

Aus dem
Universitätsklinikum Düsseldorf
Institut für Diagnostische und Interventionelle Radiologie
Direktor: Univ.-Prof. Dr. med. Gerald Antoch

**Multimodale Magnetresonanztomografie entzündlicher und degenerativer
Gelenkerkrankungen**

Habilitationsschrift zur Erlangung der venia legendi für
das Fach Radiologie des Fachbereichs Medizin
der Heinrich-Heine Universität Düsseldorf

vorgelegt von

Dr. med. Daniel Benjamin Abrar

2021

Inhalt

Abkürzungen	3
A. Kurze Zusammenfassung	6
B. Literaturangaben der zugrundeliegenden Forschungsarbeiten	12
C. Ausführliche Zusammenfassung und Diskussion.....	15
I. Einleitung.....	15
II. Untersuchungen und Ergebnisse.....	26
III. Diskussion.....	46
E. Literaturverzeichnis	55
F. Danksagung	77
G. Zugrunde liegende Forschungsarbeiten	79

Für Johanna

Abkürzungen

AIS	Adolescent idiopathic scoliosis = juvenile idiopathische Skoliose
b	biological
CEST	Chemical Exchange Saturation Transfer
CI	Konfidenzintervall
CRP	C-reaktives Protein
dGEMRIC	Delayed gadolinium enhance magnetic resonance imaging of cartilage
DMARD	Disease modifying drug
ER	Elite-Ruderer
fs	Fettgesättigt (fat-saturated)
GAG	Glykosaminoglykan
MRT	Magnetresonanztomografie
OA	Arthrose (osteoarthritis)
PDw	Protonendichte gewichtet
PsA	Psoriasisarthritis
PsAMRIS	Psoriatic Arthritis Magnetic Resonance Imaging Score
RA	Rheumatoide Arthritis
RAMRIS	Rheumatoid Arthritis Magnetic Resonance Imaging Score

r-axSpA	Radiografisch nachweisbare axiale Spondyloarthritis
SpA	Spondyloarthritis
STIR	Short Tau Inversion Recovery
T1w	T1 gewichtet
T2T	Treat-to-target
T2w	T2 gewichtet
ts	Targeted-synthesized

A. Kurze Zusammenfassung

Erkrankungen des Bewegungsapparates gehören zu den häufigsten Gründen für den Arztbesuch und sind weltweit die führende Ursache für Schmerz und Behinderung [1]. In der Folge ergeben sich zusätzlich zum individuellen Leidensdruck der Patienten enorme wirtschaftliche Kosten für die Gesellschaft [2]. So belaufen sich die Kosten für Erkrankungen des Bewegungsapparates alleine in den USA jährlich auf nahezu eine Billion US-Dollar [3]. Die verschiedenen Erkrankungen des Bewegungsapparates unterscheiden sich dabei sowohl hinsichtlich ihres zeitlichen Verlaufes und der betroffenen Körperregion als auch im Hinblick auf ihre Ätiologie. So tragen zum einen akute Verletzungen, wie Frakturen, Bandrisse oder Knorpelschäden, zum anderen chronische Erkrankungen, wie Arthrose (*osteoarthritis*, OA), Arthritiden oder Lumbago zum bunten Strauß möglicher Erkrankungen des Bewegungsapparates bei [4]. Dabei nimmt die Vielseitigkeit der Behandlungsmöglichkeiten dieser Erkrankungen stetig zu, insbesondere das weite Feld entzündlicher Gelenkerkrankungen, wie der rheumatoiden Arthritis (RA) oder der Psoriasis-Arthritis (PsA), wurde durch die Entwicklung der biologischen und gezielt synthetischen erkrankungsmodifizierenden Arzneimittel (*biological* und *targeted-synthesized disease modifying drugs*, *bDMARD* und *tsDMARD*) revolutioniert [5–8]. Durch die frühzeitige Behandlung mit diesen *DMARDs* kann durch stetige Therapiekontrolle (sog. *treat-to-target* Prinzip, *T2T*) häufig eine dauerhafte Remission erreicht werden [9–11]. Um eine derartige Erkrankung des Bewegungsapparates rechtzeitig behandeln zu können, ist eine möglichst frühzeitige Diagnose entscheidend. Seit ihrer Etablierung finden bildgebende Verfahren breite Anwendung in der Diagnostik muskuloskelettaler Erkrankungen [12–14].

Konventionelle Radiografie, Computertomografie und Magnetresonanztomografie (MRT) erlauben die sensitive, häufig sofortige und nahezu ubiquitär verfügbare Diagnose und Therapiekontrolle typischer traumatischer, degenerativer oder entzündlicher Erkrankungen des Bewegungsapparates [15–18]. Seit ihrer Entwicklung in den 1980er Jahren nimmt dabei die Bedeutung der MRT stetig zu [19, 20]. Ihre hohe Ortsauflösung, der exzellente Weichteilkontrast und die fehlende Anwendung ionisierender Strahlung machen die MRT zum Stützpfiler muskuloskelettaler Bildgebung [21, 22]. Entzündliche Weichteilveränderungen von Synovialis, Sehnen, Muskeln, Faszien und Subkutis lassen sich dabei ebenso detailliert abbilden wie knöcherne Pathologien wie Erosionen, Frakturen und Tumore [23–27]. Über diese strukturell-morphologischen Möglichkeiten der MRT hinaus, gibt es inzwischen moderne MRT-Verfahren, die auf molekularer Ebene unter anderem den Gelenkknorpel kompositionell analysieren können [28–31]. So erlaubt beispielsweise die Glykosaminoglykan (GAG) *Chemical Exchange Saturation Transfer (CEST)* Bildgebung den Nachweis von Proteoglykanen im hyalinen Gelenkknorpel und in Bandscheiben [32–34]. Da der Proteoglykanverlust ein frühes Zeichen von Knorpelschäden ist, wie sie im Rahmen degenerativer oder entzündlicher Gelenkveränderungen auftreten, können so potentielle Gelenkerkrankungen biochemisch-sensitiv erkannt werden, bevor diese strukturell manifest werden.

In der vorliegenden Habilitationsschrift wird die multimodale MRT entzündlicher und degenerativer Gelenkerkrankungen untersucht. Dabei kommen nicht-invasive Methoden der kompositionellen Knorpelbildung bei entzündlichen Gelenkerkrankungen des peripheren und Achsenskeletts sowie bei Patienten mit unspezifischen Rückenschmerzen und Leistungssportlern zum Einsatz. Außerdem

wird der Stellenwert hochauflösender MRT mit speziellen Empfangsspulen für die Detektion, Unterscheidung und Therapiekontrolle typischer rheumatischer Gelenkerkrankungen näher beleuchtet.

Die erste Arbeit untersucht den diagnostischen Stellenwert der hochauflösenden MRT von Ringbändern bei Patienten mit PsA im Vergleich zu Patienten mit RA und gesunden Kontrollpersonen. Im Rahmen dessen wurden die Finger D2-5 der obigen Studienpopulation mittels 3 Tesla (T) MRT und einer speziellen 16-Kanalhandspule untersucht, um so entzündliche und strukturelle Veränderungen der Ringbänder zu detektieren. Dabei zeigte sich, dass Patienten mit PsA ausgeprägtere Veränderungen der Ringbänder als die Vergleichskohorte aus RA-Patienten und Gesunden aufweisen. Ringbandveränderungen sind daher als für die PsA typisch anzusehen und können bei der Unterscheidung zwischen RA und PsA hilfreich sein.

Die zweite Arbeit befasst sich mit der Etablierung und Optimierung eines *gagCEST* Untersuchungsprotokolls, das mit einer klinisch-anwendbaren Untersuchungsdauer von unter acht Minuten bei einer Magnetfeldstärke von 3 T anwendbar ist. Dazu wurden zunächst Bloch-Mc-Connell Simulationsexperimente durchgeführt, um ein optimales *gagCEST*-Protokoll zu etablieren. Anschließend wurde der tibiotalare Gelenkknorpel von Patienten nach osteochondraler Läsion des Talus sowie von gesunden Kontrollpersonen mit dem optimierten Protokoll untersucht. Dabei zeigten sich sowohl eine gute Reproduzierbarkeit der Ergebnisse als auch signifikante Unterschiede zwischen Patienten und Kontrollpersonen. Somit konnte diese Machbarkeitsstudie die Durchführbarkeit von *gagCEST* am tibiotalaren Gelenkknorpel bei 3 T belegen.

In der dritten Arbeit wurden die symptomatischen Hände von Patienten mit RA und PsA mit einer dezidierten Handspule und 3 T MRT untersucht, um systematisch erkrankungsassoziierte Veränderungen zu erfassen und mögliche Unterschiede zwischen beiden Entitäten herauszuarbeiten. Zur exakten Analyse wurden die standardisierten und validierten Scores für RA und PsA, der RA *MRI* und PsA *MRI Score* (*RAMRIS* und *PsAMRIS*) erhoben [35, 36]. Diese bilden typische erkrankungsassoziierte Veränderungen, wie Synovialitis, Tenovaginitis, Osteoödem und Erosionen ab. In der Studienpopulation konnte gezeigt werden, dass die PsA signifikant häufiger mit extraartikulär gelegenen, entzündlichen Veränderungen einhergeht als die RA und mit diesem Merkmal eine Differenzierung beider Entitäten erleichtert werden kann.

Die vierte Arbeit analysierte systematisch den GAG-Gehalt lumbaler Bandscheiben (*intervertebral disks, IVDs*) von Patienten mit radiografisch nachgewiesener axialer Spondyloarthropathie (r-axSpA) im Vergleich zu altersgleichen Kontrollpersonen. Zudem wurden typische erkrankungsassoziierte Veränderungen der Wirbelsäule, wie beispielsweise Syndesmophyten und Spondylitis, mittels morphologischer Standard-MRT erfasst. Dabei zeigten sich signifikant niedrigere *IVD-gagCEST*-Werte bei Patienten. Zudem zeigte sich ein Zusammenhang zwischen niedrigen *IVD-gagCEST*-Werten und dem Vorliegen von Syndesmophyten.

In der fünften Arbeit wurde untersucht, ob und inwieweit Knorpeldegeneration mit Entzündung des Synovialis in den Fingergelenken von Patienten mit PsA assoziiert ist. Dazu wurde der Proteoglykangehalt des Gelenkknorpels der Fingergelenke mittels *delayed gadolinium-enhanced MRI of cartilage (dGEMRIC)* analysiert. Die Methode ist ein biochemisch-sensitives Verfahren zur Evaluation der Knorpelzusammensetzung. Zudem wurde mittels *dynamic contrast-enhanced*

(DCE) MRT, der sogenannten Perfusionsbildgebung, die Durchblutung der Synovialis und somit letztlich die Ausprägung bestehender Synovialitis betrachtet. Dabei zeigte sich ein Zusammenhang zwischen Proteoglykanverlust und Ausprägung der Synovialitis.

Die sechste Arbeit evaluiert eine vereinfachte Version des *PsAMRIS*, den sogenannten *sPsAMRIS*, der eine schnellere Analyse erkrankungsassoziierter Veränderungen an den Fingergelenken von Patienten mit PsA erlaubt und dabei eine gleichwertige Sensitivität für Veränderungen wahrt.

In der siebten Arbeit wurden die Fingergelenke von Patienten mit RA und PsA mittels *dGEMRIC* hinsichtlich der Zusammensetzung des Gelenkknorpels, also dem Proteoglykangehalt, untersucht. Hier zeigte sich, dass kein signifikanter Unterschied zwischen beiden Armen der Studienpopulation besteht. Somit ist von einer Beteiligung des Gelenkknorpels im Erkrankungsverlauf beider Entitäten auszugehen.

Die Arbeiten acht bis zehn untersuchten den Proteoglykangehalt lumbaler Bandscheiben in unterschiedlichen Kollektiven mittels *gagCEST* Bildgebung. Dabei konnte gezeigt werden, dass Patienten mit unspezifischer Lumbago, Radikulopathie und juveniler idiopathischer Skoliose (*adolescent idiopathic scoliosis, AIS*) signifikant niedrigere *IVD-gagCEST*-Werte aufweisen als gesunde Kontrollpersonen. Zudem weisen *IVDs*, die unmittelbar an Bandscheibenherniationen oder an die Endpunkte einer skoliotischen Hauptkrümmung grenzen, niedrige *gagCEST*-Werte auf als entferntere *IVDs*. Die zehnte Arbeit untersuchte Elite-Ruderer aus der deutschen Nationalmannschaft im Verlauf ihres jährlichen Trainingszyklus. Dabei wurde festgestellt, dass in lumbalen

IVDs ein belastungsabhängiges *Remodeling* stattfindet. So wurden in der Belastungsphase höhere *IVD-gagCEST*-Werte als in der Ruhephase festgestellt. Zusammenfassend zeigen die zehn Arbeiten neue und vertiefende Erkenntnisse über moderne MRT-Verfahren, die zum einen hochauflösende Bilder feiner Gelenkstrukturen und zum anderen kompositionelle Informationen über Gelenkknorpel und Bandscheiben vermitteln. So können degenerative und entzündliche Gelenkveränderungen sowohl strukturell als auch ultrastrukturell sichtbar gemacht werden, was als Ansatzpunkt für zukünftige Implementierung in Diagnostik und Therapiekontrolle entzündlicher und degenerativer Gelenkerkrankungen dienen kann.

B. Literaturangaben der zugrundeliegenden Forschungsarbeiten

1. Abrar DB, Schleich C, Nebelung S, Frenken M, Radke KL, Vordenbäumen S, Brinks R, Schneider M, Ostendorf B, McGonagle D, Sewerin P. High-resolution MRI of flexor tendon pulleys using a 16-channel hand coil: disease detection and differentiation of psoriatic and rheumatoid arthritis. Arthritis Res Ther. 2020 Mar 2;22(1):40.

Impact Factor (IF): 4,103

2. Abrar DB, Schleich C, Radke KL, Frenken M, Stabinska J, Ljimini A, Wittsack HJ, Antoch G, Bittersohl B, Hesper T, Nebelung S, Müller-Lutz A. Detection of early cartilage degeneration in the tibiotalar joint using 3 T gagCEST imaging: a feasibility study. MAGMA. 2020 Jul 28.

IF: 1,832

3. Abrar DB, Schleich C, Brinks R, Goertz C, Schneider M, Nebelung S, Sewerin P. Differentiating rheumatoid and psoriatic arthritis: a systematic analysis of high-resolution magnetic resonance imaging features-preliminary findings. Skeletal Radiol. 2020 Aug 26.

IF: 1,618

4. Abrar DB, Schleich C, Tsiami S, Müller-Lutz A, Radke KL, Holthausen N, Frenken M, Boschheidgen M, Antoch G, Mücke J, Sewerin P, Braun J, Nebelung S, Baraliakos X. Functional MR imaging beyond structure and inflammation-radiographic axial spondyloarthritis is associated with proteoglycan depletion of the lumbar spine. Arthritis Res Ther. 2020 Sep 17;22(1):219.

IF: 4,103

5. Abrar DB, Schleich C, Müller-Lutz A, Frenken M, Radke KL, Vordenbäumen S, Schneider M, Ostendorf B, Sewerin P. Cartilage Degradation in Psoriatic Arthritis Is Associated With Increased Synovial Perfusion as Detected by Magnetic Resonance Imaging. Front Med (Lausanne). 2020 Sep 25;7:539870.

IF: 3,9

6. Abrar DB, Schleich C, Brinks R, Goertz C, Frenken M, Schneider M, Nebelung S, Sewerin P. Introduction of a Simplified Psoriatic Arthritis Magnetic Resonance Imaging Score (sPsAMRIS): A Potential Tool for Treatment Monitoring in Peripheral Psoriatic Arthritis. Diagnostics (Basel). 2020 Dec 15;10(12):E1093.

IF: 3,110

7. Abrar DB, Schleich C, Frenken M, Vordenbäumen S, Richter J, Schneider M, Ostendorf B, Nebelung S, Sewerin P. DGEMRIC in the Assessment of Pre-Morphological Cartilage Degeneration in Rheumatic Disease: Rheumatoid Arthritis vs. Psoriatic Arthritis. Diagnostics (Basel). 2021 Jan 20;11(2):E147.

IF: 3,110

8. Frenken M, Nebelung S, Schleich C, Müller-Lutz A, Radke KL, Kamp B, Boschheidgen M, Wollschläger L, Bittersohl B, Antoch G, Konieczny MR, Abrar DB. Non-Specific Low Back Pain and Lumbar Radiculopathy: Comparison of Morphologic and Compositional MRI as Assessed by gagCEST Imaging at 3T. Diagnostics. 2021; 11(3):402. <https://doi.org/10.3390/diagnostics11030402>

IF: 3,110

9. Wollschläger LM, Nebelung S, Schleich C, Müller-Lutz A, Radke KL, Frenken M, Boschheidgen M, Prost M, Antoch G, Konieczny MR, Abrar DB. Evaluating Lumbar Intervertebral Disc Degeneration on a Compositional Level Using Chemical Exchange Saturation Transfer: Preliminary Results in Patients with Adolescent Idiopathic Scoliosis. *Diagnostics (Basel)*. 2021 May 22;11(6):934. doi: 10.3390/diagnostics11060934

IF: 3,110

10. Frenken M, Schleich C, Radke KL, Müller-Lutz A, Benedikter C, Franz A, Antoch G, Bittersohl B, Abrar DB, Nebelung S (shared last authorship). Imaging of exercise-induced spinal remodeling in elite rowers. *J Sci Med Sport*. 2021 Aug 8:S1440-2440(21)00195-X. doi: 10.1016/j.jsams.2021.07.015

IF: 4,319

C. Ausführliche Zusammenfassung und Diskussion

I. Einleitung

Erkrankungen des Bewegungsapparates gehören weltweit zu den häufigsten Ursachen für Arztbesuch, Arbeitsunfähigkeit und chronische Schmerzen [37]. Zu dieser Erkrankungsgruppe gehören unter anderem entzündliche und degenerative Gelenkerkrankungen, die in allen Altersgruppen vertreten und insgesamt gleichmäßig zwischen beiden Geschlechtern verteilt sind [38, 39]. Sozioökonomisch sind sowohl entzündliche als auch degenerative Gelenkerkrankungen eine große Last für die Gesundheitssysteme, so belaufen sich die jährlichen Kosten für einen Patienten mit OA auf bis zu €12.000 und für einen Patienten mit Arthritis auf bis zu €5000 [40, 41]. Wenn sie zu spät oder nicht behandelt werden, gehen Gelenkerkrankungen mit Gelenkdestruktion, chronischen Schmerzen und schließlich Funktionsverlust einher [42]. Daher sind die frühe Diagnose und Therapie entscheidend für den Erkrankungsverlauf. Zwar stehen die körperliche Untersuchung und laborchemische Diagnostik, insbesondere bei entzündlichen Gelenkerkrankungen, weiterhin im Vordergrund, allerdings spielen bildgebende Verfahren seit jeher eine wichtige Rolle und sind von zunehmender Bedeutung [35, 36].

1. Degenerative Gelenkerkrankungen

Die häufigsten degenerativen Gelenkerkrankungen sind die OA am peripheren Skelett und die degenerative Bandscheibenerkrankung (*degenerative disk disease, DDD*) an der Wirbelsäule.

Die OA ist die häufigste Gelenkerkrankung überhaupt: allein die Prävalenz der Gonarthrose wird auf weltweit bis zu 300 Millionen Patienten geschätzt [43].

Bislang ist die OA trotz Behandlung eine irreversible Erkrankung, die mit einer erheblichen Einschränkung der körperlichen Aktivität und Lebensqualität aufgrund chronischer Schmerzen und Funktionsverlust einhergeht. Grundsätzlich ist zwischen primärer (=idiopathischer) und sekundärer OA zu unterscheiden. Ursachen für eine sekundäre OA sind Trauma, vorausgegangene Operationen oder angeborene Fehlbildungen. Die OA wird anhand konventioneller Radiografien diagnostiziert und entsprechend ihres Schweregrades nach Kellgren-Lawrence eingeteilt: 0 (Normalbefund, keine OA) bis 4 (fortgeschrittene Verminderung der Gelenkspaltweite, Deformität der gelenkbildenden Knochenanteile, schwere OA) [44]. Die Pathogenese der OA ist sehr komplex und ist keine bloße Abnutzungserscheinung [39]. Bei der OA spielen zahlreiche Faktoren eine Rolle, beispielsweise biomechanische Gegebenheiten, die die Synthese und Freisetzung von Entzündungsmediatoren bedingen und somit die Entstehung, Persistenz und Aggravation von erkrankungsassoziierten Schmerzen begünstigen. Korrespondierend sind erhöhte Konzentrationen proinflammatorischer Zyto- und Chemokine innerhalb der Synovia nachweisbar [45]. Im Erkrankungsverlauf sind darüber hinaus auch alle weiteren Gelenkbestandteile, insbesondere jedoch der Gelenkknorpel beteiligt. Dies führt sowohl zu einer pathologischen Gelenkkinematik als auch zu Synovialitis und abermals Produktion und Freisetzung proinflammatorischer Mediatoren und Proteasen.

Die Lumbago ist die häufigste Vertreterin aller muskuloskelettaler Erkrankungen und weist eine Lebenszeitprävalenz von bis zu 85% auf [46]. Die häufigste Ursache für Rückenschmerzen sind dabei Bandscheibenerkrankungen, wobei Bandscheibenvorfälle und die *DDD* hierunter insbesondere zu erwähnen sind [47]. Im Jugendalter spielen hingegen andere Erkrankungen eine Rolle, wie

beispielsweise die *AIS* [48]. *DDD* beschreibt den pathologischen Strukturverlust der *IVD* als Folge einer zellvermittelten Antwortkaskade auf multifaktorielle Einflüsse, wie beispielsweise Traumata, Entzündung, genetische Prädisposition und beschleunigte Alterungsprozesse [49]. So werden erhöhte Konzentrationen kataboler Enzyme sowie proinflammatorischer und nozizeptiver Zytokine bei Vorliegen einer *DDD* nachgewiesen. Diese führen zu verfrühten ultrastrukturellen Matrixveränderungen von Annulus fibrosus (AF) und Nucleus pulposus (NP). Dieser kompositionelle Strukturverlust ist initial durch den Verlust von GAGs, Proteoglykanen und Kollagenen sowie später durch irreversiblen Wasserverlust gekennzeichnet. Durch diese Dehydratation und den letztlich resultierenden strukturellen Substanzverlust verliert die *IVD* ihre physiologische Funktion als mechanischer Stoßdämpfer der Wirbelsäule [50]. Bildgebung in Form konventioneller Radiografien, aber auch MRT spielen seit jeher eine Rolle bei der Abklärung von Rückenschmerzen. Dabei sind sie bislang insbesondere zum Nachweis von Bandscheibenvorfällen, Frakturen und Tumoren als Schmerzursache unerlässlich. Aber auch Veränderungen, die in Zusammenschau mit der klinischen Untersuchungen zu einer *DDD* passen, lassen sich mittels MRT zuverlässig und sensitiv erkennen [50].

Da bislang kausale Behandlungsansätze für die *OA* oder die *DDD* fehlen, sind die Erkennung und Vermeidung von Risikofaktoren sowie die Früherkennung von potentiell reversiblen Initialstadien von hoher klinischer Relevanz. Diese Früherkennung kann potentiell durch moderne MRT-Verfahren unterstützt werden.

2. Entzündliche Gelenkerkrankungen

Entzündliche Gelenkerkrankungen, die sogenannten Arthritiden, können sowohl infektiös und parainfektiös als auch primär autoimmun bedingt sein. Die häufigsten autoimmun-vermittelten Arthritiden sind die RA und PsA am peripheren und die r-axSpA am Achsenskelett. Allein in Deutschland bis zu 2 Millionen Menschen an einer dieser Arthritiden. Hinsichtlich ihrer Pathophysiologie stehen die RA als primär synoviale Erkrankung den beiden primär enthesealen Erkrankungen PsA und axSpA gegenüber. Die RA wird durch Entzündungsmediatoren vermittelt, die zu einer Synovialitis, insbesondere an kleinen Gelenken, führen. Über die Synovialis wandern Entzündungszellen an den sogenannten *bare areas* in den Knochen ein und führen hier zu einer Osteitis und zu Erosionen [51, 52]. Letztlich kommt es auch zu einer Zerstörung von Gelenkknorpel und Bändern sowie zu einer Entzündung von Sehnen(-scheiden) und den umliegenden Weichteilen.

Im Gegensatz dazu sind die PsA und r-axSpA primär Erkrankungen der Enthesen [53–57]. Enthesen sind der osteoligamentäre oder osteotendinöse Ansatz von Bändern und Sehnen am Knochen. Dieser besteht aus einem Mischgewebe aus Bindegewebe, Knorpel, Synovialis und Knochen und wird auch als synovioenthesealer Komplex bezeichnet [53]. Bei der PsA kommt es typischerweise über den Ansatz der Kollateralbandapparates zur Entzündung der kleinen Fingergelenke, wobei auch die primäre Inflammation des Ringbänder beschrieben ist [27, 54]. Die r-axSpA beginnt klassischerweise mit der Entzündung der Anheftungen des AF an den Wirbelkörperendplatten als Form der Enthesitis [58, 59]. Über die entheseale Inflammation kommt es bei allen Erkrankungen dieser Gruppe sekundär zu Synovialitis, Osteitis, Erosionen, Tenosynovialitis und Knorpeldestruktion, sodass die Endstrecke große Überschneidungen mit der RA aufweist [60].

Werden Arthritiden nicht oder zu spät behandelt, kommt es zu einer fortschreitenden Gelenkdestruktion mit Fehlstellung und Bewegungseinschränkung, die letztlich zu einem Funktionsverlust führen können. Um dies zu verhüten, sind eine frühe Diagnose und Therapie von höchster Priorität. Zwar stehen körperliche Untersuchung und laborchemische Diagnostik bei Primärdiagnose weiterhin im Vordergrund, allerdings sind bildgebende Verfahren, wie Sonografie, konventionelles Röntgen und nicht zuletzt auch die MRT, weit verbreitet und von zunehmender Bedeutung [61–67]. Die Bildgebung hilft nicht nur bei der Primärdiagnostik, sondern hat ihre Stärken insbesondere bei der Differentialdiagnostik unterschiedlicher Arthritiden und bei der Therapiekontrolle. Eine regelmäßige Therapiekontrolle (*T2T*-Prinzip) ist seit einigen Jahren sowohl bei der RA als auch der PsA etabliert, um eine dauerhafte Remission zu erreichen und zu erhalten [6, 9, 11]. Dabei kommen moderne Medikamente zum Einsatz, sog. bDMARD und tsDMARD, die eine individualisierte Therapie für jeden Patienten ermöglichen.

3. MRT

Seit ihrer Einführung in den frühen 1980er Jahren hat sich die MRT zu einer unersetzbaren Säule der muskuloskelettalen Bildgebung entwickelt. Mit ihrem exzellenten Weichteilkontrast und der ausgezeichneten Ortsauflösung, die mithilfe einer inzwischen weit verbreiteten Anwendung von modernen 3 T Geräten und fortschrittlichen Empfangsspulen klinischer Standard ist, können heutzutage alle Regionen und Gewebetypen des Bewegungsapparates zuverlässig abgebildet und beurteilt werden. So sind Frakturen und Knochenmarkveränderungen, aber auch synoviale, ligamentäre und kartilaginäre Pathologien zuverlässig darstellbar. Zwar

hat sie gegenüber Computertomografie und Sonografie auch Nachteile, wie die längere Messzeit und die höheren Kosten, allerdings stehen diesen Nachteilen die fehlende Strahlenbelastung und die fehlende Untersucherabhängigkeit als Vorteile gegenüber. Neben der hochauflösenden morphologischen Standard-MRT existieren zudem zahlreiche kompositionelle Verfahren, die ultrastrukturelle Analysen bestimmter Gewebetypen erlauben. Insbesondere für Gelenkknorpel und Bandscheibe existieren verschiedene kompositionelle Methoden, die im Folgenden näher beleuchtet werden.

a) Morphologische Hochfeld-MRT

Die MRT ist ein bildgebendes Verfahren, das nicht auf ionisierender Strahlung, sondern auf Spin-Spin-Interaktionen in einem externen Magnetfeld basiert. Hinsichtlich der basalen Grundlagen der MRT wird auf die bestehende und exzellente Primär- und Sekundärliteratur verwiesen [68, 69]. Die in der wissenschaftlichen Praxis bereits etablierten Hochfeld (3 T) MRT Geräte, finden seit längerer Zeit auch in der klinischen Routine breite Anwendung und machen so fortgeschrittene MRT Verfahren auch in der täglichen Praxis möglich, insbesondere wenn sie durch dezidierte Sende- und Empfangsspulen ergänzt werden. Vorteile der Hochfeldtechnik sind ein verbessertes Signal-zu-Rausch Verhältnis (*signal to noise ratio, SNR*), eine höhere Ortsauflösung und reduzierte Untersuchungszeiten. Da das MR-Signal proportional zum statischen Magnetfeld zum Quadrat ist, ergibt sich rechnerisch eine Verbesserung der *SNR* um den Faktor zwei. Aufgrund der gleichzeitigen Zunahme von Suszeptibilitätsartefakten bei höheren Feldstärken beträgt die tatsächliche Verbesserung der *SNR* bis zu 60% [70]. Eine verbesserte Ortsauflösung mit einer Verkleinerung der

Schichtdicke, des Untersuchungsvolumens (*field of view, FoV*) und der Pixelgröße geht zwingend auf Kosten der *SNR*. Daraus ergibt sich, dass bei der Verwendung von 3 T Geräten und dezidierten Empfangsspulen hochaufgelöste Bilder mit geringer Schichtdicke, kleinem *FoV* und kleiner Pixelgröße angefertigt werden können, die eine detaillierte Abbildung kleinster Strukturen, wie beispielsweise den kleinen Fingergelenken, erlauben, ohne dabei eine Verschlechterung der *SNR* zu erwarten [71].

aa) Anwendung RA und PsA

Die MRT erlaubt die zuverlässige Detektion erkrankungstypischer Gelenkveränderungen, wie beispielsweise Synovialitis, Tenovaginitis, Erosionen und Osteitis [72–77]. Dabei ist sie insbesondere bei der Erkennung von Knochenmarkveränderungen, also dem typischen Knochenmarködem, Goldstandard, denn diese können weder von der Sonografie noch der Computertomografie dargestellt werden. Bislang ist die MRT zwar noch kein Bestandteil der offiziellen Diagnosekriterien der RA und PsA, allerdings findet sie in Form des RA und PsA MR Imaging Scores (RAMRIS und PsAMRIS) wissenschaftliche Anwendung [35, 36, 78, 79]. Beide sind Summenscores, die semi-quantitativ erkrankungsassoziierte Veränderungen des Handgelenkes, der Handwurzel (RA) und der metacarpophalangeal (MCP)-Gelenke (beide) sowie der proximalen interphalangeal (PIP-) und distalen interphalangeal (DIP-) Gelenke (PsA) auf flüssigkeitssensitiven und kontrastmittelgestützten Sequenzen erfassen und in einem Summenwert angeben. Sowohl beim RAMRIS als auch beim PsAMRIS werden Punkte für das Vorliegen und die Ausprägung von Synovialitis, Flexor-Tenosynovialitis, Erosionen und Knochenmarködem vergeben. Der

RAMRIS schließt noch das Merkmal Gelenkspaltverschmälerung, der PsAMRIS die Merkmale periartikuläre Inflammation und Osteoproliferationen mit ein. So können nicht nur fragliche klinische Diagnosen und Differentialdiagnosen bestätigt oder ausgeschlossen werden, sondern auch der Verlauf und das Therapieansprechen valide beurteilt werden.

ab) Anwendung r-axSpA

Bei der r-axSpA und der non-r-axSpA sind die MRT der Sakroiliakalgelenke und der Nachweis einer floriden Sakroiliitis Bestandteil der primären Diagnosekriterien [80–82]. Veränderungen der Wirbelsäule sind bislang nicht Teil dieser Kriterien, allerdings lassen sich typische Veränderungen wie die anteriore und posteriore Spondylitis, Erosionen der Wirbelkörperabschlussplatten, Syndesmophyten, Verknöcherungen der Längsbänder und die Ankylose der Wirbelsegmente zuverlässig und sensitiv nachweisen [83–86].

ac) DDD

Die strukturell manifeste *DDD* lässt sich nicht-invasiv mittels der MRT abbilden, wobei dazu vor allem sagittale T2-gewichtete (T2w) Sequenzen Anwendung finden, um den Flüssigkeitsgehalt der Bandscheibe zu beurteilen. Gemäß der etablierten und validierten Pfirrmann Klassifikation wird der strukturell manifeste Grad der *IVD* Degeneration anhand der T2w Signalintensität und der Höhe der jeweiligen *IVD* bestimmt, wobei ein Grad ≤ 2 nicht-degenerierten und ein Grad ≥ 3 degenerierten *IVDs* entspricht [87]. Auch Veränderungen der Wirbelkörperabschlussplatten, die typische Folge der *DDD* sind können mittels der

MRT beurteilt werden, s. dazu beispielsweise die verbreitete Modic-Klassifikation [88].

b) Kompositionelle MRT Bildgebung von Gelenkknorpel und Bandscheibe

Frühe, potentiell reversible Veränderungen des Gelenkknorpels im Rahmen einer OA, einer RA oder einer PsA sowie der IVD bei der DDD lassen sich trotz hochauflösender MRT mittels morphologischer Standardsequenzen nicht abbilden. Dazu sind spezielle, sog. kompositionelle Methoden, wie die *gagCEST* oder *dGEMRIC* Bildgebung erforderlich.

Der avaskuläre Gelenkknorpel setzt sich aus Chondrozyten und der extrazellulären Matrix zusammen. Die extrazelluläre Matrix besteht vor allem aus Wasser (>70%) und zu geringeren Anteilen aus Typ II Kollagenfasern und sogenannten Proteoglykanen. Proteoglykane setzen sich aus einem Kernprotein und hydrophilen Polysaccharidketten, den GAGs, zusammen [39]. Während die Kollagenfasern durch ihr verzweigtes Netzwerk Scherstabilität verleihen, binden die GAGs Wasser und bedingen so die mechanische Dämpferfunktion des Knorpels. Frühe Veränderungen des Gelenkknorpels bei degenerativen Veränderungen beginnen mit einem GAG-Verlust [30, 89, 90]. Somit kann der GAG-Verlust als ein frühes, potentiell reversibles Zeichen der OA gewertet werden. Der Goldstandard der GAG-spezifischen kompositionellen MRT ist die sog. *dGEMRIC*. Dabei werden die anionischen Eigenschaften gadoliniumhaltiger (Gd^{3+}), intravenös verabreichter Kontrastmittel genutzt, die vor allem bei $Gd-DTPA^{2-}$ beschrieben wurden. Gd^{3+} -Kontrastmittel führt durch seine paramagnetischen Eigenschaften zu einer Verkürzung der T1-Zeit. Im gesunden Knorpel reichert Kontrastmittel jedoch kaum an, sodass es hier kaum eine messbare Veränderung

der T1 Zeit gibt [91]. Kommt es jedoch im Rahmen einer OA oder RA zu einem Verlust an GAG, können die nun frei gewordenen Bindungsstellen durch Gd³⁺ besetzt werden und es kommt zu einer relevanten Verminderung der T1-Zeit [28, 92, 93]. Niedrige T1-Zeiten korrelieren dabei mit dem GAG-Gehalt des untersuchten Knorpels. Dieser Zusammenhang konnte histologisch bestätigt werden [94, 95]. Vorarbeiten konnten bereits die potentielle Anwendungsmöglichkeit von *dGEMRIC* bei der RA aufzeigen, wobei für die PsA bislang keine Daten existieren [96–98].

Im Gegensatz zu *dGEMRIC* ist die *gagCEST* Bildgebung ein kompositionelles Verfahren, das keiner intravenösen Kontrastmittelgabe bedarf [99]. Die Methode beruht auf dem physiologischen chemischen Austausch von Protonen, die in zwei unterschiedlichen sog. „Protonenpools“ vorliegen [100]. Der eine Pool sind die GAG-gebundenen Protonen, die sog. Lösungsprotonen, der andere die an Wasser gebundenen, die sog. Wasserprotonen. Entscheidend ist, dass die Protonen der beiden Pools eine unterschiedliche Resonanzfrequenz aufweisen. Werden die Lösungsprotonen nun durch einen frequenzselektiven Radiofrequenzpuls gesättigt und in der Folge mittels chemischen Austausches auf den Wasserpool übertragen, sinkt auch die Magnetisierung des Wassers und somit das messbare Wassersignal. Dieser Signalabfall des Wassers korreliert negativ mit dem GAG-Gehalt der angeregten Schicht. Der Frequenzbereich von 0,9-1,9 ppm ist durch die OH⁻ Gruppen der GAGs GAG-spezifisch. In diesem Bereich ist eine sog. Asymmetrie, der sogenannte *CEST*-Effekt messbar [101]. Dieser *CEST*-Effekt wird als Magnetisierungstransfer-Asymmetrie-Ratio (MTR_{asym}) angegeben und gibt das Verhältnis von gesättigtem zu ungesättigtem Wasser in Prozent an.

Die *gagCEST* Methode wurde besonders häufig an *IVDs*, jedoch auch am hyalinen Gelenkknorpel bereits angewandt [102–106]. *IVDs* bestehen aus einem äußeren Faserring, dem AF, und dem davon umgebendem gallertigen NP. Der NP weist einen sehr hohen GAG-Gehalt auf und ähnlich zum hyalinen Gelenkknorpel kommt es im Rahmen früher degenerativer Veränderungen zum GAG-Verlust, bevor morphologische MRT-Verfahren eine strukturell manifeste *DDD* feststellen können.

II. Untersuchungen und Ergebnisse

1. **Arbeit:** Abrar DB, Schleich C, Nebelung S, Frenken M, Radke KL, Vordenbäumen S, Brinks R, Schneider M, Ostendorf B, McGonagle D, Sewerin P. High-resolution MRI of flexor tendon pulleys using a 16-channel hand coil: disease detection and differentiation of psoriatic and rheumatoid arthritis. Arthritis Res Ther. 2020 Mar 2;22(1):40.

Die periphere PsA ist eine sehr häufige entzündliche Gelenkerkrankung, die eine gemeinsame Endstrecke mit der RA aufweist, nämlich eine ausgeprägte Gelenkdestruktion und erhebliche Funktionseinschränkung [107, 108]. Dem entgegen unterscheiden sich beide Entitäten hinsichtlich ihrer Pathogenese deutlich; während die RA eine primär synoviale Erkrankung ist, entsteht die PsA an Entesen, also Band- oder Sehnenansätzen [53, 54, 109]. Dazu zählen die sogenannten synovioenthesealen Komplexe, zu denen auch die Ringbänder der Fingerbeugesehnen gehören [110–112]. Da die Unterscheidung zwischen RA und PsA im klinischen Alltag häufig nicht eindeutig ist und somit die notwendige frühe Diagnose und Therapie erschwert wird, sind diagnostische Mittel für die Unterscheidung beider Erkrankungen erforderlich [113–115]. Ziel dieser Arbeit war daher den Stellenwert morphologischer Ringbandveränderungen mittels hochauflösender 3 T MRT zur Differenzierung von PsA und RA unter Verwendung einer neuartigen 16-Kanal Handspule zu untersuchen.

17 Patienten mit aktiver PsA, 20 Patienten mit aktiver RA und 16 gesunde Probanden wurden mittels hochauflösender 3-T-MRT und einer speziellen 16-Kanal-Handspule untersucht. Die Bilder wurden von drei unabhängigen Radiologen hinsichtlich des Ausmaßes entzündlicher Veränderungen, der

Ringbanddicke und des PsAMRIS sowie seiner Subscores analysiert. Für Korrelationsanalysen wurde die Spearman rho-Korrelation berechnet.

Die Ringbänder waren bei PsA-Patienten signifikant dicker als bei RA-Patienten (mittlerer Unterschied 0,16 mm, $p < 0,001$) und Probanden (mittlerer Unterschied 0,2 mm, $p < 0,001$). Zudem zeigten sie ein höheres Ausmaß an assoziierten entzündlichen Veränderungen (mittlerer Unterschied zu RA 4,7, $p = 0,048$; mittlerer Unterschied zu den Probanden 14,65, $p < 0,001$). Zusätzlich gab es eine starke Korrelation zwischen der Entzündung der Ringbänder und dem PsAMRIS sowie seinen akut-entzündlichen Subscores, also der Tenovaginitis der Beugesehnen, der Synovialitis und der periartikulären Entzündung (beispielhaft für den zweiten Finger: Synovialitis $\rho = 0,72$, Tenovaginitis der Beugesehnen $\rho = 0,7$, PsAMRIS insgesamt $\rho = 0,72$, $p < 0,01$). Ähnlich starke Korrelationen zeigten sich in den Fingern 3-5. Schwächere Korrelationen zeigten sich bei RA (Synovialitis $\rho = 0,49$, Tenovaginitis der Beugesehnen $\rho = 0,49$, periartikuläre Entzündung $\rho = 0,4$).

Zusammenfassend konnte somit gezeigt werden, dass PsA zu deutlichen akut-entzündlichen und strukturellen Veränderungen der Ringbänder führt, die stärker ausgeprägt sind als bei Patienten mit RA und Gesunden. Die Beurteilung von MRT-Veränderungen der Ringbänder ist für die Krankheitserkennung bei PsA sowie für deren Unterscheidung von RA und gesunden Individuen somit von potentieller Bedeutung.

2. Arbeit: Abrar DB, Schleich C, Radke KL, Frenken M, Stabinska J, Ljimini A, Wittsack HJ, Antoch G, Bittersohl B, Hesper T, Nebelung S, Müller-Lutz A. Detection of early cartilage degeneration in the tibiotalar joint using 3 T gagCEST imaging: a feasibility study. MAGMA. 2020 Jul 28.

Die kompositionelle MRT vermag Knorpelveränderungen zu detektieren, die unwiderruflichen, morphologisch-manifesten Veränderungen vorausgehen [28, 29, 31]. Sie ermöglichen die Detektion des Proteoglykanverlustes, also dem potentiell reversiblen Initialstadium der OA [116]. Goldstandard war dabei bislang *dGEMRIC*, ein kontrastmittelgestütztes, histologisch validiertes Verfahren, das spezifisch für Proteoglykane ist [95, 117]. Aufgrund neuerer Einschränkungen bei der Verwendung gadoliniumbasierter Kontrastmittel, sind jedoch kontrastmittelfreie Alternativen in den wissenschaftlichen Fokus gerückt, unter anderem die *gagCEST* Bildgebung [118–120]. Allerdings wurde dieses Verfahren bei schmalen Gelenkknorpel und 3 T MRT Geräten bislang nur spärlich eingesetzt. Ziel dieser Arbeit war daher die Etablierung und Optimierung eines stabilen 3 T-*gagCEST*-Bildgebungsprotokolls zur Beurteilung des tibiotalaren Gelenkknorpels bei gesunden Probanden und Patienten nach Sprunggelenksverletzung.

Zunächst wurde mithilfe von Bloch-McConnell-Simulationen ein 3 T *gagCEST* Sequenzprotokoll mit einer Messdauer von weniger als 07:30 min optimiert. Dieses Protokoll wurde anschließend verwendet, um den *gagCEST*-Effekt des tibiotalaren Gelenkknorpels von 17 gesunden Probanden und fünf Patienten mit traumatischen osteochondralen Läsionen des Talus zu analysieren.

Die MTRasym, d.h. die *gagCEST*-Effektgröße, war bei den Patienten signifikant geringer als bei den gesunden Probanden ($0,34 \pm 1,9\%$ vs. $1,49 \pm 0,11\%$; $p < 0,001$). Die Intra- und Inter-Rater-Reproduzierbarkeit war mit einem durchschnittlichen Intraclass-Korrelationskoeffizienten (ICC) von 0,97 und einem Einzelmessungs-ICC von 0,91 ($p < 0,01$) exzellent.

Zusammenfassend waren prämorphologische Knorpelveränderungen des oberen Sprunggelenkes auf der Basis des optimierten 3 T *gagCEST*-Bildgebungsprotokolls quantitativ beurteilbar. Somit wurde eine stabile Quantifizierung der *gagCEST*-Effektgrößen bei Patienten und Gesunden in klinisch praktikabler Messzeit ermöglicht.

3. Arbeit: Abrar DB, Schleich C, Brinks R, Goertz C, Schneider M, Nebelung S, Sewerin P. Differentiating rheumatoid and psoriatic arthritis: a systematic analysis of high-resolution magnetic resonance imaging features- preliminary findings. Skeletal Radiol. 2020 Aug 26.

Rheumatische Gelenkerkrankungen, wie die RA und PsA, führen unbehandelt zu Gelenkdestruktion und erheblicher funktioneller Beeinträchtigung [42, 121]. Dabei sind die frühe Erkennung und Therapie entzündlicher Gelenkerkrankung für einen günstigen Krankheitsverlauf entscheidend [6, 7, 11]. Da sich die Therapieregime für die verschiedenen peripheren Gelenkerkrankungen inzwischen unterscheiden, ist die diagnostische Differenzierung von RA und PsA von wesentlicher Bedeutung, bleibt jedoch im klinischen Alltag aufgrund ihrer überlappenden Phänotypen bisweilen eine Herausforderung [122, 123]. Ziel dieser Studie war es daher, den diagnostischen Wert der MRT für die diagnostische Differenzierung beider Entitäten systematisch zu untersuchen.

17 Patienten mit PsA und 28 Patienten mit RA wurden mittels hochauflösender 3 T-MRT und einer speziellen 16-Kanal-Handspule untersucht. Alle Bilder wurden gemäß RAMRIS und PsAMRIS auf Vorliegen und Ausprägung von Synovialitis, Tenovaginitis der Beugesehnen, Knochenmarködem, Erosionen, periartikulärer Entzündung, Osteoproliferation und Gelenkspaltverschmälerung analysiert. Anschließend wurden odds ratios berechnet, um die Assoziationsstärke zwischen diesen bildgebenden sowie demographischen Merkmalen und dem Ergebnis RA vs. PsA zu bestimmen.

PsA konnte durch extrakapsuläre entzündliche Veränderungen (PsAMRIS-Sub-Score "periartikuläre Entzündung") von RA unterschieden werden, wobei die odds

für das Vorliegen der Diagnose „RA“ an allen MCP-Gelenken gering ((OR von 0,06, $p < 0,01$) und somit die odds für Diagnose „PsA“ im Umkehrschluss hoch waren. Ein Vorhersagemodell, das auf den Merkmalen basierte, die am stärksten mit dem Vorhandensein von RA oder PsA assoziiert waren, zeigte eine ausgezeichnete Differenzierungsfähigkeit beider Entitäten mit einer Fläche unter der Kurve (*area under the curve*) von 98,1 %.

Die hochauflösende MRT hilft bei der Identifizierung relevanter Bildgebungsmerkmale, die die klinische Differenzierung von entzündlichen Gelenkerkrankungen unterstützen können. Auf MCP-Ebene waren extrakapsuläre entzündliche Veränderungen stark mit PsA assoziiert und können daher zur bildgebenden Differenzierung von PsA und RA beitragen.

4. Arbeit: Abrar DB, Schleich C, Tsiami S, Müller-Lutz A, Radke KL, Holthausen N, Frenken M, Boschheidgen M, Antoch G, Mucke J, Sewerin P, Braun J, Nebelung S, Baraliakos X. Functional MR imaging beyond structure and inflammation-radiographic axial spondyloarthritis is associated with proteoglycan depletion of the lumbar spine. Arthritis Res Ther. 2020 Sep 17;22(1):219.

Die r-axSpA ist der bekannteste Vertreter der axialen Spondyloarthropathien [124]. Sie führt zu Rückenschmerz, Bewegungseinschränkung und letztlich zu schwerwiegendem Funktionsverlust. Im Rahmen der Diagnostik nimmt die MRT einen zunehmend wichtigen Stellenwert ein, was durch den Einschluss in die Assessment of SpondyloArthritis Society (ASAS) Klassifikationskriterien widergespiegelt wird [125, 126]. Typische Veränderungen sind dabei Syndesmophyten, aseptische Spondylodiszitis sowie Spondylitis [127, 128]. Auch Knorpelveränderungen sind in der Literatur beschrieben [129, 130]. Ob und inwieweit lumbale Bandscheiben betroffen sind, ist bislang jedoch nur spärlich untersucht worden [131]. Ziel der Arbeit war es daher den GAG-Gehalt der lumbalen Bandscheiben von Patienten mit r-axSpA und gesunden Probanden zu vergleichen und die Assoziation von GAG-Verlust und krankheitsbezogenen klinischen und bildgebenden Merkmalen zu untersuchen.

Die Lendenwirbelsäule von 50 r-axSpA-Patienten (Durchschnittsalter $50 \pm 10,5$ Jahre) und 30 gleichartigen Probanden wurde mit 3-T-MRT und konventionellen Röntgenaufnahmen untersucht. Das MRT-Protokoll umfasste morphologische Sequenzen und die *gagCEST*-Technik. Die morphologischen Bilder wurden von drei Radiologen auf entzündliche Aktivität,

Fettablagerungen, Bandscheibendegeneration und strukturelle Veränderungen auf konventionellen Röntgenaufnahmen analysiert. Zu den klinischen und serologischen Messwerten gehörten der Bath-AS-Disease-Activity- (BASDAI) und Bath-AS-Function- (BASFI) Index sowie der C-reaktive Protein (CRP)-Serumspiegel. Die *gagCEST*-Werte beider Gruppen wurden mit Hilfe eines gemischten linearen Modells verglichen. Es wurden Kendall-Tau-Korrelationsanalysen durchgeführt.

Die *GagCEST*-Werte waren bei r-axSpA-Patienten signifikant niedriger ($2,0 \pm 1,7\%$) als bei gesunden Probanden ($2,4 \pm 1,8\%$), $p = 0,001$. Geringe, aber signifikante Korrelationen wurden zwischen *gagCEST*-Werten und CRP-Werten ($\tau = - 0,14$, $p = 0,007$), BASFI ($\tau = - 0,18$, $p < 0,001$) und dem Vorhandensein von Syndesmophyten ($\tau = - 0,17$, $p = 0,001$) gefunden. Es wurden keine signifikanten Korrelationen mit den BASDAI-, Entzündungs- und Fettablagerungs-MRI-Scores gefunden.

Lumbale Bandscheiben von r-axSpA-Patienten unterliegen einer signifikanten GAG-Depletion, die unabhängig mit Syndesmophytenbildung, funktioneller Behinderung und erhöhten serologischen Entzündungsmarkern assoziiert ist. Über den Nachweis einer pathophysiologischen Rolle der Bandscheiben bei r-axSpA hinaus deuten diese Ergebnisse darauf hin, dass die *gagCEST*-Bildgebung eine ergänzende bestätigende Rolle bei der Beurteilung krankheitsbezogener pathologischer MRT-Befunde bei r-axSpA haben könnte.

5. Arbeit: Abrar DB, Schleich C, Müller-Lutz A, Frenken M, Radke KL, Vordenbäumen S, Schneider M, Ostendorf B, Sewerin P. Cartilage Degradation in Psoriatic Arthritis Is Associated With Increased Synovial Perfusion as Detected by Magnetic Resonance Imaging. Front Med (Lausanne). 2020 Sep 25;7:539870.

Ähnlich der RA geht auch die PsA mit Knorpelveränderungen peripherer Gelenke einher. In Vorarbeiten konnte gezeigt werden, dass früher Knorpelverlust mit akut-entzündlichen Gelenkveränderungen- gemessen am RAMRIS- assoziiert ist [98]. Für die RA konnten frühere Studien mithilfe kompositioneller MRT des Gelenkknorpels, und der dynamischen kontrastverstärkten MRT (*DCE-MRT*) zeigen, dass frühe Veränderungen des Gelenkknorpels stark mit synovialer Entzündung assoziiert sind [98, 132]. Das Ziel dieser Studie war es festzustellen, ob eine akute Entzündung mit frühem Knorpelverlust in kleinen Fingergelenken von Patienten mit PsA assoziiert ist. MCP-, PIP- und DIP-Gelenke von 17 Patienten mit aktiver PsA wurden mittels hochauflösender 3 T *dGEMRIC* und *DCE MRT* unter Verwendung einer dedizierten 16-Kanal-Handspule untersucht. Es wurden semiquantitative und quantitative Perfusionsparameter berechnet. Die Bilder wurden von zwei unabhängigen Gutachtern auf *dGEMRIC*-Indizes, *PsAMRIS*, Gesamtknorpeldicke und Gelenkspaltweite analysiert. Wir fanden signifikante negative Korrelationen zwischen Perfusionsparametern und *dGEMRIC*-Indizes, mit dem höchsten Wert an den MCP-Gelenken (KTrans: $\tau = -0,54$, $p = 0,01$; Kep: $\tau = -0,02$, $p = 0,90$; IAUC: $\tau = -0,51$, $p = 0,015$; Initial Slope: $\tau = -0,54$, $p = 0,01$; Peak: $\tau = -0,67$, $p = 0,002$). Heterogene Korrelationen wurden zwischen den Perfusionsparametern und dem *PsAMRIS*-Gesamtwert und den *PsAMRIS*-Synovialitis-Sub-Scores festgestellt. Es wurde keine signifikante Korrelation

zwischen Perfusionsparametern und Gelenkspaltweite und/oder Knorpeldicke festgestellt. Wie mittels *DCE-MRT* und *dGEMRIC* untersucht, besteht ein möglicher Zusammenhang zwischen frühem Knorpelverlust und akuter synovialer Entzündung in kleinen Fingergelenken von PsA-Patienten.

6. Arbeit: Abrar DB, Schleich C, Brinks R, Goertz C, Frenken M, Schneider M, Nebelung S, Sewerin P. Introduction of a Simplified Psoriatic Arthritis Magnetic Resonance Imaging Score (sPsAMRIS): A Potential Tool for Treatment Monitoring in Peripheral Psoriatic Arthritis. Diagnostics (Basel). 2020 Dec 15;10(12):E1093.

Zwar sind Erkennung und Therapiekontrolle der PsA weiterhin primär klinisch geprägt, jedoch nimmt die MRT einen zunehmend wichtigeren Stellenwert ein [27, 36, 133]. Dies findet auch in dem 2009 eingeführten *PsAMRIS* Ausdruck, einem semi-quantitativen Summenscore, der verschiedene akut- und chronisch-entzündliche Gelenkveränderungen der Fingergelenke, wie beispielsweise Erosionen, Synovialitis und Osteoödem, nach ihrer Ausprägung evaluiert und zusammenfasst [36]. Zwar ist der *PsAMRIS* sehr sensitiv für typische erkrankungsassoziierte Gelenkveränderungen, jedoch ist er sehr umfangreich und daher zeitaufwändig in seiner Erhebung. Daher war das Ziel dieser Studie, zu untersuchen, ob eine vereinfachte (*simplified, s*) Version des *PsAMRIS*, der sogenannte *sPsAMRIS*, ein potenzielles Werkzeug für die Therapieüberwachung bei PsA ist.

Die klinisch dominante Hand von 17 Patienten mit aktiver PsA wurde mittels 3 T MRT zu Studienbeginn und nach 6 Monaten untersucht. Die Auswertung erfolgte durch zwei muskuloskelettale Radiologen nach Vorgaben des *PsAMRIS* und des *sPsAMRIS*, einer vereinfachten Version, die auf der vorherigen Auswertung der Veränderungsempfindlichkeit durch standardisierte Antwortmittel (*standardized response means, SRMs*) basiert. Beide Scores wurden durch Berechnung der

SRMs des Gesamt- und jedes Sub-Scores und der relativen Wirksamkeit (*relative efficacy, RE*) nach Bootstrapping verglichen.

Die *PsAMRIS*-Sub-Scores der MCP-Gelenke D3 und 4 sowie des PIP-Gelenkes D4 wiesen die höchsten *SRM* (jeweils -0,07) auf, was auf die höchste Sensitivität für Veränderungen hinweist, und wurden daher in den *sPsAMRIS* aufgenommen. Im Vergleich zu *PsAMRIS* zeichnete sich der *sPsAMRIS* durch höhere *SRMs* (*sPsAMRIS*: -0,13 vs. *PsAMRIS*: -0,02) und eine höhere *RE* (29,46) aus. *sPsAMRIS* und *PsAMRIS* wiesen bei Studienbeginn ($r = 0,75$, $p < 0,01$ (Pearson's correlation)) und bei der 6-monatigen Verlaufskontrolle ($r = 0,64$, $p = 0,01$) eine hohe Korrelation auf. Der mittlere Zeitaufwand für die Erhebung des Scores pro MRT-Untersuchung war bei Verwendung des *sPsAMRIS* ($140,1 \pm 21,25$ s) im Vergleich zum regulären *PsAMRIS* ($469 \pm 87,03$ s) signifikant reduziert ($p < 0,001$). Aufgrund der ähnlichen Ansprechbarkeit auf Veränderungen im Vergleich zum Standard-*PSAMRIS* und der Zeiteffizienz könnte der *sPsAMRIS* ein potenzielles diagnostisches Werkzeug zur semiquantitativen Beurteilung und Überwachung der Therapie bei PsA sein.

7. Arbeit: Abrar DB, Schleich C, Frenken M, Vordenbäumen S, Richter J, Schneider M, Ostendorf B, Nebelung S, Sewerin P. *dGEMRIC* in the Assessment of Pre-Morphological Cartilage Degeneration in Rheumatic Disease: Rheumatoid Arthritis vs. Psoriatic Arthritis. *Diagnostics* (Basel). 2021 Jan 20;11(2):E147.

Die Schädigung des Gelenkknorpels ist ein bekanntes Merkmal der RA. Studien der letzten zwei Jahrzehnte haben die Bedeutung von Knorpelschädigung in der Pathogenese und im Krankheitsverlauf der RA intensiv untersucht [134–136]. Obwohl Knorpelverlust auch ein bekanntes Merkmal der PsA ist, ist die Studienlage im Vergleich zur RA spärlich und seine Rolle in der Pathogenese, für die Krankheitsüberwachung und für die Differenzierung von der RA weitgehend unklar [137]. Mittels *dGEMRIC* untersuchten wir daher MCP- und PIP-Gelenke bei PsA-Patienten und verglichen diese mit RA-Patienten, um Hinweise für die Knorpelbeteiligung im Krankheitsverlauf der PsA zu erlangen.

Insgesamt 17 Patienten mit aktiver PsA und 20 Patienten mit aktiver RA wurden mittels hochauflösender 3 T *dGEMRIC* und einer speziellen 16-Kanal-Handspule untersucht. Die Bilder wurden von zwei unabhängigen Radiologen hinsichtlich der *dGEMRIC*-Indizes und der Gelenkspaltweite auf MCP- und PIP-Gelenkebene analysiert.

Es konnten keine signifikanten Unterschiede der *dGEMRIC*-Werte zwischen beiden Studienpopulationen gefunden werden (PsA 472,25 ms, RA 461,11 ms; $p = 0,763$). Bei allen RA- und den meisten PsA-Patienten zeigten die PIP-Gelenke signifikant niedrigere *dGEMRIC*-Indizes als die MCP-Gelenke (RA: D2: $p = 0,009$, D3: $p = 0,008$, D4: $p = 0,002$, D5: $p = 0,002$; PsA: D3: $p = 0,001$, D4: $p = 0,004$).

Die Gelenkspaltweite war in den meisten Gelenke ähnlich und es wurden keine signifikanten Unterschiede gefunden.

Die molekulare Zusammensetzung des MCP- und PIP-Gelenkknorpels von PsA-Patienten ist ähnlich wie die von RA-Patienten, was die wissenschaftliche und klinische Machbarkeit der kompositionellen MRT bei diesen Krankheitsentitäten zeigt. Muster und Schweregrad der ultrastrukturellen Knorpeldegradation der Fingergelenke können daher bei PsA- und RA-Patienten über die reine Morphologie hinaus beurteilt werden.

8. Arbeit: Frenken M, Nebelung S, Schleich C, Müller-Lutz A, Radke KL, Kamp B, Boschheidgen M, Wollschläger L, Bittersohl B, Antoch G, Konieczny MR, Abrar DB. Non-Specific Low Back Pain and Lumbar Radiculopathy: Comparison of Morphologic and Compositional MRI as Assessed by gagCEST Imaging at 3T. *Diagnostics*. 2021; 11(3):402.

Rückenschmerz ist eine Volkskrankheit, die eine große sozioökonomische und auch individuelle Belastung darstellt [138]. Die meisten Fälle lassen sich als unspezifische Lumbago definieren, dem keine eindeutige strukturelle Ursache, wie beispielsweise eine Fraktur oder ein Bandscheibenvorfall, zugrunde liegt [139]. Ein Faktor, der potentiell zu unspezifischer Lumbago beiträgt, ist die lumbale *DDD* [140]. Die MRT ist eine sehr sensitive Methode Bandscheibendegeneration zu detektieren. Unter Verwendung von *gagCEST*- wurde in dieser Studie der GAG-Gehalt lumbaler Bandscheiben von Patienten mit unspezifischer Lumbago, Radikulopathie und asymptomatischen Probanden vergleichend untersucht, um die Assoziation von klinischer Manifestation und GAG-Gehalt zu klären. Insgesamt 18 Patienten (Durchschnittsalter 57,5 ±22,5 Jahre) mit Radikulopathie, 16 altersgleiche Patienten mit chronischer unspezifischer Lumbago und 20 altersgleiche wurden mittels morphologischer und kompositioneller MRT mit einem 3 T Scanner untersucht. In allen Kohorten wurde der GAG-Gehalt der lumbalen *IVDs* mittels *gagCEST*-MRT bestimmt. Eine Bewertung der morphologischen Bandscheibendegeneration auf Basis der Pfirrmann-Klassifikation und T2-w Sequenzen diente als Referenz [87]. Für die statistische Auswertung wurde ein lineares gemischtes Modell verwendet, das für multiple Faktoren adjustiert wurde. *IVDs* von Patienten mit Lumbago zeigten niedrigere *gagCEST*-Werte als die von

Probanden (Lumbago: 1,3% [99% Konfidenzintervall (CI): 1,0; 1,6] vs. Probanden: 1,9 % [99 % KI: 1,6; 2,2]). Die *IVDs* von Patienten mit Radikulopathie (1,8 % [99 % KI: 1,4; 2,1]) unterschieden sich jedoch nicht von Patienten mit Lumbago oder Probanden. Bei Patienten mit Radikulopathie zeigten *IVDs*, die direkt an Bewegungssegmente mit Bandscheibenvorfällen angrenzten, niedrigere *gagCEST*-Werte als davon weiter entfernte *IVDs* (angrenzend: 0,9% [99% CI: 0,3; 1,5], entfernt: 2,1% [99% CI: 1,7; 2,5]). Die fortgeschrittene GAG-Depletion bei Lumbago und in *IVDs*, die direkt an Bandscheibenvorfälle angrenzen, deutet auf einen engen Zusammenhang von klinischer Pathologie und kompositioneller Degeneration hin.

9. Arbeit: Wollschläger LM, Nebelung S, Schleich C, Müller-Lutz A, Radke KL, Frenken M, Boschheidgen M, Prost M, Antoch G, Konieczny MR, Abrar DB. Evaluating Lumbar Intervertebral Disc Degeneration on a Compositional Level Using Chemical Exchange Saturation Transfer: Preliminary Results in Patients with Adolescent Idiopathic Scoliosis. *Diagnostics (Basel)*. 2021 May 22;11(6):934. doi: 10.3390/diagnostics11060934.

Die *AIS* ist die häufigste Form der idiopathischen Skoliose [48]. Sie ist typischerweise mit Rückenschmerzen und Bewegungseinschränkung assoziiert. Bei der *AIS* kommt es durch die veränderte Biomechanik und ungleichmäßige Lastverteilung zu einer vorzeitigen Degeneration der *IVDs*, die wiederum mit Rückenschmerzen vergesellschaftet ist [141]. Die Degeneration der lumbalen *IVDs* ist durch strukturelle und kompositionelle Veränderungen gekennzeichnet, wobei letztere nicht durch morphologische Standard-Sequenzen, sondern lediglich durch moderne, biochemisch-sensitive Verfahren, wie beispielsweise *gagCEST*, untersucht werden können [142]. In dieser Studie wurde der GAG-Gehalt der *IVDs* von Patienten mit *AIS* und gesunden Kontrollpersonen mit Hilfe der *gagCEST* Bildgebung untersucht. Zehn *AIS*-Patienten (Durchschnittsalter $18,3 \pm 8,2$ Jahre) und 16 gesunde Probanden (Durchschnittsalter $25,5 \pm 1,7$ Jahre) wurden einbezogen. Klinisch- morphologische Standard-MRT-Bilder (T1w-, T2w- und STIR-Sequenzen) zum Ausschluss weiterer Wirbelsäulenerkrankungen und zur Beurteilung der *IVD*-Degeneration anhand des Pfirrmann-Scores sowie kompositionelle *gagCEST*-Sequenzen wurden mit einem 3 T-MRT aufgenommen. Bei *AIS*-Patienten wurde die am weitesten distal gelegene skoliotische Krümmung anhand von konventionellen Röntgenaufnahmen der gesamten Wirbelsäule und

morphologischen MRTs bestimmt. Die *IVDs* wurden danach eingeteilt, ob sie von der skoliotischen Deformität betroffen waren, d. h. proximal (betroffen, *affected, aIVDs*) oder distal (nicht betroffen, *unaffected uaIVDs*) zum Neutralwirbel der am weitesten distal gelegenen skoliotischen Krümmung. Zum Vergleich der mittleren *gagCEST*-Werte wurden lineare gemischte Modelle verwendet. Über alle Segmente hinweg wiesen die *IVDs* der *AIS*-Patienten signifikant niedrigere *gagCEST*-Werte auf als die der Probanden: 2,76 [2,32, 3,20]% (*AIS*), 3,51 [3,16, 3,86]% (Probanden); $p = 0,005$. Bei den *gagCEST*-Werten wurden keine signifikanten Unterschiede zwischen *aIVDs* und *uaIVDs* festgestellt. Zusammenfassend kann die *gagCEST*-Bildgebung als effektives diagnostisches Hilfsmittel prospektiv eingesetzt werden, um frühe degenerative Veränderungen bei Patienten mit *AIS* zu erkennen.

10. Arbeit: Frenken M, Schleich C, Radke KL, Müller-Lutz A, Benedikter C, Franz A, Antoch G, Bittersohl B, Abrar DB, Nebelung S (shared last authorship). Imaging of exercise-induced spinal remodeling in elite rowers. *J Sci Med Sport*. 2021 Aug 8:S1440-2440(21)00195-X. doi: 10.1016/j.jsams.2021.07.015.

Rudern geht mit einer erhöhten Belastung für lumbale *IVDs* einher. Daher führt Rudern als Leistungssport zu einer vorzeitigen Bandscheibendegeneration und zu Bandscheibenvorfällen [143]. Im Verlauf der Bandscheibendegeneration ist der Verlust von Proteoglykanen ein Frühzeichen [144, 145]. Dieser Proteoglykanverlust kann mittels morphologischer Standard-MRT nicht detektiert werden [146]. Allerdings sind mittlerweile neuer, kompositionelle Verfahren, wie die *gagCEST*-Bildgebung, verfügbar, die eine kompositionelle Analyse von Bandscheiben und die Erkennung frühen Proteoglykanverlustes ermöglichen [147, 148]. Da das Wissen über den trainingsinduzierten lumbaler *IVDs* in-vivo gering ist, wurde in dieser Studie mittels kompositioneller MRT untersucht, wie sich die lumbalen *IVDs* in Abhängigkeit von langfristigem Training bei Spitzensportlern und altersgleichen Kontrollpersonen verändern.

Prospektiv wurden die Lendenwirbelsäulen von 17 Elite-Ruderern (ERs) der deutschen Ruder-Nationalmannschaft (Durchschnittsalter: 23,9 ± 3,3 Jahre) in einem klinischen 3 T-MRT untersucht. Die Untersuchungen wurden zweimal während des jährlichen Trainingszyklus durchgeführt, d.h. während der trainingsintensiven Saisonvorbereitung (t0) und 6 Monate später während der Erholung nach dem Wettkampf (t1). Die Kontrollpersonen (n = 22, Durchschnittsalter: 26,3 ± 1,9 Jahre) wurden einmal zu den entsprechenden Zeitpunkten untersucht (t0: n = 11; t1: n = 11). Der GAG-Gehalt lumbaler *IVDs* (n

= 195) wurde segmentweise mittels *gagCEST* bestimmt. Um den Einfluss der Kohorte und anderer Variablen auf den GAG-Gehalt zu bewerten, wurden lineare gemischte Modelle erstellt.

Während der Vorsaison waren die *IVD*-GAG-Werte der ERs signifikant höher als die der Kontrollen (ERs (t0): $2,58 \pm 0,27$ % (Mittelwert \pm Standardabweichung); Kontrollen(t0): $1,43 \pm 0,36$ %; $p \leq 0,001$), während der Erholung nach dem Wettkampf waren diese Unterschiede nicht mehr vorhanden (ERs(t1): $2,11 \pm 0,18$ %; Kontrollen(t1): $1,89 \pm 0,24$ %; $p = 0,362$).

Professionelles Rudern auf Spitzenniveau ist vorübergehend mit signifikant höheren *gagCEST*-Werten assoziiert, was auf einen erhöhten lumbalen *IVD*-GAG-Gehalt und starke Remodellierungseffekte als Reaktion auf das Training hinweist. Über das professionelle Rudern hinaus kann ein Ganzkörpertraining zur Stärkung der Körpermitte dazu beitragen, die Widerstandsfähigkeit der Lendenwirbelsäule als potenzielles therapeutisches Ziel bei der Behandlung von Rückenschmerzen zu verbessern.

III. Diskussion

Die dieser Habilitationsschrift zugrundeliegenden Arbeiten zeigen den Stellenwert und potentiellen Nutzen hochaufgelöster Standard- sowie kompositioneller, biochemisch-sensitiver MRT Sequenzen im Rahmen degenerativer (OA und DDD) und entzündlicher (PsA, r-axSpA und RA) Gelenkerkrankungen an Hand- und Fingergelenken, Sprunggelenk und der Lendenwirbelsäule auf.

Mittels hochaufgelöster 3 T MRT und einer dezidierten Handspule konnten wir in Patienten mit PsA, RA und einer gesunden Kontrollgruppe die A1- und A2-Ringbänder darstellen. Interessanterweise bilden Sehnen und Ringbänder funktionelle Entesen, wobei die Ringbänder mit einer fibrocartilaginären Komponente die Beugesehnen diskontinuierlich umgeben und ihr Abheben bei Flexion verhindern [149]. Da die PsA im Gegensatz zur RA einer primär enthesale Erkrankung ist, konnten wir ausgeprägtere entzündliche Veränderungen der zudem dickeren Ringbänder bei PsA- im Gegensatz zu RA-Patienten aufzeigen. Auch im Vergleich zur gesunden Vergleichsgruppe zeigten sich signifikante Unterschiede hinsichtlich entzündlicher Veränderungen und Ringbanddicke. Somit bestätigen unsere Ergebnisse erste Daten anderer Arbeitsgruppen, die bei der PsA ein „tiefes Koebnerphänomen“, also eine enthesale Entzündung durch mechanische Reizung vermutet haben und ähnliche Veränderungen an der Ringbändern in MRT und Sonografie nachweisen konnten [27, 110, 112]. Diese Ergebnisse tragen somit sowohl zum besseren Verständnis der Pathogenese der PsA als auch zur Differenzierung von der RA bei. Die Unterscheidung von RA und PsA ist zwar in der Regel klinisch und laborchemisch möglich, da sich das Verteilungsmuster der peripheren Arthritis zwischen beiden Entitäten divergiert und die PsA eine seronegative Arthritis ist, allerdings bleibt die Unterscheidung

zwischen seronegativer RA und einer PsA mit symmetrischem Befallsmuster eine Herausforderung. [65, 122, 150–153]. Aufgrund der inzwischen teils unterschiedlichen Therapieregime mit bDMARDs und tsDMARDs ist eine Differenzierung der Entitäten jedoch von großer Relevanz. In einer der vorliegenden Arbeiten strebten wir daher den systematischen Vergleich typischer erkrankungsassoziierter Gelenkveränderungen an, indem wir die Dimensionen des PsAMRIS für Patienten mit RA und PsA anwendeten. Dabei zeigte sich, dass die PsA häufiger mit einer periartikulären Inflammation einhergeht, also der extrakapsulären Entzündung der periartikulären Weichteile, und somit mit hoher diagnostischer Sicherheit von der RA differenziert werden kann. Einschränkend ist zu berücksichtigen, dass die beiden verglichenen Kollektive klein und die Ergebnisse nur als Indiz und möglicher Ausgangspunkt für Untersuchungen in größeren Kollektiven dienen können. Unter Berücksichtigung der Pathophysiologie beider Erkrankungen sind die Ergebnisse jedoch nicht überraschend, denn die Dactylitis ist bei den entheseal vermittelten PsA ein Charakteristikum [154]. Auch andere Arbeitsgruppen fanden ähnliche Ergebnisse in MRT-Studien [67, 155]. Für die RA konnte bereits in zahlreichen Studien gezeigt werden, dass Knorpelveränderungen mittels *dGEMRIC* detektiert werden können, diese mit bestimmten erkrankungsassozierten Gelenkveränderungen und dynamischer Gelenk-MRT korrelieren und sie als Verlaufsparemeter geeignet sind [96–98, 156]. Zwar ist für die PsA eine Beteiligung des Gelenkknorpels ebenfalls bekannt, allerdings sind Studien dazu spärlich [137]. Da Knorpelzustand und Gelenkfunktionalität eng miteinander verknüpft sind, haben wir den Gelenkknorpel der kleinen Fingergelenke bei Patienten mit PsA mittels *dGEMRIC* untersucht und mit RA Patienten und dynamischer MRT Gelenke, sog. MR-Perfusion, verglichen.

So konnten wir zeigen, dass sich die *dGEMRIC*-Werte beider Kollektive nicht signifikant unterschieden und daher eine Knorpelbeteiligung bei der PsA zu beobachten ist und sich diese mittels *dGEMRIC*-Bildgebung darstellen lässt. In der RA ist bislang nicht abschließend geklärt, ob Knorpelschaden Folge oder Begleitphänomen synovialer und artikulärer Entzündung ist. Es wurde lediglich eine Korrelation zwischen Knorpelschaden und Entzündung beschrieben [62, 64, 132, 156]. Diese Ergebnisse werden durch unsere Arbeit zum Vergleich von synovialer Entzündung und Knorpelschaden gemessen anhand MR-Perfusion und *dGEMRIC* bestätigt, denn wir konnten eine Assoziation zwischen niedrigen *dGEMRIC*-Werten und erhöhten Perfusionsparametern nachweisen. Somit ergibt sich auch für die PsA der Hinweis, dass eine Verknüpfung von synovialer Entzündung und Knorpelveränderungen existiert.

Nicht zuletzt aufgrund der 2017 durch die europäische Arzneimittelagentur erlassenen Restriktionen hinsichtlich der Verwendung GD-haltiger Kontrastmittel aufgrund möglicher Ablagerungen im Gehirn nehmen kompositionelle MRT Verfahren an Bedeutung zu, die keiner intravenösen Kontrastmittelgabe bedürfen. Eine dieser Methoden ist die *gagCEST*-Methode. Diese wurde initial für 7 T Systeme entwickelt, ist jedoch mittlerweile auch bei 3 T anwendbar. Die meisten *gagCEST* Studien existieren für Bandscheibenveränderungen, da der GAG-Gehalt des NP im Vergleich zum teils sehr dünnen Gelenkknorpel peripherer Gelenke sehr hoch ist. In den hier präsentierten Arbeiten konnten wir *gagCEST* erfolgreich an den LWS von Patienten mit *A/S*, Lumbago, Radikulopathie und mit *r-axSpA* sowie von Leistungssportlern anwenden.

Dabei fanden wir in einem kleinen Kollektiv von *A/S*-Patienten niedrigere GAG-Werte in lumbalen, morphologisch nicht-degenerierten *IVDs* als in denen einer

gesunden, signifikant älteren Vergleichsgruppe. Dies legt nahe, dass die veränderte Biomechanik im Rahmen der skoliotischen Fehlhaltung bereits früh zu ultrastrukturellen Veränderungen der *IVDs* führt. Dies könnte aus zwei Gründen von Bedeutung sein. Zum einen könnte der frühere Nachweis degenerativer Veränderungen Änderungen der Therapieplanung nach sich ziehen, da eine vermehrte Degeneration zu einer zunehmend veränderten Biomechanik führt. Effektive konservative Maßnahmen sind jedoch insbesondere im Wachstum möglich, sodass eine frühe Therapie zu vorteilhaft ist. Zum anderen könnte der Nachweis früher degenerativer Veränderungen sich auf eine mögliche operative Therapie auswirken, denn ist Gegenstand intensiver Forschung wieviele Segmente eine spinale Fusion umfassen sollte, um das Risiko einer Anschlussdegeneration möglichst gering zu halten [157, 158]. Sind bestimmte *IVDs* aber bereits präoperativ ultrastrukturell verändert, könnte hier ein anderes Vorgehen indiziert sein. Dies bleibt jedoch zum gegenwärtigen Zeitpunkt spekulativ und könnte Ausgangspunkt zukünftiger Studien sein. Patienten mit Lumbago weisen im Vergleich zu Patienten mit Radikulopathie und einer gesunden Vergleichsgruppe niedrigere *gagCEST* Werte in morphologisch nicht-degenerierten *IVDs* auf. Vergleich man bei Patienten mit Radikulopathie jene *IVDs*, die unmittelbar an einen Bandscheibenprolaps grenzen, so sind hier niedrigere *gagCEST* Werte nachweisbar als in *IVDs* die weiter entfernt liegen. Zudem ist der GAG-Gehalt dieser Bandscheiben geringer als der der Vergleichsgruppe. Es bleibt unklar, ob dieser niedrigere GAG-Gehalt in den angrenzenden *IVDs* Folge einer durch den Bandscheibenvorfall veränderten Biomechanik oder lediglich Folge der selben biomechanischen Belastung ist, die zum besagten Prolaps geführt hat. Die Tatsache, dass die GAG-Werte der Radikulopatienten insgesamt denen der

Vergleichsgruppen glichen, spricht eher für die erste These. Auch eine Studie von Masui et al. deutet in diese Richtung; hier wurden Patienten mit Bandscheibenvorfall über sieben Jahre mittels MRT nachuntersucht. Es konnten zunehmende degenerative *IVD*-Veränderungen nachgewiesen werden, wobei in der Baselineuntersuchung noch keine *IVD*-Degeneration erkennbar war [159]. Sollte sich dieser Zusammenhang in Folgestudien bestätigen, könnte man mittels kompositioneller Bildgebung *IVD* identifizieren, die in der Folge eines Bandscheibenvorfalls besonders gefährdet sind vorzeitig zu degenerieren.

In 50 Patienten mit r-axSpA konnte gezeigt werden, dass ihre *IVDs* einen geringeren GAG-Gehalt aufweisen als die einer gesunden Vergleichsgruppe. Vorherige Studien demonstrierten bereits, dass hyaliner Gelenknorpel im Rahmen der r-axSpA betroffen ist und Knorpelschäden eine relevante Rolle in der Pathogenese der Erkrankung spielen [130, 160–165]. Dabei ist insbesondere der abschlussplattennahe Knorpel betroffen, der unmittelbar den *IVDs* anliegt. Hier wird zudem diskutiert, ob Knorpelschäden der Bildung von Syndesmophyten vorausgehen [166]. In dem eng zusammenhängenden Gefüge eines Bewegungssegmentes der Wirbelsäule könnte die Detektion sehr früher *IVD*-Veränderungen daher von Bedeutung für Pathophysiologie, aber auch Therapiekontrolle sein. Zudem konnten wir zeigen, dass GAG-Verlust mit dem Vorliegen von Syndesmophyten und funktionellen Einschränkungen der r-axSpA Patienten korreliert, jedoch nicht mit dem Vorliegen akut- oder chronisch entzündlicher Knochenmarkveränderungen der Wirbelkörper. Niedrige GAG-Werte bei r-axSpA Patienten sind möglicherweise der Pathogenese, können jedoch auch Ausdruck verminderter körperlicher Aktivität sein, denn aus einer Arbeit von Roos et al. ist bekannt, dass körperliche Aktivität zu einem erhöhten

GAG-Gehalt im Gelenkknorpel führt [167]. Diese Beobachtungen werden auch durch die zehnte vorliegende Arbeit untermauert, in der wir 17 Elite-Ruderer der deutschen Nationalmannschaft während ihres jährlichen Trainingszyklus prospektiv untersucht haben. Dabei konnten wir während des Belastungsmaximums in der Wettkampfvorbereitung höhere GAG-Werte in ihren lumbalen *IVDs* detektieren als in der Erholungsphase nach der Wettkampfsaison und im Vergleich zu einer altersgleichen Kontrollgruppe. In der Erholungsphase glichen die GAG-Werte denen der Kontrollgruppe. Diese Ergebnisse legen anabole Anpassungsreaktionen von *IVDs* auf körperliche Belastung nahe. Weshalb Spitzensportler dennoch ein höheres Risiko für die Entwicklung von Bandscheibenvorfällen haben, obwohl sie durch das „GAG-Remodeling“ an die höhere Belastung angepasst sein müssten, bleibt unklar [168]. Eine mögliche Erklärung ist das sog. „anabole Belastungsfenster“ [169, 170]. Dieses besagt, dass optimale Anpassungen von *IVDs* nur in einem bestimmten Belastungsumfang möglich sind. Belastungen außerhalb dieses spezifischen Bereiches setzen keine anabolen Anpassungsreaktionen in Gang, sondern können mechanisch bedingt zu strukturellen Schäden führen.

Zwar ist die *gagCEST* Methode an Bandscheiben besonders etabliert und robust, allerdings konnten wir in der zweiten Arbeit dieser Habilitationsschrift erstmalig ein *gagCEST* Protokoll für die Untersuchung des tibiotalaren Gelenkknorpels bei 3 T etablieren. Die Schwierigkeit besteht in der nur sehr geringen Dicke des Knorpels und der damit verbundenen schlechten Ortsauflösung bei 3 T. Zunächst wurde in Experimenten mittels Bloch-McConnell-Simulationen ein optimales *gagCEST* Protokoll etabliert. Dieses wurde dann in einer gesunden Kohorte im Vergleich zu Patienten mit osteochondralen Läsionen des Talus in seiner klinischen

Anwendbarkeit getestet. Dabei konnten robuste und reproduzierbare Ergebnisse erhoben werden. Zudem fanden wir in der Patientgruppe niedrige GAG-Werte als in der gesunden Kontrollgruppe. Da Patienten mit osteochondralen Läsionen für die Entwicklung einer sekundären OA gefährdet sind, ist die *gagCEST*-Bildgebung hier von potentiell Interesse, um zunehmende Knorpelveränderungen im Verlauf zu erkennen und ggf. zu behandeln, bevor diese zu einer manifesten OA führen.

Zusammenfassend zeigen die dieser Habilitationsschrift zugrundeliegenden Arbeiten die breite Anwendungsmöglichkeit multimodaler MRT Bildgebung für die Erkennung, Beurteilung und Verlaufskontrolle entzündlicher und degenerativer Gelenkerkrankungen. Zudem können insbesondere kompositionelle MRT Verfahren zum besseren Verständnis der Pathophysiologie beitragen und sind zukünftig eine mögliche Option zur Früherkennung bestimmter Erkrankungen, da sie beispielsweise Knorpelveränderungen aufzeigen können, bevor diese strukturell-morphologisch erkennbar sind.

D. Ausblick

Die in dieser Habilitationsschrift genutzten multimodalen MRT-Verfahren haben breite Anwendungsmöglichkeiten in der Diagnostik und Therapiekontrolle muskuloskelettaler Erkrankungen, insbesondere bei entzündlichen und degenerativen Gelenkerkrankungen.

Die hochauflösende MRT findet bereits breite Anwendung in der klinischen Routine, sodass schon heute eine detaillierte Betrachtung von kleinsten Strukturen möglich ist. Durch die Weiterentwicklung dezidierter Spulensysteme und MRT-Parameter werden diese hochauflösenden MRT Sequenzen in der Zukunft noch schneller und robuster werden. Damit wird die MRT Mittel der ersten Wahl für die Darstellung kleiner Gelenke an Extremitäten, aber auch an der Wirbelsäule und dem kraniozervikalen Übergang sein.

Kompositionelle MRT Verfahren von Gelenkknorpel und Bandscheibe sind in der Wissenschaft etablierte Verfahren, haben jedoch bislang nicht den Sprung in die routinemäßige klinische Anwendung geschafft. Betrachtet man jedoch den großen sozioökonomischen Einfluss von entzündlichen und degenerativen Gelenkerkrankungen und die bisher häufig fehlenden kausalen Therapieansätze, so erscheinen MRT Verfahren, die eine Früherkennung in noch reversiblen Erkrankungsstadien ermöglichen, als sehr nützlich und von großem Interesse. GAG-spezifische MRT Verfahren können GAG-Verlust aufzeigen bevor es zu strukturell manifesten Knorpel-/Bandscheibenschäden gekommen ist. Somit lässt sich potentiell gefährdetes Gewebe erkennen und präventive Therapiemaßnahmen können möglicherweise irreversible Schäden verhindern. Insbesondere die gagCEST-Bildgebung erscheint dabei zukunftssträchtig, da sie keiner Kontrastmittelgabe bedarf und somit keine Gefahr für

Gadoliniumablagerungen im Körper der Patienten besteht. Neben den in dieser Habilitationsschrift aufgezeigten Verfahren finden in unserer Arbeitsgruppe weitere kompositionelle Verfahren, wie Natriumbildgebung und T1rho-Bildgebung sowie T2 Mapping Verfahren Anwendung.

E. Literaturverzeichnis

- 1 Malik KM, Beckerly R, Imani F. Musculoskeletal Disorders a Universal Source of Pain and Disability Misunderstood and Mismatched: A Critical Analysis Based on the U.S. Model of Care. *Anesth Pain Med* 2018;8(6).
- 2 Yelin E, Weinstein S, King T. An update on the burden of musculoskeletal diseases in the U.S. *Semin Arthritis Rheum* 2019;49(1):1–2.
- 3 Yelin E, Weinstein S, King T. The burden of musculoskeletal diseases in the United States. *Semin Arthritis Rheum* 2016;46(3):259–60.
- 4 Weinstein SL. The Burden of Musculoskeletal Conditions. *J Bone Joint Surg Am* 2016;98(16):1331.
- 5 Heidari B. Rheumatoid Arthritis: Early diagnosis and treatment outcomes. *Caspian J Intern Med* 2011;2(1):161–70.
- 6 Coates LC, Helliwell PS. Treating to target in psoriatic arthritis: how to implement in clinical practice. *Ann Rheum Dis* 2016;75(4):640–43.
- 7 Coates LC. Treating to target in psoriatic arthritis. *Curr Opin Rheumatol* 2015;27(2):107–10.
- 8 Singh JA, Guyatt G, Ogdie A, et al. Special Article: 2018 American College of Rheumatology/National Psoriasis Foundation Guideline for the Treatment of Psoriatic Arthritis. *Arthritis Care Res (Hoboken)* 2019;71(1):2–29.
- 9 Coates LC, Lubrano E, Perrotta FM, et al. What Should Be the Primary Target of "Treat to Target" in Psoriatic Arthritis? *J Rheumatol* 2019;46(1):38–42.
- 10 Møller-Bisgaard S, Hørslev-Petersen K, Ejbjerg B, et al. Effect of Magnetic Resonance Imaging vs Conventional Treat-to-Target Strategies on Disease

Activity Remission and Radiographic Progression in Rheumatoid Arthritis: The IMAGINE-RA Randomized Clinical Trial. *JAMA* 2019;321(5):461–72.

11 van Vollenhoven R. Treat-to-target in rheumatoid arthritis - are we there yet? *Nat Rev Rheumatol* 2019;15(3):180–86.

12 Taljanovic MS, Hunter TB, Fitzpatrick KA, et al. Musculoskeletal magnetic resonance imaging: importance of radiography. *Skeletal Radiol* 2003;32(7):403–11. doi:10.1007/s00256-003-0648-7 [published Online First: 3 June 2003].

13 Ahn JM, El-Khoury GY. Role of magnetic resonance imaging in musculoskeletal trauma. *Top Magn Reson Imaging* 2007;18(3):155–68.

14 Oostveen JC, van de Laar MA. Magnetic resonance imaging in rheumatic disorders of the spine and sacroiliac joints. *Semin Arthritis Rheum* 2000;30(1):52–69.

15 Grigoryan M, Roemer FW, Mohr A, et al. Imaging in spondyloarthropathies. *Curr Rheumatol Rep* 2004;6(2):102–09.

16 Hayashi D, Guermazi A, Crema MD, et al. Imaging in osteoarthritis: what have we learned and where are we going? *Minerva Med* 2011;102(1):15–32.

17 Boesen M, Kubassova O, Bouert R, et al. Correlation between computer-aided dynamic gadolinium-enhanced MRI assessment of inflammation and semi-quantitative synovitis and bone marrow oedema scores of the wrist in patients with rheumatoid arthritis--a cohort study. *Rheumatology (Oxford)* 2012;51(1):134–43.

18 Østergaard M, Boesen M. Imaging in rheumatoid arthritis: the role of magnetic resonance imaging and computed tomography. *Radiol Med* 2019;124(11):1128–41. doi:10.1007/s11547-019-01014-y [published Online First: 18 March 2019].

- 19 Chung M, Dahabreh IJ, Hadar N, et al. Emerging MRI Technologies for Imaging Musculoskeletal Disorders Under Loading Stress. Rockville (MD) 2011.
- 20 Munk PL, Vellet AD, Romano C, et al. The emerging role of magnetic resonance imaging in rheumatology. *Can Assoc Radiol J* 1994;45(4):270–76.
- 21 Dean Deyle G. The role of MRI in musculoskeletal practice: a clinical perspective. *J Man Manip Ther* 2011;19(3):152–61.
- 22 Del Grande F, Guggenberger R, Fritz J. Rapid Musculoskeletal MRI in 2021: Value and Optimized Use of Widely Accessible Techniques. *AJR Am J Roentgenol* 2021;216(3):704–17. doi:10.2214/AJR.20.22901 [published Online First: 3 February 2021].
- 23 Meier R, Kraus TM, Schaeffeler C, et al. Bone marrow oedema on MR imaging indicates ARCO stage 3 disease in patients with AVN of the femoral head. *Eur Radiol* 2014;24(9):2271–78. doi:10.1007/s00330-014-3216-8 [published Online First: 28 May 2014].
- 24 Waldt S, Gersing A, Brügel M. Measurements and classifications in spine imaging. *Semin Musculoskelet Radiol* 2014;18(3):219–27. doi:10.1055/s-0034-1375565 [published Online First: 4 June 2014].
- 25 Baumert B, Wörtler K, Steffinger D, et al. Assessment of the internal craniocervical ligaments with a new magnetic resonance imaging sequence: three-dimensional turbo spin echo with variable flip-angle distribution (SPACE). *Magn Reson Imaging* 2009;27(7):954–60. doi:10.1016/j.mri.2009.01.012 [published Online First: 17 March 2009].
- 26 Wörtler K, Schaeffeler C. Akute Sportverletzungen und chronische Überlastungsschäden an Vor- und Mittelfuß. *Radiologe* 2015;55(5):417–32.

- 27 Tan AL, Fukuba E, Halliday NA, et al. High-resolution MRI assessment of dactylitis in psoriatic arthritis shows flexor tendon pulley and sheath-related enthesitis. *Ann Rheum Dis* 2015;74(1):185–89.
- 28 Guermazi A, Alizai H, Crema MD, et al. Compositional MRI techniques for evaluation of cartilage degeneration in osteoarthritis. *Osteoarthr Cartil* 2015;23(10):1639–53. doi:10.1016/j.joca.2015.05.026 [published Online First: 5 June 2015].
- 29 Guermazi A, Roemer FW. Compositional MRI assessment of cartilage: what is it and what is its potential for sports medicine? *Br J Sports Med* 2016;50(15):896–97. doi:10.1136/bjsports-2015-095146 [published Online First: 28 October 2015].
- 30 Burstein D, Velyvis J, Scott KT, et al. Protocol issues for delayed Gd(DTPA)(2-)-enhanced MRI (dGEMRIC) for clinical evaluation of articular cartilage. *Magn Reson Med* 2001;45(1):36–41.
- 31 Link TM. Editorial comment: the future of compositional MRI for cartilage. *Eur Radiol* 2018;28(7):2872–73. doi:10.1007/s00330-018-5457-4 [published Online First: 30 April 2018].
- 32 Einarsson E, Peterson P, Önnarfjord P, et al. The role of cartilage glycosaminoglycan structure in gagCEST. *NMR Biomed* 2020;33(5):e4259. doi:10.1002/nbm.4259 [published Online First: 30 January 2020].
- 33 Schreiner MM, Zbýň Š, Schmitt B, et al. Reproducibility and regional variations of an improved gagCEST protocol for the in vivo evaluation of knee cartilage at 7 T. *MAGMA* 2016;29(3):513–21. doi:10.1007/s10334-016-0544-5 [published Online First: 10 March 2016].

- 34 Müller-Lutz A, Schleich C, Pentang G, et al. Age-dependency of glycosaminoglycan content in lumbar discs: A 3t gagcEST study. *J Magn Reson Imaging* 2015;42(6):1517–23.
- 35 Østergaard M, Peterfy CG, Bird P, et al. The OMERACT Rheumatoid Arthritis Magnetic Resonance Imaging (MRI) Scoring System: Updated Recommendations by the OMERACT MRI in Arthritis Working Group. *J Rheumatol* 2017;44(11):1706–12.
- 36 Ostergaard M, McQueen F, Wiell C, et al. The OMERACT psoriatic arthritis magnetic resonance imaging scoring system (PsAMRIS): definitions of key pathologies, suggested MRI sequences, and preliminary scoring system for PsA Hands. *J Rheumatol* 2009;36(8):1816–24.
- 37 Nwaru CA, Nygård C-H, Virtanen P. Musculoskeletal pain and re-employment among unemployed job seekers: a three-year follow-up study. *BMC Public Health* 2016;16:531. doi:10.1186/s12889-016-3200-0 [published Online First: 8 July 2016].
- 38 van der Woude D, van der Helm-van Mil AHM. Update on the epidemiology, risk factors, and disease outcomes of rheumatoid arthritis. *Best Pract Res Clin Rheumatol* 2018;32(2):174–87.
- 39 Martel-Pelletier J, Barr AJ, Cicuttini FM, et al. Osteoarthritis. *Nat Rev Dis Primers* 2016;2:16072. doi:10.1038/nrdp.2016.72 [published Online First: 13 October 2016].
- 40 Huscher D, Merkesdal S, Thiele K, et al. Cost of illness in rheumatoid arthritis, ankylosing spondylitis, psoriatic arthritis and systemic lupus erythematosus in Germany. *Ann Rheum Dis* 2006;65(9):1175–83. doi:10.1136/ard.2005.046367 [published Online First: 15 March 2006].

- 41 Salmon JH, Rat AC, Sellam J, et al. Economic impact of lower-limb osteoarthritis worldwide: a systematic review of cost-of-illness studies. *Osteoarthr Cartil* 2016;24(9):1500–08. doi:10.1016/j.joca.2016.03.012 [published Online First: 23 March 2016].
- 42 Aletaha D, Funovits J, Smolen JS. Physical disability in rheumatoid arthritis is associated with cartilage damage rather than bone destruction. *Ann Rheum Dis* 2011;70(5):733–39.
- 43 Oliveria SA, Felson DT, Reed JI, et al. Incidence of symptomatic hand, hip, and knee osteoarthritis among patients in a health maintenance organization. *Arthritis Rheum* 1995;38(8):1134–41.
- 44 KELLGREN JH, LAWRENCE JS. Radiological assessment of osteoarthrosis. *Ann Rheum Dis* 1957;16(4):494–502.
- 45 Robinson WH, Lepus CM, Wang Q, et al. Low-grade inflammation as a key mediator of the pathogenesis of osteoarthritis. *Nat Rev Rheumatol* 2016;12(10):580–92. doi:10.1038/nrrheum.2016.136 [published Online First: 19 August 2016].
- 46 Cassidy JD, Côté P, Carroll LJ, et al. Incidence and course of low back pain episodes in the general population. *Spine (Phila Pa 1976)* 2005;30(24):2817–23.
- 47 Hemanta D, Jiang X-X, Feng Z-Z, et al. Etiology for Degenerative Disc Disease. *Chin Med Sci J* 2016;31(3):185–91.
- 48 Konieczny MR, Senyurt H, Krauspe R. Epidemiology of adolescent idiopathic scoliosis. *J Child Orthop* 2013;7(1):3–9.
- 49 Wu PH, Kim HS, Jang I-T. Intervertebral Disc Diseases PART 2: A Review of the Current Diagnostic and Treatment Strategies for Intervertebral Disc Disease.

Int J Mol Sci 2020;21(6). doi:10.3390/ijms21062135 [published Online First: 20 March 2020].

50 Taher F, Essig D, Lebl DR, et al. Lumbar degenerative disc disease: current and future concepts of diagnosis and management. *Adv Orthop* 2012;2012:970752. doi:10.1155/2012/970752 [published Online First: 2 April 2012].

51 Tan AL, Tanner SF, Conaghan PG, et al. Role of metacarpophalangeal joint anatomic factors in the distribution of synovitis and bone erosion in early rheumatoid arthritis. *Arthritis Rheum* 2003;48(5):1214–22.

52 Bugatti S, Caporali R, Manzo A, et al. Involvement of subchondral bone marrow in rheumatoid arthritis: lymphoid neogenesis and in situ relationship to subchondral bone marrow osteoclast recruitment. *Arthritis Rheum* 2005;52(11):3448–59.

53 McGonagle D, Lories RJU, Tan AL, et al. The concept of a "synovio-entheseal complex" and its implications for understanding joint inflammation and damage in psoriatic arthritis and beyond. *Arthritis Rheum* 2007;56(8):2482–91.

54 McGonagle D, Tan AL. The enthesis in psoriatic arthritis. *Clin Exp Rheumatol* 2015;33(5 Suppl 93):S36-9.

55 Schett G, Lories RJ, D'Agostino M-A, et al. Enthesitis: from pathophysiology to treatment. *Nat Rev Rheumatol* 2017;13(12):731–41.

56 Sudoł-Szopińska I, Kwiatkowska B, Prochorec-Sobieszek M, et al. Enthesopathies and enthesitis. Part 1. Etiopathogenesis. *J Ultrason* 2015;15(60):72–84.

57 Sudol-Szopińska I, Kwiatkowska B, Prochorec-Sobieszek M, et al. Enthesopathies and enthesitis. Part 2: Imaging studies. *J Ultrason* 2015;15(61):196–207.

58 Dubash S, McGonagle D, Marzo-Ortega H. New advances in the understanding and treatment of axial spondyloarthritis: from chance to choice. *Ther Adv Chronic Dis* 2018;9(3):77–87. doi:10.1177/2040622317743486 [published Online First: 14 December 2017].

59 Zhu W, He X, Cheng K, et al. Ankylosing spondylitis: etiology, pathogenesis, and treatments. *Bone Res* 2019;7:22. doi:10.1038/s41413-019-0057-8 [published Online First: 5 August 2019].

60 Appel H, Loddenkemper C, Miossec P. Rheumatoid arthritis and ankylosing spondylitis - pathology of acute inflammation. *Clin Exp Rheumatol* 2009;27(4 Suppl 55):S15-9.

61 Chandran V, Abji F, Perruccio AV, et al. Serum-based soluble markers differentiate psoriatic arthritis from osteoarthritis. *Ann Rheum Dis* 2019 (accessed 26 Apr 2019).

62 Cimmino MA, Parodi M, Innocenti S, et al. Dynamic magnetic resonance of the wrist in psoriatic arthritis reveals imaging patterns similar to those of rheumatoid arthritis. *Arthritis Res Ther* 2005;7(4):R725-31.

63 Colebatch AN, Edwards CJ, Østergaard M, et al. EULAR recommendations for the use of imaging of the joints in the clinical management of rheumatoid arthritis. *Ann Rheum Dis* 2013;72(6):804–14.

64 Schwenzer NF, Kötter I, Henes JC, et al. The role of dynamic contrast-enhanced MRI in the differential diagnosis of psoriatic and rheumatoid arthritis. *AJR Am J Roentgenol* 2010;194(3):715–20.

- 65 Zabotti A, Salvin S, Quartuccio L, et al. Differentiation between early rheumatoid and early psoriatic arthritis by the ultrasonographic study of the synovio-entheseal complex of the small joints of the hands. *Clin Exp Rheumatol* 2016;34(3):459–65.
- 66 McGonagle D, Hermann K-GA, Tan AL. Differentiation between osteoarthritis and psoriatic arthritis: implications for pathogenesis and treatment in the biologic therapy era. *Rheumatology (Oxford)* 2015;54(1):29–38 (accessed 26 Apr 2019).
- 67 Narváez J, Narváez JA, Albert M de, et al. Can magnetic resonance imaging of the hand and wrist differentiate between rheumatoid arthritis and psoriatic arthritis in the early stages of the disease? *Semin Arthritis Rheum* 2012;42(3):234–45.
- 68 Currie S, Hoggard N, Craven IJ, et al. Understanding MRI: basic MR physics for physicians. *Postgrad Med J* 2013;89(1050):209–23. doi:10.1136/postgradmedj-2012-131342 [published Online First: 7 December 2012].
- 69 Sands MJ, Levitin A. Basics of magnetic resonance imaging. *Semin Vasc Surg* 2004;17(2):66–82.
- 70 Collins CM. Radiofrequency Field Calculations for High Field MRI. In: *Ultra High Field Magnetic Resonance Imaging*. Boston, MA: Springer US 2006:209–48.
- 71 Alizai H, Chang G, Regatte RR. MRI of the Musculoskeletal System: Advanced Applications using High and Ultrahigh Field MRI. *Semin Musculoskelet Radiol* 2015;19(4):363–74. doi:10.1055/s-0035-1563735 [published Online First: 19 November 2015].

- 72 Buchbender C, Sewerin P, Mattes-György K, et al. Utility of combined high-resolution bone SPECT and MRI for the identification of rheumatoid arthritis patients with high-risk for erosive progression. *Eur J Radiol* 2013;82(2):374–79.
- 73 Buchbender C, Ostendorf B, Mattes-György K, et al. Synovitis and bone inflammation in early rheumatoid arthritis: high-resolution multi-pinhole SPECT versus MRI. *Diagn Interv Radiol* 2013;19(1):20–24.
- 74 Tan AL, Grainger AJ, Tanner SF, et al. A high-resolution magnetic resonance imaging study of distal interphalangeal joint arthropathy in psoriatic arthritis and osteoarthritis: are they the same? *Arthritis Rheum* 2006;54(4):1328–33.
- 75 Sudoł-Szopińska I, Matuszewska G, Kwiatkowska B, et al. Diagnostic imaging of psoriatic arthritis. Part I: etiopathogenesis, classifications and radiographic features. *J Ultrason* 2016;16(64):65–77.
- 76 Spadaro A, Lubrano E. Psoriatic arthritis: imaging techniques. *Reumatismo* 2012;64(2):99–106.
- 77 Sankowski AJ, Lebkowska UM, Cwikła J, et al. Psoriatic arthritis. *Pol J Radiol* 2013;78(1):7–17 (accessed 26 Apr 2019).
- 78 Kay J, Upchurch KS. ACR/EULAR 2010 rheumatoid arthritis classification criteria. *Rheumatology (Oxford)* 2012;51 Suppl 6:vi5-9.
- 79 Tillett W, Costa L, Jadon D, et al. The CIASsification for Psoriatic ARthritis (CASPAR) criteria--a retrospective feasibility, sensitivity, and specificity study. *J Rheumatol* 2012;39(1):154–56.
- 80 Rudwaleit M, Braun J, Sieper J. ASAS-Klassifikationskriterien für axiale Spondyloarthritis. *Z Rheumatol* 2009;68(7):591–93.

81 Braun J, van den Berg R, Baraliakos X, et al. 2010 update of the ASAS/EULAR recommendations for the management of ankylosing spondylitis. *Ann Rheum Dis* 2011;70(6):896–904.

82 Zochling J, van der Heijde D, Burgos-Vargas R, et al. ASAS/EULAR recommendations for the management of ankylosing spondylitis. *Ann Rheum Dis* 2006;65(4):442–52.

83 Baraliakos X, Davis J, Tsuji W, et al. Magnetic resonance imaging examinations of the spine in patients with ankylosing spondylitis before and after therapy with the tumor necrosis factor alpha receptor fusion protein etanercept. *Arthritis Rheum* 2005;52(4):1216–23.

84 Appel H, Loddenkemper C, Grozdanovic Z, et al. Correlation of histopathological findings and magnetic resonance imaging in the spine of patients with ankylosing spondylitis. *Arthritis Res Ther* 2006;8(5):R143.

85 Machado P, Landewé R, Braun J, et al. Both structural damage and inflammation of the spine contribute to impairment of spinal mobility in patients with ankylosing spondylitis. *Ann Rheum Dis* 2010;69(8):1465–70.

86 Baraliakos X, Hermann K-GA, Xu S, et al. Spinal mobility in the cervical and lumbar spine correlates with magnetic resonance imaging findings for inflammatory and structural changes in patients with active ankylosing spondylitis. *Clin Exp Rheumatol* 2020.

87 Pfirrmann CW, Metzdorf A, Zanetti M, et al. Magnetic resonance classification of lumbar intervertebral disc degeneration. *Spine (Phila Pa 1976)* 2001;26(17):1873–78.

88 Modic MT, Masaryk TJ, Ross JS, et al. Imaging of degenerative disk disease. *Radiology* 1988;168(1):177–86.

89 Burstein D, Gray ML. Is MRI fulfilling its promise for molecular imaging of cartilage in arthritis? *Osteoarthr Cartil* 2006;14(11):1087–90. doi:10.1016/j.joca.2006.07.001 [published Online First: 9 August 2006].

90 Bashir A, Gray ML, Hartke J, et al. Nondestructive imaging of human cartilage glycosaminoglycan concentration by MRI. *Magn Reson Med* 1999;41(5):857–65.

91 Bittersohl B, Miese FR, Dekkers C, et al. T2* mapping and delayed gadolinium-enhanced magnetic resonance imaging in cartilage (dGEMRIC) of glenohumeral cartilage in asymptomatic volunteers at 3 T. *Eur Radiol* 2013;23(5):1367–74.

92 Sewerin P, Schleich C, Vordenbäumen S, et al. Update on imaging in rheumatic diseases: cartilage. *Clin Exp Rheumatol* 2018;36 Suppl 114(5):139–44.

93 Miese FR, Ostendorf B, Wittsack H-J, et al. Knorpelqualität an den Fingergelenken: delayed Gd(DTPA)²-enhanced MRI of the cartilage (dGEMRIC) bei 3T. *Rofa* 2010;182(10):873–78.

94 Bittersohl B, Kircher J, Miese FR, et al. T2* mapping and delayed gadolinium-enhanced magnetic resonance imaging in cartilage (dGEMRIC) of humeral articular cartilage--a histologically controlled study. *J Shoulder Elbow Surg* 2015;24(10):1644–52.

95 Schmaranzer F, Arendt L, Liechti EF, et al. Do dGEMRIC and T2 Imaging Correlate With Histologic Cartilage Degeneration in an Experimental Ovine FAI Model? *Clin Orthop Relat Res* 2019;477(5):990–1003.

96 Sewerin P, Schleich C, Brinks R, et al. Assessing Associations of Synovial Perfusion, Cartilage Quality, and Outcome in Rheumatoid Arthritis Using Dynamic Contrast-enhanced Magnetic Resonance Imaging. *J Rheumatol* 2019.

- 97 Sewerin P, Müller-Lutz A, Abrar DB, et al. Prevention of the progressive biochemical cartilage destruction under methotrexate therapy in early rheumatoid arthritis. *Clin Exp Rheumatol* 2019;37(2):179–85.
- 98 Herz B, Albrecht A, Englbrecht M, et al. Osteitis and synovitis, but not bone erosion, is associated with proteoglycan loss and microstructure damage in the cartilage of patients with rheumatoid arthritis. *Ann Rheum Dis* 2014;73(6):1101–06.
- 99 Deng M, Yuan J, Chen WT, et al. Evaluation of Glycosaminoglycan in the Lumbar Disc Using Chemical Exchange Saturation Transfer MR at 3.0 Tesla: Reproducibility and Correlation with Disc Degeneration. *Biomed Environ Sci* 2016;29(1):47–55.
- 100 Kim M, Chan Q, Anthony M-P, et al. Assessment of glycosaminoglycan distribution in human lumbar intervertebral discs using chemical exchange saturation transfer at 3 T: feasibility and initial experience. *NMR Biomed* 2011;24(9):1137–44.
- 101 Latz D, Frenken M, Schiffner E, et al. Assessment of glycosaminoglycan content in intervertebral discs of patients with leg length discrepancy: A pilot study. *J Orthop* 2019;16(5):363–67.
- 102 Lee YH, Yang J, Jeong H-K, et al. Assessment of the patellofemoral cartilage: Correlation of knee pain score with magnetic resonance cartilage grading and magnetization transfer ratio asymmetry of glycosaminoglycan chemical exchange saturation transfer. *Magn Reson Imaging* 2017;35:61–68.
- 103 Togao O, Hiwatashi A, Wada T, et al. A Qualitative and Quantitative Correlation Study of Lumbar Intervertebral Disc Degeneration Using

Glycosaminoglycan Chemical Exchange Saturation Transfer, Pfirrmann Grade, and T1-ρ. *AJNR Am J Neuroradiol* 2018;39(7):1369–75.

104 Schleich C, Bittersohl B, Miese F, et al. Glycosaminoglycan chemical exchange saturation transfer at 3T MRI in asymptomatic knee joints. *Acta Radiol* 2016;57(5):627–32.

105 Saar G, Zhang B, Ling W, et al. Assessment of glycosaminoglycan concentration changes in the intervertebral disc via chemical exchange saturation transfer. *NMR Biomed* 2012;25(2):255–61.

106 Müller-Lutz A, Schleich C, Pentang G, et al. Age-dependency of glycosaminoglycan content in lumbar discs: A 3t gagcEST study. *J Magn Reson Imaging* 2015;42(6):1517–23.

107 Sewerin P, Brinks R, Schneider M, et al. Prevalence and incidence of psoriasis and psoriatic arthritis. *Ann Rheum Dis* 2019;78(2):286–87.

108 Ritchlin CT, Colbert RA, Gladman DD. Psoriatic Arthritis. *N Engl J Med* 2017;376(21):2095–96.

109 McGonagle D, Tan AL, Møller Døhn U, et al. Microanatomic studies to define predictive factors for the topography of periarticular erosion formation in inflammatory arthritis. *Arthritis Rheum* 2009;60(4):1042–51.

110 Furlan A, Stramare R. The thickening of flexor tendons pulleys: a useful ultrasonographical sign in the diagnosis of psoriatic arthritis. *J Ultrasound* 2018;21(4):309–14.

111 Graceffa D, Bonifati C, Lora V, et al. Ultrasound assessment of enthesitis thickness in psoriasis and psoriatic arthritis: A cross-sectional study. *Indian J Dermatol Venereol Leprol* 2019;85(2):175–81.

- 112 Tinazzi I, McGonagle D, Aydin SZ, et al. 'Deep Koebner' phenomenon of the flexor tendon-associated accessory pulleys as a novel factor in tenosynovitis and dactylitis in psoriatic arthritis. *Ann Rheum Dis* 2018;77(6):922–25.
- 113 Merola JF, Espinoza LR, Fleischmann R. Distinguishing rheumatoid arthritis from psoriatic arthritis. *RMD Open* 2018;4(2):e000656.
- 114 Boutry N, do Carmo CCM, Flipo R-M, et al. Early rheumatoid arthritis and its differentiation from other joint abnormalities. *Eur J Radiol* 2009;71(2):217–24.
- 115 Narváez J, Narváez JA, Albert M de, et al. Can magnetic resonance imaging of the hand and wrist differentiate between rheumatoid arthritis and psoriatic arthritis in the early stages of the disease? *Semin Arthritis Rheum* 2012;42(3):234–45.
- 116 Matzat SJ, van Tiel J, Gold GE, et al. Quantitative MRI techniques of cartilage composition. *Quant Imaging Med Surg* 2013;3(3):162–74.
- 117 Holstein A, Zilkens C, Bittersohl B, et al. Delayed gadolinium-enhanced MRI of cartilage (dGEMRIC) and morphologic MRI of cartilage in the long-term follow-up after Legg-Calvé-Perthes disease (LCPD). *J Med Imaging Radiat Oncol* 2011;55(3):259–65.
- 118 Brinkhof S, Nizak R, Khlebnikov V, et al. Detection of early cartilage damage: feasibility and potential of gagCEST imaging at 7T. *Eur Radiol* 2018;28(7):2874–81.
- 119 Brinkhof S, Nizak R, Sim S, et al. In vivo biochemical assessment of cartilage with gagCEST MRI: Correlation with cartilage properties. *NMR Biomed* 2021;34(3):e4463. doi:10.1002/nbm.4463 [published Online First: 22 December 2020].

120 Einarsson E, Peterson P, Önnarfjord P, et al. The role of cartilage glycosaminoglycan structure in gagCEST. *NMR Biomed* 2020;33(5):e4259.

121 Krakowski P, Gerkowicz A, Pietrzak A, et al. Psoriatic arthritis - new perspectives. *Arch Med Sci* 2019;15(3):580–89.

122 Merola JF, Espinoza LR, Fleischmann R. Distinguishing rheumatoid arthritis from psoriatic arthritis. *RMD Open* 2018;4(2):e000656. doi:10.1136/rmdopen-2018-000656 [published Online First: 13 August 2018].

123 Shiraishi M, Fukuda T, Igarashi T, et al. Differentiating Rheumatoid and Psoriatic Arthritis of the Hand: Multimodality Imaging Characteristics. *Radiographics* 2020;40(5):1339–54. doi:10.1148/rg.2020200029 [published Online First: 31 July 2020].

124 Khmelinskii N, Regel A, Baraliakos X. The Role of Imaging in Diagnosing Axial Spondyloarthritis. *Front Med (Lausanne)* 2018;5:106. doi:10.3389/fmed.2018.00106 [published Online First: 17 April 2018].

125 Braun J, van den Berg R, Baraliakos X, et al. 2010 update of the ASAS/EULAR recommendations for the management of ankylosing spondylitis. *Ann Rheum Dis* 2011;70(6):896–904.

126 van der Heijde DM, Revicki DA, Gooch KL, et al. Physical function, disease activity, and health-related quality-of-life outcomes after 3 years of adalimumab treatment in patients with ankylosing spondylitis. *Arthritis Res Ther* 2009;11(4):R124.

127 Sudół-Szopińska I, Płaza M, Pracoń G. Selected issues in diagnostic imaging of spondyloarthritides: psoriatic arthritis and juvenile spondyloarthritis. *Reumatologia* 2016;54(6):310–17.

- 128 Schett G, Coates LC, Ash ZR, et al. Structural damage in rheumatoid arthritis, psoriatic arthritis, and ankylosing spondylitis: traditional views, novel insights gained from TNF blockade, and concepts for the future. *Arthritis Res Ther* 2011;2011. <http://arthritis-research.com/supplements/13/S1/S4> (accessed 26 Apr 2019).
- 129 Appel H, Kuhne M, Spiekermann S, et al. Immunohistochemical analysis of hip arthritis in ankylosing spondylitis: evaluation of the bone-cartilage interface and subchondral bone marrow. *Arthritis Rheum* 2006;54(6):1805–13.
- 130 Bleil J, Sieper J, Maier R, et al. Cartilage in facet joints of patients with ankylosing spondylitis (AS) shows signs of cartilage degeneration rather than chondrocyte hypertrophy: implications for joint remodeling in AS. *Arthritis Res Ther* 2015;17(1).
- 131 Schleich C, Müller-Lutz A, Matuschke F, et al. Glycosaminoglycan chemical exchange saturation transfer of lumbar intervertebral discs in patients with spondyloarthritis. *J Magn Reson Imaging* 2015;42(4):1057–63. doi:10.1002/jmri.24877 [published Online First: 11 March 2015].
- 132 Müller-Lutz A, Schleich C, Sewerin P, et al. Comparison of quantitative and semiquantitative dynamic contrast-enhanced MRI with respect to their correlation to delayed gadolinium-enhanced MRI of the cartilage in patients with early rheumatoid arthritis. *J Comput Assist Tomogr* 2015;39(1):64–69.
- 133 Schraml C, Schwenzer NF, Martirosian P, et al. Assessment of synovitis in erosive osteoarthritis of the hand using DCE-MRI and comparison with that in its major mimic, the psoriatic arthritis. *Acad Radiol* 2011;18(7):804–09.

134 Buchbender C, Scherer A, Kröpil P, et al. Cartilage quality in rheumatoid arthritis: comparison of T2* mapping, native T1 mapping, dGEMRIC, $\Delta R1$ and value of pre-contrast imaging. *Skeletal Radiol* 2012;41(6):685–92.

135 Miese FR, Ostendorf B, Wittsack H-J, et al. Knorpelqualität an den Fingergelenken: delayed Gd(DTPA)²-enhanced MRI of the cartilage (dGEMRIC) bei 3T. *Rofo* 2010;182(10):873–78.

136 Miese F, Kröpil P, Ostendorf B, et al. Motion correction improves image quality of dGEMRIC in finger joints. *Eur J Radiol* 2011;80(3):e427-31.

137 Bhattaram P, Chandrasekharan U. The joint synovium: A critical determinant of articular cartilage fate in inflammatory joint diseases. *Semin Cell Dev Biol* 2017;62:86–93. doi:10.1016/j.semcdb.2016.05.009 [published Online First: 19 May 2016].

138 Wu A, March L, Zheng X, et al. Global low back pain prevalence and years lived with disability from 1990 to 2017: estimates from the Global Burden of Disease Study 2017. *Ann Transl Med* 2020;8(6):299.

139 Billis EV, McCarthy CJ, Oldham JA. Subclassification of low back pain: a cross-country comparison. *Eur Spine J* 2007;16(7):865–79. doi:10.1007/s00586-007-0313-2 [published Online First: 17 March 2007].

140 Deane JA, McGregor AH. Current and future perspectives on lumbar degenerative disc disease: a UK survey exploring specialist multidisciplinary clinical opinion. *BMJ Open* 2016;6(9):e011075. doi:10.1136/bmjopen-2016-011075 [published Online First: 15 September 2016].

141 Bertram H, Steck E, Zimmerman G, et al. Accelerated intervertebral disc degeneration in scoliosis versus physiological ageing develops against a

background of enhanced anabolic gene expression. *Biochem Biophys Res Commun* 2006;342(3):963–72.

142 Haneder S, Apprich SR, Schmitt B, et al. Assessment of glycosaminoglycan content in intervertebral discs using chemical exchange saturation transfer at 3.0 Tesla: preliminary results in patients with low-back pain. *Eur Radiol* 2013;23(3):861–68.

143 Hosea TM, Hannafin JA. Rowing Injuries. *Sports Health* 2012;4(3):236–45.

144 Liu X, Krishnamoorthy D, Lin L, et al. A method for characterising human intervertebral disc glycosaminoglycan disaccharides using liquid chromatography-mass spectrometry with multiple reaction monitoring. *Eur Cell Mater* 2018;35:117–31.

145 Müller-Lutz A, Schleich C, Pentang G, et al. Age-dependency of glycosaminoglycan content in lumbar discs: A 3t gagcEST study. *J Magn Reson Imaging* 2015;42(6):1517–23.

146 Schleich C, Müller-Lutz A, Blum K, et al. Facet tropism and facet joint orientation: risk factors for the development of early biochemical alterations of lumbar intervertebral discs. *Osteoarthr Cartil* 2016;24(10):1761–68.

147 Müller-Lutz A, Schleich C, Schmitt B, et al. Gender, BMI and T2 dependencies of glycosaminoglycan chemical exchange saturation transfer in intervertebral discs. *Magn Reson Imaging* 2016;34(3):271–75.

148 Müller-Lutz A, Schleich C, Schmitt B, et al. Improvement of gagCEST imaging in the human lumbar intervertebral disc by motion correction. *Skeletal Radiol* 2015;44(4):505–11. doi:10.1007/s00256-014-2034-z [published Online First: 23 October 2014].

149 McGonagle D, Marzo-Ortega H, Benjamin M, et al. Report on the Second international Enthesitis Workshop. *Arthritis Rheum* 2003;48(4):896–905.

150 Baraliakos X, Kleyer A, Simon D, et al. Bildgebung bei der Psoriasisarthritis und Aspekte der röntgenologischen Progression. *Z Rheumatol* 2020;79(1):40–52.

151 Finzel S, Englbrecht M, Engelke K, et al. A comparative study of periarticular bone lesions in rheumatoid arthritis and psoriatic arthritis. *Ann Rheum Dis* 2011;70(1):122–27. doi:10.1136/ard.2010.132423 [published Online First: 11 October 2010].

152 Moll JM, Johnson G, Wright V. Psoriatic arthritis: a unique family. *Rheumatol Rehabil* 1974;13(3):154–57.

153 Moll JM, Wright V. Psoriatic arthritis. *Semin Arthritis Rheum* 1973;3(1):55–78.

154 Kaeley GS, Eder L, Aydin SZ, et al. Dactylitis: A hallmark of psoriatic arthritis. *Semin Arthritis Rheum* 2018;48(2):263–73.

155 Forney MC, Winalski CS, Schils JP. Magnetic resonance imaging of inflammatory arthropathies of peripheral joints. *Top Magn Reson Imaging* 2011;22(2):45–59.

156 Vordenbäumen S, Schleich C, Lögters T, et al. Dynamic contrast-enhanced magnetic resonance imaging of metacarpophalangeal joints reflects histological signs of synovitis in rheumatoid arthritis. *Arthritis Res Ther* 2014;16(5):452.

157 Jones M, Badreddine I, Mehta J, et al. The Rate of Disc Degeneration on MRI in Preoperative Adolescent Idiopathic Scoliosis. *Spine J* 2017;17(11):S332.

158 Connolly PJ, Schroeder HP von, Johnson GE, et al. Adolescent idiopathic scoliosis. Long-term effect of instrumentation extending to the lumbar spine. *J Bone Joint Surg Am* 1995;77(8):1210–16.

- 159 Masui T, Yukawa Y, Nakamura S, et al. Natural history of patients with lumbar disc herniation observed by magnetic resonance imaging for minimum 7 years. *J Spinal Disord Tech* 2005;18(2):121–26.
- 160 Bleil J, Maier R, Hempfing A, et al. Granulation Tissue Eroding the Subchondral Bone Also Promotes New Bone Formation in Ankylosing Spondylitis. *Arthritis Rheumatol* 2016;68(10):2456–65.
- 161 Bleil J, Maier R, Hempfing A, et al. Histomorphologic and histomorphometric characteristics of zygapophyseal joint remodeling in ankylosing spondylitis. *Arthritis Rheumatol* 2014;66(7):1745–54.
- 162 CRUICKSHANK B. Lesions of cartilaginous joints in ankylosing spondylitis. *J Pathol Bacteriol* 1956;71(1):73–84.
- 163 CRUICKSHANK B. Histopathology of diarthrodial joints in ankylosing spondylitis. *Ann Rheum Dis* 1951;10(4):393–404.
- 164 Oei EHG, Wick MC, Müller-Lutz A, et al. Cartilage Imaging: Techniques and Developments. *Semin Musculoskelet Radiol* 2018;22(2):245–60 (accessed 30 Apr 2019).
- 165 Braun HJ, Gold GE. Advanced MRI of articular cartilage. *Imaging Med* 2011;3(5):541–55.
- 166 Koning A de, Schoones JW, van der Heijde D, et al. Pathophysiology of axial spondyloarthritis: Consensus and controversies. *Eur J Clin Invest* 2018;48(5):e12913.
- 167 Roos EM, Dahlberg L. Positive effects of moderate exercise on glycosaminoglycan content in knee cartilage: a four-month, randomized, controlled trial in patients at risk of osteoarthritis. *Arthritis Rheum* 2005;52(11):3507–14.

168 Witwit WA, Kovac P, Sward A, et al. Disc degeneration on MRI is more prevalent in young elite skiers compared to controls. *Knee Surg Sports Traumatol Arthrosc* 2018;26(1):325–32. doi:10.1007/s00167-017-4545-3 [published Online First: 13 April 2017].

169 Belavý DL, Quittner MJ, Ridgers N, et al. Running exercise strengthens the intervertebral disc. *Sci Rep* 2017;7:45975. doi:10.1038/srep45975 [published Online First: 19 April 2017].

170 Wilke HJ, Neef P, Caimi M, et al. New in vivo measurements of pressures in the intervertebral disc in daily life. *Spine (Phila Pa 1976)* 1999;24(8):755–62.

F. Danksagung

Mein besonderer Dank gilt Herrn Professor Dr. med. Gerald Antoch, der mir den Weg in die Radiologie ermöglicht und mich sowohl bei meinem klinischen als auch wissenschaftlichem Werdegang immer unterstützt hat.

Zudem bedanke ich mich bei Herrn PD Dr. med. Christoph Schleich, der mich für die muskuloskelettale Radiologie begeistert und mich mit offenen Armen in seine Arbeitsgruppe aufgenommen hat. Auch Herrn PD Dr. Sven Nebelung gebührt mein außerordentlicher Dank, denn er war ein steter Quell neuer Ideen und mein wissenschaftlicher Mentor.

Meiner Arbeitsgruppe, Frau Dr. med. Dipl.Ing. Miriam Frenken, Frau Dr. med. Lena Wilms, Frau PD Dr. rer. nat. Anja Müller-Lutz, Herrn Professor Dr. rer. Nat. Hans-Jörg Wittack, Herrn Ludger Radke, M. Sc. Und Herrn Benedikt Kamp, M. Sc. danke ich herzlich für die außergewöhnliche Zusammenarbeit, die von großer Hilfsbereitschaft und freundschaftlichem Austausch geprägt war.

Meinen engen Kooperationspartnern, allen voran den Herren PD Dr. med. Philipp Sewerin aus der Klinik für Rheumatologie und den Herren PD Dres. Bernd Bittersohl, Markus Konieczny und Tobias Hesper danke ich für ausgezeichnete Zusammenarbeit und Synergie.

Darüber hinaus gilt mein Dank allen Mitarbeitern des Instituts für Diagnostische und Interventionelle Radiologie für die stets kollegiale und freundschaftliche Zusammenarbeit im klinischen Alltag sowie die Unterstützung der wissenschaftlichen Projekte.

Allen voran danke ich jedoch meiner Familie, vor allem meiner liebsten Johanna, die endloser Quell meiner Motivation und Inspiration ist, meinen Eltern Petra und Amir, meinen Großeltern Jutta und Franz-Josef, meinen Geschwistern Alida, Sascha und Kai und meinem kleinen Sonnenschein Yuna sowie meinen Freunden, denn sie haben mich in allen Phasen meines privaten und beruflichen Werdegangs unterstützt und hatten immer ein offenes Ohr für meine Probleme und Widrigkeiten. Für ihre uneingeschränkte Unterstützung und bedingungslose Liebe bin ich auf ewig dankbar.

G. Zugrunde liegende Forschungsarbeiten

Die Sonderdrucke erfolgen im Rahmen der Autorenrechte.

RESEARCH ARTICLE

Open Access



High-resolution MRI of flexor tendon pulleys using a 16-channel hand coil: disease detection and differentiation of psoriatic and rheumatoid arthritis

Daniel B. Abrar^{1†}, Christoph Schleich^{1†}, Sven Nebelung¹, Miriam Frenken¹, Karl Ludger Radke¹, Stefan Vordenbäumen², Ralph Brinks², Matthias Schneider², Benedikt Ostendorf², Dennis McGonagle³ and Philipp Sewerin^{2*} 

Abstract

Background: To evaluate the value of 3 Tesla (T) magnetic resonance imaging (MRI) changes of flexor tendon pulleys for the differentiation of psoriatic (PsA) and rheumatoid arthritis (RA), using a novel 16-channel high-resolution hand coil.

Methods: Seventeen patients with active PsA, 20 patients with active RA, and 16 healthy controls (HC) underwent high-resolution 3 T MRI using the dedicated 16-channel hand coil. Images were analyzed by three independent readers for the degree of inflammatory changes, thickness of flexor tendon pulleys, and comparison to the outcome measures for RA clinical trials (OMERACT) PsA MRI score (PsAMRIS) and to its sub-scores. For correlation analyses, Spearman rho correlation was calculated.

Results: Flexor tendon pulleys were thicker in PsA than in RA patients (mean difference 0.16 mm, $p < 0.001$) and HC (mean difference 0.2 mm, $p < 0.001$) and showed a higher degree of associated inflammatory changes (mean difference from RA 4.7, $p = 0.048$; mean difference from HC 14.65, $p < 0.001$). Additionally, there was a strong correlation of accessory pulley inflammation and PsAMRIS and its acute-inflammatory sub-scores, flexor tenosynovitis, synovitis, and periarticular inflammation (for the second digit synovitis $\rho = 0.72$, flexor tenosynovitis $\rho = 0.7$, overall PsAMRIS $\rho = 0.72$, $p < 0.01$). Similar robust correlations were evident in digits 3–5. Weaker correlations were evident in RA (synovitis $\rho = 0.49$, flexor tenosynovitis $\rho = 0.49$, periarticular inflammation $\rho = 0.4$).

Conclusion: The assessment of MRI changes of flexor tendon pulleys is potentially beneficial for disease detection in PsA, as well as for its distinction from RA and HC.

Trial registration: 2014123117, December 2014.

Keywords: Psoriatic arthritis, Pulley, PsAMRIS, Enthesitis, Rheumatoid arthritis, Synovio-entheseal-complex

* Correspondence: philipp.sewerin@med.uni-duesseldorf.de

[†]Daniel B. Abrar and Christoph Schleich contributed equally to this work.

²Policlinic and Hiller Research Unit for Rheumatology, UKD, Heinrich Heine University Düsseldorf, Moorenstrasse 5, 40225 Düsseldorf, Germany

Full list of author information is available at the end of the article



© The Author(s). 2020 **Open Access** This article is licensed under a Creative Commons Attribution 4.0 International License, which permits use, sharing, adaptation, distribution and reproduction in any medium or format, as long as you give appropriate credit to the original author(s) and the source, provide a link to the Creative Commons licence, and indicate if changes were made. The images or other third party material in this article are included in the article's Creative Commons licence, unless indicated otherwise in a credit line to the material. If material is not included in the article's Creative Commons licence and your intended use is not permitted by statutory regulation or exceeds the permitted use, you will need to obtain permission directly from the copyright holder. To view a copy of this licence, visit <http://creativecommons.org/licenses/by/4.0/>. The Creative Commons Public Domain Dedication waiver (<http://creativecommons.org/publicdomain/zero/1.0/>) applies to the data made available in this article, unless otherwise stated in a credit line to the data.

Background

Psoriatic arthritis (PsA) is a very common chronic inflammatory disease that affects joints and ultimately leads to joint destruction and functional disabilities [1, 2]. Regarding its clinical presentation, PsA shares many similarities with rheumatoid arthritis (RA), which potentially complicates the distinction between both entities, especially in cases of symmetric and seronegative RA [3–5]. However, PsA and RA differ in their pathophysiology: RA is considered to be a synovial disease that exhibits secondary spread to the adjacent bone; PsA on the other hand characteristically affects entheses, such as tendon and ligament insertion sites. These can be classified as fibrous and fibrocartilaginous and belong to the so-called synovio-entheseal complex [6–10]. Additionally, tendons build so-called functional entheses with associated ligamentous structures, such as flexor tendon pulleys [11]. These pulleys have a fibrocartilaginous component and discontinuously wrap around the flexor tendons preventing their bowstringing during flexion [12]. Recent studies have shown that inflammation and thickening of flexor tendon pulleys are potentially due to mechanical stress (“deep Koebner response”) and may lead to the initial development of flexor tenosynovitis and dactylitis, that are major features of PsA [13–15].

As in RA, remission is the ultimate goal of disease-modifying therapy in PsA. Hence, early accurate diagnosis and treatment are pivotal for a favorable clinical outcome [16]. Additionally, distinct pharmacological options and treat-to-target strategies exist for both diseases which underlines the importance of an unequivocal distinction [3, 17, 18]. Even though not yet included in the Classification Criteria for PsA (CASPAR), magnetic resonance imaging (MRI) is becoming increasingly important and widely used for diagnosis and the monitoring of therapy for PsA [19–21]. The Outcome Measures for Rheumatoid Arthritis Clinical Trials (OMERACT) working group has developed a semi-quantitative PsA MRI (sum-)score (PsAMRIS) that is highly sensitive for disease-related joint changes and is widely used for therapy monitoring [22–24]. However, until most recently, enthesitis was not included in any MRI score, despite being a hallmark of PsA [25, 26]. Indeed, enthesitis is difficult to accurately evaluate in small joints using conventional MRI or with high-resolution MRI surface coils that can only visualize a small area. We

addressed this by using a dedicated 16-channel high-resolution hand coil to permit a global evaluation of digits in PsA and RA. Herein, we describe our findings indicating that this technique has considerable potential to differentiate between RA and PsA hand involvement.

Methods

Patients

Seventeen patients (mean age 53.7 ± 11.6 ; minimum/maximum 26/72 years, male/female 9/8) fulfilling the CASPAR criteria with a mean disease duration of 2.6 ± 3.3 years and peripheral joint involvement and dactylitis were prospectively recruited for the “Analysis of the Dactylic Melange” (ADAM) research initiative. All patients had failed methotrexate (MTX) monotherapy and were escalated to Etanercept (Enbrel® 50 mg s.c. fortnightly) after a baseline MRI scan.

Additionally, 20 therapy naïve patients (mean age 46 ± 15.7 , minimum/maximum 19/67 years, male/female 9/11), fulfilling the ACR/EULAR 2010 criteria for RA with a mean disease duration < 6 months (mean duration 11 ± 7 weeks) from the “Cartilage in early RA” (CARERA) study, were included. Patients were allowed a daily dose of oral prednisone at < 10 mg. After a baseline scan, patients received either MTX monotherapy or a combination of MTX and adalimumab. Patients were blinded for their therapy regime. PsA and RA patient characteristics are visualized in Table 1.

Furthermore, 16 patients (mean age 39 ± 16.1 , minimum/maximum 17/78 years, male/female 9/7) with no history of arthritis were retrospectively recruited as healthy controls (HC). MRI studies were performed due to clinical reasons (e.g., suspected carpal ganglion) in our daily routine. At the time of retrospective recruitment, all subjects of HC were over 18 years of age. The study was approved by the local ethics committee (MOLKP-719, 4962R). Written and informed consent was obtained from all patients before initiation of the study.

MR imaging

For MR imaging, a 3 T MRI scanner (Magnetom Skyra, Siemens Healthineers, Erlangen, Germany) and a dedicated 16-channel hand coil (Fig. 1; 3 T Tim Coil, Siemens Healthineers, Erlangen, Germany) were used, allowing for

Table 1 Characteristics of the study population. For patients with psoriatic arthritis (PsA) and rheumatoid arthritis (RA), as well as healthy controls the population size, the mean age in years \pm standard deviation and range, the mean disease duration (except HC) in years (PsA) and weeks (RA) \pm standard deviation and range and the sex are presented

	PsA patients	RA patients	HC
Population size	17	20	16
Age [years]	53.7 ± 11.6 (26–72)	46 ± 15.7 (19–67)	39 ± 16.1 (range 17–78)
Disease duration	2.6 ± 3.3 (1–8 years)	11 ± 7 (2–24 weeks)	–
Sex [male/female]	9 males/8 females	11 males/9 females	9 males/7 females

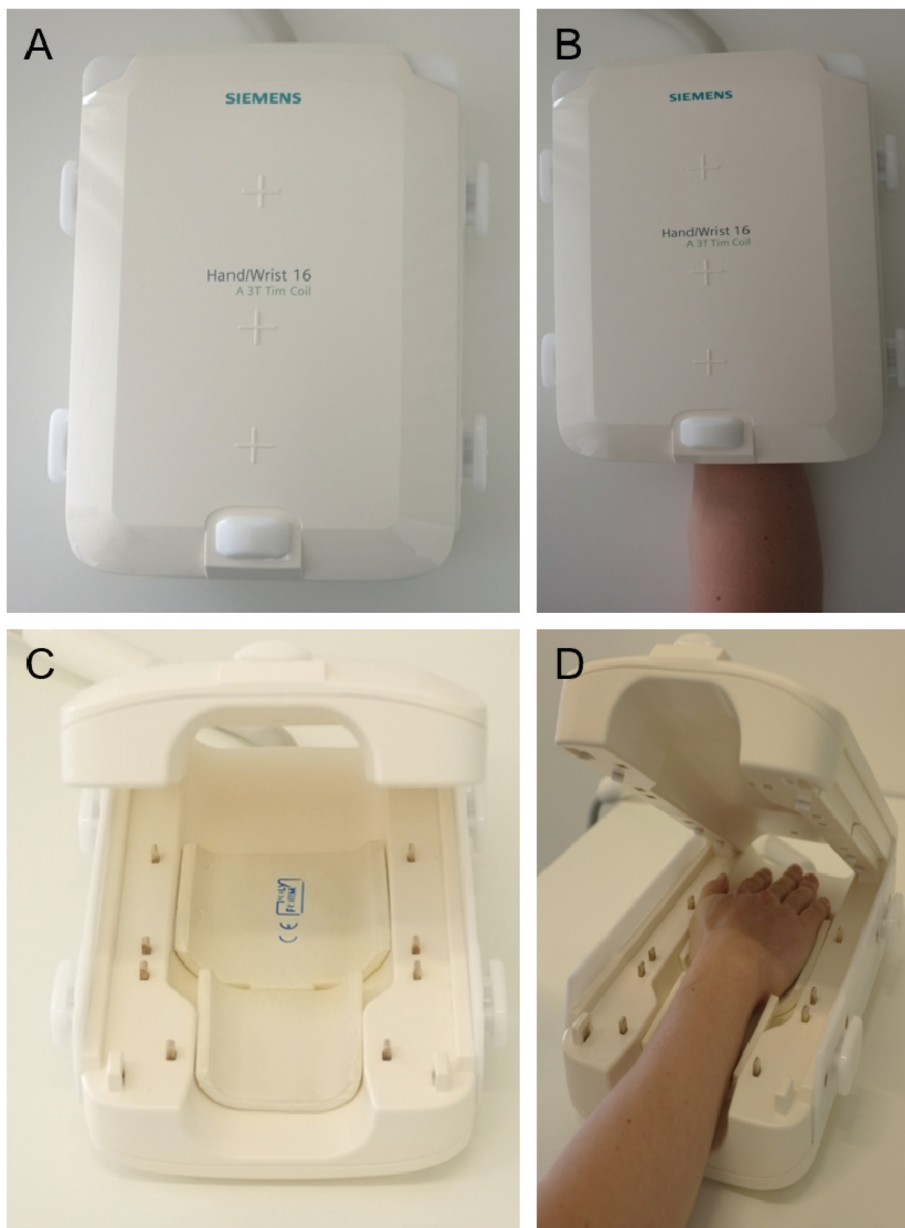


Fig. 1 16-channel hand coil

a high-resolution imaging over a wide area. PsA patients received a baseline (T0) and a follow-up (T1) scan with an approximately 6.2 ± 0.85 months (minimum/maximum: 5/8 months) interval in between. A baseline (T0) and two follow-up (T1 and T2) scans were performed in the RA population with approximately 2.8 ± 0.1 months (minimum/maximum 2.6/3 months) between T0 and T1 and 5.6 ± 0.1 months (minimum/maximum 5.4/5.8 months) between T0 and T2. For HC only a single scan was performed. In patients, all baseline scans were used for further image analysis.

The imaging protocol followed the recommendations of the OMERACT working group for PsA and RA [21, 27]. In PsA patients this included pre- and post-contrast (DOTA⁻, Dotarem, Guerbet, Villepinte, France; intravenous-injection of 0.4 ml/kg bodyweight) T1-weighted turbo spin echo (TSE) and non-contrast-enhanced fat-saturated T2-weighted TSE or short tau inversion recovery (STIR) sequences in two different orthogonal planes. The field of view covered MCP, PIP and DIP of digits 2–5. In RA patients the protocol included the following sequences: pre- and post-contrast (DOTA⁻, Dotarem, Guerbet, Villepinte,

France intravenous-injection of 0.4 ml/kg bodyweight) coronal T1-weighted TSE and transversal fat-saturated T1-weighted spin echo (SE) after contrast agent application as well as a coronal STIR. The field of view covered MCP 2–5, carpometacarpal, carpal, radiocarpal, and distal radioulnar joints.

In control patients, our in-house standard protocol was used, which included the same sequences as detailed for the RA patients above. In addition, a transversal fat-saturated proton-density-weighted sequence was acquired. The field of view differed according to the clinical region of interest. All participants were scanned in the prone position with their clinically dominant hand extended overhead and the palm facing down (“superman position”).

The sequence parameters were as follows:

PsA: coronal T1 TSE (TR/TE in ms, PsA: 862/27, RA: 862/27; flip angle in °, PsA: 150, RA: 150; slice thickness in mm, PsA: 2.5, RA: 2.5; field of view in mm, PsA: 140, RA: 130; pixel size: PsA: 0.3 × 0.3 mm, RA: 0.3 × 0.3; acquisition matrix: 512 × 512), coronal STIR (TR/TE in ms, PsA: 5560/31, RA: 5560/31; flip angle in °, PsA: 120, RA: 120; slice thickness in mm, PsA: 2.5, RA: 2.5; field of view in mm, PsA: 140, RA: 130; pixel size: PsA: 0.3 × 0.3 mm, RA: 0.3 × 0.3 mm; acquisition matrix: 448 × 314), sagittal PD TSE fat-saturated (only PsA: TR/TE in ms 3150/47, flip angle 150°, slice thickness 2.5 mm, field of view 150 mm; pixel size: 0.3 × 0.3 mm; acquisition matrix: 448 × 182), transversal T2 TSE fat-saturated (only PsA: TR/TE in ms: 5693.8/89, flip angle 180°, slice thickness 3.0 mm, field of view: 160 mm; pixel size: 0.3 × 0.3 mm; acquisition matrix: 512 × 358), transversal T1 SE fat-saturated after iv contrast (TR/TE in ms, PsA: 807/16, RA: 702/16; flip angle in °, PsA: 90, RA: 90; slice thickness in mm, PsA: 3.0, RA: 2.5; field of view in mm, PsA: 130, RA: 120; pixel size: PsA: 0.3 × 0.3 mm, RA: 0.3 × 0.3 mm; acquisition matrix: 384 × 288) and coronal T1 TSE after iv contrast (TR/TE in ms, PsA: 862/27, RA: 862/27; flip angle in °, PsA: 150, RA: 150; slice thickness in mm, PsA: 2.5, RA: 2.5; field of view in mm, PsA: 140, RA: 140; pixel size: PsA: 0.3 × 0.3 mm, RA: 0.3 × 0.3 mm; acquisition matrix: 512 × 512).

Image analysis

MR images were independently read and analyzed by two radiologists (one attending physician [CS], one resident physician [DBA]) with long-term experience in musculoskeletal imaging of > 8 years (CS) and all trained in RAMRIS and PsAMRIS-Scoring according to the OMERACT guidelines [15, 16]. In case of different findings, the readers decided by common consensus with the assisting opinion of a third reader (PS, rheumatologist with 8 years of experience in musculoskeletal imaging). Readers were blinded to the diagnosis of the patients. Flexor tendon pulleys A1 and A2 were analyzed

in digits 2 to 5. Each pulley was evaluated regarding its thickness in millimeter and its intrinsic and/or surrounding signal intensity at the radial, ulnar, and volar aspect of each pulley (see Figs. 2 and 3 for typical changes). The PsAMRIS was adapted due to the clear visualization of the pulleys with abnormalities being scored as 0–3 as per PsAMRIS scoring at other sites such as synovium and tenosynovium [21]. Consequently, the score reflected the maximum degree of enhancing and/or hyperintense signals within the pulley complex perpendicular to the pulley at its most inflamed part and scores indicated the absence of any abnormality (score 0), the involvement of < 50% of the pulley thickness (score 1), of ≥ 50–< 100% (score 2), and ≥ its entire thickness (score 3). For each pulley, we took the sum of the radial, ulnar, and volar grading regarding the surrounding and/or intrinsic inflammatory changes and the mean of the radial and ulnar thickness of the pulley itself in millimeter measured at its thickest part. Hence, measurements were not necessarily performed on the same slice. Additionally, PsA and RA patients were evaluated according to PsAMRIS at the MCP, PIP, and DIP (the latter two only in PsA patients) joint level of digits 2–5 for synovitis (score 0–3), flexor tenosynovitis (score 0–3), bone edema (score 0–3), erosion (score 0–10), proliferation (score 0 or 1), and periarticular inflammation (score 0 or 1) [21].

Statistical analysis

All statistical analyses were performed using SPSS software (IBM, version 22, Armonk, NY, USA). For descriptive analysis, the mean, standard deviation, minimum, and maximum are presented. Mean values were compared with a one-way analysis of variance (ANOVA) and a post hoc Scheffé test. For correlation analyses, Spearman rho correlation coefficient (ρ) was used. Correlation strength was graded as suggested by Cohen [28]: small (< 0.3), moderate (0.3–0.5), and large (> 0.5).

Due to a large number of comparisons between PsA patients, RA patients, and healthy controls, Bonferroni correction was applied, and the level of significance was set to $p \leq 0.05/3 = 0.0167$. Three patient cohorts were comparatively evaluated and therefore may be considered as separate experiments. In a stricter statistical sense, correction of all 66 sub-experiments (i.e., 3 cohorts, 2 assessed MRI characteristics, and 11 anatomical flexor tendon pulley levels) ought to be performed; however, the increased risk of producing false negatives secondary to overly conservative statistical analyses rendered this option impractical. Accordingly, we decided to use (design-adapted) Bonferroni correction and look for consistent and significant changes of the pulleys as a function of disease entity instead of relying on statistical formalism. Inter- and intra-rater reliability for

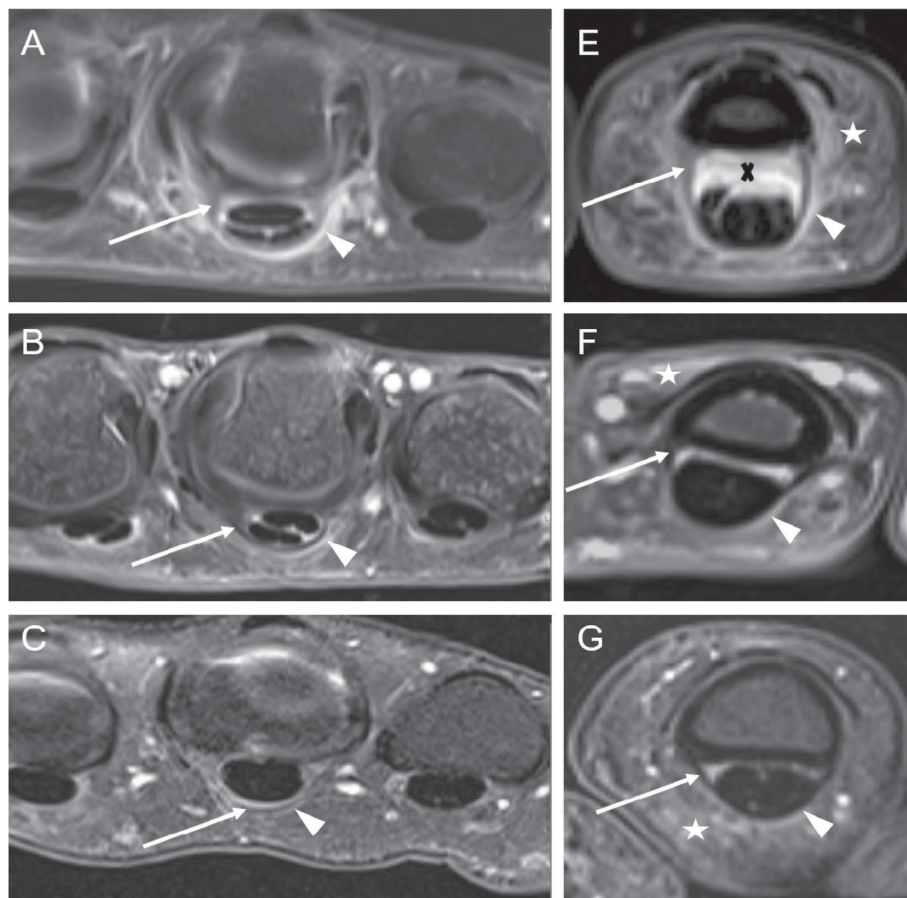


Fig. 2 High-resolution MRI of the Hand - Figure 2

pulley thickness and pulley inflammatory changes were calculated by two-way mixed intraclass correlation coefficients (single-measure ICC (sICC) for intra-rater and average measure ICC (aICC) for inter-rater reliability).

Results

PsAMRIS (sub-scores) at MCP joint level in PsA and RA patients

Descriptive analysis of inflammation sub-scores according to PsAMRIS are illustrated in Table 1 for PsA and in Table 2 for RA patients. Synovitis, flexor tenosynovitis, and periarticular inflammation (extracapsular changes) were commonly found in all PsA and RA patients. Bone edema and bone erosions, on the other hand, were less frequently seen, whereas bone proliferations were rarely detected. Periarticular inflammation (extracapsular changes) and bone erosions were significantly more frequently detected in PsA than in RA patients ($p = 0.003$ and $p < 0.001$) as originally described in hand joints [29]. Regarding all other sub-scores, no significant differences could be detected.

Inflammatory changes and thickness of the flexor tendon pulleys

Mean values of inflammatory changes and thickness of the A1 and A2 flexor tendon pulleys in PsA and RA patients and in HC are summarized in Tables 3 and 4. Visualization of flexor pulley changes in Figs. 2 and 3.

PsA patients had significantly thicker A1 and A2 flexor tendon pulleys in most fingers as compared to RA and HC (overall mean difference compared to RA: 0.19 mm, $p < 0.001$; overall mean difference compared to HC: 0.16 mm, $p < 0.001$).

Additionally, PsA patients showed significantly more inflammatory changes (higher sum-scores) at A1 and A2 flexor tendon pulleys in all fingers as compared to HC (mean difference 14.65, $p < 0.001$). Furthermore, inflammatory changes of all flexor tendon pulleys were higher in PsA than in RA patients (mean difference 4.17; $p = 0.048$). Compared to HC, RA patients had a similar thickness, but more intense inflammatory changes of pulleys (mean difference 9.95, $p < 0.001$). sICC was 0.88 and aICC 0.93.

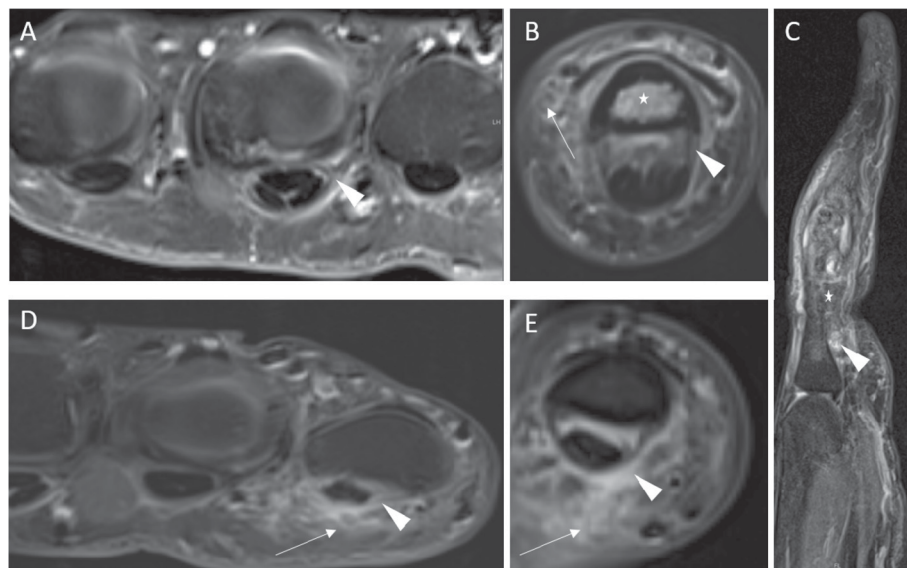


Fig. 3 High-resolution MRI of the Hand - Figure 3

Correlation of flexor tendon pulley inflammation and pulley thickness and PsAMRIS (–sub-scores)

Values for Spearman rho correlation coefficients of flexor tendon pulley inflammation and pulley thickness and PsAMRIS (–sub-scores) for PsA and RA patients are displayed in Table 5.

In PsA patients, there was a strong correlation between pulley inflammation and overall PsAMRIS as well as inflammatory PsAMRIS sub-scores (synovitis, peri-articular inflammation, and flexor tenosynovitis) at most fingers. A heterogeneous (low to high) correlation was found for pulley inflammation and bone erosion and edema, whereas the correlation of pulley inflammation and bone proliferation was mostly weak. Furthermore, pulley inflammation and thickness showed a weak correlation.

Table 2 Mean PsAMRIS values ± standard deviation for each inflammation parameter at MCP joint level in PsA and RA patients

PsAMRIS value	MCP		p value
	PsA	RA	
Overall	23.41 ± 4.89	20.45 ± 4.17	0.071
Synovitis	9.18 ± 2.1	10.35 ± 1.87	0.084
Flexor tenosynovitis	4.76 ± 1.44	5.05 ± 1.61	0.572
Periarticular inflammation	6.47 ± 1.66	4.15 ± 2.24	0.003
Bone edema	0.6 ± 1.18	0.4 ± 1.27	0.643
Bone erosion	2.29 ± 1.49	0.5 ± 0.76	< 0.001
Bone proliferation	0.12 ± 0.33	0	0.163

p values for the comparison of means between PsA and RA patients. After (adapted) Bonferroni correction, p values < 0.0167 were considered significant and are given in bold type

In RA patients, we also found a significant, but weaker, correlation between pulley inflammation and overall PsAMRIS as well as inflammatory PsAMRIS sub-scores as compared to PsA. Correlation coefficients for bone erosion and bone edema were low to intermediate.

Discussion

Psoriatic arthritis has a prominent enthesal disease component manifesting at the so-called synovio-enthesal complex, that includes flexor tendon pulleys [9]. In this study, we evaluated the value of high-resolution 3 T MRI changes of flexor tendon pulleys in PsA patients for disease detection as well as a distinction from RA and HC using a dedicated 16-channel hand coil.

According to our results, PsA patients had significantly thicker A1 and A2 flexor tendon pulleys than RA patients or HC. Between the latter, on the other hand, there were no significant differences in pulley thickness. These findings of pulley thickening in PsA patients confirm the prior ultrasound studies of Tinazzi et al., who evaluated a small population of patients with PsA, RA, non-arthritis psoriasis (Pso), and healthy individuals [14]. They hypothesized that the distinctive thickening of flexor tendon pulleys in PsA could be due to “deep Koebnerization,” an adaptation of entheses to mechanical stress, according to dermal hyperplasia and thickening in Pso, commonly known as “Koebner phenomena” [14]. Even more recently, Furlan et al. also found thickened A1 pulleys in PsA patients using ultrasound and concluded that pulley thickness could potentially be used to differentiate PsA from other forms of arthritis [30]. In addition, Graceffa et al. also demonstrated enthesal thickening in larger entheses in PsA and Pso patients, and

Table 3 Mean values ± standard deviation and intergroup comparisons of flexor tendon pulley inflammatory changes in PsA, RA, and HC patients

Finger + pulley	PsA Inflammatory changes	RA	HC	PsA vs RA <i>p</i> values	PsA vs HC	RA vs HC
D2 A1	2.82 ± 1.25	2.55 ± 1.43	0.94 ± 1.14	0.82	0.001	< 0.003
D2 A2	2.06 ± 1.08	1.75 ± 1.55	0.75 ± 1.03	0.77	0.02	0.08
D3 A1	3.24 ± 1.59	2.6 ± 1.16	0.69 ± 0.98	0.35	< 0.001	< 0.001
D3 A2	3.28 ± 1.62	1.85 ± 1.56	0.94 ± 1.03	0.02	< 0.001	0.2
D4 A1	2.65 ± 1.37	2.05 ± 1.24	0.5 ± 0.79	0.33	< 0.001	0.002
D4 A2	2.5 ± 1.12	1.7 ± 1.05	1.13 ± 1.11	0.1	0.002	0.32
D5 A1	2.18 ± 1.15	1.5 ± 1.57	0.38 ± 0.70	0.27	0.001	0.036
D5 A2	2.22 ± 1.27	1.95 ± 1.53	0.69 ± 0.98	0.82	0.007	0.03
D2–5 A1	10.88 ± 4.30	8.7 ± 3.15	2.5 ± 2.87	0.194	< 0.001	< 0.001
D2–5 A2	10.06 ± 3.11	7.25 ± 3.65	3.5 ± 3.51	0.031	< 0.001	0.004
D2–5 A1 + 2	20.65 ± 6.57	15.95 ± 7.01	6 ± 6.3	0.048	< 0.001	< 0.001

After (adapted) Bonferroni correction, *p* values < 0.0167 were considered significant and are printed in bold type

assumed that these distinct changes were triggered by inflammation [31]. Along with our findings, this contributes to the concept of “enthesitis being a hallmark of PsA,” even though we only considered patients with PsA, but not with Pso [25]. Further studies evaluating differences of pulley thickness and inflammation between patients with PsA, skin Pso, and nail Pso would be of great interest. Our high-resolution MRI study is the first to demonstrate these distinct PsA features using an alternative imaging method to sonography. Both modalities, ultrasound and MRI, are validated high-resolution imaging modalities for the evaluation of inflammatory joint changes in PsA such as thickening and inflammatory edema of tendons and ligaments. As compared to ultrasound, MRI is highly reproducible and can detect additional disease-related imaging features that ultrasound would miss such as bone marrow edema [32, 33]. MRI, however, is more time-consuming, less dynamic,

more expensive, and reliant on considerably larger infrastructural requirements [33]. In addition, this study demonstrated that flexor tendon pulleys of PsA patients were not only thicker than those of HC and RA patients, but also showed more frequent and intense inflammatory changes in their course and at their insertion sites. However, these findings were only numerically (not statistically) significant regarding RA patients. In 2015, Tan et al. had already demonstrated that MRI inflammatory changes of finger entheses were more frequent and severe in PsA patients than in HC, but they only evaluated fingers with acute dactylitis and did not use a dedicated 16-channel hand coil as we did in this study [13]. In particular when assessing small soft tissue structures as the A1 and A2 pulleys whose mean thickness we determined as 0.63 mm in healthy individuals (Table 4), MRI technique needs to be optimized regarding sequence parameter settings and coil and scanner

Table 4 Mean values ± standard deviation and intergroup comparisons of flexor tendon pulley thickness in PsA, RA, and HC patients

Finger + pulley	PsA Pulley thickness in mm	RA	HC	PsA vs RA <i>p</i> value	PsA vs HC	RA vs HC
D2 A1	0.86 ± 0.14	0.63 ± 0.10	0.62 ± 0.16	< 0.001	< 0.001	0.99
D2 A2	0.79 ± 0.13	0.54 ± 0.09	0.6 ± 0.11	< 0.001	< 0.001	0.45
D3 A1	0.82 ± 0.19	0.6 ± 0.09	0.64 ± 0.11	< 0.001	0.002	0.76
D3 A2	0.83 ± 0.11	0.58 ± 0.12	0.66 ± 0.18	< 0.001	0.006	0.269
D4 A1	0.71 ± 0.16	0.6 ± 0.09	0.61 ± 0.09	0.03	0.09	0.94
D4 A2	0.79 ± 0.12	0.58 ± 0.12	0.63 ± 0.13	< 0.001	0.008	0.54
D5 A1	0.76 ± 0.21	0.58 ± 0.08	0.64 ± 0.13	0.005	0.1	0.56
D5 A2	0.71 ± 0.21	0.61 ± 0.08	0.61 ± 0.12	0.13	0.15	1
D2–5 A1	0.79 ± 0.18	0.6 ± 0.09	0.63 ± 0.13	< 0.001	< 0.001	0.74
D2–5 A2	0.78 ± 0.15	0.58 ± 0.22	0.63 ± 0.14	< 0.001	< 0.001	0.21
D2–5 A1 + 2	0.79 ± 0.17	0.59 ± 0.19	0.63 ± 0.13	< 0.001	< 0.001	0.35

After (adapted) Bonferroni correction, *p* values < 0.0167 were considered significant and are printed in bold type

Table 5 Spearman rho correlation coefficient (ρ) for the score of inflammatory changes of flexor tendon pulleys (A1 and A2) and PsAMRIS sub-scores, total PsAMRIS, and flexor tendon pulley thickness at D2–5 in PsA and RA patients

	D2		D3		D4		D5	
	PsA	RA	PsA	RA	PsA	RA	PsA	RA
Synovitis	0.72	0.49	0.48	0.36	0.4	0.2	0.83	0.11
Flexor tenosynovitis	0.7	0.49	0.91	0.46	0.7	0.48	0.76	0.41
Periarticular inflammation	0.49	0.49	0.62	0.32	0.77	0.49	0.6	0.53
Bone erosion	0.37	0.16	0.43	0.31	0.13	na	0.62	0.28
Bone edema	0.52	– 0.34	0.66	0.39	0.36	na	0.28	na
Bone proliferation	– 0.03	na	– 0.05	na	– 0.44	na	0.05	na
Overall PsAMRIS	0.72	0.46	0.81	0.47	0.45	0.63	0.80	0.46
Pulley thickness	0.23		0.11		0.22		0.07	

na = non applicable

After (adapted) Bonferroni correction, p values < 0.0167 were considered significant and are printed in bold type

configurations enable true high-resolution imaging. Consequently, we achieved in-plane pixel dimensions of $0.3 \times 0.3 \text{ mm}^2$.

Our findings show inflammation of pulleys at both dactylitic and non-dactylitic fingers and, therefore, expand the value of pulley involvement beyond the scope of dactylitis. Potentially this is partly due to a higher image resolution using a 16-channel hand coil in the present study and suggests that the non-dactylitic tenosynovitis in PsA is also linked to pulley inflammation.

Furthermore, despite similar findings regarding pulley thickness, our data also showed more pulley-associated inflammation in RA patients than in HC. Considering that RA is primarily a synovial disease that is known to secondarily affect adjacent structures, such as flexor tendons, the involvement of entheses, and hence pulleys, seems evident. However, previous studies have shown that RA, despite involving the synovio-enthesal complex, primarily affects its synovial aspect; PsA on the other hand shows a stronger affection of its enthesal component [34]. Along with our findings of more intense and more frequent involvement of pulleys in PsA than in RA, this supports the idea of PsA being more predominantly an enthesal and extracapsular disease and contributes to the distinction of the two entities. In addition, it remains for future studies to assess whether these differences between both entities become more distinct in more distal pulleys, i.e., A 3–5. Since early diagnosis and treatment is pivotal for a better outcome in both entities and treatment options are increasingly diverging due to the development of biological and targeted synthesized disease-modifying anti-rheumatic drugs (bDMARD and tsDMARD), an early distinction between the two would be highly beneficial.

The presented data shows only a weak correlation between inflammatory changes and thickness of A1 and A2 flexor tendon pulleys in PsA patients. This could be due to the patient population of non-early PsA patients

that show side-by-side signs of acute inflammation and post-inflammatory changes in different joints/entheses. Thus, on the one hand, thickened pulleys could be associated with acute inflammation, while, on the other hand, being a result of previous inflammation. Baraliakos et al. also demonstrated that chronic changes of entheses can occur without inflammation present in patients with peripheral spondyloarthritis [35]. Despite a weak correlation between pulley thickness and inflammation, we found a strong correlation between pulley inflammation and overall PsAMRIS, flexor tenosynovitis, periarticular inflammation and synovitis, and to a lesser extent with bone erosion and bone edema sub-score. It is worth noting though that our population of PsA patients' scores for the PsAMRIS item "periarticular inflammation" were higher than in previous studies [24, 36]. However, in contrast to these studies, we have recruited patients who fulfilled the CASPAR criteria and additionally suffered from dactylitis of at least one digit. Since periarticular inflammation is considered an imaging core feature of dactylitis, our study design might have led to an overrepresentation of that particular PsAMRIS item. PsAMRIS and its sub-scores are validated tools for the detection and monitoring of disease-related joint changes. Therefore, inflammatory changes of pulleys could also be appropriate for the evaluation of disease-driven joint involvement [24]. In early 2019, Mathew et al. introduced a preliminary enthesitis-based MRI scoring system, named "Heel Enthesitis Scoring System" (HEMRIS) that emphasizes the value of enthesal changes for the diagnosis and monitoring of PsA [26].

The following limitations to this study must be considered when interpreting its results; as our study has only a small patient cohort size, our results have to be considered preliminary. Accordingly, further investigations with larger patient cohorts are required. The mean disease duration of the PsA and RA study population differed by approximately 109 weeks (RA 11, PsA 120

weeks). Applying current definitions, we hence compare non-early PsA with early RA populations (early RA: disease duration < 12 months; early PsA: disease duration < 24 months) [37, 38]. Thus, the comparability of both populations is potentially limited and the differences regarding inflammatory changes of the pulleys might be affected by differences in disease duration; however, because PsA is a very heterogeneous disease, the definition of disease onset and, therefore, an “early” patient population is challenging. In addition, enthesitis is a sign of acute inflammation, and hence not limited to advanced disease stages. Since the evaluation of enthesitis, namely inflammatory changes of flexor tendon pulleys, was our main goal, we consider the divergent disease duration only a minor limitation. However, in future investigations, study populations with a similar disease duration are required.

Even though the readers were blinded to the patients’ diagnosis, different field-of-views of certain sequences might have corrupted proper blinding.

Unfortunately, we did not systematically count swollen and tender joints in a per-digit and per-joint manner at the time of recruitment for the MRI studies. Thus, we cannot further elucidate the association of inflammatory pulley changes and their clinical manifestation. Therefore, future studies are required that further investigate the association of imaging features and clinical findings. MRI generally has a limited spatial resolution. Since flexor tendon pulleys frequently have a thickness of < 1 mm there is an increased risk of measuring inaccuracy due to partial volume effects, which may bring about substantial inter- and intra-rater variability. However, our findings show a good intra- and inter-rater reliability that is in coherence with previous studies regarding MRI measurements of pulleys and may also be the result of the optimized measurement setup that allows high-resolution imaging [39].

Conclusion

In conclusion, the assessment of high-resolution MRI changes of flexor tendon pulleys using a 16-channel hand coil could be used for disease detection in PsA and is potentially beneficial for the distinction from RA and HC.

Abbreviations

ACR: American College of Rheumatology; ADAM: Analysis of the DActylic Melange; aICC: Average measure ICC; bDMARD: Biological DMARD; CAR-ERA: Cartilage in early RA; CASPAR: Classification criteria for psoriatic arthritis; DIP: Distal interphalangeal; DMARD: Disease-modifying drug; EULAR: European League Against Rheumatism; HC: Healthy control; ICC: Intraclass correlation coefficient; MCP: Metacarpophalangeal; MRI: Magnetic resonance imaging; MTX: Methotrexate; OMERACT: Outcome measures in rheumatoid arthritis clinical trials; PD: Proton density; PIP: Proximal interphalangeal; PsA: Psoriatic arthritis; PsAMRIS: Psoriatic arthritis magnetic resonance imaging score; RA: Rheumatoid arthritis; RAMRIS: Rheumatoid arthritis magnetic resonance imaging score; SE: Spin

echo; sICC: Single measure ICC; STIR: Short tau inverse recovery; T: Tesla; T2T: Treat to target; TE: Echo time; TR: Relaxation time; tsDMARD: Targeted synthetic DMARD; TSE: Turbo spin echo

Acknowledgements

We thank Mrs. Erika Rädisch for the technical acquisition of all MRI studies.

Authors’ contributions

DBA contributed to the acquisition, analysis, and interpretation of data, and helped to draft and design the work. CS, DMCG, and PS contributed to the conception and design of the study, interpreted and analyzed data, and helped to draft, design, and revise the work. SN, MF, RB, and KLR contributed to the interpretation and analysis of data, helped to draft, design, and revise the work. SV, MS, and BO contributed to the design and conception of the study, helped draft, design, and revise the work. All authors read and approved the final manuscript.

Funding

DBA was supported by the local research committee of the medical faculty. PS and SV received funding from Pfizer Germany with the “Pfizer GiP Inflammation Germany Research Initiative 2014.” PS and BO received funding from AbbVie Deutschland GmbH & Co. KG for the “Delayed Gadolinium-enhanced MR Imaging of Cartilage—A pilot study to measure the effect of Adalimumab plus MTX versus Placebo plus MTX on cartilage in early RA patients (CAR-ERA) Study”. PS received a grant from the German “Bundesministerium für Bildung und Forschung” (BMBF), ArthroMark (01EC1009). SN has been supported by grants from the “Deutsche Forschungsgemeinschaft” (DFG) (NE 2136/3-1).

Availability of data and materials

The datasets used and/or analyzed during the current study are available from the corresponding author on reasonable request.

Ethics approval and consent to participate

The study was approved by the local ethics committee (MO-LKP-719, 4962R).

Consent for publication

Written and informed consent was obtained from all patients before the initiation of the study.

Competing interests

The authors declare that they have no competing interests.

Author details

¹Institute for Diagnostic and Interventional Radiology, UKD, Heinrich Heine University Düsseldorf, Moorenstrasse 5, 40225 Düsseldorf, Germany.

²Policlinic and Hiller Research Unit for Rheumatology, UKD, Heinrich Heine University Düsseldorf, Moorenstrasse 5, 40225 Düsseldorf, Germany. ³NIHR Leeds Musculoskeletal Biomedical Research Unit, Leeds Teaching Hospitals Trust and The University of Leeds, Leeds, UK.

Received: 27 November 2019 Accepted: 20 February 2020

Published online: 02 March 2020

References

1. Sewerin P, Brinks R, Schneider M, Haase I, Vordenbäumen S. Prevalence and incidence of psoriasis and psoriatic arthritis. *Ann Rheum Dis*. 2019;78:286–7.
2. Ritchlin CT, Colbert RA, Gladman DD. Psoriatic arthritis. *N Engl J Med*. 2017; 376:957–70.
3. Merola JF, Espinoza LR, Fleischmann R. Distinguishing rheumatoid arthritis from psoriatic arthritis. *RMD Open*. 2018;4:e000656.
4. Boutry N, do Carmo CCM, Flipo R-M, Cotten A. Early rheumatoid arthritis and its differentiation from other joint abnormalities. *Eur J Radiol*. 2009;71: 217–24.
5. Narváez J, Narváez JA, de Albert M, Gómez-Vaquero C, Nolla JM. Can magnetic resonance imaging of the hand and wrist differentiate between rheumatoid arthritis and psoriatic arthritis in the early stages of the disease? *Semin Arthritis Rheum*. 2012;42:234–45.
6. Sommer OJ, Kladošek A, Weiler V, Czembirek H, Boeck M, Stiskal M. Rheumatoid arthritis: a practical guide to state-of-the-art imaging, image interpretation, and clinical implications. *Radiographics*. 2005;25:381–98.

7. Benjamin M, Moriggi B, Brenner E, Emery P, McGonagle D, Redman S. The "entheses organ" concept: why enthesopathies may not present as focal insertional disorders. *Arthritis Rheum.* 2004;50:3306–13.
8. Benjamin M, McGonagle D. The anatomical basis for disease localisation in seronegative spondyloarthropathy at entheses and related sites. *J Anat.* 2001;199:503–26.
9. McGonagle D, Lories RJU, Tan AL, Benjamin M. The concept of a "synovio-enthesal complex" and its implications for understanding joint inflammation and damage in psoriatic arthritis and beyond. *Arthritis Rheum.* 2007;56:2482–91.
10. McGonagle D, Gibbon W, Emery P. Classification of inflammatory arthritis by enthesitis. *Lancet.* 1998;352:1137–40.
11. McGonagle D, Marzo-Ortega H, Benjamin M, Emery P. Report on the second international Enthesitis Workshop. *Arthritis Rheum.* 2003;48:896–905.
12. Gupta P, Lenchik L, Wuertzer SD, Pacholke DA. High-resolution 3-T MRI of the fingers: review of anatomy and common tendon and ligament injuries. *AJR Am J Roentgenol.* 2015;204:W314–23.
13. Tan AL, Fukuba E, Halliday NA, Tanner SF, Emery P, McGonagle D. High-resolution MRI assessment of dactylitis in psoriatic arthritis shows flexor tendon pulley and sheath-related enthesitis. *Ann Rheum Dis.* 2015;74:185–9.
14. Tinazzi I, McGonagle D, Aydin SZ, Chessa D, Marchetta A, Macchioni P. 'Deep Koebner' phenomenon of the flexor tendon-associated accessory pulleys as a novel factor in tenosynovitis and dactylitis in psoriatic arthritis. *Ann Rheum Dis.* 2018;77:922–5.
15. Kaeley GS, Eder L, Aydin SZ, Gutierrez M, Bakewell C. Dactylitis: a hallmark of psoriatic arthritis. *Semin Arthritis Rheum.* 2018;48:263–73.
16. Lubrano E, Mesina F, Caporali R. Clinical remission in rheumatoid arthritis and psoriatic arthritis. *Clin Exp Rheumatol.* 2018;36(5):900–10.
17. Coates LC. Treating to target in psoriatic arthritis. *Curr Opin Rheumatol.* 2015;27:107–10.
18. Coates LC, Rahman P, Psaradellis E, Rampakakis E, Osborne B, Lehman AJ, et al. Validation of new potential targets for remission and low disease activity in psoriatic arthritis in patients treated with golimumab. *Rheumatology (Oxford).* 2019;58(3):522–26.
19. Helliwell PS, Taylor WJ. Classification and diagnostic criteria for psoriatic arthritis. *Ann Rheum Dis.* 2005;64(Suppl 2):ii3–8.
20. Coates LC, McGonagle DM, Hodgson R, Gisoni P, Kavanaugh AF, Qureshi AA, et al. Imaging in psoriasis and psoriatic arthritis: GRAPPA 2008. *J Rheumatol.* 2010;37:448–52.
21. Congi L, Roussou E. Clinical application of the CASPAR criteria for psoriatic arthritis compared to other existing criteria. *Clin Exp Rheumatol.* 2010;28:304–10.
22. Østergaard M, McQueen F, Wiell C, Bird P, Bøyesen P, Ejlberg B, et al. The OMERACT psoriatic arthritis magnetic resonance imaging scoring system (PsAMRIS): definitions of key pathologies, suggested MRI sequences, and preliminary scoring system for PsA hands. *J Rheumatol.* 2009;36:1816–24.
23. Østergaard M, Bird P, Gandjbakhch F, Eshed I, Haugen IK, Haavardsholm EA, et al. The OMERACT MRI in arthritis working group - update on status and future research priorities. *J Rheumatol.* 2015;42:2470–2.
24. Glinatsi D, Bird P, Gandjbakhch F, Mease PJ, Bøyesen P, Peterfy CG, et al. Validation of the OMERACT psoriatic arthritis magnetic resonance imaging score (PsAMRIS) for the hand and foot in a randomized placebo-controlled trial. *J Rheumatol.* 2015;42:2473–9.
25. Kaeley GS, Eder L, Aydin SZ, Gutierrez M, Bakewell C. Enthesitis: a hallmark of psoriatic arthritis. *Semin Arthritis Rheum.* 2018;48:35–43.
26. Mathew AJ, Krabbe S, Eshed I, Gandjbakhch F, Bird P, Pedersen SJ, et al. The OMERACT MRI in enthesitis initiative: definitions of key pathologies, suggested MRI sequences, and a novel heel Enthesitis scoring system. *J Rheumatol.* 2019.
27. Østergaard M, Peterfy CG, Bird P, Gandjbakhch F, Glinatsi D, Eshed I, et al. The OMERACT rheumatoid arthritis magnetic resonance imaging (MRI) scoring system: updated recommendations by the OMERACT MRI in arthritis working group. *J Rheumatol.* 2017;44:1706–12.
28. Cohen J. A power primer. *Psychol Bull.* 1992;112:155–9.
29. Jevtic V, Watt I, Rozman B, Kos-Golja M, Demsar F, Jarh O. Distinctive radiological features of small hand joints in rheumatoid arthritis and seronegative spondyloarthritis demonstrated by contrast-enhanced (Gd-DTPA) magnetic resonance imaging. *Skelet Radiol.* 1995;24:351–5.
30. Furlan A, Stramare R. The thickening of flexor tendons pulleys: a useful ultrasonographic sign in the diagnosis of psoriatic arthritis. *J Ultrasound.* 2018;21:309–14.
31. Graceffa D, Bonifati C, Lora V, Saraceni PL, de Felice C, Chimenti MS, et al. Ultrasound assessment of entheses thickness in psoriasis and psoriatic arthritis: a cross-sectional study. *Indian J Dermatol Venereol Leprol.* 2019;85:175–81.
32. Anandarajah A. Imaging in psoriatic arthritis. *Clin Rev Allergy Immunol.* 2013;44:157–65.
33. Lento PH, Primack S. Advances and utility of diagnostic ultrasound in musculoskeletal medicine. *Curr Rev Musculoskelet Med.* 2008;1:24–31.
34. Zabotti A, Salvin S, Quartuccio L, de Vita S. Differentiation between early rheumatoid and early psoriatic arthritis by the ultrasonographic study of the synovio-enthesal complex of the small joints of the hands. *Clin Exp Rheumatol.* 2016;34:459–65.
35. Baraliakos X, Kiltz U, Appel H, Dybowski F, Igelmann M, Kalthoff L, et al. Chronic but not inflammatory changes at the Achilles' tendon differentiate patients with peripheral spondyloarthritis from other diagnoses - results from a prospective clinical trial. *RMD Open.* 2017;3:e000541.
36. Bøyesen P, McQueen FM, Gandjbakhch F, Lillegraven S, Coates L, Wiell C, et al. The OMERACT psoriatic arthritis magnetic resonance imaging score (PsAMRIS) is reliable and sensitive to change: results from an OMERACT workshop. *J Rheumatol.* 2011;38:2034–8.
37. Gladman DD. Early psoriatic arthritis. *Rheum Dis Clin N Am.* 2012;38:373–86.
38. Heidari B. Rheumatoid arthritis: early diagnosis and treatment outcomes. *Caspian J Intern Med.* 2011;2:161–70.
39. Hirschmann A, Sutter R, Schweizer A, Pfirrmann CWA. MRI of the thumb: anatomy and spectrum of findings in asymptomatic volunteers. *AJR Am J Roentgenol.* 2014;202:819–27.

Publisher's Note

Springer Nature remains neutral with regard to jurisdictional claims in published maps and institutional affiliations.

Ready to submit your research? Choose BMC and benefit from:

- fast, convenient online submission
- thorough peer review by experienced researchers in your field
- rapid publication on acceptance
- support for research data, including large and complex data types
- gold Open Access which fosters wider collaboration and increased citations
- maximum visibility for your research: over 100M website views per year

At BMC, research is always in progress.

Learn more [biomedcentral.com/submissions](https://www.biomedcentral.com/submissions)





Detection of early cartilage degeneration in the tibiotalar joint using 3 T gagCEST imaging: a feasibility study

Daniel B. Abrar¹ · Christoph Schleich¹ · Karl Ludger Radke¹ · Miriam Frenken¹ · Julia Stabinska¹ · Alexandra Ljimini¹ · Hans-Jörg Wittsack¹ · Gerald Antoch¹ · Bernd Bittersohl² · Tobias Hesper² · Sven Nebelung¹ · Anja Müller-Lutz¹

Received: 31 March 2020 / Revised: 10 July 2020 / Accepted: 14 July 2020
© The Author(s) 2020

Abstract

Objective To establish and optimize a stable 3 Tesla (T) glycosaminoglycan chemical exchange saturation transfer (gagCEST) imaging protocol for assessing the articular cartilage of the tibiotalar joint in healthy volunteers and patients after a sustained injury to the ankle.

Methods Using Bloch–McConnell simulations, we optimized the sequence protocol for a 3 T MRI scanner for maximum gagCEST effect size within a clinically feasible time frame of less than 07:30 min. This protocol was then used to analyze the gagCEST effect of the articular cartilage of the tibiotalar joint of 17 healthy volunteers and five patients with osteochondral lesions of the talus following ankle trauma. Reproducibility was tested with the intraclass correlation coefficient.

Results The mean magnetization transfer ratio asymmetry (MTR_{asym}), i.e., the gagCEST effect size, was significantly lower in patients than in healthy volunteers ($0.34 \pm 1.9\%$ vs. $1.49 \pm 0.11\%$; $p < 0.001$ [linear mixed model]). Intra- and inter-rater reproducibility was excellent with an average measure intraclass correlation coefficient (ICC) of 0.97 and a single measure ICC of 0.91 ($p < 0.01$).

Discussion In this feasibility study, pre-morphological tibiotalar joint cartilage damage was quantitatively assessable on the basis of the optimized 3 T gagCEST imaging protocol that allowed stable quantification gagCEST effect sizes across a wide range of health and disease in clinically feasible acquisition times.

Keywords Cartilage · Magnetic resonance imaging · Proteoglycans · Osteoarthritis · Molecular imaging

Introduction

To this day and age, several magnetic resonance imaging (MRI) techniques have emerged that go beyond mere morphological depiction of joint cartilage. Such compositional MRI techniques allow the detection of early degenerative changes of the articular cartilage, e.g., loss of proteoglycans, that precede morphological damage and hence are considered an early, and more importantly, reversible, stage of osteoarthritis (OA) [1]. Because of its proteoglycan-specificity, the gold-standard technique of compositional MRI of cartilage is delayed gadolinium-enhanced MRI of cartilage (dGEMRIC) [2, 3]. However, due to recent restrictions imposed on gadolinium-based contrast agents, alternative compositional MRI techniques that do not rely on the administration of contrast agents have received ever-increasing scientific and clinical attention [4]. Among these techniques, glycosaminoglycan chemical

Daniel B. Abrar and Christoph Schleich have contributed equally to this work.

Sven Nebelung and Anja Müller-Lutz have contributed equally to this work.

Electronic supplementary material The online version of this article (<https://doi.org/10.1007/s10334-020-00868-y>) contains supplementary material, which is available to authorized users.

✉ Daniel B. Abrar
DanielBenjamin.Abrar@med.uni-duesseldorf.de

¹ Department of Diagnostic and Interventional Radiology, Medical Faculty, University Hospital Düsseldorf, University Düsseldorf, Moorenstraße 5, 40225 Düsseldorf, Germany

² Department of Orthopedic and Trauma Surgery, Medical Faculty, Heinrich-Heine University Düsseldorf, Düsseldorf, Germany

exchange saturation transfer (gagCEST) imaging assesses the specific GAG content in human articular cartilage and its depletion, which is considered an early sign of cartilage degeneration [5].

GagCEST imaging is based upon the chemical exchange of water protons between GAG and bulk water molecules. To induce a CEST effect, solute protons are saturated by a frequency-specific radiofrequency (RF) pulse and then transferred to bulk water by chemical exchange, which consequently reduces its signal. The normalized signal can then be used to quantify the CEST effect at a GAG-specific frequency range of 0.9–1.9 ppm via analysis of the magnetization transfer ratio asymmetry (MTR_{asym}), which correlates with the GAG concentration [5, 6]. For additional details on the basic principles of CEST imaging, the interested reader is referred to earlier excellent reviews [7, 8]. Several studies showed promising results using gagCEST imaging at the spine [9–12]. However, data on the joints of the lower extremity with substantially thinner cartilage are sparse. In 2016, our group demonstrated promising results for the application of gagCEST at the knee joint [13]. Kogan et al. applied gagCEST imaging on a 7 T MRI scanner to assess the ankle joint of healthy volunteers [14]. Even though these results were promising, gagCEST imaging of the ankle joint has not yet been established on a 3 T MRI scanner. To achieve a more widespread scientific and clinical adaptation of the technique, the clinical utility has to be demonstrated on a broader scale, which -given the limited availability of 7 T MRI scanners- necessitates the technique's implementation on more widely available 3 T MRI scanners.

Tibiotalar joint injuries are common [15]. Osteochondral lesions of the talus (OLT), defined as an injury of the cartilage layer and the underlying subchondral bone, are frequent injuries in active populations that can be seen in up to 73% of all traumatic ankle injuries [16]. OLTs may predispose the joint to premature OA and ought to be diagnosed in an early and reliable manner as a timely diagnosis is a pre-requisite for appropriate treatment [17].

The aim of this study was (a) to develop and optimize a gagCEST imaging protocol for the articular cartilage of the tibiotalar joint that is clinically feasible and fits into diagnostic workflows and (b) to apply this imaging protocol to a population of healthy volunteers and patients with OLT after an ankle injury to prove clinical utility and validity. We hypothesized that -based on the developed and optimized gagCEST imaging protocol- (a) imaging of the articular cartilage of the tibiotalar joint would be possible in a clinical population and in clinically feasible time frames and (b) patients after variable ankle injuries (representative of the patient population undergoing MRI diagnostics in the clinic) demonstrate lower gagCEST effects compared to healthy volunteers.

Methods

Simulations

In a first step, simulations using the two-pool (water and GAG (-OH and -NH) Bloch–McConnell equation [18, 19] and a customized script (implemented in MATLAB [R2018a, The MathWorks, MA, USA] and to be downloaded at https://github.com/cest-sources/BM_sim_fit/) [20] were applied for the optimization of a pulsed gagCEST sequence [20–22]. The equations were solved analytically [19]. Based on this script, the CEST effect was simulated without the application of a saturation pulse. The radiofrequency field strength B_1 , the pulse duration t_p and the number of CEST saturation pulses n_p were varied using a constant duty cycle (DC) of 0.5. To keep the specific absorption rate (SAR) within the safe range, local SAR was restricted accordingly. Therefore, the maximum pulse duration was secondarily restricted by the scanner to a maximum of 300 ms. For water, simulations were performed with relaxation times as reported earlier, i.e., $T_1 = 1.2$ s and $T_2 = 0.039$ s and a concentration of 88 M [23, 24]. The following parameters were used for GAG-OH protons: exchange rate = 1000 Hz, concentration 0.3 M, $T_1 = 1$ s, $T_2 = 0.01$ s and chemical shift = 1 ppm, and for GAG-NH protons: exchange rate = 50 Hz, concentration = 0.1 M, $T_1 = 1$ s, $T_2 = 0.01$ s and chemical shift = 3.2 ppm [24, 25]. The different variations of the parameters used in the simulation are displayed in Table 1; output parameters were z-spectra and MTR_{asym} curves. For each parameter, the maximum MTR_{asym} value was analytically determined at a step size of 0.01, 0.02 and 0.05 ppm at frequency offsets of 0.9–1.9 ppm, 0.5–1.5 ppm and 1–1.5 ppm. The optimized protocol in terms of the largest gagCEST effect at a reasonable acquisition time was used for the subsequent in-vivo studies.

Table 1 Details of sequence parameters used for simulating each parameter's contribution to quantitatively assess GAG exchange processes based on Bloch–McConnell simulations

Experiment	n_p	t_p (ms)	B_1 [μ T]
1	6	100	0.2; 0.4; 0.6; 0.8; 1.0; 1.2; 1.4
2	6	100; 200; 300	1.0
3	2; 4; 6; 8; 10; 12; 14	100	1.0

In each experiment, one of the three parameters (number of pulses n_p , pulse duration t_p , and radiofrequency-field strength B_1) was systematically varied

In-vivo study

Study population

19 healthy volunteers (mean age 23.0 ± 3.8 , range 20–37 years, 11 males, 8 females) and six patients (mean age 31.7 ± 9.3 , range 20–44 years, two males, four females) after earlier ankle injury were recruited from 06/2018 to 01/2019 via dedicated specialist consultations at our Department of Orthopedic and Trauma Surgery. The predefined inclusion criterion for patients was an isolated traumatic OLT lesion as diagnosed in earlier MRI studies. At the time of recruitment, patients were graded according to the Anderson modification of the Berndt and Harty classification and four patients had grade 1 and two patients grade 2b OLT lesions [15, 16]. Predefined exclusion criteria for healthy volunteers included all forms of primary or secondary OA of the ankle as well as other bone and joint disorders such as OLT, rheumatoid arthritis, avascular necrosis, gouty arthritis, septic arthritis, Paget disease or osteochondritis dissecans. Volunteers were also excluded if they had acute or chronic ankle pain or a history of serious trauma or surgery to the index ankle joint.

The MRI data sets of one patient and two healthy volunteers had to be excluded from image analysis due to excessive motion artifacts. The mean disease duration of patients was 22 ± 30 months (range 1–60 months). Written and informed consent was obtained from all patients before the initiation of the study. The study was approved by the local ethics committee (Ethical Committee of the University Hospital Düsseldorf, study number: 3980).

MRI studies

All imaging studies were performed on a 3 T MRI scanner (Magnetom Prisma, Siemens Healthineers, Erlangen, Germany) using a dedicated receive-only 16-channel foot–ankle coil (Foot/Ankle 16, Siemens Healthineers). Patients and volunteers were scanned in the supine position with a neutral ankle position of 90° dorsiflexion. Positioning aids, sandbags and medical tape were used to reduce motion artifacts.

The MRI protocol included standard morphological sequences, i.e., sagittal (sag) and coronal (cor) Proton Density-weighted (PDw) fat-saturated (fs) sequences, transversal (tra) T2-weighted turbo-spin echo (TSE), and cor T1-weighted TSE sequences. In addition to the actual gagCEST sequence as detailed below, water saturation shift referencing (WASSR), T1 mapping gradient echo (GE) and T2 multi-spin-echo (SE) mapping sequences with five different echo times (13.8, 27.6, 41.4, 55.2 and 69 ms) were acquired. Of note, the latter two sequences were only acquired in the healthy volunteers and not in the patients. GagCEST imaging was performed using a two-dimensional (2D) radiofrequency (RF)-spoiled GE sequence

with a pulsed CEST pre-saturation module consisting of 8 Gaussian-shaped RF pulses with a duty cycle of 0.5. 26 images with pre-saturation pulses at different offset frequencies around the bulk water resonance were obtained. Among these images was one reference image with a frequency offset of 300 ppm. The maximum frequency offset ($\Delta\omega$) was 4 ppm with a step size of 0.33 ppm. In a fraction of the healthy volunteer cohort ($n = 10$, mean age 22.4 ± 1.8 , range 20–25 years, seven males, three females) radiofrequency field strengths and pulse durations were systematically varied to optimize the protocol at the beginning of the study. More specifically, three different radiofrequency field strengths ($B_1 = 0.6, 0.8$ and $1.0 \mu\text{T}$) and three different pulse durations ($t_p = 100, 200$ and 300 ms) were used. Based on the results of the simulations, i.e., the largest measured MTR_{asym} values, we used a radiofrequency field strength of $B_1 = 0.8$ and a pulse duration $t_p = 300$ ms in the remaining healthy volunteer and patient cohorts. For the WASSR sequence, 22 images with pre-saturation and a reduced radiofrequency field strength ($B_1 = 0.25 \mu\text{T}$) were obtained. The maximum frequency offset was decreased to $\Delta\omega = 1$ ppm with a step size of 0.1 ppm. For WASSR and CEST sequences, motion correction was applied. The acquisition time was 5:01 min for the CEST and 2:22 min for the WASSR sequence. The total acquisition times for the compositional MRI sequences were: 24:21 min for the initial 10 healthy volunteers ($3 \times 5:05$ min CEST, $1 \times 2:22$ min WASSR, $6 \times 1:14$ min T1) and 7:27 min for the remaining 7 healthy volunteers and the 5 patients ($1 \times 5:05$ min CEST and $1 \times 2:22$ min WASSR). The acquisition time for the morphological sequences was 18 min, resulting in a total scan time of 42:21 min for the initial 10 volunteers and 25:27 min for the consecutive 7 volunteers and the 5 patients.

Detailed parameters of the morphological and compositional sequences are given in Tables 2 and 3.

Image analysis

All images were independently analyzed by two radiologists (DBA, 3 years of training in musculoskeletal imaging; CS, 8 years of training in musculoskeletal imaging) who were blinded to the volunteers' or patients' data. First, all studies were read to determine the individual joint's overall status with a particular focus on the integrity of tibiotalar cartilage. Also, OLTs were -if present- classified according to Hepple et al. [26]. Second, using the unsaturated WASSR image, both readers independently identified the cartilage layers of the tibiotalar joint and quantified its biophysical properties in a standardized manner by placing an ellipsoid-shaped region-of-interest (ROI) in the median plane onto both cartilage layers at the central load-bearing region of the tibiotalar joint. Each ROI was placed distant to the tibial and talar bone cortex and the anterior and posterior joint

Table 2 Detailed sequence parameters of morphological MRI sequences

Imaging parameter	Sagittal fs PDw	Coronal fs PDw	Transversal T2w TSE	Coronal T1w TSE
FOV (mm)	160×160	160×160	160×160	160×160
Slice thickness (mm)	3	3	3	3
TE (ms)	40	40	78	17
TR (ms)	4000	4000	4600	700
Resolution (mm/pixel)	0.31×0.42	0.31×0.42	0.31×0.39	0.28×0.4
Flip angle (°)	150	150	150	140
Acquisition matrix	512×384	512×384	512×410	576×403

Field of view (FOV), slice thickness, echo time (TE), repetition time (TR), resolution, flip angle, and acquisition matrix are given for sagittal and coronal fat-saturated proton-density-weighted (fs PDw), transversal T2-weighted turbo spin echo (T2w TSE) and coronal T1-weighted TSE (T1w TSE) sequences

Table 3 Detailed sequence parameters of compositional MRI sequences

Imaging parameter	WASSR	gagCEST	T1 map	T2 map
FOV (mm)	160×160	160×160	160×160	160×160
Slice thickness (mm)	5	5	7	3 mm
TE (ms)	3.5	3.5	11	13.8/27.6, 41.4/55.2/69
TR (ms)	7.2	7.2	6000	1000
TI (ms)			25/50/100/500/1000/2000	
Resolution (mm/pixel)	0.6×0.6	0.6×0.6	0.6×0.6	0.4×0.4
Flip angle (°)	15	15	180	180
Pulsed CEST saturation module				
Frequency range (ppm – ppm)	– 1 to 1	– 3 to 3		
Number of Dynamic Scans	21 + 1	25 + 1 reference image		
Number of saturation pulses	1	8		
Pulse Duration t_p (ms)	54	300 (100, 200)		
Interpulse Duration (ms)	–	300		
B_1 amplitude (μ T)	0.2	0.8 (0.6, 1.0)		

In healthy volunteers, pulse duration t_p and B_1 amplitude were evaluated at 100, 200, and 300 ms and at 0.6, 0.8, and 1.0 μ T, respectively, while in patients, the following parameter settings were used: 300 ms and 0.8 μ T

WASSR water saturation, gagCEST glycosaminoglycan chemical exchange saturation transfer imaging, FOV field of view, TE echo time, TR repetition time, TI inversion time

areas to reduce partial volume artifacts due to the presence of cortical bone and potentially excessive amounts of joint fluid (Fig. 1). The second reader repeated the ROI placement at a different time point to allow for the assessment of inter-rater reliability.

For the analysis of the MTR_{asym} curve, i.e., the CEST effect, we used an in-house script implemented in Matlab (MATLAB R2018a, The MathWorks, Inc., MA, USA). Prior to further evaluation, B_0 field inhomogeneities were corrected by the WASSR maximum-symmetry algorithm with the calculation of a pixel-wise frequency offset curve [27, 28]. These offset-corrected CEST-curves divided by the signal without pre-saturation (S_0) were defined as the so-called z-spectrum ($Z(\omega)$). The maximum frequency offset of each z-spectrum was $\Delta\omega = 3$ ppm. Next, we used the

magnetization transfer asymmetry (MTR_{asym}) (defined as $MTR_{asym}(\Delta\omega) = Z(-\Delta\omega) - Z(\Delta\omega)$) for the evaluation of the gagCEST effect [29]. MTR_{asym} maps were calculated using the average value of MTR_{asym} in the GAG-specific range of $\Delta\omega = 0.9 - 1.9$ ppm [30]. In addition, the B_0 -corrected and -normalized spectra were fitted using Lorentzian function analysis to account for the GAG-OH, GAG-NH, water pools at -1 ppm, the nuclear Overhauser effect at -1 and -2.8 ppm and the magnetization transfer pool at -2.43 ppm [31, 32]. In the following, the Lorentzian-fitted gagCEST effect is given as GAG-OH amplitude.

T1 and T2 relaxation times calculations in ten healthy volunteers were also performed in Matlab. In a pixel-wise manner, acquired data was fitted and calculated based on the following equations:

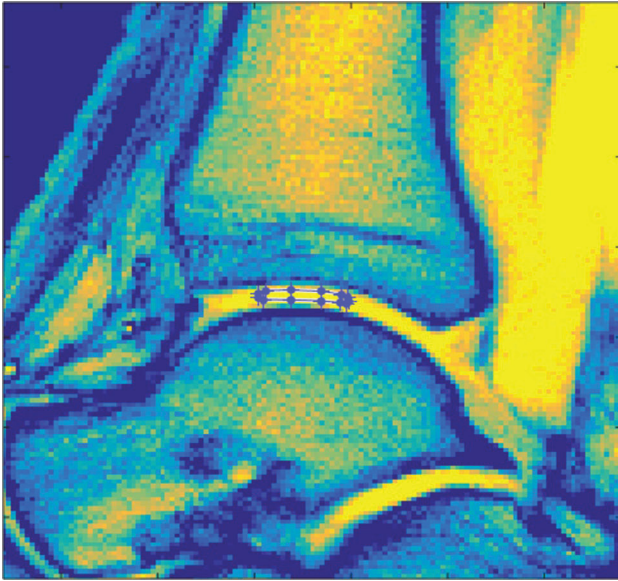


Fig. 1 Exemplary image detailing the region-of-interest (ROI) definition. Water saturation shift referencing sequence (WASSR) image of the tibiotalar joint of a 29-year-old healthy male. Manual definition of the ROI in the central weight-bearing region of the tibiotalar joint was performed individually by two radiologists to include the cartilage layers of the tibiotalar joints while reducing partial volume artifacts due to cortical bone and/or joint fluid

$$T1: M_z(t) = M_z^0 - (M_z^0 - M_z(0)) \exp\left(\frac{-t}{T_1}\right)$$

$$T2: M_{xy}(t) = M_{xy}(0) \exp\left(\frac{-t}{T_2}\right)$$

with T1 and T2 being the sought relaxation times, $M_z(t)$ the total magnetization in the z -direction, and $M_{xy}(t)$ the total magnetization in the xy -plane at time point t .

Statistical analysis

SPSS software (IBM, version 22, Armonk, NY, USA) was used for all statistical analyses by KLR and DBA. For descriptive analysis, mean gagCEST values \pm standard deviation, median, and range (minimum–maximum) were calculated for healthy volunteers and patients. For optimization of the imaging protocol radiofrequency field strength and pulse duration were systematically varied and then compared using a multivariate analysis of variance (MANOVA) and a post-hoc Scheffé-test. For the comparison of gagCEST values between both cohorts, a multivariable statistical analysis was performed using a linear mixed model (LMM). The established model included a subject-specific random intercept, the factors healthy volunteer/patient, age, gender and the interaction of these factors assuming a fixed linear effect

on the gagCEST values. Results of this model are given in Table 1 of the Supplementary Material. The LMM was fitted using a restricted maximum likelihood approach (REML). Based on this final model, the mean differences of gagCEST values were calculated and evaluated for significance. For correlation analyses of MTR_{asym} values and GAG-OH amplitudes, Pearson's correlation was determined and quantified using the correlation coefficient r . Correlation strength was graded as suggested by Cohen [33]: small (0.1–0.3), moderate (0.3–0.5), and large (>0.5). p values <0.05 were considered significant. For the evaluation of inter- and intrarater reliability, single and average measure intraclass correlation coefficients (sICC and aICC) were calculated based on the ROIs drawn by the two raters.

Results

Simulations

The results of the systematic simulations are illustrated in Figs. 2 and 3.

- Variation of t_p .
Maximum MTR_{asym} values were 1.33 % at 0.9–1.9 ppm with $t_p = 200$ ms, 1.07 % at 0.5–1.5 ppm with $t_p = 100$ ms and 1.37 % at 1.0–1.5 ppm with $t_p = 100$ ms (Fig. 3a).
- Variation of n_p .
The CEST effect increases with the number of applied saturation pulses (n_p) (Fig. 3b). Eight applied pulses reach 98% of the maximum gagCEST effect that could be obtained with 14 pulses at all ranges (0.9–1.9 ppm, 0.5–1.5 ppm and 1.0–1.5 ppm). Maximum MTR_{asym} values with eight applied pulses were 1.33 % at 0.9–1.9 ppm, 1.02 % at 0.5–1.5 ppm and 1.33 % at 1.0–1.5 ppm.
- Variation of B_1 .

The CEST effect increases with increasing B_1 until it reaches a maximum (Fig. 3c). Due to the spillover effect, MTR_{asym} values decrease beyond the maximum. Maximum MTR_{asym} values were 1.33 % at 0.9–1.9 ppm and a B_1 of 1 μ T, 1.17 % at 0.5–1.5 ppm and a B_1 of 0.8 μ T and 1.37 % at 1.0–1.5 ppm and a B_1 of 1 μ T.

In-vivo studies

Morphological MRI of patients and healthy volunteers

Apart from the presence of OLTs as outlined below and a moderate joint effusion, the overall joint status of three of

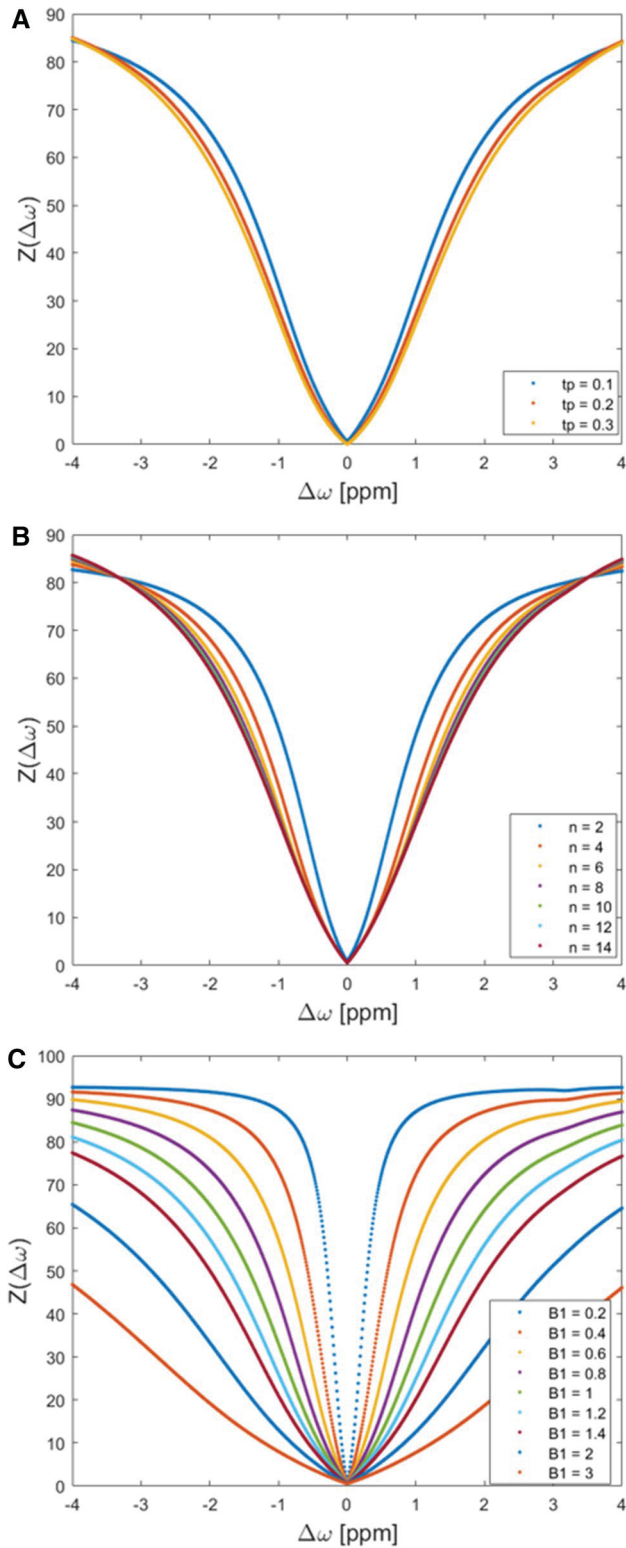


Fig. 2 Simulations results detailing the effects of variations in CEST framework conditions. Pulse durations t_p (100, 200, and 300 ms) (a), number of applied pulses n_p ($n=2-14$) (b), and radiofrequency field strengths B_1 (0.2–3 μT) (c) were systematically varied. Each colored curve represents a simulated parameter value and gives the z-spectrum at different offset frequencies (0–4 ppm)

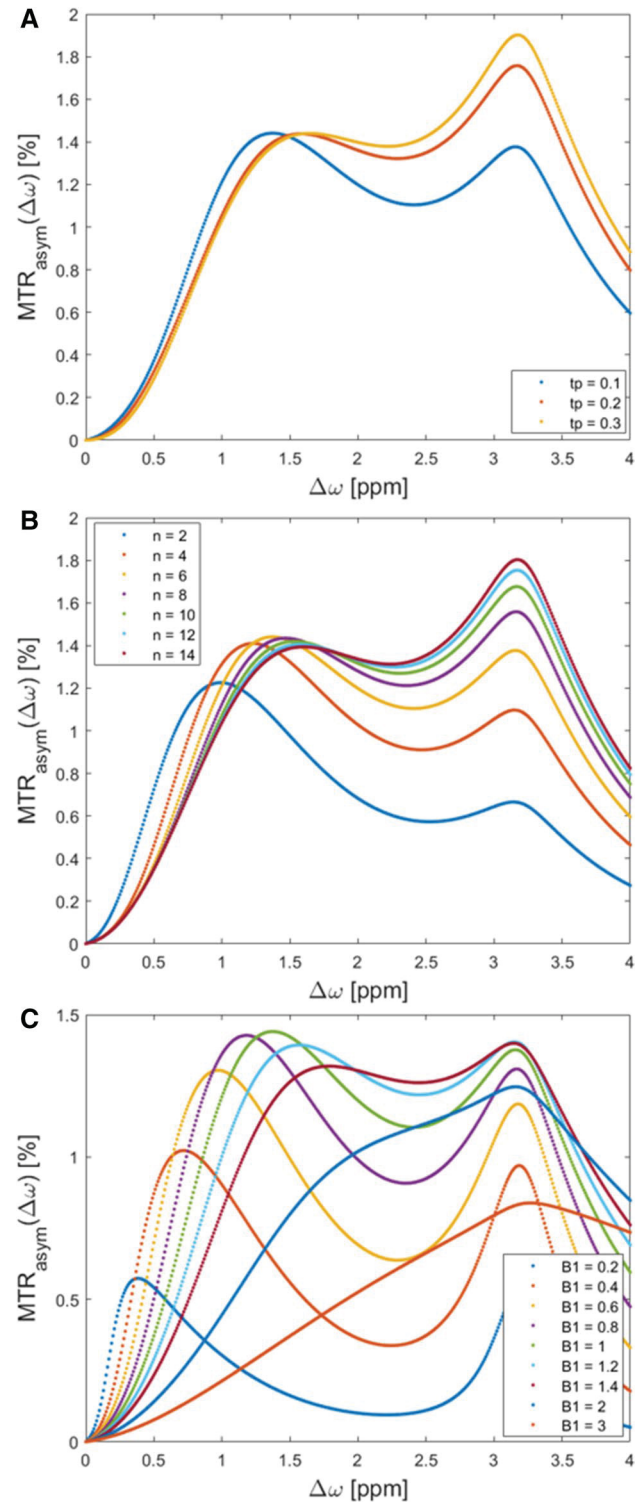


Fig. 3 Simulations results detailing the effects of variations in CEST framework conditions. Pulse durations t_p (100, 200, and 300 ms) (a), number of applied pulses n_p ($n=2-14$) (b), and radiofrequency field strengths B_1 (0.2–1.4 μT) (c) were systematically varied. Each colored curve represents a simulated parameter value and gives the maximum magnetization transfer ratio asymmetry at different offset frequencies (0–4 ppm)

five patients was unremarkable. In them, we did not find any bone marrow lesions, subchondral thickening, osteophytes or joint space narrowing. In two patients, we noted signs of secondary OA with osteophytes, joint space narrowing, subchondral sclerosis, and moderate joint effusion. The joint status of healthy volunteers was unremarkable without any structural alterations. Within the entire study population, the following accessory ossicles were found: Os tibiale externum in six individuals, Os trigonum in three individuals, Os supratolare in one individual.

Staging of OLTs was performed according to the Heppner classification (stages 1–5, 1: articular cartilage damage only, 2a: cartilage injury with underlying fracture and surrounding edema, 2b: 2a without surrounding edema, 3: detached, but undisplaced fragment, 4: detached and displaced fragment, 5: subchondral cyst). The following stages were observed in the patient cohort: one individual with stage 2a, one individual with stage 3, one individual with stage 4 and two individuals with stage 5.

Implementation of the optimized protocol in 10 healthy volunteers

Table 4 gives the details of the MTR_{asym} values in 10 healthy volunteers as a function of systematically varied parameter settings of B_1 (0.6, 0.8, and 1.0 μT) and t_p (100, 200, and 300 ms).

a. Variation of B_1 .

The mean MTR_{asym} values had a maximum of $1.7 \pm 1.4\%$ at 0.8 μT and tended to be -even though non-significantly- numerically higher than at 1.0 μT ($0.5 \pm 1.0\%$, $p = 0.073$) and at 0.6 μT ($1.3 \pm 1.1\%$, $p = 0.759$).

b. Variation of t_p .

The highest mean MTR_{asym} values were found at $t_p = 300$ ms that were significantly higher than at $t_p = 100$ ms (1.67

vs. 0.12 %, $p < 0.004$) and tended to be higher than at $t_p = 200$ ms (1.67 vs 0.71 %, $p = 0.092$).

Implementation of the optimized protocol in all healthy volunteers and patients

a. MTR_{asym} values and GAG-OH amplitude of healthy volunteers vs. patients.

Using the optimized imaging protocol (with the following framework conditions: radiofrequency-field strength $B_1 = 0.8$, pulse duration $t_p = 300$ ms and number of pulses $n_p = 8$), the mean MTR_{asym} value of the tibiotalar joint cartilage in patients was $0.3 \pm 0.2\%$ (95 % confidence interval [CI] 0–0.7) and in healthy volunteers was $1.5 \pm 0.9\%$ (95 % CI 1.3–1.7) ($p < 0.001$). MTR_{asym} values are visualized in Fig. 3. Corresponding gagCEST maps are given in Fig. 4.

Gag-OH amplitudes of the tibiotalar joint cartilage in patients were $0.8 \pm 0.4\%$ (95% CI 0–1.6) and in healthy volunteers $2.0 \pm 0.2\%$ (CI 1.6–2.4) ($p = 0.013$). We found strong and significant correlations between mean MTR_{asym} values and gagOH amplitudes ($r = 0.56$, $p = 0.006$).

No significant differences were found between the volunteers that were used for protocol optimization and the remaining volunteers (volunteer cohort 1: MTR_{asym} : $1.5 \pm 0.9\%$, volunteer cohort 2: MTR_{asym} : $1.4 \pm 0.9\%$, $p = 0.715$).

The reproducibility of the MTR_{asym} values of all ROIs was excellent (aICC= 0.97, 95% confidence intervals 0.82/0.95, $p < 0.001$ and sICC= 0.91, 95% CI 0.93/0.98, $p < 0.001$).

b. T1 and T2 relaxation times in healthy volunteers.

The in-vivo measurements in healthy volunteers showed a mean T1 relaxation time of 940 ± 120 ms (range 720–1080 ms) and a mean T2 relaxation time of 35 ± 7 ms (range 26–48 ms) (Figs. 5, 6).

Table 4 Magnetization transfer ratio asymmetry (MTR_{asym}) values as a function of systematically varied B_1 and t_p in 10 healthy volunteers

Offset frequency [ppm]	B_1 (μT)	t_p (ms)	MTR_{asym} (%)	p value
0.9–1.9	0.6	100	0.37 ± 0.78	100 vs. 200 ms: < 0.001
		200	0.75 ± 0.65	100 vs. 300 ms: < 0.001
		300	1.34 ± 1.05	200 vs. 300 ms: 0.016
	0.8	100	0.12 ± 0.47	0.6 vs. 0.8:
		200	0.71 ± 0.81	1.0
		300	1.67 ± 1.35	0.6 vs. 1.0: 0.001
	1.0	100	0.27 ± 0.78	0.8 vs. 1.0: < 0.001
		200	0.94 ± 1.02	
		300	0.49 ± 0.95	

MTR_{asym} values are given as mean \pm standard deviation

Means were compared using a multivariate analysis of variance (MANOVA) followed by a post-hoc Scheffé test

p values < 0.05 were considered significant and are given in bold type

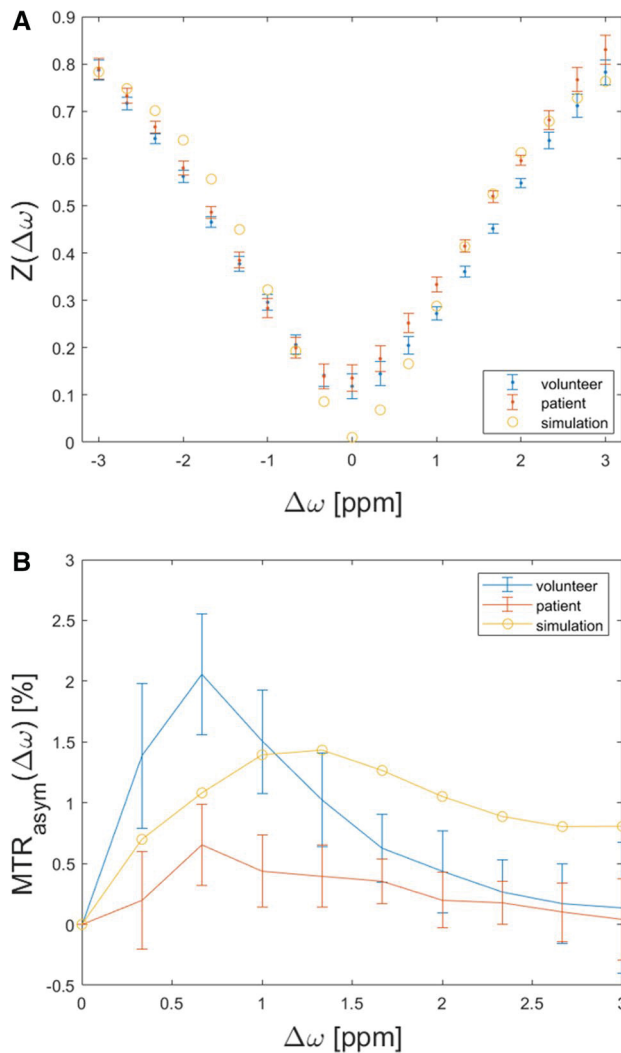


Fig. 4 Illustration of Z-spectra (a) and MTR_{asym} (b) curves of the simulation (blue), a volunteer (yellow) and a patient (orange). CEST framework conditions were $B_1=0.8$, $t_p=300$ ms and $n_p=8$. Simulations results For the patient's and volunteer's curves means (dots) and standard deviations (whiskers) are given. Of note, the GAG-NH peak is only visible in the simulation, but not in-vivo

Discussion

The most important finding of this study is that following comprehensive and systematic sequence optimization-gagCEST imaging of the tibiotalar joint is feasible using a clinical standard 3 T MRI scanner, fits into clinical workflows with an acquisition time of less than 07:30 min, and yields stable and reproducible results that allow compositional cartilage assessment. In addition, we demonstrated that the tibiotalar joint cartilage of patients with known tibiotalar joint injury, especially OLT, have significantly lower gagCEST values than healthy volunteers.

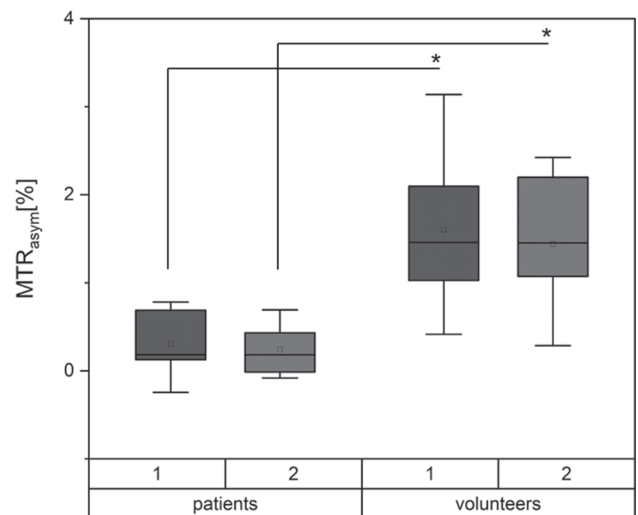


Fig. 5 Comparison of MTR_{asym} values in patients and healthy volunteers. Data are presented as means (thick line), medians (square boxes), standard deviation (boxes), and ranges (whiskers). For each cohort, two separate boxes are presented: 1 gives the MTR_{asym} values of the ROI defined by rater 1. Box 2 depicts the MTR_{asym} values of the corresponding ROIs of rater 2. p values < 0.05 were considered significant and are highlighted with an asterisk

Compositional MRI exceeds the mere morphological depiction of cartilage and allows for the detection of early cartilage changes that precede morphological alterations, i.e., loss of proteoglycans, as an early, potentially treatable stage of OA. GagCEST can be used for the detection and treatment monitoring of very early OA [34]. Despite this great clinical need, research on gagCEST imaging in general has been limited by the numerous technical complexities involved such as homogeneous magnetic field properties, long scan times, low SNR, and high field strengths (optimally ≥ 7.0 T) that are considered necessary for cartilage imaging [35]. Moreover, with the majority of imaging studies focusing on the knee joint, data on the tibiotalar joint is sparse [14]. This is mainly due to the joint's limited cartilage thickness, measuring only about 2 mm in healthy individuals and the known limited spatial resolution of gagCEST imaging [36, 37]. In this study, we set out to establish and optimize a gagCEST imaging protocol with reasonable scan times, sufficient SNR, and high reproducibility at 3.0 T for the potential implementation in the clinical setting.

GagCEST imaging can be modified by altering the number of applied saturation pulses, pulse durations and radiofrequency field strengths. To find the optimal setting of these parameters that allow for both a high gagCEST effect size and reasonable acquisition time, we used the Bloch-McConnell simulation before proceeding with the *in-vivo* measurements [38]. The simulation experiments showed a maximum effect size at a radiofrequency field strength of $0.8 \mu\text{T}$.

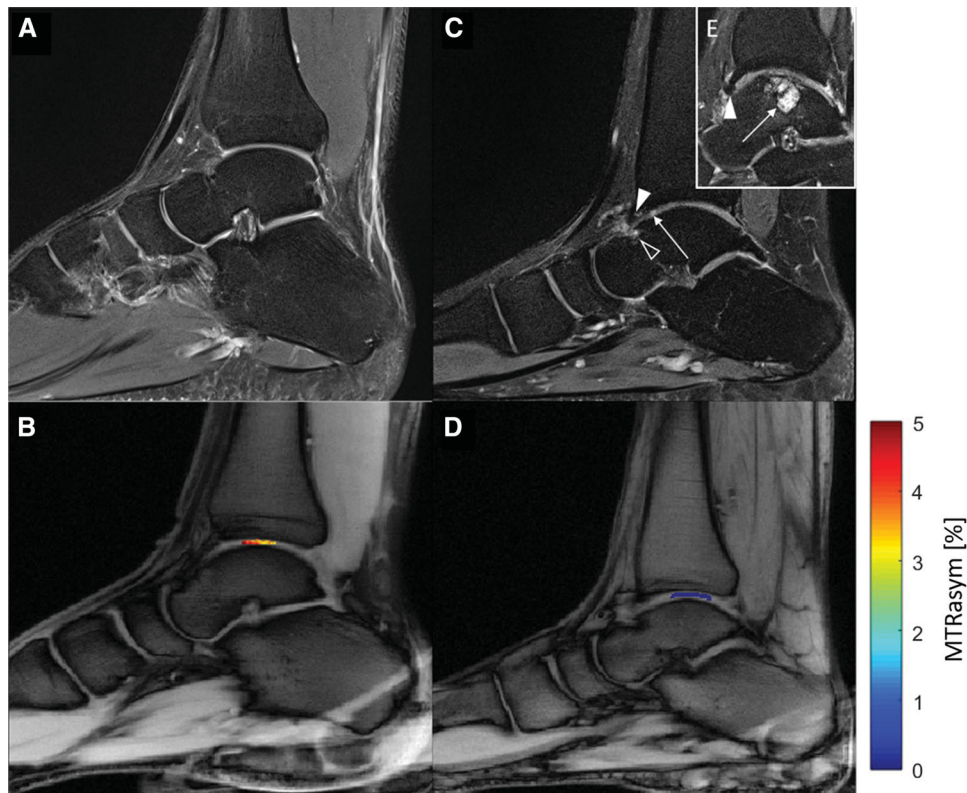


Fig. 6 Sagittal proton-density weighted (PDw) images and corresponding glycosaminoglycan chemical exchange saturation transfer (gagCEST) maps of a 29-year-old healthy male (**a** and **b**) and an age-matched male patient with an established osteochondral lesion of the talus (OLT; **c**, **d**, **e**). **a** Unremarkable tibiotalar joint with no sign of cartilage damage, osteoarthritis or OLT. **c** Osteochondral lesion of the anterior talus (black arrowhead), osteophyte of the anterior tibia (white arrowhead), and intra-tissue signal hyperintensity of the anterior tibiotalar joint cartilage indicative of focal cartilage damage (long

arrow). **e** More medial to (**c**), presence of a large cystic OLT in the weight-bearing aspect of the talus (long arrow) representing a stage 5 OLT according to the Hepple classification and an osteophyte of the anterior tibia (arrowhead). Overall, the tibiotalar joint cartilage is focally thinned, inhomogeneous, and irregular. **b** and **d** The tibiotalar joint cartilage of the healthy volunteer has higher gagCEST values than the patient (color-coded gagCEST maps overlaid onto T1w morphological image)

The effect size decreased at higher field strengths due to the ‘spillover effect’: With an increasing B_1 amplitude, the spillover effect leads to direct saturation of the water pool instead of the soluble proton pool and hence results in decreases of the gagCEST effect [39]. When tested in healthy volunteers, we noted numerically higher MTR_{asym} values and GAG-OH amplitudes at 0.8 than at 1.0 μT , but not than at 0.6 μT . The effect size increased with the applied number of pulses with a MTR_{asym} of 0.98% at 14 pulses; however, at eight applied pulses, the MTR_{asym} reached 0.98% of the maximum effect size. To keep the acquisition time as short as possible at a maximum gagCEST effect size, we decided to use eight pulses. Moreover, the effect size was found to be increased with increasing pulse durations. Due to limitations secondary to the specific absorption rate (SAR); however, the maximum pulse durations to be used in vivo were limited to 300 ms [40]. By trend, we found higher MTR_{asym} values in vivo at a pulse duration of 300 ms (as compared to 100 and 200 ms)—even though these differences were only partially significant.

After simulations and in-vivo experiments, our final gagCEST protocol consisted of 8 applied pulses with a pulse duration of 300 ms at a radiofrequency field strength of 0.8 μT and a constant duty cycle of 0.5 aiming for a minimized scan time. We used WASSR to improve the differentiation of the water and GAG peak as well as to correct for B_0 field inhomogeneities [27]. Using this protocol, we found excellent reproducibility of gagCEST values as measured by one individual rater and between two independent raters (aICC=0.97 and sICC=0.91). These values for reproducibility were even higher than presented in previous studies focusing on gagCEST of peripheral joints [34]. A good reproducibility is beneficial not only for future studies, but also for the perspective of clinical implementation of the technique [41].

The acquisition time of the optimized gagCEST sequence was 5:01 min, followed by an additional 2:22 min for the WASSR sequence. Thus, the sequence requires 7:23 min. Hence, our scan time is comparable to the one presented

by Kogan et al., who conducted the only previous study on gagCEST imaging of the ankle joint, and even shorter than several gagCEST studies focusing on the knee joint [13, 14, 42]. Additionally, the gagCEST imaging protocol was designed for 3 T scanners, which is the commonly used field strength for musculoskeletal imaging in clinical practice [43]. Thus, our protocol may be applied in both research and clinical contexts to further advance the clinical utility of gagCEST imaging of the tibiotalar joint. However, it still has to be considered less sensitive at detecting early cartilage changes than imaging protocols applied at 7 T scanners, especially if the latter are designed as volumetric multi-slice approaches [14]. Volumetric protocols have been implemented at 3 T scanners for gagCEST imaging of the knee joint and generally allow for better localization of cartilage changes. Consequently, future adaptation of volumetric protocols for gagCEST imaging of the tibiotalar joint seems of great scientific and clinical interest.

In addition to providing a stable and reproducible protocol, we observed significant differences between healthy volunteers and patients with OLTs. Since this study was the first of its kind comparing healthy individuals with patients using gagCEST at the ankle joint, we chose a patient cohort with morphologically damaged cartilage to demonstrate feasibility of this technique. In the future, we intend to study patients after ankle trauma without morphological apparent cartilage lesions to assess the presence of pre-morphological tissue damage.

Despite its strengths, our study has limitations. Our measured T1 and T2 relaxation times were shorter than the ones used for the simulations, but were overall comparable to the current literature [44].

Synovial fluid in general and joint effusion in particular are known to interfere with gagCEST imaging due to the presence of GAGs [1, 45]. Therefore, we placed our ROIs in the center of the tibiotalar joint at a distance to the anterior and posterior anatomical recesses, where joint fluid may collect and distort our measurements. *Á priori*, we excluded patients with manifest joint effusion as visible in the morphological sequences. However, since we included both cartilage layers, i.e., both tibial and talar, in one single ROI, the odds are high that synovial fluid might have contaminated our gagCEST measures. Future studies should, therefore, use sequences that use fluid suppression. Moreover, our study population was small, which may be explained by the fact that we set out to implement a clinically applicable imaging protocol for gagCEST imaging. Nonetheless, future studies need to be conducted to corroborate our findings in larger patient numbers. Furthermore, we did not compare our findings to the gold-standard technique dGEMRIC. Since

dGEMRIC relies on gadolinium-based contrast agents and its use is restricted due to ethical reasons, we consider this only a minor limitation. Last, we used a two-pool exchange model considering only the water- and the GAG-OH pool for the simulation. This model might be partially inaccurate for *in-vivo* applications, because of other influencing factors such as the GAG-NH pool, the nuclear Overhauser effect (NOE), and the magnetization transfer (MT) that were not included in our simulation because of lacking application-specific-framework fitting parameters for the NOE and MT. However, for the eventual quantification of the *in-vivo* measurements we used both the MTR_{asym} values and the Lorentzian fit analyses. While the former accounts only for the water and the GAG-OH pool the latter also takes the GAG-NH, NOE and magnetization transfer pools into consideration. As both were strongly correlated, we consider the merge simple two-pool exchange model to be sufficient for *in-vivo* quantification purposes.

In this feasibility study, pre-morphological tibiotalar joint cartilage damage was quantitatively assessable on the basis of an optimized 3 T gagCEST imaging protocol that allowed a stable gagCEST effect quantification both in normal and degenerated cartilage in clinically feasible acquisition times.

Acknowledgements Open Access funding provided by Projekt DEAL. DBA was supported by the local research committee of the medical faculty. SN has been supported by grants from the “Deutsche Forschungsgemeinschaft” (DFG) (NE 2136/3-1).

Author contributions DBA: study conception and design. Acquisition of data. Analysis and interpretation of data. Drafting of manuscript. CS: study conception and design. Acquisition of data. Analysis and interpretation of data. Critical revision. KLR: study conception and design. Acquisition of data. Analysis and interpretation of data. Critical revision. MF: study conception and design. Analysis and interpretation of data. Critical revision. JS: study conception and design. Analysis and interpretation of data. Critical revision. AL: study conception and design. Analysis and interpretation of data. Critical revision. H-JW: study conception and design. Analysis and interpretation of data. Critical revision. GA: study conception and design. Critical revision. BB: study conception and design. Critical revision. TH: study conception and design. Acquisition of data. Critical revision. SN: study conception and design. Analysis and interpretation of data. Critical revision. AM-L: study conception and design. Acquisition of data. Analysis and interpretation of data. Critical revision.

Compliance with ethical standards

Conflict of interest The authors declare that they have no conflict of interest.

Ethical standards All procedures performed in studies involving human participants were in accordance with the ethical standards of the institutional and/or national research committee and with the 1964 Helsinki Declaration and its later amendments or comparable ethical standards.

Open Access This article is licensed under a Creative Commons Attribution 4.0 International License, which permits use, sharing, adaptation, distribution and reproduction in any medium or format, as long as you give appropriate credit to the original author(s) and the source, provide a link to the Creative Commons licence, and indicate if changes were made. The images or other third party material in this article are included in the article's Creative Commons licence, unless indicated otherwise in a credit line to the material. If material is not included in the article's Creative Commons licence and your intended use is not permitted by statutory regulation or exceeds the permitted use, you will need to obtain permission directly from the copyright holder. To view a copy of this licence, visit <http://creativecommons.org/licenses/by/4.0/>.

References

- Guermaz A, Alizai H, Crema Md et al (2015) Compositional mri techniques for evaluation of cartilage degeneration in osteoarthritis. *Osteoarthr Cartil* 23(10):1639–1653
- Matzat SJ, Van Tiel J, Gold GE et al (2013) Quantitative mri techniques of cartilage composition. *Quant Imaging Med Surg* 3(3):162–174
- Matzat J, Kogan F, Fong W et al (2014) Imaging strategies for assessing cartilage composition in osteoarthritis. *Curr Rheumatol Rep* 16(11):1–9. <https://doi.org/10.1007/S11926-014-0462-3>
- Kanda T (2019) The new restrictions on the use of linear gadolinium-based contrast agents In Japan. *Magn Reson Med Sci* 18(1):1–3
- Ling W, Regatte RR, Navon G et al (2008) Assessment of glycosaminoglycan concentration in vivo by chemical exchange-dependent saturation transfer (Gagcest). *Proc Natl Acad Sci USA* 105(7):2266–2270
- Williamson DC, Närväinen J, Hubbard PI et al (2006) Effects of radiation damping on Z-spectra. *J Magn Reson* 183(2):203–212
- Vinogradov E, Sherry AD, Lenkinski RE (2013) Cest: from basic principles to applications, challenges and opportunities. *J Magn Reson* 229:155–172
- Kogan F, Hariharan H, Reddy R (2013) Chemical exchange saturation transfer (cest) imaging: description of technique and potential clinical applications. *Curr Radiol Rep* 1(2):102–114
- Müller-Lutz A, Schleich C, Schmitt B et al (2016) Gender, bmi and T2 dependencies of glycosaminoglycan chemical exchange saturation transfer in intervertebral discs. *Magn Reson Imaging* 34(3):271–275
- Pulickal T, Boos J, Konieczny M et al (2019) Mri identifies biochemical alterations of intervertebral discs in patients with low back pain and radiculopathy. *Eur Radiol* 29(12):6443–6446
- Schleich C, Müller-Lutz A, Blum K et al (2016) Facet tropism and facet joint orientation: risk factors for the development of early biochemical alterations of lumbar intervertebral discs. *Osteoarthr Cartil* 24(10):1761–1768
- Schleich C, Müller-Lutz A, Eichner M et al (2016) Glycosaminoglycan chemical exchange saturation transfer of lumbar intervertebral discs in healthy volunteers. *Spine* 41(2):146–152
- Schleich C, Bittersohl B, Miese F et al (2016) Glycosaminoglycan chemical exchange saturation transfer at 3t mri in asymptomatic knee joints. *Acta Radiol* 57(5):627–632
- Kogan F, Hargreaves BA, Gold GE (2017) Volumetric multislice gagCEST imaging of articular cartilage: optimization and comparison with T1rho. *Magn Reson Med* 77(3):1134–1141
- Jr Steele, Tj D, Ae F et al (2018) Osteochondral lesions of the talus. *Foot Ankle Orthop* 3(3):247301141877955
- Posadzy M, Desimpel J, Vanhoenacker F (2017) Staging of osteochondral lesions of the talus: mri and cone beam Ct. *J Belg Soc Radiol* 101(Suppl 2):1
- Looze CA, Capo J, Ryan MK et al (2017) Evaluation and management of osteochondral lesions of the talus. *Cartilage* 8(1):19–30
- Zaiss M, Bachert P (2013) Chemical exchange saturation transfer (Cest) And Mr Z-spectroscopy in vivo: a review of theoretical approaches and methods. *Phys Med Biol* 58(22):R221–R269
- Zaiss M, Zu Z, Xu J et al (2014) A Combined analytical solution for chemical exchange saturation transfer and semi-solid magnetization transfer. *Nmr Biomed* 28(2):217–230
- Zaiss M, Angelovski G, Demetriou E et al (2018) Qesp and quest revisited—fast and accurate quantitative cest experiments. *Magn Reson Med* 79(3):1708–1721
- Schmitt B, Zaiss M, Zhou J et al (2011) Optimization of pulse train presaturation for cest imaging in clinical scanners. *Magn Reson Med* 65(6):1620–1629
- Roeloffs V, Meyer C, Bachert P et al (2015) Towards quantification of pulsed spinlock and cest at clinical mr scanners: an analytical interleaved saturation-relaxation (isar) approach. *Nmr Biomed* 28(1):40–53
- Stanisz GJ, Odobina EE, Pun J et al (2005) T1, T2 relaxation and magnetization transfer in tissue at 3T. *Magn Reson Med* 54(3):507–512
- Singh A, Haris M, Cai K et al (2012) Chemical exchange saturation transfer magnetic resonance imaging of human knee cartilage at 3 T and 7 T. *Magn Reson Med* 68(2):588–594
- Saar G, Zhang B, Ling W et al (2012) Assessment of glycosaminoglycan concentration changes in the intervertebral disc via chemical exchange saturation transfer. *Nmr Biomed* 25(2):255–261
- Hepple S, Winson IG, Glew D (1999) Osteochondral lesions of the talus: a revised classification. *Foot Ankle Int* 20(12):789–793
- Kim M, Gillen J, Landman BA et al (2009) Water saturation shift referencing (wassr) for chemical exchange saturation transfer (cest) experiments. *Magn Reson Med* 61(6):1441–1450
- Müller-Lutz A, Schleich C, Schmitt B et al (2015) Improvement of gagCEST imaging in the human lumbar intervertebral disc by motion correction. *Skeletal Radiol* 44(4):505–511
- Müller-Lutz A, Schleich C, Pentang G et al (2015) Age-dependency of glycosaminoglycan content in lumbar discs: a 3T gagCEST study. *J Magn Reson Imaging* 42(6):1517–1523
- Müller-Lutz A, Cronenberg T, Schleich C et al (2017) Comparison of glycosaminoglycan chemical exchange saturation transfer using gaussian-shaped and off-resonant spin-lock radiofrequency pulses in intervertebral disks. *Magn Reson Med* 78(1):280–284
- Zaiss M, Schmitt B, Bachert P (2011) Quantitative separation of cest effect from magnetization transfer and spillover effects by lorentzian-line-fit analysis of Z-spectra. *J Magn Reson* 211(2):149–155
- Deng M, Yuan J, Chen WT et al (2016) Evaluation of glycosaminoglycan in the lumbar disc using chemical exchange saturation transfer mr at 30 tesla: reproducibility and correlation with disc degeneration. *Biomed Environ Sci* 29(1):47–55
- Cohen J (1992) A power primer. *Psychol Bull* 112(1):155–159
- Brinkhof S, Nizak R, Khlebnikov V et al (2018) Detection of early cartilage damage: feasibility and potential of gagcest imaging at 7T. *Eur Radiol* 28(7):2874–2881
- Martín Noguero T, Raya JG, Wessell DE et al. (2019) Functional mri for evaluation of hyaline cartilage extracellular matrix, a physiological-based approach. *Br J Radiol* 92(1103):20190443. <https://www.ncbi.nlm.nih.gov/pmc/articles/PMC3473592/pdf/Bjr-83-476.pdf>.
- Millington SA, Li B, Tang J et al (2007) Quantitative and topographical evaluation of ankle articular cartilage using high resolution mri. *J Orthop Res* 25(2):143–151

37. Krusche-Mandl I, Schmitt B, Zak L et al (2012) Long-term results 8 years after autologous osteochondral transplantation: 7 T gagcest and sodium magnetic resonance imaging with morphological and clinical correlation. *Osteoarthr Cartil* 20(5):357–363
38. Abergel D, Palmer AG (2004) Approximate solutions of the bloch-mcconnell equations for two-site chemical exchange. *ChemPhysChem* 5(6):787–793
39. Zaiss M, Xu J, Goerke S et al (2014) Inverse Z-spectrum analysis for spillover-, Mt-, and T1 -corrected steady-state pulsed cest-mri—application to Ph-weighted mri of acute stroke. *Nmr Biomed* 27(3):240–252
40. Wang Z, Collins CM (2010) Effect of Rf pulse sequence on temperature elevation for a given time-average Sar. *Concepts Magn Reson Part B Magn Reson Eng* 37b(4):215–219
41. Dickersin K, Mayo-Wilson E (2018) Standards for design and measurement would make clinical research reproducible and usable. *Proc Natl Acad Sci USA* 115(11):2590–2594
42. Krishnamoorthy G, Nanga RPR, Bagga P et al (2016) High quality 3d gagcest imaging of in vivo human knee cartilage at 7T. *Magn Reson Med* 77(5):1866–1873
43. Tp F, Nc A, Jp W et al (2018) Musculoskeletal imaging: current practice and future directions. *Semin Musculoskelet Radiol* 22(5):564–581
44. Wiener E, Pfirrmann CWA, Hodler J (2010) Spatial variation in T1 of healthy human articular cartilage of the knee joint. *Br J Radiol* 83(990):476–485 (**Accessed 23 Mar 2020**)
45. Kulkarni P, Deshpande S, Koppikar S et al (2016) Glycosaminoglycan measured from synovial fluid serves as a useful indicator for progression of osteoarthritis and complements Kellgren-Lawrence score. *Bba Clin* 6:1–4

Publisher's Note Springer Nature remains neutral with regard to jurisdictional claims in published maps and institutional affiliations.



Differentiating rheumatoid and psoriatic arthritis: a systematic analysis of high-resolution magnetic resonance imaging features—preliminary findings

Daniel B. Abrar¹ · Christoph Schleich¹ · Ralph Brinks² · Christine Goertz² · Matthias Schneider² · Sven Nebelung¹ · Philipp Sewerin²

Received: 23 May 2020 / Revised: 7 August 2020 / Accepted: 16 August 2020
© The Author(s) 2020

Abstract

Background Because of overlapping phenotypical presentations, the diagnostic differentiation of rheumatoid arthritis (RA) and psoriatic arthritis (PsA) remains challenging. Thus, this study aimed to examine the diagnostic value of distinct imaging features obtained by high-resolution 3-T MRI for the diagnostic differentiation.

Materials and methods Seventeen patients with PsA and 28 patients with RA were imaged at high resolution using 3-T MRI scanners and a dedicated 16-channel hand coil. All images were analyzed according to the outcome measures in rheumatology clinical trials' (OMERACT) RAMRIS (Rheumatoid Arthritis Magnetic Resonance Imaging Score) and PsAMRIS (Psoriatic Arthritis Magnetic Resonance Imaging Score) for the presence and intensity of synovitis, flexor tenosynovitis, bone edema, bone erosion, periarticular inflammation, bone proliferation, and joint space narrowing. Next, odds ratios (OR) were calculated to determine the strength of the associations between these imaging features, demographic characteristics, and the outcome RA vs. PsA.

Results PsA could be differentiated from RA by extracapsular inflammatory changes (PsAMRIS sub-score “periarticular inflammation”), with low odds for the presence of RA (OR of 0.06, $p < 0.01$) at all metacarpophalangeal (MCP) joints. A prediction model informed by the items that were strongest associated with the presence of RA or PsA demonstrated excellent differentiating capability with an area under the curve of 98.1%.

Conclusion High-resolution imaging is beneficial for the identification of relevant imaging features that may assist the clinical differentiation of inflammatory conditions of the hand. At the MCP level, extracapsular inflammatory changes were strongly associated with PsA and may consequently allow the imaging differentiation of PsA and RA.

Keywords Psoriatic arthritis · Rheumatoid arthritis · MRI · PsAMRIS · RAMRIS · Metacarpophalangeal joint

Christoph Schleich, Sven Nebelung and Philipp Sewerin contributed equally to this work.

Electronic supplementary material The online version of this article (<https://doi.org/10.1007/s00256-020-03588-5>) contains supplementary material, which is available to authorized users.

✉ Daniel B. Abrar
danielbenjamin.abrar@med.uni-duesseldorf.de

¹ Medical Faculty, Department of Diagnostic and Interventional Radiology, University Dusseldorf, 40225 Dusseldorf, Germany

² Policlinic and Hiller Research Unit of Rheumatology, UKD, Heinrich Heine University Düsseldorf, Moorenstrasse 5, 40225 Dusseldorf, Germany

Introduction

Rheumatoid arthritis (RA) and psoriatic arthritis (PsA) are chronic inflammatory conditions that cause progressive destruction of cartilage and bone [1]. Even though these entities share pathophysiological features and phenotypical manifestations, several studies hypothesized that RA and PsA differ ultimately in their pattern of joint involvement [2]. This is reflected by the current entheses organ concept that highlights the role of fibrocartilaginous insertion sites of tendons and ligaments in the pathogenesis of PsA [3, 4]. In contrast, RA is considered a synovial disease with secondary involvement of periarticular insertion sites and ligaments [5].

Despite the fact that imaging plays only a minor role in commonly applied clinical classification schemes [6, 7], characteristic imaging features exist for both entities and may be

visualized using radiography, ultrasound, or magnetic resonance imaging (MRI) [8]. MRI can provide crucial information on a range of pathological manifestations such as synovitis, enthesitis, bone edema, erosion, and osteoproliferation [9, 10]. Even though MRI is not used as the primary diagnostic imaging modality for RA or PsA, it is increasingly used to evaluate treatment response. The outcome measures in rheumatology clinical trials (OMERACT) initiative established MRI scores for PsA and RA, i.e. PsAMRIS (Psoriatic Arthritis Magnetic Resonance Imaging Score) and RAMRIS (Rheumatoid Arthritis Magnetic Resonance Imaging Score) [11, 12]. However, despite great progress over the last years in defining typical imaging features, there remains significant overlap between both entities that challenges unambiguous diagnosis [13]. Especially in polyarticular disease, distinction with certainty can be difficult. Consequently, recent studies outlined certain imaging features that might assist differentiation in these “borderline” cases but have not been able to provide measures or means for valid and reliable differentiation [14]. In addition to truly overlapping phenotypical manifestations of the two diseases, this diagnostic limitation may be the result of insensitive imaging modalities. In MRI, field strength needs to be invested adequately to achieve proper image resolution, signal-to-noise ratio, and contrast to best differentiate the disease entities, in particular when imaging delicate structures such as the small finger joints, the entheses, and the nails for subtle changes. This may be hampered when field strength is low (i.e. ≤ 1.5 T) and coils are inadequate [15–17].

In the past, RA and PsA patients have received the same therapy regimes, rendering diagnostic differentiation largely irrelevant. The benefit of a tailored treat-to-target approach for each type of arthritis [18, 19], however, and the development and increasing application of biological disease-modifying drugs (bDMARD) and targeted synthetic disease-modifying drugs (tsDMARDs) has made the diagnostic differentiation between RA and PsA increasingly important to guide treatment in each individual patient.

In the present study, we aimed to systematically assess and quantify the diagnostic value of a range of inflammatory and noninflammatory MRI features obtained at high resolution in differentiating rheumatoid and psoriatic arthritis using clinical classification criteria as reference. We hypothesized that the distribution, severity, and tissue involvement of these imaging features (a) was variable in both entities and (b) could be used to quantitatively assess each imaging feature’s contribution to the diagnosis of RA or PsA.

Materials and methods

Study population

Characteristics of the study populations are summarized in Table 1.

Table 1 Demographic characteristics of the study populations. For patients with psoriatic (PsA) and rheumatoid arthritis (RA), the mean age in years \pm standard deviation (SD) and range, the mean disease duration in years (PsA) and weeks (RA) \pm SD and range, and the sex are presented

	PsA patients	RA patients
Population size	17	28
Age (years)	53.7 \pm 11.6 (26–72)	55 \pm 11.4 (39–74)
Disease duration	2.6 \pm 3.3 (1–8 years)	6.3 \pm 10.1 (2–23 weeks)
Sex (male/female)	9 males/8 females	9 males/19 females

A total of 17 patients with PsA (mean age 53.7 \pm 11.6; range 26–72 years; 9 males, 8 females), who fulfilled the CASPAR criteria [5], had a mean disease duration of 2.6 \pm 3.3 years, and suffered from peripheral joint involvement, were prospectively recruited for the “Analysis of the DActylic Melange” (ADAM) research initiative [10]. All patients had failed monotherapy with the conventional synthetic disease-modifying antirheumatic drug (csDMARD) methotrexate (MTX) and were escalated to anti-TNF therapy following an MRI scan.

Additionally, 28 patients with RA (mean age 55.0 \pm 11.4 years; range 39–74 years; 9 males, 19 females), who fulfilled the ACR/EULAR 2010 criteria for RA and had a mean disease duration < 6 months (mean 6.3 \pm 10.1; range 2–23 weeks), were prospectively recruited from the German ArthroMark initiative cohort [20]. All patients were treated with MTX without any increase in dosage nor change to other medications.

Exclusion criteria for both arms of the total study population were pregnancy, current breastfeeding, age < 18 years, metal implants, implanted medical devices (e.g. ventriculoperitoneal shunts), claustrophobia, asthma, known malignancy, and known osteoarthritis of the hands.

Disease activity was assessed by the Disease Activity Score 28 (DAS28, remission < 2.6 , low 2.6 to < 3.2 , moderate 3.2 to 5.1, high > 5.1) [21] for RA and the Disease Activity index for PsA (DAPSA, remission 0–4, low 5 to 14, moderate 5 to 28, high > 28) [22] for PsA patients, which are commonly used quantitative measures to assess disease activity and progress in RA and PsA, respectively [23, 24]. In our study, the mean DAS28 was 4.69 \pm 0.84 and the mean DAPSA was 26.89 \pm 18.23. In addition, serum C-reactive protein (CRP) levels were determined for both cohorts (RA 0.96 \pm 0.93 mg/dL; PsA 1.1 \pm 1.7 mg/dL).

The present study was approved by the local ethical committee (Ethical Committee of the Medical Faculty of the University of Düsseldorf, Germany, study number: 3828 and 4962R. Trial registration: 2014123117). Written and informed consent was obtained from all patients prior to initiation.

MRI studies

In PsA patients, MR imaging of the clinically dominant hand was performed using a 3-T MRI scanner (Magnetom Skyra, Siemens Healthineers, Erlangen, Germany). In RA patients, a 3-T MRI scanner (Magnetom Trio, A Tim System; Siemens Healthineers) was used. In both scanners, patients were examined in a prone position with their arm extended overhead and the palm facing down (“superman position”). For high-resolution scanning, a dedicated 16-channel hand coil (3-T Tim receive-only coil, Siemens Healthineers) was used, allowing for a high-resolution imaging over a wider area compared with previous high-resolution strategies.

The imaging protocol was implemented in line with the recommendations of the OMERACT working group [11, 25] and included pre- and post-contrast T1-weighted (T1w) and non-contrast fat-saturated T2w/STIR images in two different orthogonal planes. More specifically, the following sequences of the clinically dominant hand were obtained: coronal short tau inversion recovery (STIR) and T1w turbo spin echo (TSE) sequences. Following intravenous injection of the contrast agent (gadolinium-based, 0.4 mL/kg body weight gadoteric acid [Gd-DOTA], Dotarem, Guerbet Villepinte, France for PsA and [Gd-DTPA], Magnevist; Schering, Berlin, Germany, in RA patients), coronal and transversal T1wTSE sequences with spectral fat suppression were applied. The field of view covered the metacarpophalangeal (MCP) and the proximal and distal interphalangeal (PIP, DIP) joints in PsA patients, and the wrist, the carpus, and the MCP joints in RA patients.

Detailed sequence parameters are given in Table 2.

Image analysis

MR images were randomized and then independently read and analyzed by two radiologists (both trained in musculoskeletal imaging and in PsAMRIS and RAMRIS scoring with 3 (DBA) and 8 (CS) years of experience) according to the OMERACT guidelines [11, 26]. In case of different findings, the raters decided by common agreement with the assisting opinion of a third rater (PS, rheumatologist with 8 years of experience). The raters were blinded to patients’ data and treatment and did not partake in data collection. According to the definitions of the OMERACT guidelines [11, 25], images were evaluated for synovitis (score 0–3), flexor tenosynovitis (score 0–3), periarticular inflammation (score 0 or 1), bone edema (score 0–3), bone erosion (score 0–10), bone proliferation (score 0 or 1), and joint space narrowing (score 0 or 1) of the MCP joints of digits 2–5, with higher scores indicating more severe inflammatory changes. Typical changes are depicted in Figs. 1, 2, and 3.

Statistical analysis

All statistical analyses were performed by RB using the R project for statistical computing (version 3.5.1, The R Foundation for Statistical Computing, <https://www.r-project.org/>). For descriptive analysis, the mean, standard deviation, minimum, and maximum were determined. For each item of the scores, age and sex, univariate logistic regression models, odds ratios (OR), and 95% confidence intervals (CI) were calculated. The results of these analyses are shown in a forest plot (Fig. 3). *p* values < 0.05 were considered significant.

Table 2 Detailed magnetic resonance imaging (MRI) sequence parameters

Sequence	Orientation	TR/TE (ms)	Flip angle (°)	Slice thickness (mm)	FoV (mm × mm)	Acquisition matrix (pixels)	Pixel size (mm/pixel)	
T1w TSE	PsA	Coronal	862/27	150	2.5	140 × 140	512 × 512	0.27 × 0.27
	RA		862/27	150	2.5	130 × 130	512 × 512	0.25 × 0.25
T1w TSE + contrast	PsA	Coronal	862/27	150	2.5	140 × 140	512 × 512	0.27 × 0.27
	RA		862/27	150	2.5	130 × 130	512 × 512	0.25 × 0.25
STIR	PsA	Coronal	5560/31	120	2.5	140 × 140	448 × 314	0.31 × 0.41
	RA		5560/31	120	2.5	130 × 130	448 × 314	0.29 × 0.41
T2w TSE fs	PsA	Transversal	5694	89	3.0	160 × 160	512 × 358	0.31 × 0.45
	RA		na	na	na	na	na	na
PD TSE fs	PsA	Sagittal	3150/47	150	2.5	150 × 150	448 × 182	0.33 × 0.82
	RA		na	na	na	na	na	na
T1 TSE fs + contrast	PsA	Transversal	807/16	90	2.5	130 × 130	384 × 288	0.31 × 0.42
	RA		702/16	90	2.5	130 × 130	384 × 288	0.31 × 0.42

Imaging plane, echo and repetition time (TE/TR), flip angle, slice thickness, field of view (FoV), pixel size, and number of slices are given for all sequences (short tau inversion recovery, T2-weighted fat-saturated turbo spin echo (T2w TSE fs), T1w TSE, proton density TSE fs (PD))

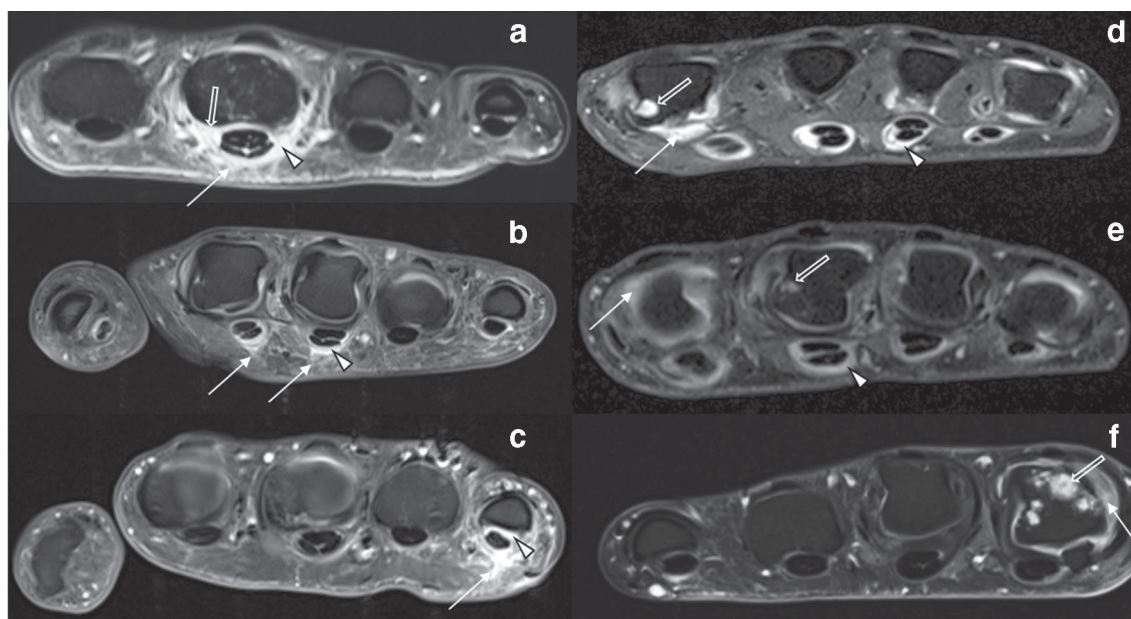


Fig. 1 Overview of representative MRI findings in psoriatic arthritis (PsA) and rheumatoid arthritis (RA). Transversal T1w fat-saturated contrast-enhanced sequences of selected MCP joints of three patients each with PsA (**a–c**) and RA (**d–f**). **a** 39-year-old male. Severe periarticular inflammation (white arrow) with additional flexor tenosynovitis (arrowhead) and synovitis (open arrow). **b** 43-year-old male. Moderate periarticular inflammation (white arrow) with flexor tenosynovitis (open arrow). **c** 39-year-old female. Severe periarticular inflammation (white

arrow) with corresponding flexor tenosynovitis (arrowhead). **d** 48-year-old female. Widespread synovitis (white arrow), bone erosions (open arrow), and severe flexor tenosynovitis (arrowhead). **e** 39-year-old male. Bone erosion (open arrow), synovitis (white arrow), and severe flexor tenosynovitis (arrowhead). **f** 43-year-old male. Multiple bone erosions (open arrow) and synovitis (white arrow). Note the absence of periarticular inflammation in **d–f** despite significant inflammatory joint changes at the joint level

Based on these data, we set up a prediction model related to age, gender, periarticular inflammation (volar portion of MCP 5), and bone erosion (proximal joint portion of MCP 5) that attempted to correctly identify PsA- and RA-associated imaging features to establish a diagnosis. The resulting coefficients of the prediction model on the link scale of the logistic regression, i.e. log-OR, are given in Supplementary Table 1. Consequently, receiver operating characteristics (ROC) were calculated. Of note, the variables age, gender, periarticular inflammation, and bone erosion were selected due to their OR (strongest and second strongest OR of two different score items) and potential clinical practicability and availability (gender, age, and one particular digit). $OR > 1$ indicates that the respective variable is associated with the outcome RA. Variables linked to the outcome PsA, or strictly speaking “not RA,” have $OR < 1$. Confidence bounds for the prediction model were estimated by the bootstrap method [27] (based on $B = 5000$ bootstraps with replacement) and application of the percentile method [28]. Based on the ROC, an area under the curve (AUC) was obtained, which is an index that indicates the diagnostic value of a test (set) and varies from 0.5 (no apparent accuracy) to 1.0 (perfect accuracy) [29]. Inter- and intra-rater reliability were calculated by two-way mixed intraclass correlation coefficients (single-measure intraclass correlation coefficient (sICC) for intra-rater; average-measure ICC (aICC) for inter-rater reliability).

Results

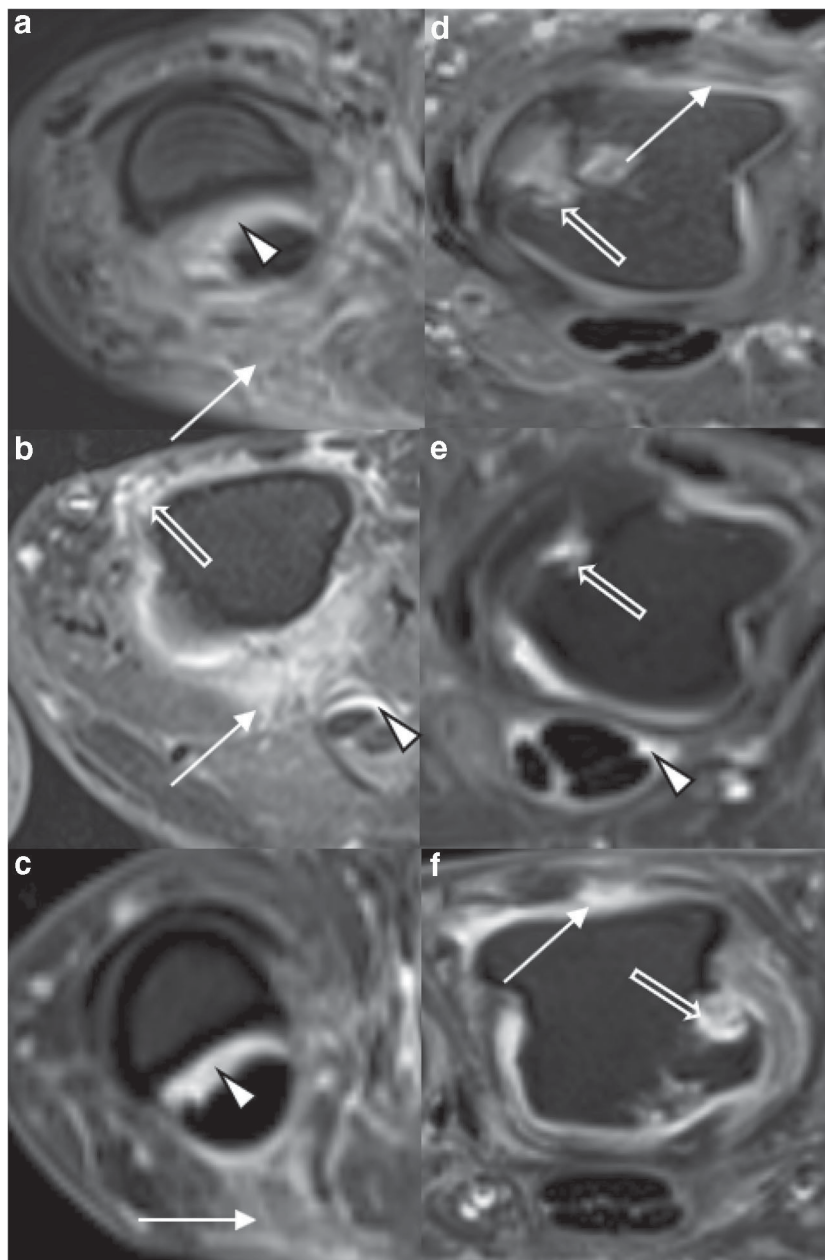
Distribution of RAMRIS and PsAMRIS sub-scores inter- and intra-rater reliability

Frequency, distribution, and means as well as standard deviations for each scored item are listed in Table 3. Typical disease-related findings are illustrated in Figs. 1 and 2. sICC and aICC were > 0.9 .

Odds ratios for gender, age, and RAMRIS and PsAMRIS sub-scores for the outcome RA vs. PsA

The odds ratios (OR) for gender, age, and RAMRIS and PsAMRIS items for the outcome RA are presented in Table 4. Periarticular inflammation of the dorsal and volar aspects of MCP 3–5 as well as of the volar aspect of MCP2 were strongly associated with the presence of PsA, as indicated by small ORs ($OR < 0.15$ [$p < 0.05$]). By trend, periarticular inflammation of the dorsal aspect of MCP2 and bone erosion at the proximal portion of MCP5 were similarly associated with the presence of PsA, yet not statistically significantly. In contrast, bone erosion at the distal portion of MCP3 was associated with the presence of RA, yet not significantly.

Fig. 2 Detailed view of representative MRI findings in psoriatic arthritis (PsA) and rheumatoid arthritis (RA). Transversal T1w fat-saturated contrast-enhanced sequences of selected MCP joints of three patients each with PsA (**a–c**) and RA (**d–f**). **a** 29-year-old female. Severe periarticular inflammation (white arrow) with additional flexor tenosynovitis (arrowhead). **b** 47-year-old female. Severe periarticular inflammation (white arrow) with synovitis (open arrow) and flexor tenosynovitis (arrowhead). **c** 37-year-old male. Moderate periarticular inflammation (white arrow) with corresponding flexor tenosynovitis (arrowhead). **d** 55-year-old male. Widespread synovitis (white arrow) and multiple bone erosions (arrowhead). **e** 48-year-old female. Bone erosion (open arrow) and slight flexor tenosynovitis (arrowhead). **f** 39-year-old male. Bone erosion (open arrow) and synovitis (white arrow). Note the absence of periarticular inflammation in **d–f** despite significant inflammatory joint changes at the joint level



Throughout, flexor tenosynovitis was strongly and significantly associated with the presence of RA, as indicated by large ORs ($OR > 6$ [$p < 0.05$]). Other imaging features did not demonstrate strong or significant association with either disease entity.

Prediction model including four variables

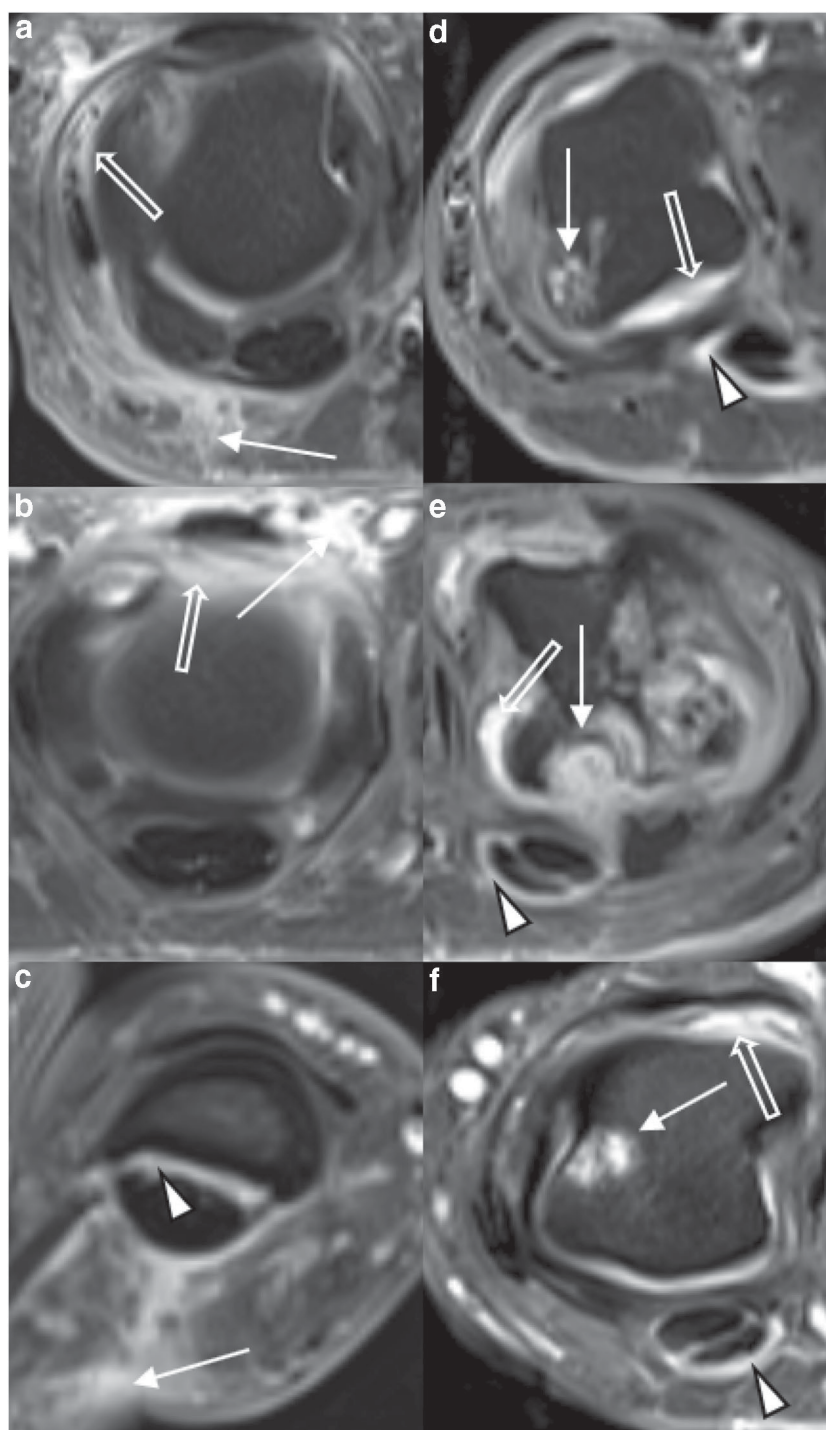
Gender, age, and the imaging features of erosion of the proximal and periarticular inflammation of the volar joint portion of MCP5 were used to calculate a prediction model for the differentiation between RA and PsA. On the basis of this model, an area under the curve (AUC) of 98.1% (CI =

0.955–1.0) was determined (Fig. 4), therefore accounting for excellent accuracy in distinguishing RA and PsA.

Discussion

The most important finding of the present study is that the clinical differentiation of inflammatory conditions of the hand may be facilitated by high-resolution MRI features. At the MCP level, extracapsular inflammation was strongly associated with PsA, while flexor tenosynovitis was associated with RA.

Fig. 3 Detailed view of representative MRI findings in PsA and RA. Transversal T1w fat-saturated contrast-enhanced sequences of selected MCP joints of three patients each with PsA (a–c) and RA (d–f). **a** 34-year-old male. Severe periarticular inflammation (white arrow) with additional mild synovitis (open arrow). **b** 42-year-old female. Severe dorsal periarticular inflammation (white arrow) with synovitis (open arrow). **c** 44-year-old female. Severe periarticular inflammation (white arrow) with corresponding mild flexor tenosynovitis (arrowhead). **d** 39-year-old male. Widespread synovitis (white arrow) with moderate flexor tenosynovitis (arrowhead) and large bone erosion (white arrow). **e** 41-year-old male. Multiple large bone erosions (white arrow) and severe synovitis (open arrow) with mild flexor tenosynovitis (arrowhead). **f** 56-year-old female. Bone erosion (white arrow) with moderate flexor tenosynovitis (arrowhead) and moderate synovitis (open arrow). Note the absence of periarticular inflammation in d–f despite significant inflammatory joint changes at the joint level



Even though the diagnostic differentiation is considered challenging [13], our results indicate that optimized imaging in terms of spatial resolution, signal-to-noise ratio, and contrast can depict subtle changes that may help in clinical decision-making. This is the reason why we used high-resolution MRI studies to explore potentially distinctive imaging features for the differentiation between RA and PsA.

Our results demonstrate that all evaluated imaging features, i.e. synovitis, flexor tenosynovitis, periarticular inflammation, joint space narrowing, bone erosion, bone edema, and bone proliferation can be detected in PsA patients [30]. Except for bone proliferation, all features could also be found in RA patients, which again indicates the considerable morphological overlap between both disease entities. Notably, bone

Table 3 Distribution, frequency, and severity of combined RAMRIS and PsAMRIS sub-scores of metacarpophalangeal (MCP) joint 2–5 in patient cohorts with psoriatic arthritis (PsA) or rheumatoid arthritis (RA). Data are presented as [frequency in %] and median (interquartile range) for the MCP joint of each digit (D2–D5) and overall. *na* not applicable

Item		Joint portion	D2	D3	D4	D5	Overall
Synovitis	PsA	na	[100%] 2 (2–3)	[100%] 3 (2–3)	[100%] 2 (2–3)	[100%] 2 (1–3)	9 (7–11)
	RA	na	[100%] 3 (2–3)	[100%] 3 (2–3)	[100%] 2 (1–3)	[100%] 2 (1–3)	9.5 (7–11)
Flexor tenosynovitis	PsA	na	[100%] 1 (1–1)	[94%] 1 (1–2)	[94%] 1 (1–1)	[88%] 1 (1–2)	5 (4–6)
	RA	na	[100%] 2 (1–2)	[96%] 1 (1–2)	[86%] 1 (1–2)	[89%] 1 (1–2)	5 (4–7)
Periarticular inflammation	PsA	Volar	[82%] 1 (1–1)	[76%] 1 (1–1)	[88%] 1 (1–1)	[88%] 1 (1–1)	4 (3–4)
		Dorsal	[65%] 1 (0–1)	[76%] 1 (1–1)	[65%] 1 (0–1)	[82%] 1 (1–1)	4 (2–4)
	RA	Volar	[14%] 0 (0–0)	[7%] 0 (0–0)	[7%] 0 (0–0)	[4%] 0 (0–0)	0 (0–0)
		Dorsal	[46%] 0 (0–1)	[35%] 0 (0–1)	[21%] 0 (0–0)	[21%] 0 (0–0)	1 (0–2)
Bone edema	PsA	Proximal	0 [6%] 0 (0–0)	[12%] [12%] 0 (0–0)	0 0	[6%] [6%] 0 (0–0)	0 (0–0)
		Distal	0 (0–0)	[12%] 0 (0–0)	0	[6%] 0 (0–0)	0 (0–0)
	RA	Proximal	[4%] 0 (0–0)	[11%] 0 (0–0)	0	0	0 (0–0)
		Distal	[4%] 0 (0–0)	[11%] 0 (0–0)	[4%] 0 (0–0)	0	0 (0–0)
Bone erosion	PsA	Proximal	[53%] 0 (0–1)	[47%] 0 (0–1)	[35%] 0 (0–1)	[29%] 0 (0–1)	2 (1–3)
		Distal	[12%] 0 (0–0)	[6%] 0 (0–0)	[6%] 0 (0–0)	[6%] 0 (0–10)	0 (0–0)
	RA	Proximal	[36%] 0 (0–1)	[36%] 0 (0–1)	[18%] 0 (0–0)	[14%] 0 (0–0)	0.5 (0–2.25)
		Distal	[29%] 0 (0–1)	[18%] 0 (0–0)	0	[7%] 0 (0–0)	0 (0–1)
Bone proliferation	PsA	na	[6%] 0 (0–0)	0	[6%] 0 (0–0)	0	0 (0–0)
	RA	na	0	0	0	0	0
Joint space narrowing	PsA	na	[29%] 0 (0–1)	[59%] 1 (0–1)	[65%] 1 (0–1)	[41%] 0 (0–1)	2 (0.25–3.75)
	RA	na	[29%] 0 (0–1)	[50%] 0.5 (01)	[68%] 1 (01)	[0.32%] 0 (0–1)	2 (1–3.25)

proliferation itself can be considered as a reliable predictor for PsA, even though it could not be included into the presented prediction model due to its rare occurrence in the PsA patient cohort. This may be a consequence of the relatively short disease duration in our patients.

On the other hand, regarding periarticular inflammation, our results show a significant predominance in PsA patients, as reflected by the low odds ratio for the diagnosis RA. Periarticular inflammation is included as a sub-score in the OMERACT PsAMRIS, but not in its RA equivalent, RAMRIS [11, 12, 25]. Both scoring systems are validated semi-quantitative sub-scores for the detection and monitoring of PsA-/RA-related joint changes. By definition, periarticular inflammation is present if increased water content or abnormal

contrast-enhancement at extraarticular sites such as soft tissues or entheses can be detected in designated MRI sequences [11, 31]. Previous studies have shown that PsA is an enthesal disease, primarily affecting the so-called “enthesal organs” or the synovio-enthesal complex [4, 32, 33], which consist of tendons and their sheaths as well as ligaments and their insertion sites [34]. Research further indicates that enthesal changes are associated with inflammation of extraarticular tissue [35, 36]; thus, periarticular inflammation is potentially more frequently found in PsA due to its enthesal-driven pathophysiology [37]. Accordingly, in 1995, Jevtic et al. demonstrated that periarticular inflammation is more frequent in PsA than in RA patients, at least at the PIP joint level [38]. Moreover, recent ultrasound and MRI studies have shown that

Table 4 Odds ratios (OR) for gender, age, and individual RAMRIS and PsAMRIS sub-scores with 2.5 and 97.5% confidence intervals (CI) for the outcome RA versus PsA. JSN joint space narrowing. Statisticallysignificant values are given in italics and further stratified into **p* value < 0.05; ***p* value < 0.01. *na* not applicable. D2–D5 indicate digits 2–5

Item	D2		D3		D4		D5	
	OR	CI	OR	CI	OR	CI	OR	CI
Gender	2.32	0.73/7.69	2.32	0.73/7.69	2.32	0.73/7.69	2.32	0.73/7.69
Age	1	0.95/1.06	1	0.95/1.06	1	0.95/1.06	1	0.95/1.06
Synovitis	1.36	0.56/3.33	0.7	0.27/1.65	0.72	0.31/1.64	0.94	0.46/1.89
Flexor tenosynovitis	<i>6.08**</i>	1.84/29.19	1.03	0.44/2.49	1.95	0.73/6.16	1	0.44/2.32
Periarticular inflammation								
Volar	<i>0.036**</i>	0.01/0.16	<i>0.02**</i>	0/0.12	<i>0.01**</i>	0/0.06	<i>0.01**</i>	0/0.04
Dorsal	0.47	0.13/1.6	<i>0.17*</i>	0.04/0.62	<i>0.15**</i>	0.04/0.54	<i>0.06**</i>	0.01/0.24
Bone edema								
Proximal	9.85e06	4.79e–206/na	1.51	0.6/7.11	na	na	3.65e–08	na/7.53 e204
Distal	0.5	0.03/1.98	1.14	0.55/2.82	9.85 e06	4.79e–206/na	na	na
Bone erosion								
Proximal	0.68	0.28/1.64	1.16	0.72/2.2	0.52	0.16/1.57	0.4	0.09/1.77
Distal	1.83	0.61/7.75	3.04	0.76/4.8	3.65e–08	na/7.53 e204	1.23	0.11/20.78
Bone proliferation	3.65e–08	na/7.53 e204	na	na	3.65 e–08	na/7.53 e204	na	na
JSN	0.1	0.26/3.81	1.13	0.46/2.95	0.83	0.31/2.19	0.59	0.18/1.85

periarticular inflammation is not only a characteristic feature of PsA but is even more frequently detected than in RA [37, 39, 40]. However, literature data are not conclusive as others have reported no difference between RA and PsA concerning extraarticular inflammatory changes and enthesitis [41]. Most likely, these different definitions of morphological changes in both diseases is due to the heterogeneity of PsA and the

limited image resolution and signal yield of low-field MRI scanners that may have prevented the detection of subtle changes in small joints. Against this background, our data lend evidence to the use of high-resolution MRI sequences, as in this study, because they seem beneficial for detecting subtle extracapsular changes in efforts to differentiate the two entities.

In the present study, we established a prediction model comprised of demographic characteristics, i.e. age and gender, and imaging features, i.e. periarticular inflammation and erosion at MCP5. The model performed exquisitely well in differentiating both entities as indicated by the AUC value of 98.1, indicating excellent accuracy in differentiating RA from PsA. Even though our model can give an indication of the variables that need particular attention when it comes to the eventual differentiation of both entities, these findings should be treated with caution. First, our sample size was small, and thus the model certainly lacks generalizability until it has been validated in a separate cohort of RA and PsA patients, in particular in terms of different disease stages. Long-standing inflammatory conditions most likely undergo phenotypical changes that are not yet captured by the model. Second, the model was developed on the basis of the best-performing classifiers, which—of course—boosts its diagnostic performance. That is why our findings and the derived prediction model can only be regarded as preliminary and require future studies for their validation. Yet, we consider this methodology a starting point for future research efforts that not only include larger patient cohorts but also variable phenotypical

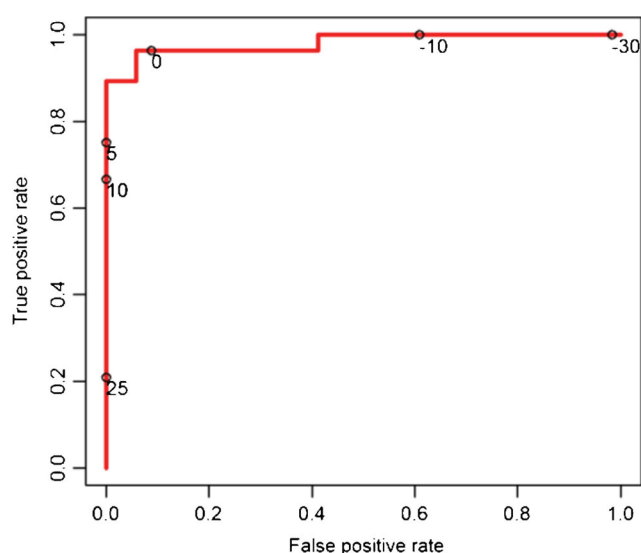


Fig. 4 Receiver operating characteristics (ROC) curve to illustrate the diagnostic ability of the calculated prediction model to determine the outcome RA. Given are different discrimination thresholds (circles with adjoined numbers). Area under the curve (AUC) = 98.1%

presentations, disease stages, and previous medication regimens. After validation, however, the developed prediction model could be of great clinical significance since the distinction between RA and PsA can be challenging by mere clinical and serological means, especially in borderline cases. With the introduction of treat-to-target therapy regimens in both entities and the increasing development and application of bDMARDs and tsDMARDs, the early diagnostic differentiation between the two diseases has become increasingly important to guide therapy in each individual patient [18, 19].

The only other imaging feature that was significantly associated with one of the two disease entities was flexor tenosynovitis, which was strongly associated with the presence of RA, as already shown in previous studies [10, 40, 42]. Only for MCP2 did we find significant values, while for MCP4, a similar, yet nonsignificant, trend was seen. For MCP2 and 3, however, flexor tenosynovitis was equally distributed between the two entities. One possible explanation for these discrepancies may be the fact that flexor tenosynovitis occurs frequently in both RA and PsA, without a predominant association with one disease entity over the other [31, 43, 44]. Accordingly, this item has been included in both OMERACT MRI scores, RAMRIS and PsAMRIS [11, 25]. Even though Marzo-Ortega et al. detected flexor tenosynovitis more frequently in RA than in PsA, their patient sample was too small to be certain of a significant association [40]. Our own findings demonstrated a similar pattern, with a higher overall prevalence of flexor tenosynovitis in RA patients. Due to conflicting results in different studies including our own, each involving small and selective patient cohorts, no solid conclusions may be drawn as flexor tenosynovitis at the MCP joint level may be associated with both disease entities.

Regarding all other evaluated imaging features, we found an overall homogenous distribution between both entities, with slight differences by trend that are neither statistically nor (most likely) clinically significant.

In addition to mere morphological MRI, compositional imaging techniques have emerged over the last years and have become a powerful tool for diagnosis and monitoring of various musculoskeletal disorders, including inflammatory joint conditions such as RA [45, 46]. Among them, delayed gadolinium enhanced MRI of cartilage (dGEMRIC) is still the gold-standard technique, even though techniques that do not rely on the application of intravenous contrast agents such as T2/T2* mapping or sodium imaging are of increasing scientific and clinical interest [47–50]. However, research on compositional MRI in PsA is sparse, with yet only one single study published [51]. In future studies, nevertheless, compositional MRI techniques could potentially further facilitate the characterization and distinction of RA and PsA.

When interpreting our results, the following limitations must be considered.

First and foremost, both patient cohorts were small and, due to our study's exploratory design, our results can only be considered as preliminary and need further validation in future studies with larger study populations. Secondly, our PsA cohort may not be representative of the full spectrum of disease stages because all included PsA patients suffered from severe dactylitis in at least one finger. As dactylitis is associated with high disease activity [36], the imaging correlates identified in this study may be predisposed towards higher disease severity, thereby rendering the incidence and severity of enthesitis and periarticular inflammation overly high. Similarly, flexor tenosynovitis may also be overrepresented since it is known to be associated with dactylitis, too [36, 52]. Third, the mean disease duration of both study cohorts differed substantially. With a mean disease duration of 6 and 160 weeks, we compared (very) "early" RA to "long-standing" PsA. Of note, current guidelines define "early" RA in terms of a disease duration of less than 12 months, while "early" PsA is defined as a disease duration of less than 24 months [53, 54]. Thus, the comparability of both cohorts and their respective imaging features in terms of frequency, distribution, and severity is certainly limited. However, periarticular inflammation is a sign of acute inflammation and therefore not limited to late stages of the disease. Since periarticular inflammation is the most predictive feature of our investigation and both patient cohorts had overall similar disease activity as quantified by DAS28 and DAPSA, this limitation seems relevantly attenuated; nonetheless, our findings are only preliminary until confirmed in patient cohorts with equal disease durations. Fourth, we only assessed the imaging features at the MCP joint level. Most likely, the diagnostic differentiation of not just RA vs. PsA but also each entity's phenotypical manifestation needs to focus on joint levels beyond such as the interphalangeal and intercarpal joints. Future research ought to be directed at quantitatively defining the imaging features there, too. Further, despite the fact readers had been blinded to patient data, different fields-of-view of certain MRI sequences might have corrupted proper blinding. The potential bias was mitigated by the fact that (i) the MCP joints selected for quantitative imaging feature assessment had been imaged using similar sequence and acquisition parameter settings, thereby allowing comparative evaluation, and that (ii) two independent readers analyzed all images in a coherent and standardized manner using the scoring systems of the official OMERACT guidelines. The fact that both readers' performance was characterized by high inter-reader reliability pays testimony to the validity of their comparative evaluation at the MCP joint level. Additionally, our results have a limited generalizability because of the different prior therapeutic regimens, yet the clinical presentation of increased disease activity was overall comparable. Therefore, we consider the results to be representative of a clinical setting, even though—admittedly—the methodological inaccuracy makes direct comparisons

difficult and different types of DMARDs and different treatment durations potentially change intensity, distribution, and quality/dimension of disease-related imaging sub-scores. Last, it is of relevance that MRI can support, but not replace, clinical assessment in the differentiation of inflammatory arthritis. Once the developed prediction model has been validated and substantiated in larger studies and proven to perform well in clinical practice, the clinical differentiation of inflammatory joint diseases may be greatly aided by MRI.

Conclusion

High-resolution imaging based on optimized sequence protocols, adequate magnetic field strengths, and dedicated coil technology is beneficial for the identification of relevant imaging features that may support the clinical differentiation of inflammatory conditions of the hand. At the MCP level, periarticular inflammation was strongly associated with PsA and may consequently guide diagnostic decision-making when it comes to differentiating PsA and RA.

Acknowledgments Alexander Lautwein, MD, Stefan Vorderbümen, MD, Miriam Frenken, MD, and Benedikt Ostendorf, MD, scientifically contributed to this work. We thank Mrs. Erika Rädisch for technically performing all MRI scans.

Funding information Open Access funding provided by Projekt DEAL. The project was funded by the “Pfizer GIP Inflammation Germany Research Initiative 2014” to PS and by a grant from the German “Bundesministerium für Bildung und Forschung” (BMBF), ArthroMark (01EC1009). DBA was supported by an internal research grant of the local research committee of the medical faculty. SN has been supported by grants from the “Deutsche Forschungsgemeinschaft” (DFG) (NE 2136/3-1).

Data availability The datasets used and/or analyzed during the current study are available from the corresponding author upon reasonable request.

Compliance with ethical standards

Conflict of interest The authors declare that they have no competing interests.

Open Access This article is licensed under a Creative Commons Attribution 4.0 International License, which permits use, sharing, adaptation, distribution and reproduction in any medium or format, as long as you give appropriate credit to the original author(s) and the source, provide a link to the Creative Commons licence, and indicate if changes were made. The images or other third party material in this article are included in the article's Creative Commons licence, unless indicated otherwise in a credit line to the material. If material is not included in the article's Creative Commons licence and your intended use is not permitted by statutory regulation or exceeds the permitted use, you will need to obtain permission directly from the copyright holder. To view a copy of this licence, visit <http://creativecommons.org/licenses/by/4.0/>.

References

- Rahman P, Nguyen E, Cheung C, et al. Comparison of radiological severity in psoriatic arthritis and rheumatoid arthritis. *J Rheumatol*. 2001;28(5):1041–4.
- Finzel S, Englbrecht M, Engelke K, et al. A comparative study of periarticular bone lesions in rheumatoid arthritis and psoriatic arthritis. *Ann Rheum Dis*. 2011;70(1):122–7.
- Benjamin M, McGonagle D. The anatomical basis for disease localisation in seronegative spondyloarthropathy at entheses and related sites. *J Anat*. 2001;199(Pt 5):503–26.
- McGonagle D. Imaging the joint and entheses: insights into pathogenesis of psoriatic arthritis. *Ann Rheum Dis*. 2005;64(Suppl 2):ii58–60.
- Taylor W, Gladman D, Helliwell P, et al. Classification criteria for psoriatic arthritis: development of new criteria from a large international study. *Arthritis Rheum*. 2006;54(8):2665–73.
- Tillett W, Costa L, Jadon D, et al. The CIASSification for Psoriatic ARthritis (CASPAR) criteria—a retrospective feasibility, sensitivity, and specificity study. *J Rheumatol*. 2012;39(1):154–6.
- Coates LC, Gossec L, Ramiro S, et al. New GRAPPA and EULAR recommendations for the management of psoriatic arthritis. *Rheumatology (Oxford)*. 2017;56(8):1251–3.
- Aletaha D, Neogi T, Silman AJ, et al. 2010 rheumatoid arthritis classification criteria: an American College of Rheumatology/European League Against Rheumatism collaborative initiative. *Arthritis Rheum*. 2010;62(9):2569–81.
- Aleo E, Migone S, Prono V, et al. Imaging techniques in psoriatic arthritis: update 2012–2014 on current status and future prospects. *J Rheumatol Suppl*. 2015;93:53–6.
- Abrar DB, Schleich C, Nebelung S, et al. High-resolution MRI of flexor tendon pulleys using a 16-channel hand coil: disease detection and differentiation of psoriatic and rheumatoid arthritis. *Arthritis Res Ther*. 2020;22(1):40.
- Ostergaard M, McQueen F, Wiell C, et al. The OMERACT psoriatic arthritis magnetic resonance imaging scoring system (PsAMRIS): definitions of key pathologies, suggested MRI sequences, and preliminary scoring system for PsA hands. *J Rheumatol*. 2009;36(8):1816–24.
- Ostergaard M, Peterfy C, Conaghan P, et al. OMERACT rheumatoid arthritis magnetic resonance imaging studies. Core set of MRI acquisitions, joint pathology definitions, and the OMERACT RA-MRI scoring system. *J Rheumatol*. 2003;30(6):1385–6.
- Merola JF, Espinoza LR, Fleischmann R. Distinguishing rheumatoid arthritis from psoriatic arthritis. *RMD Open*. 2018;4(2):e000656 (accessed 22 Feb 2019).
- Sudoł-Szopińska I, Pracoń G. Diagnostic imaging of psoriatic arthritis. Part II: magnetic resonance imaging and ultrasonography. *J Ultrason*. 2016;16(65):163–74.
- Anderson ML, Skinner JA, Felmlee JP, et al. Diagnostic comparison of 1.5 Tesla and 3.0 Tesla preoperative MRI of the wrist in patients with ulnar-sided wrist pain. *J Hand Surg [Am]*. 2008;33(7):1153–9.
- Lenk S, Ludescher B, Martirosan P, et al. 3.0 T high-resolution MR imaging of carpal ligaments and TFCC. *Rofo*. 2004;176(5):664–7.
- Wieners G, Detert J, Streitparth F, et al. High-resolution MRI of the wrist and finger joints in patients with rheumatoid arthritis: comparison of 1.5 Tesla and 3.0 Tesla. *Eur Radiol*. 2007;17(8):2176–82.
- Singh JA, Saag KG, Bridges SL, et al. American College of Rheumatology Guideline for the treatment of rheumatoid arthritis. *Arthritis Rheumatol (Hoboken, NJ)*. 2016. 2015;68(1):1–26.
- Gossec L, Coates LC, de Wit M, et al. Management of psoriatic arthritis in 2016: a comparison of EULAR and GRAPPA recommendations. *Nat Rev Rheumatol*. 2016;12(12):743–50.

20. Sewerin P, Schleich C, Brinks R, et al. Assessing associations of synovial perfusion, cartilage quality, and outcome in rheumatoid arthritis using dynamic contrast-enhanced magnetic resonance imaging. *J Rheumatol*. 2020;47(1):15–9.
21. Anderson J, Caplan L, Yazdany J, et al. Rheumatoid arthritis disease activity measures: American College of Rheumatology recommendations for use in clinical practice. *Arthritis Care Res*. 2012;64(5):640–7.
22. Schoels MM, Aletaha D, Alasti F, Smolen JS. Disease activity in psoriatic arthritis (PsA): defining remission and treatment success using the DAPSA score. *Ann Rheum Dis*. 2016;75(5):811–8. <https://doi.org/10.1136/annrheumdis-2015-207507>.
23. van Riel PLCM, Renskers L. The Disease Activity Score (DAS) and the Disease Activity Score using 28 joint counts (DAS28) in the management of rheumatoid arthritis. *Clin Exp Rheumatol*. 2016;34(5 Suppl 101):S40–4.
24. Schoels M, Aletaha D, Funovits J, et al. Application of the DAREA/DAPSA score for assessment of disease activity in psoriatic arthritis. *Ann Rheum Dis*. 2010;69(8):1441–7.
25. Østergaard M, Peterfy CG, Bird P, et al. The OMERACT rheumatoid arthritis magnetic resonance imaging (MRI) scoring system: updated recommendations by the OMERACT MRI in Arthritis Working Group. *J Rheumatol*. 2017;44(11):1706–12.
26. Glinatsi D, Lillegraven S, Haavardsholm EA, et al. Validation of the OMERACT magnetic resonance imaging joint space narrowing score for the wrist in a multireader longitudinal trial. *J Rheumatol*. 2015;42(12):2480–5.
27. Calmettes G, Drummond GB, Vowler SL. Making do with what we have: use your bootstraps. *Adv Physiol Educ*. 2012;36(3):177–80.
28. Ialongo C. Confidence interval for quantiles and percentiles. *Biochem Med (Zagreb)*. 2019;29(1):10101.
29. Hanley JA, McNeil BJ. The meaning and use of the area under a receiver operating characteristic (ROC) curve. *Radiology*. 1982;143(1):29–36.
30. Felbo SK, Terslev L, Østergaard M. Imaging in peripheral and axial psoriatic arthritis: contributions to diagnosis, follow-up, prognosis and knowledge of pathogenesis. *Clin Exp Rheumatol*. 2018;36 Suppl 114(5):24–4.
31. Healy PJ, Groves C, Chandramohan M, et al. MRI changes in psoriatic dactylitis—extent of pathology, relationship to tenderness and correlation with clinical indices. *Rheumatology (Oxford)*. 2008;47(1):92–5.
32. Benjamin M, Moriggl B, Brenner E, et al. The “entheses organ” concept: why enthesopathies may not present as focal insertional disorders. *Arthritis Rheum*. 2004;50(10):3306–13.
33. Benjamin M, McGonagle D. The entheses organ concept and its relevance to the spondyloarthropathies. *Adv Exp Med Biol*. 2009;649:57–70.
34. Benjamin M, Toumi H, Ralphs JR, et al. Where tendons and ligaments meet bone: attachment sites (entheses) in relation to exercise and/or mechanical load. *J Anat*. 2006;208(4):471–90.
35. Kaeley GS, Eder L, Aydin SZ, et al. Enthesitis: a hallmark of psoriatic arthritis. *Semin Arthritis Rheum*. 2018;48(1):35–43.
36. Kaeley GS, Eder L, Aydin SZ, et al. Dactylitis: a hallmark of psoriatic arthritis. *Semin Arthritis Rheum*. 2018;48(2):263–73.
37. Gutierrez M, Filippucci E, Salaffi F, et al. Differential diagnosis between rheumatoid arthritis and psoriatic arthritis: the value of ultrasound findings at metacarpophalangeal joints level. *Ann Rheum Dis*. 2011;70(6):1111–4 (accessed 21 Mar 2019).
38. Jevtic V, Watt I, Rozman B, Kos-Golja M, Demsar F, Jarh O. Distinctive radiological features of small hand joints in rheumatoid arthritis and seronegative spondyloarthritis demonstrated by contrast-enhanced (Gd-DTPA) magnetic resonance imaging. *Skelet Radiol*. 1995;24(5):351–5.
39. Fournié B, Margarit-Coll N, Champetier de Ribes TL, et al. Extrasynovial ultrasound abnormalities in the psoriatic finger. Prospective comparative power-Doppler study versus rheumatoid arthritis. *Joint Bone Spine*. 2006;73(5):527–31.
40. Marzo-Ortega H, Tanner SF, Rhodes LA, et al. Magnetic resonance imaging in the assessment of metacarpophalangeal joint disease in early psoriatic and rheumatoid arthritis. *Scand J Rheumatol*. 2009;38(2):79–83.
41. Ibrahim G, Groves C, Chandramohan M, et al. Clinical and ultrasound examination of the Leeds Enthesitis Index in psoriatic arthritis and rheumatoid arthritis. *ISRN Rheumatol*. 2011;2011:731917 (accessed 21 Mar 2019).
42. Saran S, Bagarhatta M, Saigal R. Diagnostic accuracy of ultrasonography in detection of destructive changes in small joints of hands in patients of rheumatoid arthritis: a comparison with magnetic resonance imaging. *J Assoc Physicians India*. 2016;64(11):26–30.
43. Eshed I, Feist E, Althoff CE, et al. Tenosynovitis of the flexor tendons of the hand detected by MRI: an early indicator of rheumatoid arthritis. *Rheumatology (Oxford)*. 2009;48(8):887–91.
44. Forney MC, Winalski CS, Schils JP. Magnetic resonance imaging of inflammatory arthropathies of peripheral joints. *Top Magn Reson Imaging*. 2011;22(2):45–59.
45. Sewerin P, Schleich C, Vordenbäumen S, et al. Update on imaging in rheumatic diseases: cartilage. *Clin Exp Rheumatol*. 2018;36 Suppl 114(5):139–44.
46. Vordenbäumen S, Schleich C, Lögters T, et al. Dynamic contrast-enhanced magnetic resonance imaging of metacarpophalangeal joints reflects histological signs of synovitis in rheumatoid arthritis. *Arthritis Res Ther*. 2014;16(5):452.
47. Nebelung S, Tingart M, Pufe T, et al. Ex vivo quantitative multiparametric MRI mapping of human meniscus degeneration. *Skelet Radiol*. 2016;45(12):1649–60.
48. Mori V, Sawicki LM, Sewerin P, et al. Differences of radiocarpal cartilage alterations in arthritis and osteoarthritis using morphological and biochemical magnetic resonance imaging without gadolinium-based contrast agent administration. *Eur Radiol*. 2019;29(5):2581–8.
49. Müller-Lutz A, Kamp B, Nagel AM, et al. Sodium MRI of human articular cartilage of the wrist: a feasibility study on a clinical 3T MRI scanner. *MAGMA*. 2020. <https://doi.org/10.1007/s10334-020-00856-2>.
50. Nebelung S, Brill N, Tingart M, et al. Quantitative OCT and MRI biomarkers for the differentiation of cartilage degeneration. *Skelet Radiol*. 2016;45(4):505–16.
51. Abrar DB, Schleich C, Nebelung S, et al. Proteoglycan loss in the articular cartilage is associated with severity of joint inflammation in psoriatic arthritis—a compositional magnetic resonance imaging study. *Arthritis Res Ther*. 2020;22(1):124.
52. Healy PJ, Helliwell PS. Dactylitis: pathogenesis and clinical considerations. *Curr Rheumatol Rep*. 2006;8(5):338–41.
53. Heidari B. Rheumatoid arthritis: early diagnosis and treatment outcomes. *Caspian J Intern Med*. 2011;2(1):161–70.
54. Gladman DD. Early psoriatic arthritis. *Rheum Dis Clin N Am*. 2012;38(2):373–86.

RESEARCH ARTICLE

Open Access



Functional MR imaging beyond structure and inflammation—radiographic axial spondyloarthritis is associated with proteoglycan depletion of the lumbar spine

Daniel B. Abrar^{1*}, Christoph Schleich¹, Styliani Tsiami², Anja Müller-Lutz¹, Karl Ludger Radke¹, Neela Holthausen¹, Miriam Frenken¹, Matthias Boschheidgen¹, Gerald Antoch¹, Johanna Mucke³, Philipp Sewerin³, Juergen Braun², Sven Nebelung^{1†} and Xenofon Baraliakos^{2†}

Abstract

Background: To compare the glycosaminoglycan (GAG) content of lumbar intervertebral disks (IVDs) of patients with ankylosing spondylitis (AS) and healthy volunteers and to investigate the association of GAG depletion and disease-related clinical and imaging features.

Methods: Lumbar spines of 50 AS patients (mean age 50 ± 10.5 years) and 30 age-matched volunteers were studied with 3-T magnetic resonance imaging (MRI) and conventional radiographs (CR). The MRI protocol included high-resolution morphological sequences and the compositional GAG chemical exchange saturation transfer imaging technique (gagCEST). Morphological images were analyzed by three raters for inflammatory activity, fat deposition, disk degeneration, and structural changes on CR. Clinical and serological measures included the Bath AS Disease Activity (BASDAI) and Bath AS Function (BASFI) Indices and C-reactive protein (CRP) levels. GagCEST values of both groups were compared using a linear mixed model. Kendall-Tau correlation analyses were performed.

Results: GagCEST values were significantly lower in AS patients ($2.0 \pm 1.7\%$) vs. healthy volunteers ($2.4 \pm 1.8\%$), $p = 0.001$. Small, yet significant correlations were found between gagCEST values and CRP levels ($r = -0.14$, $p = 0.007$), BASFI ($r = -0.18$, $p < 0.001$) and presence of syndesmophytes ($r = -0.17$, $p = 0.001$). No significant correlations were found with BASDAI, inflammation, and fat deposition MRI scores.

Conclusions: Lumbar spines of r-AS patients undergo significant GAG depletion, independently associated with syndesmophyte formation, functional disability, and increased serological inflammation markers. Beyond establishing a pathophysiological role of the cartilage in AS, these findings suggest that gagCEST imaging may have an adjunct confirmatory role in the assessment of disease-related pathological MRI findings in axial spondyloarthritis.

(Continued on next page)

* Correspondence: danielbenjamin.abrar@med.uni-duesseldorf.de

†Sven Nebelung and Xenofon Baraliakos contributed equally to this work.

¹Department of Diagnostic and Interventional Radiology, University Düsseldorf, Medical Faculty, 40225 Düsseldorf, Germany

Full list of author information is available at the end of the article



© The Author(s). 2020 **Open Access** This article is licensed under a Creative Commons Attribution 4.0 International License, which permits use, sharing, adaptation, distribution and reproduction in any medium or format, as long as you give appropriate credit to the original author(s) and the source, provide a link to the Creative Commons licence, and indicate if changes were made. The images or other third party material in this article are included in the article's Creative Commons licence, unless indicated otherwise in a credit line to the material. If material is not included in the article's Creative Commons licence and your intended use is not permitted by statutory regulation or exceeds the permitted use, you will need to obtain permission directly from the copyright holder. To view a copy of this licence, visit <http://creativecommons.org/licenses/by/4.0/>. The Creative Commons Public Domain Dedication waiver (<http://creativecommons.org/publicdomain/zero/1.0/>) applies to the data made available in this article, unless otherwise stated in a credit line to the data.

(Continued from previous page)

Trial registration: 3980 (<https://studienregister.med.uni-duesseldorf.de>)

Keywords: Ankylosing spondylitis, Magnetic resonance imaging, gagCEST, Spine, Rheumatic diseases, Spondyloarthropathy

Introduction

Ankylosing spondylitis (AS), also called radiographic spondyloarthritis (r-axSpA), as the prototype disease of all axSpA, is a chronic inflammatory disease that predominantly affects the sacroiliac joints (SIJ) and the spine [1]. It leads to back pain, restricted mobility, and, if left untreated, to ankylosis and severe functional disability [2, 3]. As of today, magnetic resonance imaging (MRI) is a cornerstone imaging technique for identification and may also be helpful in treatment monitoring of axSpA [4]. This is reflected by the inclusion of MRI of the SIJ into the Assessment of SpondyloArthritis Society (ASAS) classification criteria [5]. However, MRI of the spine was not included in these criteria due to the lack of specificity when compared to degenerative spinal lesions [6]. Nonetheless, in current clinical and research practice, MRI of both the SIJ and the spine is widely used due to its non-invasiveness, superior soft tissue contrast, high spatial resolution, functional capability, and absence of ionizing radiation.

On the other hand, new bone formation is a key feature of chronic stages of axSpA and contributes to the burden of the disease and functional disability beyond mere inflammation-related symptoms [7–9]. Earlier studies demonstrated that joint remodeling in patients with r-axSpA is characterized by incipient cartilage loss, subchondral infiltration of fibrous tissue, and later on eventual formation of new bone [10, 11]. In an earlier study, our group demonstrated the feasibility of glycosaminoglycan chemical exchange saturation transfer imaging (gagCEST) of the lumbar intervertebral disks (IVD) in a pilot study of 9 patients with axSpA [12]. GagCEST imaging is a compositional MRI technique that relies on the chemical exchange of water protons between GAG and bulk water molecules. For the induction of a CEST effect, a pool of solute protons is saturated by a frequency-specific radiofrequency (RF) pulse at different offset frequencies around the water resonance and then transferred to the bulk water pool via chemical exchange, which consequently reduces its signal. The signal is then used to quantify the CEST effect at the GAG-specific frequency range (0.9–1.9 ppm) by analysis of the magnetization transfer ratio asymmetry (MTR_{asym}), which correlates with the underlying GAG concentration of the given IVD [13–15].

The aim of this study was to systematically assess the association of GAG depletion in lumbar IVDs with structural and inflammatory imaging features as well as

clinical and serological reference measures in a larger patient population of r-axSpA patients and controls.

Building on preliminary evidence that suggested a role for advanced imaging techniques in the evaluation of r-axSpA [12, 16, 17], we hypothesized that (a) lumbar IVDs of patients with r-axSpA contained less GAG than a group of age-matched volunteers and (b) that GAG depletion was associated with disease-related acute and chronic inflammation and structural changes of the adjacent vertebrae as well as functional limitations.

Methods

Study population

Fifty patients with active r-axSpA according to the ASAS classification criteria [5] (mean age 50 ± 10.5 , range 25–69 years) and mean disease duration of 13 ± 11 years (range, 0–40 years) were prospectively recruited. R-axSpA was defined as definitive radiographic sacroiliitis on the sacroiliac joint conventional radiography according to the New York criteria [18, 19]. At the time of recruitment, 44/50 patients received biological disease-modifying antirheumatic drugs (bDMARDs), while the other 6 patients were not treated with any permanent medication. In addition, 30 volunteers (mean age 47 ± 13.5 , range 30–76 years) were included as a control group. The exclusion criteria for all participants were prior spine surgery, a body mass index < 18.5 or > 30 kg/m², radiculopathy, known disk extrusion, congenital spine deformities, and being underage. For the control group, the exclusion criteria were expanded to chronic lower back pain (LBP), acquired spine deformities, and chronic inflammatory diseases affecting the musculoskeletal system.

Written informed consent was acquired from all participants before the initiation of the study. The study was approved by the local ethical committee (Ethical Committee, Medical Faculty, University of Düsseldorf, Germany, study number 5087R).

The characteristics of the study population are given in Table 1.

Imaging studies

MRI studies of the lumbar spine of all participants were performed on a clinical 3-T scanner (Magnetom Prisma, Siemens Healthineers, Erlangen, Germany) with a 32-channel body and a 24-channel spine matrix coil (both Siemens Healthineers) in the supine position.

Table 1 Demographic, clinical, serological, and functional information of the study population

	Patients	Volunteers
Age [years]	50 ± 10.5	47 ± 13.5
Sex [female/male]	14/36	15/15
Disease duration [years]	9 ± 7	na
CRP level [mg/dL]	0.75 ± 0.76	na
BASDAI [0–10]	5.13 ± 1.84	na
BASFI [0–10]	5.36 ± 2.15	na
Medication	bDMARD [<i>n</i> = 44] None [<i>n</i> = 6]	na

Data are given as means ± standard deviations. Only for the radiographic axial spondylarthritis (r-axSpA) patients were data on disease durations, CRP levels, and functional scores, i.e., Bath Ankylosing Spondylitis Disease Activity and Bath Ankylosing Spondylitis Function Indices (BASDAI and BASFI), available. *na* not available; *CRP* C-reactive protein, normal range 0–0.5 mg/dL; *bDMARD* biological disease-modifying drug

All MRI examinations included morphological and compositional sequences. Morphological imaging comprised T1-weighted (T1w), T2-weighted (T2w), and short tau inversion recovery (STIR) sequences in the sagittal orientation, while compositional imaging included gagCEST and water saturation shift referencing (WASSR) sequences in the sagittal orientation. The detailed sequence parameters are given in Table 2.

Additionally, standard conventional radiographs (CR) of the lumbar spines (Th12–S3) in anterior-posterior (ap) and lateral projections were obtained after the recruitment.

Image analysis

All images were blinded to the participants’ diagnoses and demographics and were then independently analyzed by two radiologists (DBA and CS) with long-

Table 2 Detailed magnetic resonance imaging (MRI) sequence parameters

Sequence	STIR		T2w TSE		T1w TSE		gagCEST		WASSR	
Imaging plane	Sagittal	Sagittal	Sagittal	Sagittal	Sagittal	Sagittal	Sagittal	Sagittal	Sagittal	Sagittal
TE/TR [ms]	57/3800	95/3500	9.5/650	5.1/10	5.1/10					
Flip angle [°]	150	160	150	10	10					
Slice thickness [mm]	4	4	4	5	5					
FoV [mm × mm]	300 × 300	300 × 300	300 × 300	300 × 300	300 × 300					
Pixel size [mm × mm]	0.8 × 0.8	0.7 × 0.7	0.7 × 0.7	1.6 × 1.6	1.6 × 1.6					
Number of slices	15	15	15	1	1					

Imaging plane, echo and repetition time (TE/TR), flip angle, slice thickness, field of view (FoV), pixel size, and number of slices are given for all sequences (short tau inversion recovery, T2-weighted turbo spin-echo (T2w TSE), T1w TSE, gagCEST, and WASSR)

standing experience in musculoskeletal imaging. In case of discrepant findings, consensus was established with the assistant opinion of a third experienced rater (SN).

The lumbar IVD segments L1/L2–L5/S1 of all participants were scored individually on sagittal T2w images according to the Pfirrmann classification [20]. Briefly, the Pfirrmann classification is based on five grades and allows dichotomization of non-degenerative (grades 1 and 2) and degenerative IVDs (grades 3–5) on the basis of intensity and structure of the nucleus pulposus (NP), its distinction from the annulus fibrosus (AF), and disk height.

Further, each lumbar segment was separately analyzed according to the Spondyloarthropathies Research Consortium of Canada (SPARCC) score, which is an MRI index for scoring inflammation of the spine [21]. To this end, each lumbar discovertebral unit (DVU) was divided into four quadrants: upper anterior, lower anterior, upper posterior, and lower posterior endplate. The presence of “acute inflammation/bone marrow edema” was assessed based on the high signal intensity on STIR images. For each DVU, three consecutive slices were selected demonstrating the most pathological slices for that particular segment. On each slice, the imaging feature “bone marrow edema” was scored present or absent resulting in a maximum score of 12 per DVU. In addition, we evaluated all lumbar segments for the presence of “fatty depositions” (as a sign of chronic inflammation) by proceeding in the same manner. The presence of “fatty deposition” was assessed based on the high signal intensity on T1w and T2w images.

Additionally, as a radiographic score, all anterior vertebral corners (VC) of the lumbar segments were evaluated (score 0–2) on lateral CR projections for the presence of syndesmophytes (score 1) or bridging syndesmophytes (score 2).

GagCEST analyses were in line with the standard post-processing practice as published previously [22, 23]. Before gagCEST analysis, motion correction was performed for both CEST and WASSR datasets using a diffeomorphic registration approach incorporated into a dedicated software (fMRLung, Siemens Healthineers) as published before [24].

As in earlier studies [25, 26], WASSR data were used to correct B_0 field inhomogeneities by the WASSR maximum-symmetry algorithm with the calculation of a pixel-wise frequency offset curve. These offset-corrected CEST curves divided by the signal without pre-saturation (S_0) were defined as the so-called z -spectrum ($Z(\omega)$). The maximum frequency offset of each z -spectrum was $\Delta\omega = 3$ ppm. Next, we used the magnetization transfer asymmetry (MTR_{asym}) (defined as $MTR_{asym}(\Delta\omega) = Z(-\Delta\omega) - Z(\Delta\omega)$) for the evaluation of the gagCEST effect [25]. MTR_{asym} maps were calculated

using the average value of MTR_{asym} in the GAG-specific range of $\Delta\omega = 0.9\text{--}1.9$ ppm. MTR_{asym} values are given in percentage. For the analysis of the CEST effect, regions of interest (ROIs) were defined based on a customized in-house script implemented in Matlab (MATLAB, R2018a, The MathWorks, Inc., MA, USA) that automatically detects lumbar IVD segments.

Then, all ROIs were automatically placed in the lumbar IVDs by an in-house written script for the Matlab software. The disk segmentation was based on Bayes classification to divide bone and ligaments from disk cartilage [27]. All automatically placed ROIs were visually confirmed for the correct position by a board-certified radiologist (CS). No ROIs had to be manually corrected. In total, nine individuals with 45 IVDs had to be excluded from the gagCEST analysis due to excessive motion artifacts (6 r-axSpA, 3 volunteers). For the sake of readability, MTR_{asym} values are referred to as gagCEST values.

Clinical evaluation

For every patient, the Bath Ankylosing Spondylitis Disease Activity Index (BASDAI) and Bath Ankylosing Spondylitis Function Index (BASFI) [28, 29] were assessed. In addition, C-reactive protein levels [mg/dL] were determined in all patients.

Statistical analysis

The SPSS software (IBM, version 22, Armonk, NY, USA) was used for all statistical analyses performed by KLR and DBA. For descriptive analysis, mean gagCEST values of the AF and the NP \pm standard deviation, median, and range (minimum-maximum) were calculated for volunteers and patients. For the comparison of gagCEST values between both cohorts and between AF and NP, a multivariable statistical analysis was performed using a linear mixed model (LMM). The model included a subject-specific random intercept, the factors healthy volunteer/patient, age, gender, and the interaction of these factors. The LMM was fitted using a restricted maximum likelihood approach (REML) [30]. Based on this final model, the mean differences of gagCEST values were calculated and evaluated for significance. For correlation analyses, the Kendall Tau correlation coefficient τ was calculated. Correlation strengths were graded as suggested by Cohen [31]: small (< 0.3), moderate ($0.3\text{--}0.5$), and large (> 0.5). p values < 0.05 were considered significant.

Results

Clinical scores: BASDAI, BASFI, and serum CRP levels

Patient characteristics and serological, clinical, and functional data are summarized in Table 1. Overall, patients showed active disease, with a mean BASDAI of 5.1 ± 1.8

and mean CRP levels of 0.8 ± 0.8 mg/dL, and also high levels of functional impairment, with a mean BASFI of 5.4 ± 2.2 .

Morphological analysis

Morphological imaging findings for the presence of syn-desmophytes and fatty depositions, and according to the Pfirrmann classification, and SPARCC are shown in Table 3. Typical disease-related MR imaging features are shown in Fig. 1.

The distribution of IVDs according to the Pfirrmann classification were as follows: total study population—grade 1 [$n = 0$], grade 2 [$n = 285$], grade 3 [$n = 99$], grade 4 [$n = 14$], and grade 5 [$n = 2$]; r-axSpA patients—grade 1 [$n = 0$], grade 2 [$n = 180$], grade 3 [$n = 58$], grade 4 [$n = 10$], and grade 5 [$n = 2$]; volunteers—grade 1 [$n = 0$], grade 2 [$n = 105$], grade 3 [$n = 41$], grade 4 [$n = 4$], and grade 5 [$n = 0$].

All scores were equally distributed between the lumbar segments, i.e., no significant differences were found between the evaluated lumbar segments at any given score (Table 3).

Comparative analysis of gagCEST values: NP vs. AF and NP vs. Pfirrmann grading

In all IVDs, the NP showed significantly higher gagCEST values than the AF (AF $1.1 \pm 1.3\%$, NP $2.2 \pm 1.8\%$, $p < 0.001$). GagCEST values were significantly affected by the morphological degeneration of the IVD as assessed by the Pfirrmann score. NPs of IVDs with Pfirrmann grades ≤ 2 , i.e., non-degenerated IVDs, had significantly higher gagCEST values than NPs of IVDs with Pfirrmann grades ≥ 3 , i.e., degenerated IVDs—NPs (Pfirrmann grades ≤ 2) $2.7 \pm 1.7\%$ and NPs (Pfirrmann grades ≥ 3) $0.7 \pm 0.9\%$; $p = 0.003$. No significant differences were found between gagCEST values of the NPs of IVDs of the different lumbar segments in patients and volunteers (L1/2 $2.1 \pm 1.7\%$, L2/3 $2.2 \pm 1.7\%$, L3/4 $2.0 \pm 1.7\%$, L4/5 $2.1 \pm 1.5\%$, L5/S1 $1.9 \pm 2.1\%$, $p = 0.06$).

Comparative analyses of gagCEST values: patients vs. volunteers

Mean gagCEST values of r-axSpA patients and volunteers as well as the comparative analysis are presented in Table 3.

Over all segments, gagCEST values of the NP of lumbar IVDs of r-axSpA patients were significantly lower than of volunteers (patients $2.0 \pm 1.7\%$, control $2.4 \pm 1.8\%$, $p = 0.001$). GagCEST maps of representative patients and volunteers confirmed these findings (Fig. 2).

Table 3 Analysis of morphological and compositional imaging features of lumbar intervertebral disks (IVDs)

Score		Segment					Overall	p value
		L1/2	L2/3	L3/4	L4/5	L5/S1		
gagCEST values [%]	Patients	2.7 ± 1.7	2.1 ± 1.7	1.9 ± 1.6	1.8 ± 1.4	1.9 ± 2.0	2.0 ± 1.7	0.001
	Volunteers	3.1 ± 1.7	2.2 ± 1.6	2.1 ± 1.6	2.4 ± 1.7	2.1 ± 2.3	2.4 ± 1.8	
Pfirrmann Score [1–5]	Patients	2.4 ± 0.7	2.5 ± 0.8	2.4 ± 0.7	2.5 ± 0.6	2.7 ± 0.8	2.5 ± 0.7	0.119
	Volunteers	2.1 ± 0.5	2.3 ± 0.7	2.4 ± 0.6	2.4 ± 0.6	2.6 ± 0.7	2.4 ± 0.6	
SPARCC acute inflammation [0–12]	Patients	1 ± 2.4	0.4 ± 1.3	0.2 ± 1	0.6 ± 1.6	0.6 ± 2.3	0.6 ± 1.8	0.318
Fatty depositions [0–12]	Patients	4.3 ± 3.9	3.4 ± 2.8	3.9 ± 3.2	4.2 ± 3.1	3.8 ± 3.1	3.9 ± 3.2	0.723
Syndesmophytes [0–2]	Patients	1.3 ± 1.3	1.2 ± 1.2	1.3 ± 1.1	1.2 ± 1.2	1.4 ± 1.4	1.3 ± 1.2	0.894

The mean imaging measures as a function of the study cohort (i.e., patient and volunteer) and intervertebral disk segment level. Data are means ± standard deviations. The mean values of the glycosaminoglycan chemical exchange saturation transfer (gagCEST) values were compared with a linear mixed model comprising a subject-specific random intercept. Overall, the mean values of the Pfirrmann grading, the SPARCC, presence of fatty depositions, and syndesmophytes of the patient and the control group were compared by the Kruskal-Wallis test. *p* values < 0.05 were considered significant. MRI scores were Pfirrmann scores, Spondyloarthritis Research Consortium of Canada (SPARCC), and the presence of fatty deposition (chronic inflammation of vertebral corners). The presence of syndesmophytes was scored by CR

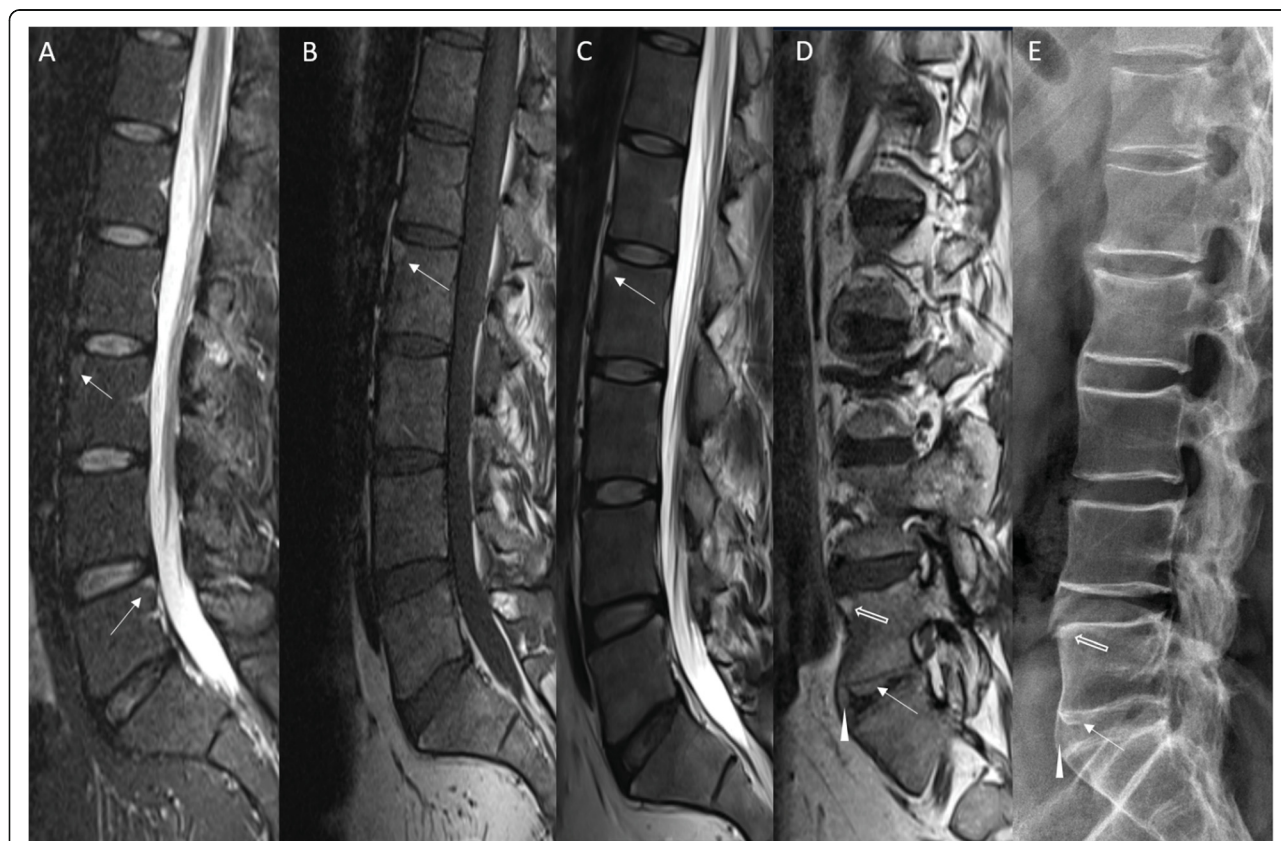


Fig. 1 Multi-modality representation of typical imaging findings in ankylosing spondylitis (AS). Morphological MRI findings (a–d) and radiographical findings (e) are demonstrated. **a–c** Sagittal short tau inversion recovery (STIR, **a**), T1-weighted (T1w, **b**), and T2-weighted (T2w, **c**) images of the lumbar spine (T12–S2) of a 31-year-old male with r-axSpA. Typical disease-related changes are acute inflammation of vertebral corners (**a**) that are visible as multi-segmental focal signal hyperintensities of the anterior and posterior corners of vertebral endplates (white arrows in **a**). Signs of chronic inflammation, i.e., fatty infiltration, of the vertebral endplate corners are detected as signal hyperintensities in T1w and T2w images (white arrows in **b** and **c**). **d, e** Sagittal T1w image (obtained laterally at the height of the neuroforaminal openings) and lateral radiographic projection of the lumbar spine of a 46-year-old male with AS. Here, chronic inflammation at a vertebral endplate corner is visible as a focal signal hyperintensity (block arrow in **d**) or focal sclerosis (block arrow in **e**) of the upper anterior corner of the vertebral body of L5. New bone formations can be seen as bridging syndesmophytes (arrowheads) and as transdiskal ankylosis (white arrows)

No significant differences were found between the gagCEST values of treated and non-treated patients (treated 2.1 ± 1.8 ; non-treated 2.1 ± 1.24 ; $p = 0.904$).

Correlation analyses

The correlations of compositional cartilage measures, i.e., gagCEST values, with serological (CRP level), clinical/functional (BASDAI and BASFI), and imaging (SPARCC, fatty depositions, syndesmophytes) scores of lumbar IVDs are presented in Table 4.

Significant, yet small and negative correlations were found between gagCEST values and CRP levels ($\tau = -0.14$, $p = 0.007$), BASFI ($\tau = -0.18$, $p < 0.001$), and syndesmophytes ($\tau = -0.17$, $p = 0.001$). No significant

correlations were found between gagCEST values and BASDAI, SPARCC, and fatty depositions.

Discussion

The most important findings of this study were that lumbar IVDs of patients with r-axSpA had significantly lower gagCEST values, i.e., a lower GAG content, than those of an age-matched control group and that these compositional changes were associated with variable structural changes on the level of the patient and the spine. More specifically, the lumbar IVDs' GAG content was associated with serological CRP levels, functional BASFI scores, and presence of syndesmophytes, while no association was observed with acute or chronic inflammation scores or patient-reported BASDAI scores.

Anecdotal evidence suggested that the composition of IVDs changed in patients with axSpA as compared to healthy volunteers [12]. Building on the preliminary findings, our study provides substantial evidence that compositional changes of the lumbar spine are associated with numerous structural and inflammatory changes in a larger and homogenous cohort of patients with r-axSpA, which is considered the prototypical axSpA disease. GAG depletion is an established sign of early cartilage changes that precedes morphologically visible damage [32, 33]. Interestingly, since the 1950s, research has indicated that cartilage loss plays a significant role in the pathophysiology of r-axSpA, too [34, 35]. Also, more recent studies have highlighted the affection of the joint cartilage in the disease course. In histological studies, Bleil et al. demonstrated that cartilage degradation as shown by cartilage thinning, increased chondrocyte apoptosis, and proteoglycan loss promoted by the invasion of the subchondral bone are hallmark changes of joint remodeling in r-axSpA [10, 36, 37]. Furthermore, they demonstrated that cartilage involvement in r-axSpA differed from OA, especially regarding the affection of the subchondral plate [10]. According to other studies, the cartilage layer of the joints is the primary site for inflammation and necessary for its induction [11]. Our results confirm these histological findings in the area of the vertebral bodies, as decreased GAG contents of morphologically unremarkable lumbar IVDs were observed in patients with r-axSpA. It was hypothesized that the development of syndesmophytes is preceded by cartilage loss [8]. These syndesmophytes are not only a mere sign of long-standing inflammation, but are the main cause of irreversible functional disability and independent from inflammation-related stiffness and pain [7]. As the prevention of radiographic disease progression is a major treatment goal in r-axSpA [38], a better

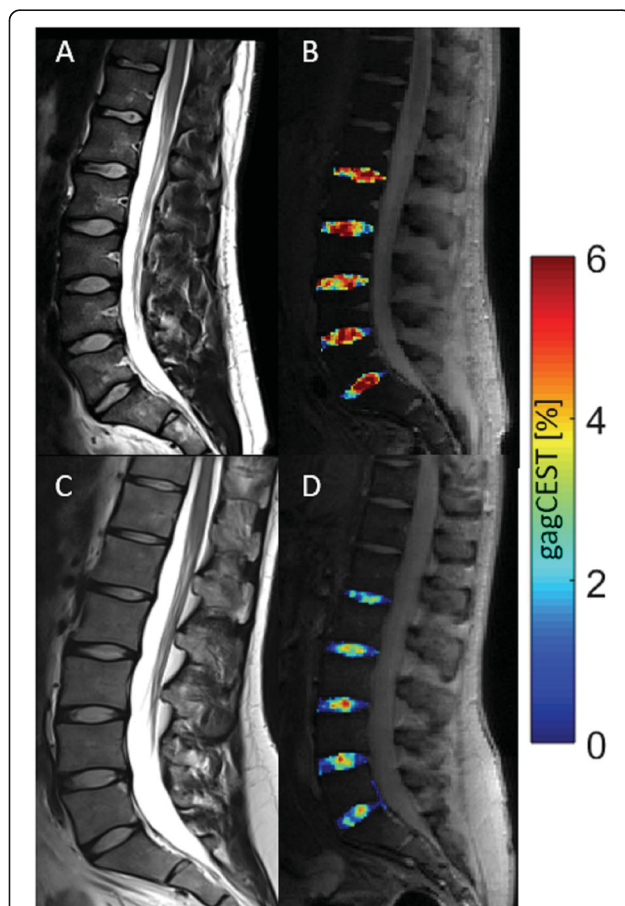


Fig. 2 Representative morphological and compositional imaging findings of the lumbar spine of a volunteer (a, b) and a patient with r-axSpA (AS; c, d). **a, c** Sagittal T2-weighted images show the absence of gross morphological signs of degeneration, in particular of the intervertebral disks (IVDs). **b, d** Sagittal gagCEST images with overlaid colored gagCEST maps for visualization of the GAG content. High GAG content as indicated by high gagCEST values is illustrated in red, while low GAG content is indicated in blue. Notably, this patient with r-axSpA demonstrated lower GAG contents than this volunteer despite non-degenerated IVDs in both individuals

Table 4 Correlation analyses of gagCEST values of lumbar IVDs and serological (CRP level), clinical/functional (BASDAI and BASFI), and imaging scores. *p* values < 0.05 were considered significant and are given in bold. Please refer to Table 3 for an explanation of the abbreviations

		Kendall Tau correlation coefficient τ	<i>p</i> value
gagCEST values vs.	CRP levels	- 0.14	0.007
	BASDAI	0.04	0.400
	BASFI	- 0.18	< 0.001
	SPARCC acute inflammation	0.06	0.285
	Fatty depositions	- 0.09	0.055
	Syndesmophytes	- 0.17	0.001

understanding of syndesmophyte formation and earlier detection of bone proliferations seems beneficial and a promising diagnostic target. It might be beneficial to evaluate cartilaginous structures for subtle changes that eventually lead to syndesmophyte formation, potentially allowing for earlier diagnosis and treatment. Therefore, considering our findings, gagCEST imaging could be of great interest for expanded disease stratification and treatment monitoring.

Our study demonstrates significant, yet small negative correlations between the GAG contents of lumbar IVDs and CRP levels, the functional BASFI score, and the presence of syndesmophytes. In contrast, no correlations were found between GAG contents and the BASDAI scores as an established patient-reported outcome of disease activity, or the SPARCC score with its focus on acute inflammation, or the presence of fatty depositions as a sign of chronic inflammatory changes of the vertebral endplates. Hence, overall, weak correlations were found for GAG content and structural changes of the spine and functional disability, but not for inflammatory imaging features and inflammation-related pain and stiffness. Considering the abovementioned concepts, it seems plausible that the GAG contents demonstrated significant correlations with structural changes and functional disability as opposed to no significant correlations with inflammatory changes and inflammation-related symptoms. Against this background, the earlier study by Roos and Dahlberg has to be considered, which demonstrated physical activity might lead to anabolic GAG remodeling [39]. In their study, patients at risk of osteoarthritis of the knee joint displayed an increase in GAG in their articular cartilage after completing a 4-month exercise routine. Considering that patients with r-axSpA are prone to physical inactivity due to the disease, the opposite effects of catabolic GAG depletion are likely.

When interpreting our results, some limitations need to be mentioned. First, gagCEST imaging of the cartilage still requires histological validation. Because of obvious ethical considerations, we could not perform IVD biopsies for histological analyses. Second, the disease

duration of our patient cohort was quite heterogeneous ranging from 0 to 40 years, which might be the reason for increased statistical variability, yet it is fully reflective of the clinical reality. Also, most of our r-axSpA patients were treated by bDMARDs with largely well-controlled symptomatology. Nonetheless, future studies should include a more homogenous study population, in particular in terms of disease duration to establish the potential value of compositional assessment of the spine across variable disease durations. Third, we only evaluated lumbar, but not thoracic IVDs, which are usually considered in established axSpA imaging scores, such as the mSASSS. However, as of today, gagCEST imaging is especially prone to movement artifacts, such as breathing, and may not be implemented at the thoracic level in the foreseeable future. Further, the proportion of females was higher in the control than in the patient group, which potentially affected the results, since anecdotal evidence suggests a higher proteoglycan content of lumbar IVDs in females than in males [26]. However, since the factor “gender” was included in the LMM that was used for our statistical analysis, we consider the differences in gender distribution only a minor limitation.

Conclusions

In conclusion, we found a significantly lower GAG content in lumbar IVDs of patients with r-axSpA compared to the healthy control group. Lower GAG contents were associated with structural alterations of the spine such as syndesmophyte formation, and functional disabilities but not with inflammatory changes of the vertebral endplates or inflammation-related pain and stiffness. Beyond establishing a pathophysiological role of the cartilage in r-axSpA, these findings suggest that—once substantiated by further studies—gagCEST imaging may have an adjunct diagnostic role in the assessment of disease severity and treatment effects in spondyloarthritis.

Abbreviations

AS: Ankylosing spondylitis; ASAS: Assessment of SpondyloArthritis International Society; axSpA: Axial spondyloarthritis; BASDAI: Bath Ankylosing Spondylitis Disease Activity Index; BASFI: Bath Ankylosing Spondylitis Function Index; CEST: Chemical exchange saturation transfer; CRP: C-reactive

protein; DMARD: Disease-modifying antirheumatic drug; FoV: Field of view; GAG: Glycosaminoglycan; IVD: Intervertebral disk; MRI: Magnetic resonance imaging; mSASSS: Modified Stoke Ankylosing Spondylitis Spinal Score; MTR_{asym}: Magnetization transfer ratio asymmetry; OA: Osteoarthritis; r-axSpA: Radiographic axial spondyloarthritis; SIJ: Sacroiliac joint; SPAR CC: Spondyloarthropathy Research Consortium of Canada; STIR: Short tau inversion recovery; TE: Echo time; TR: Repetition time; VC: Vertebral corner

Acknowledgements

We thank Mrs. Erika Rädtsch for the technical acquisition of all MRI studies.

Authors' contributions

All authors read and approved the final manuscript.

DBA: acquisition, analysis, and interpretation of the data; draft and design of the work.

CS: conception and design of the study; interpretation and analysis of the data; draft and design of the work; revision of the work.

SN, MF, JB, and KLR: interpretation and analysis of the data; draft and design of the work; revision of the work.

GA: conception and design of the study; interpretation and analysis of the data; revision of the work.

PS, NH, and AML: design and conception of the study; analysis and interpretation of the data; revision of the work.

JM, ST, and XB: design and conception of the study; draft and design of the work; revision of the work.

Funding

DBA was supported by the local research committee of the medical faculty. SN has been supported by grants from the "Deutsche Forschungsgemeinschaft" (DFG) (NE 2136/3-1). Open Access funding enabled and organized by Projekt DEAL.

Availability of data and materials

The datasets used and/or analyzed during the current study are available from the corresponding author on reasonable request.

Ethics approval and consent to participate

The study was approved by the local ethics committee (3980).

Consent for publication

Written and informed consent was obtained from all patients before the initiation of the study.

All authors agreed to the publication of this manuscript.

Competing interests

The authors declare that they have no competing interests.

Author details

¹Department of Diagnostic and Interventional Radiology, University Düsseldorf, Medical Faculty, 40225 Düsseldorf, Germany. ²Rheumazentrum Ruhrgebiet Herne, Ruhr University Bochum, Claudiusstr. 45, 44649 Herne, Germany. ³Policlinic and Hiller Research Unit of Rheumatology, UKD, Heinrich Heine University Düsseldorf, Moorenstrasse 5, 40225 Düsseldorf, Germany.

Received: 16 June 2020 Accepted: 7 September 2020

Published online: 17 September 2020

References

- Khmelnitskii N, Regel A, Baraliakos X. The role of imaging in diagnosing axial spondyloarthritis. *Front Med (Lausanne)*. 2018;5:106. Published 2018 Apr 17. <https://doi.org/10.3389/fmed.2018.00106>.
- Braun J. Axial spondyloarthritis including ankylosing spondylitis. *Rheumatology (Oxford)*. 2018;57(suppl_6):vi1–3.
- Baraliakos X, Hermann K-GA, Xu S, et al. Spinal mobility in the cervical and lumbar spine correlates with magnetic resonance imaging findings for inflammatory and structural changes in patients with active ankylosing spondylitis. *Clin Exp Rheumatol*. 2020;38(3):467–71.
- Baraliakos X, Davis J, Tsuji W, et al. Magnetic resonance imaging examinations of the spine in patients with ankylosing spondylitis before and after therapy with the tumor necrosis factor alpha receptor fusion protein etanercept. *Arthritis Rheum*. 2005;52(4):1216–23.
- Sieper J, Rudwaleit M, Baraliakos X, et al. The Assessment of SpondyloArthritis international Society (ASAS) handbook: a guide to assess spondyloarthritis. *Ann Rheum Dis*. 2009;68(Suppl 2):ii1–44.
- Hermann K-GA, Baraliakos X, van der Heijde DMFM, et al. Descriptions of spinal MRI lesions and definition of a positive MRI of the spine in axial spondyloarthritis: a consensual approach by the ASAS/OMERACT MRI study group. *Ann Rheum Dis*. 2012;71(8):1278–88.
- Landewé R, Dougados M, Mielants H, et al. Physical function in ankylosing spondylitis is independently determined by both disease activity and radiographic damage of the spine. *Ann Rheum Dis*. 2009;68(6):863–7.
- de Koning A, Schoones JW, van der Heijde D, et al. Pathophysiology of axial spondyloarthritis: consensus and controversies. *Eur J Clin Invest*. 2018; 48(5):e12913.
- Machado P, Landewé R, Braun J, et al. Both structural damage and inflammation of the spine contribute to impairment of spinal mobility in patients with ankylosing spondylitis. *Ann Rheum Dis*. 2010;69(8):1465–70.
- Bleil J, Maier R, Hempfing A, et al. Histomorphologic and histomorphometric characteristics of zygapophyseal joint remodeling in ankylosing spondylitis. *Arthritis Rheumatol (Hoboken, N.J.)*. 2014;66(7):1745–54.
- Appel H, Kuhne M, Spiekermann S, et al. Immunohistochemical analysis of hip arthritis in ankylosing spondylitis: evaluation of the bone-cartilage interface and subchondral bone marrow. *Arthritis Rheum*. 2006;54(6):1805–13.
- Schleich C, Müller-Lutz A, Matuschke F, et al. Glycosaminoglycan chemical exchange saturation transfer of lumbar intervertebral discs in patients with spondyloarthritis. *J Magn Reson Imaging*. 2015;42(4):1057–63.
- Kogan F, Hariharan H, Reddy R. Chemical exchange saturation transfer (CEST) imaging: description of technique and potential clinical applications. *Curr Radiol Rep*. 2013;1(2):102–14.
- Vinogradov E, Sherry AD, Lenkinski RE. CEST: from basic principles to applications, challenges and opportunities. *J Magn Reson*. 2012;229:155–72.
- Schleich C, Müller-Lutz A, Zimmermann L, et al. Biochemical imaging of cervical intervertebral discs with glycosaminoglycan chemical exchange saturation transfer magnetic resonance imaging: feasibility and initial results. *Skelet Radiol*. 2016;45(1):79–85.
- Wang D, Yin H, Liu W, et al. Comparative analysis of the diagnostic values of T2 mapping and diffusion-weighted imaging for sacroiliitis in ankylosing spondylitis. *Skelet Radiol*. 2020.
- Zhang M, Le Zhou HN, et al. Assessment of active and inactive sacroiliitis in patients with ankylosing spondylitis using quantitative dynamic contrast-enhanced MRI. *J Magn Reson Imaging*. 2017;46(1):71–8.
- Slobodin G, Eshed I. Non-radiographic axial spondyloarthritis. *Isr Med Assoc J*. 2015;17(12):770–6.
- van der Linden S, Valkenburg HA, Cats A. Evaluation of diagnostic criteria for ankylosing spondylitis. A proposal for modification of the New York criteria. *Arthritis Rheum*. 1984;27(4):361–8.
- Pfirrmann CW, Metzendorf A, Zanetti M, et al. Magnetic resonance classification of lumbar intervertebral disc degeneration. *Spine*. 2001;26(17):1873–8.
- Maksymowych WP, Inman RD, Salonen D, et al. Spondyloarthritis Research Consortium of Canada magnetic resonance imaging index for assessment of spinal inflammation in ankylosing spondylitis. *Arthritis Rheum*. 2005;53(4): 502–9.
- Schleich C, Müller-Lutz A, Eichner M, et al. Glycosaminoglycan chemical exchange saturation transfer of lumbar intervertebral discs in healthy volunteers. *Spine*. 2016;41(2):146–52.
- Schleich C, Müller-Lutz A, Blum K, et al. Facet tropism and facet joint orientation: risk factors for the development of early biochemical alterations of lumbar intervertebral discs. *Osteoarthr Cartil*. 2016;24(10):1761–8.
- Müller-Lutz A, Schleich C, Schmitt B, et al. Improvement of gagCEST imaging in the human lumbar intervertebral disc by motion correction. *Skelet Radiol*. 2015;44(4):505–11.
- Müller-Lutz A, Schleich C, Pentang G, et al. Age-dependency of glycosaminoglycan content in lumbar discs: a 3t gagCEST study. *J Magn Reson Imaging*. 2015;42(6):1517–23.
- Müller-Lutz A, Schleich C, Schmitt B, et al. Gender, BMI and T2 dependencies of glycosaminoglycan chemical exchange saturation transfer in intervertebral discs. *Magn Reson Imaging*. 2016;34(3):271–5.
- Zhang Z. Naïve Bayes classification in R. *Ann Transl Med*. 2016;4(12):241.
- Calin A, Jones SD, Garrett SL, et al. Bath Ankylosing Spondylitis Functional Index. *Br J Rheumatol*. 1995;34(8):793–4 <https://www.ncbi.nlm.nih.gov/pmc/articles/PMC1754665/pdf/v062p00817.pdf>.

29. Garrett S, Jenkinson T, Kennedy LG, et al. A new approach to defining disease status in ankylosing spondylitis: the Bath Ankylosing Spondylitis Disease Activity Index. *J Rheumatol*. 1994;21(12):2286–91.
30. Beaumont C. Comparison of Henderson's Method I and restricted maximum likelihood estimation of genetic parameters of reproductive traits. *Poult Sci*. 1991;70(7):1462–8.
31. Cohen J. A power primer. *Psychol Bull*. 1992;112(1):155–9.
32. Braun HJ, Gold GE. Advanced MRI of articular cartilage. *Imaging Med*. 2011; 3(5):541–55.
33. Oei EHG, Wick MC, Müller-Lutz A, et al. Cartilage imaging: techniques and developments. *Semin Musculoskelet Radiol*. 2018;22(2):245–60.
34. Cruickshank B. Histopathology of diarthrodial joints in ankylosing spondylitis. *Ann Rheum Dis*. 1951;10(4):393–404.
35. Cruickshank B. Lesions of cartilaginous joints in ankylosing spondylitis. *J Pathol Bacteriol*. 1956;71(1):73–84.
36. Bleil J, Maier R, Hempfing A, et al. Granulation tissue eroding the subchondral bone also promotes new bone formation in ankylosing spondylitis. *Arthritis Rheumatol (Hoboken, N.J.)*. 2016;68(10):2456–65.
37. Bleil J, Sieper J, Maier R, et al. Cartilage in facet joints of patients with ankylosing spondylitis (AS) shows signs of cartilage degeneration rather than chondrocyte hypertrophy: implications for joint remodeling in AS. *Arthritis Res Ther*. 2015;17:170.
38. Baraliakos X, Østergaard M, Gensler LS, et al. Comparison of the effects of secukinumab and adalimumab biosimilar on radiographic progression in patients with ankylosing spondylitis: design of a randomized, phase IIIb study (SURPASS). *Clin Drug Investig*. 2020;40(3):269–78.
39. Roos EM, Dahlberg L. Positive effects of moderate exercise on glycosaminoglycan content in knee cartilage: a four-month, randomized, controlled trial in patients at risk of osteoarthritis. *Arthritis Rheum*. 2005; 52(11):3507–14.

Publisher's Note

Springer Nature remains neutral with regard to jurisdictional claims in published maps and institutional affiliations.

Ready to submit your research? Choose BMC and benefit from:

- fast, convenient online submission
- thorough peer review by experienced researchers in your field
- rapid publication on acceptance
- support for research data, including large and complex data types
- gold Open Access which fosters wider collaboration and increased citations
- maximum visibility for your research: over 100M website views per year

At BMC, research is always in progress.

Learn more [biomedcentral.com/submissions](https://www.biomedcentral.com/submissions)





Cartilage Degradation in Psoriatic Arthritis Is Associated With Increased Synovial Perfusion as Detected by Magnetic Resonance Imaging

Daniel B. Abrar^{1†}, Christoph Schleich^{1†}, Anja Müller-Lutz¹, Miriam Frenken¹, K. Ludger Radke¹, Stefan Vordenbäumen², Matthias Schneider², Benedikt Ostendorf² and Philipp Sewerin^{2*}

OPEN ACCESS

Edited by:

Raj Sengupta,
Royal National Hospital for Rheumatic
Diseases, United Kingdom

Reviewed by:

Cheng-De Yang,
Shanghai Jiao Tong University, China
Raul Antonio Castellanos-Moreira,
Hospital Clínic de Barcelona, Spain

*Correspondence:

Philipp Sewerin
philipp.sewerin@
med.uni-duesseldorf.de

[†]These authors have contributed
equally to this work

Specialty section:

This article was submitted to
Rheumatology,
a section of the journal
Frontiers in Medicine

Received: 02 March 2020

Accepted: 21 August 2020

Published: 25 September 2020

Citation:

Abrar DB, Schleich C, Müller-Lutz A,
Frenken M, Radke KL,
Vordenbäumen S, Schneider M,
Ostendorf B and Sewerin P (2020)
Cartilage Degradation in Psoriatic
Arthritis Is Associated With Increased
Synovial Perfusion as Detected by
Magnetic Resonance Imaging.
Front. Med. 7:539870.
doi: 10.3389/fmed.2020.539870

¹ Department of Diagnostic and Interventional Radiology, Medical Faculty, University Dusseldorf, Düsseldorf, Germany,

² Department and Hiller Research Unit for Rheumatology, UKD, Heinrich Heine University Düsseldorf, Düsseldorf, Germany

Objective: Even though cartilage loss is a known feature of psoriatic arthritis (PsA), research is sparse on its role in the pathogenesis of PsA and its potential use for disease detection and monitoring. Using delayed gadolinium-enhanced magnetic resonance imaging of cartilage (dGEMRIC) and dynamic contrast-enhanced MRI (DCE MRI), research has shown that early cartilage loss is strongly associated with synovial inflammation in rheumatoid arthritis (RA). The aim of this study was to determine if acute inflammation is associated with early cartilage loss in small finger joints of patients with PsA.

Methods: Metacarpophalangeal (MCP), proximal interphalangeal (PIP), and distal interphalangeal (DIP) joints of 17 patients with active PsA were evaluated by high-resolution 3 Tesla dGEMRIC and DCE MRI using a dedicated 16-channel hand coil. Semi-quantitative and quantitative perfusion parameters were calculated. Images were analyzed by two independent raters for dGEMRIC indices, PsA MRI scores (PsAMRIS), total cartilage thickness (TCT), and joint space width (JSW).

Results: We found significant negative correlations between perfusion parameters (except K_{ep}) and dGEMRIC indices, with the highest value at the MCP joints (K_{Trans} : $\tau = -0.54$, $p = 0.01$; K_{ep} : $\tau = -0.02$, $p = 0.90$; IAUC: $\tau = -0.51$, $p = 0.015$; Initial Slope: $\tau = -0.54$, $p = 0.01$; Peak: $\tau = -0.67$, $p = 0.002$). Heterogeneous correlations were detected between perfusion parameters and both, total PsAMRIS and PsAMRIS synovitis sub-scores. No significant correlation was seen between any perfusion parameter and JSW and/or TCT.

Conclusion: As examined by DCE MRI and dGEMRIC, there is a potential association between early cartilage loss and acute synovial inflammation in small finger joints of PsA patients.

Keywords: psoriatic arthritis, magnetic resonance imaging, dGEMRIC, cartilage, compositional imaging

INTRODUCTION

Psoriatic arthritis (PsA) is a chronic autoimmune disease that ultimately leads to joint destruction and functional disability (1). As in rheumatoid arthritis (RA), early diagnosis and treatment are pivotal for a better clinical outcome (2, 3). Therefore, treat-to-target (T2T) strategies have been introduced for the treatment of PsA (4, 5). Even though magnetic resonance imaging is not yet included in the classification criteria for PsA (CASPAR), it becomes increasingly important for the early detection and monitoring of disease-related joint changes (6–8). In 2009, the Outcome Measures in Rheumatology Clinical Trials (OMERACT) working group introduced a semi-quantitative PsA MRI score (PsAMRIS) that evaluates metacarpophalangeal (MCP), proximal (PIP), and distal interphalangeal joints concerning the osteodestructive (bone erosion), osteoproliferative (bone proliferation), and acute inflammatory (synovitis, flexor tenosynovitis, periarticular inflammation) features of PsA (9). Several studies have shown that the degree of synovial contrast enhancement in arthritic joints can be quantified by dynamic contrast-enhanced MRI (DCE MRI), and hence, have found a strong correlation between the synovitis sub-score of PsAMRIS and RA MRI score (RAMRIS) and DCE MRI parameters (10–12). Furthermore, elevated synovial perfusion assessed by DCE MRI reflects histological findings of acute synovitis (13). Even though cartilage damage is a known feature of PsA, research is sparse on its value in the pathogenesis and the disease course (14). That is why it is not included in the PsAMRIS as opposed to its RA equivalent (15). Several studies using delayed gadolinium-enhanced MRI of cartilage (dGEMRIC) have shown that early cartilage loss in RA is associated with the severity of synovitis (10, 16). dGEMRIC is a histologically validated and robust method that depicts proteoglycan loss in cartilage by measurement of fixed-charge density (17, 18). Proteoglycans have negatively charged side chains that allow for the inversely proportional penetration of similarly negatively charged contrast agent molecules (e.g., gadolinium) following intravenous administration. Consequently, proteoglycan depletion leads to an accumulation of gadolinium ions in degenerated cartilage.

However, the placement of region of interests in small joints is difficult using conventional MRI or with high-resolution MRI surface coils. We, therefore, used a 16-channel high-resolution hand coil to allow for an improved evaluation of smaller joints.

Herein, we set out to evaluate if there was any association between acute inflammation and early cartilage loss in small finger joints of patients with PsA.

METHODS

Study Population

Seventeen patients with PsA (mean age 53.7 ± 11.6 ; minimum/maximum 26/72 years, male/female 9/8) fulfilling the CASPAR criteria, mean disease duration 4 ± 3.6 years, and suffering from peripheral joint involvement of at least two MCP joints and dactylitis of at least one finger were prospectively recruited for the “Analysis of the DActylic Melange” (ADAM)

research initiative. All patients had failed methotrexate (MTX) monotherapy and were escalated to etanercept therapy after a baseline MRI scan. Patient recruitment took place in the Department of Rheumatology from 06/ 2015 to 01/ 2017. The same study population has been included in a different study. However, this study has been published as a pre-print only (19).

The study was approved by the local ethics committee (study number: 4962R, “Analysis of the Dactylitic Melange (ADAM): Defining the morphological components of dactylitis in psoriatic arthritis and their responsiveness to etanercept therapy). Written and informed consent was obtained from all patients before initiation of the study. The Disease Activity Score 28 (DAS 28) was 2.42 ± 0.72 (range 1.8–4.3, median 2.2). C-reactive protein (CRP) levels were 0.87 ± 1.35 mg/dl (range 0.1–5.8 mg/dl, median 0.3 mg/dl).

MR Imaging

A 3T MRI scanner (Magentom Skyra, Siemens Healthineers, Erlangen, Germany) and a dedicated 16-channel hand coil (3T Tim Coil [receive only], Siemens Healthineers, Erlangen, Germany) was used for all patients. Patients were imaged in the prone position with their arm extended overhead (“superman position” with palm facing down).

The imaging protocol included coronal T1-weighted turbo spin echo (TSE) sequences before and after intravenous injection of an ionic gadolinium-based contrast agent (Gd-DOTA⁻ [Dotarem, Guerbet Villepinte, France] in double dose, 0.4 mmol/kg bodyweight). The intravenous injection was carried out by an injection pump followed by a saline chaser. Also, non-contrast enhanced, fat-saturated T2-weighted/short tau inversion recovery (STIR) as well as post-contrast fat-saturated T1-weighted sequences in at least two different orthogonal planes were obtained.

Compositional MRI using the dGEMRIC technique of the MCP, PIP, and DIP joints 2–5 was performed 40 min after intravenous contrast-agent administration. To this end, we used a flip-angle three-dimensional gradient-echo (GE) imaging (FLASH) sequence with two excitation flip angles (5° and 26°) as in previously published studies of our institute (17, 20, 21). 40 sagittal slices were acquired perpendicular to the joint surface. Total acquisition time was 2.25 min.

For perfusion imaging, a dynamic T1-weighted GE turbo FLASH sequence and two T1-weighted GE 3D-FLASH sequences with two different flipangles were acquired; the contrast agent was injected 20 s after sequence initiation. Total acquisition time was 7.20 min. B₁ shimming was applied to maximize image quality.

The detailed sequence parameters were as follows:

Coronal T1 turbo spin echo (TSE) (TR/TE 862/27 ms; flip angle 150° ; slice thickness 2.5 mm; field of view 140×140 mm; imaging matrix: 512×512 ; pixel size 0.3×0.3 mm), coronal STIR (TR/TE, 5560/31 ms; flip angle 120° ; slice thickness 2.5 mm; 8.0; slice thickness 3.0 mm; field of view 140×140 mm; imaging matrix: 448×312 ; pixel size 0.3×0.3 mm), sagittal proton density (PD) TSE fat-saturated (TR/TE 3150/47 ms, flip angle 150° , slice thickness 2.5 mm,

field of view 60 × 150 mm; imaging matrix: 448 × 182; pixel size 0.3 × 0.3 mm), transversal T2 TSE fat-saturated (TR/TE 5693.8/89 ms, flip angle 180°, slice thickness 3.0 mm, field of view 160 × 160 mm; imaging matrix: 512 × 358; pixel size 0.3 × 0.3 mm), transversal T1 SE fat-saturated after intravenous (iv) contrast administration (TR/TE 807/16 ms; flip angle 90°; slice thickness 3.0 mm; field of view 130 × 130 mm; imaging matrix: 384 × 288; pixel size 0.3 × 0.3 mm), coronal T1 TSE after iv contrast (TR/TE 862/27 ms; flip angle 150°; slice thickness 2.5 mm; field of view 140 × 140 mm; imaging matrix: 512 × 512; pixel size 0.3 × 0.3 mm), 3D FLASH GE (TR/TE 5.8/1.9 ms; flip angle 5/26°; slice thickness 3.0 mm; field of view 65 × 110 mm; imaging matrix: 384 × 228; pixel size 0.3 × 0.3 mm) and T1 GE Turbo FLASH (TR/TE 5.8 / 1.9 ms; flip angle 5°; slice thickness 3.0 mm; field of view 140 × 140 mm; imaging matrix: 128 × 96; pixel size 1.1 × 1.1 mm).

Image Analysis

MR images were independently read and analyzed by two radiologists (DBA and CS, trained in musculoskeletal imaging with 3 and 8 years experience) and one rheumatologist (PS, trained in musculoskeletal imaging with 8 years of experience) according to the OMCERACT PsAMRIS guidelines (9). In addition, joint space width (JSW; minimal distance in mm between the proximal and distal bone surface) and total cartilage thickness (TCT; sum of the proximal and distal cartilage layer) were measured for each MCP, PIP and DIP joint of finger 2–5. Measurements were performed perpendicular to the subchondral bone in the medial part of the joint using the inbuilt digital caliper tool of the picture archiving and communication system (PACS, Sectra Workstation IDS7, Sectra AB, Linköping, Sweden) on sagittal PDw images.

Perfusion in the MCP, PIP, and DIP joints of finger 2-5 was evaluated with quantitative and semi-quantitative analysis using The DCE Tool (The DCE Tool for ClearCanvas 2.0 SP1, <http://thedcetool.com>) as described in previously published studies of our institute (10). The quantitative analysis of this tool is based upon the Tofts model (22). Perfusion analysis requires the knowledge of T1 relaxation times. Therefore, the T1w GE 3D FLASH sequence with variable flip angles was used for a pixel-based calculation of the T1 time. For this calculation we applied the following formula:

$$T1(x, y, z) = \frac{TR}{\ln \left[\frac{\sin(\alpha_1) \cos(\alpha_2) - Q(x, y, z) \sin(\alpha_2) \cos(\alpha_1)}{\sin(\alpha_1) - Q(x, y, z) \sin(\alpha_2)} \right]}$$

where

$$Q(x, y, z) = \frac{S_{\alpha_1}(x, y, z)}{S_{\alpha_2}(x, y, z)}$$

And $S_{\alpha_1}(x, y, z)$ and $S_{\alpha_2}(x, y, z)$ are the corresponding pixel intensities to flip angles α_1 and α_2 . Then, the T1 relaxation was used for the perfusion analysis.

A region of interest (ROI) was placed on the radial and ulnar side of each joint by one reader (DBA). After ROI placement a second reader (CS) confirmed the optimal placement before each

measured signal intensity was used to determine a corresponding concentration time curve using the following formula:

$$C_{GD}(t) = \frac{S(t) - S_0}{S_0 T_{10} R}$$

where T_{10} is the native T1 time, $R = 4.5 \text{ s}^{-1} \text{ mM}^{-1}$ is the relaxivity of the contrast agent, S is the average signal intensity in the ROI and S_0 is the average signal intensity in the ROI in absence of the contrast agent. This Tofts model requires the knowledge of the arterial input function (AIF). AIF can be calculated individually from the blood signal or, alternatively, a population average can be used (22). In this study, we used an analytically described AIF population average that can be used at any temporal resolution (22).

The following perfusions parameters were calculated:

Perfusion parameters are displayed and explained in **Table 1**: K_{Trans} , k_{ep} (quantitative parameters) and IAUC (integral of the signal curve over time), initial slope and peak (semiquantitative parameters).

For compositional analyses of cartilage quality with dGEMRIC, motion correction was applied using STROKETOOL (Digital Image Solutions, Frechen, Germany, <http://www.digitalimagesolutions.de>) for all images to reduce movement artifacts. This tool has been validated for dGEMRIC analyses of the finger joints and corrects for patient motion between the measurements using a dedicated image registration method (23).

Readers were allowed to adjust the window settings as required to guarantee optimal visualization of the intra- and periarticular structures for ROI placement. T1 maps were analyzed by first defining regions-of-interest (ROIs) on the central sagittal slice. ROI outlines comprising the full thickness of the proximal and distal portion of the articular cartilage of MPC, PIP and DIP joints of finger 2-5 were manually defined on the morphological images of the 3D T1-weighted FLASH sequence with the flip angle of 5° for dGEMRIC. Particular care was taken to exclude artifacts and surrounding structures such as synovial fluid and cortical bone. Consequently, four ROIs were set per digit (i.e., metacarpal, base of proximal phalanx, apex of proximal phalanx, and base of intermediate phalanx) and 16 ROIs per patient (i.e., four ROIs of four digits) and visually checked by the second and third reader to confirm that only cartilage was included. Next, ROIs were copied to the corresponding slices of the color-coded T1 parameter maps. Further analyses involved the pixel-wise calculation post-contrast T1 values as before (17, 24, 25). More specifically, the T1 maps representing the spatially resolved dGEMRIC indices were analyzed in terms of the ROIs as defined above the mean dGEMRIC indices [ms] were recorded. All images were analyzed by two readers (DBA and CS, radiologists) who were blinded for patients' data.

Statistical Analysis

All statistical analyses were performed using SPSS software (IBM, version 22, Armonk, NY, USA). For descriptive analysis mean,

TABLE 1 | Description of quantitative and semi-quantitative perfusion parameters. IAUC: initial area under the curve.

Quantitative parameters		Semi-quantitative parameters		
K_{Trans}	k_{ep}	IAUC	Initial slope	Peak
Transfer constant between EES and blood plasma	K_{Trans}/V_e : relative volume of EES	Integral of the signal curve over time starting at the onset time (t_{onset}) of the bolus	Slope of the signal curve determined by linear regression within the initial seconds after onset	Maximal signal enhancement

EES, extravascular extracellular space.

standard deviation, minimum, and maximum were calculated. Due to the small sample size and the heterogeneity of our data, non-normal distribution was assumed. For comparison of means, Kruskal-Wallis test and a *post-hoc* Bonferroni test were performed. Correlation analysis was performed between each dGEMRIC indices, total PsAMRIS and all its sub-scores and TCT using the Kendall-Tau correlation coefficient. p -values < 0.05 were considered to be significant.

RESULTS

Descriptive Analysis of dGEMRIC Indices, Perfusion Parameters, JSW, and TCT at MCP and PIP Joints

The descriptive analysis (mean, standard deviation, and range) of dGEMRIC values, quantitative (K_{Trans} , K_{ep}) and semi-quantitative (IAUC, initial slope, peak) perfusion parameters, JSW, and TCT of MCP, PIP, and DIP joints and overall are displayed in **Table 2**.

Perfusion and dGEMRIC maps are shown in **Figure 1**.

Correlation Between Perfusion Parameters and JSW, TCT, Total PsAMRIS, Synovitis Sub-score, dGEMRIC Indices, CRP-Levels, and DAS 28

The correlation between perfusion parameters and JSW, TCT, total PsAMRIS, synovitis sub-score, DAS 28, and dGEMRIC indices is illustrated in **Table 3**.

There was no significant correlation between any perfusion parameter and JSW or TCT, neither overall nor at any joint level (MCP, PIP, DIP).

Overall, there was a significant negative correlation between dGEMRIC indices and all perfusion parameters except k_{ep} . The strongest correlation was found at the MCP joint level.

No significant correlation was seen between any perfusion parameter and overall PsAMRIS and/or synovitis sub-score at the MCP joints and overall. For PIP joints, we found a significant correlation for the parameter peak and total PsAMRIS ($\tau = 0.44$, $p = 0.032$) and for the parameters IAUC and peak and the synovitis sub-score ($\tau = 0.41$, $p = 0.042$; $\tau = 0.451$, $p = 0.032$). At the DIP level, there was a significant correlation between the perfusions parameters K_{Trans} , IAUC, initial slope, and peak and the total PsAMRIS ($\tau = 0.54$, $p = 0.07$; $\tau = 0.48$, $p = 0.018$; $\tau = 0.46$, $p = 0.024$; $\tau = 0.43$, $p = 0.032$). Further, no significant

correlations were found between perfusion parameters and DAS 28 as well as serum CRP levels.

The negative correlations between dGEMRIC values and the quantitative parameter K_{Trans} and the semi-quantitative parameter peak at the MCP joint level are depicted in **Figure 2**.

DISCUSSION

Cartilage degradation is a known feature of PsA that can reliably be assessed by dGEMRIC (26). However, as opposed to RA, research is sparse on the role of cartilage in the pathogenesis of PsA. DCE MRI is a valid tool for the evaluation of inflammation in a given joint that has been validated for many types of arthritis (11, 12). In this study, we set out to investigate the relationship between joint inflammation and cartilage loss measured by DCE MRI and dGEMRIC.

We found a significant negative correlation of dGEMRIC indices and quantitative and semi-quantitative perfusion parameters, wherein MCP and PIP joints showed the highest values. The exact reason for the missing correlations at the DIP joints remain unclear, but might be due to a constitutively different proteoglycan content of cartilage along the finger joints or a higher loss of proteoglycans at MCP and PIP than at DIP joints in this specific population of PsA patients. This indicates that molecular cartilage loss is associated with inflammatory joint changes in patients with established PsA, and hence, high inflammation of joints leads to cartilage damage. These findings concur with previous research on cartilage loss, synovial inflammation and perfusion parameters in patients with early RA (10, 16, 20). Since biochemical MRI detects molecular cartilage degradation preceding structural damage, it might be applicable as a monitoring tool for very early disease-related joint changes in PsA.

The association of perfusion parameters and PsAMRIS (sub-scores) has not yet been evaluated. Previous studies on RA showed that perfusion parameters highly correlated with RAMRIS and histological synovitis in affected patients (10, 13, 27–29). As opposed to these findings, we found heterogeneous correlations of perfusion parameters and total PsAMRIS, as well as the synovitis sub-score in PsA patients. DCE MRI is known to indicate the severity of inflammation at a given joint; that is why one could have expected a strong association between perfusion parameters and PsAMRIS. However, previous research using DCE MRI has partially shown that PsA and RA can differ regarding the degree of their synovial enhancement, despite indistinguishable appearances on non-dynamic MRI (30, 31).

TABLE 2 | Descriptive analysis (mean, standard deviation (SD) and range (maximum, minimum) of quantitative and semi-quantitative perfusion parameters, delayed Gadolinium Enhanced Magnetic Resonance Imaging of Cartilage (dGEMRIC) indices, joint space width (JSW), and total cartilage thickness (TCT) of finger 2–5 at the metacarpophalangeal (MCP), proximal interphalangeal (PIP), and distal interphalangeal (DIP) joint region and overall.

		K trans ml/g per min	K ep 1/min	IAUC mM/l per s	Initial slope mM/l per s	Peak mM/l per s	dGEMRIC in ms	TCT in mm	JSW in mm
MCP	Mean	0.06	0.18	3.08	0.0023	0.15	542.65	1.15	1.5
	SD	0.04	0.13	2.46	0.002	0.10	130.34	0.26	0.17
	Max	0.14	0.53	8.45	0.007	0.36	828.03	1.59	1.83
	Min	0.02	0.03	0.81	0.0004	0.05	340.4	0.73	1.27
PIP	Mean	0.05	0.17	2.90	0.002	0.15	411.92	0.71	1.02
	SD	0.03	0.13	2.01	0.002	0.08	104.46	0.18	0.24
	Max	0.12	0.65	7.59	0.006	0.31	639.6	1.11	1.49
	Min	0.008	0.04	0.58	0.0004	0.04	237.18	0.38	0.69
DIP	Mean	0.06	0.21	3.72	0.003	0.16	352.86	0.57	0.8
	SD	0.04	0.15	2.72	0.002	0.08	98.75	0.2	0.18
	Max	0.17	0.68	9.96	0.009	0.29	585.03	0.79	1.19
	Min	0.01	0.06	0.43	0.0003	0.04	184.35	0	0.55
Overall	Mean	0.06	277.32	3.11	0.003	0.15	436.30	0.77	1.07
	SD	0.03	802.71	1.88	0.002	0.07	110.09	0.2	0.18
	Max	0.12	3141.11	7.67	0.006	0.30	670.98	1.13	1.44
	Min	0.01	0.04	0.57	0.0004	0.05	253.98	0.40	0.75
p-value	MCP vs PIP	0.359	0.591	0.864	0.531	1.00	0.019	0.029	<0.001
	MCP vs DIP	0.724	0.803	0.558	0.818	0.848	0.001	0.02	0.007
	PIP vs DIP	0.079	0.918	0.874	0.896	0.848	0.491	0.566	0.116

Mean values of each parameter were compared with a Kruskal-Wallis test and a post-hoc Bonferroni test. P-values <0.05 were considered significant and are given in bold type.

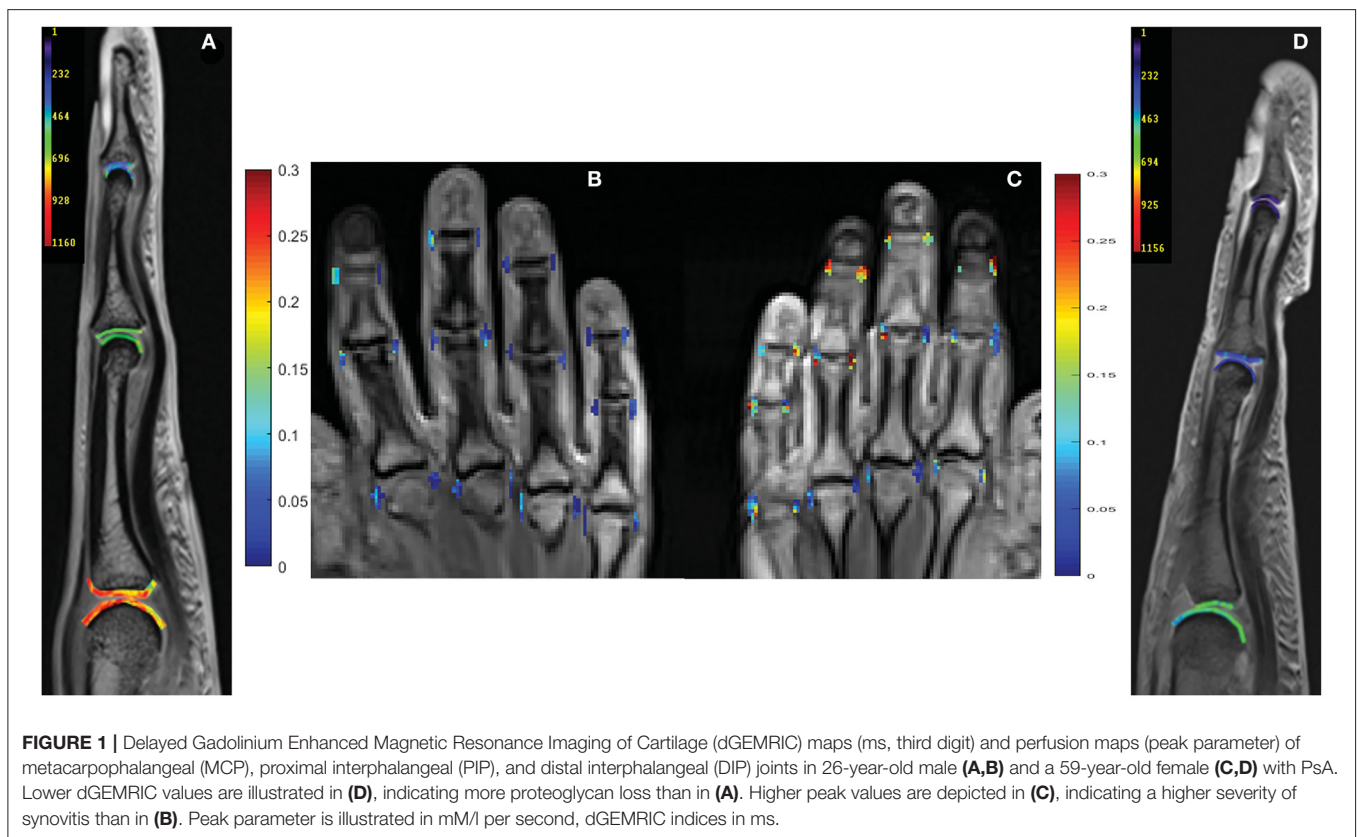
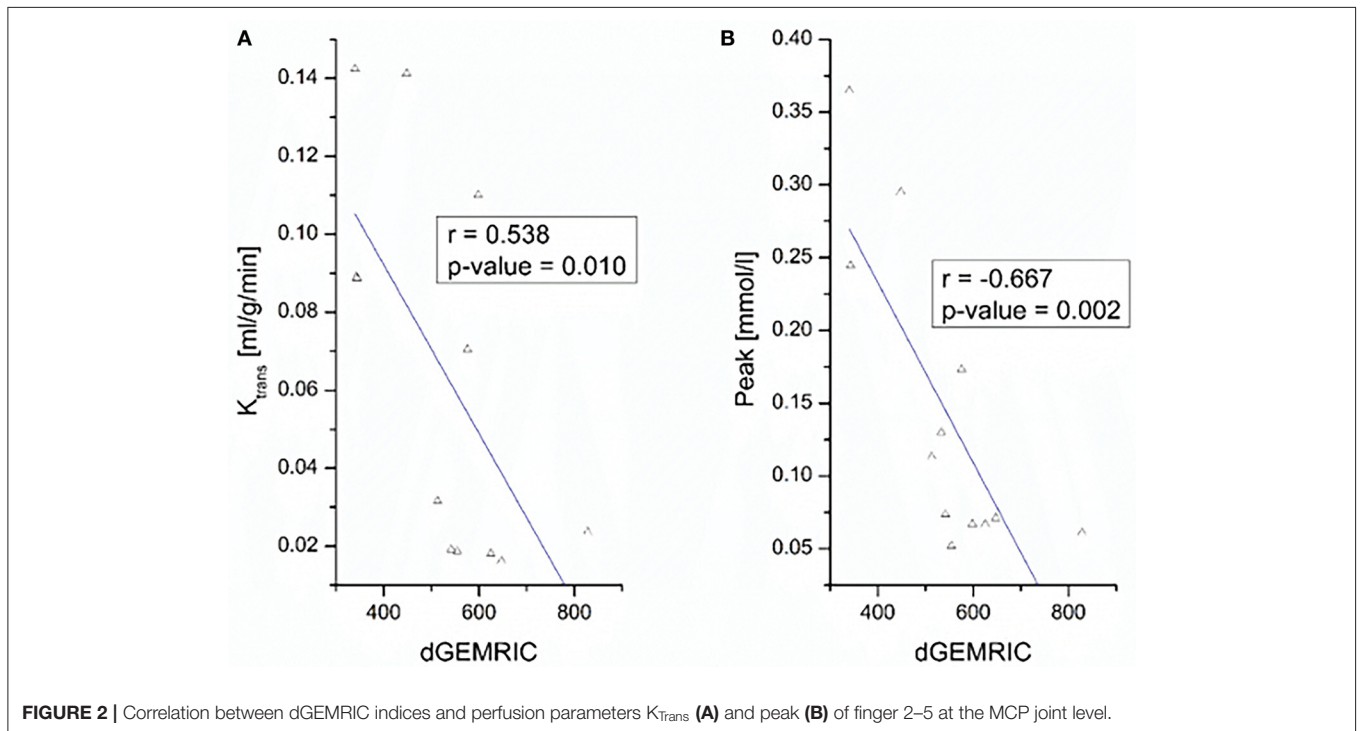


FIGURE 1 | Delayed Gadolinium Enhanced Magnetic Resonance Imaging of Cartilage (dGEMRIC) maps (ms, third digit) and perfusion maps (peak parameter) of metacarpophalangeal (MCP), proximal interphalangeal (PIP), and distal interphalangeal (DIP) joints in 26-year-old male (A,B) and a 59-year-old female (C,D) with PsA. Lower dGEMRIC values are illustrated in (D), indicating more proteoglycan loss than in (A). Higher peak values are depicted in (C), indicating a higher severity of synovitis than in (B). Peak parameter is illustrated in mM/l per second, dGEMRIC indices in ms.

TABLE 3 | Kendall Tau correlation τ between quantitative and semi-quantitative perfusion parameters and dGEMRIC indices, total Psoriatic arthritis magnetic resonance imaging score (PsAMRIS), PsAMRIS sub-score “synovitis.”

		K_{Trans}		K_{ep}		IAUC		Initial slope		Peak	
		τ	p	τ	p	τ	p	τ	p	τ	p
Overall	JSW	0.1	0.35	-0.1	0.33	0.05	0.64	0.02	0.84	0.04	0.69
	TCT	0.03	0.8	-0.12	0.26	0	0.97	-0.12	0.91	-0.12	0.91
	dGEMRIC	-0.27	0.014	-0.29	0.008	-0.29	0.008	0.32	0.004	-0.26	0.02
	PsAMRIS	-0.44	0.826	-0.27	0.188	0.09	0.661	0.13	0.51	0.18	0.38
	Synovitis	0.17	0.409	-0.12	0.545	0.26	0.205	0.26	0.205	0.35	0.088
	DAS 28	0.19	0.335	-0.04	0.854	0.27	0.169	0.014	0.952	0.32	0.108
MCP	JSW	0.2	0.3	-0.01	0.96	0.03	0.87	0.03	0.87	0.12	0.55
	TCT	-0.21	0.3	-0.17	0.41	-0.25	0.2	-0.25	0.2	-0.25	0.2
	dGEMRIC	-0.54	0.01	-0.02	0.90	-0.51	0.015	-0.54	0.01	-0.67	0.002
	PsAMRIS	0.02	0.912	-0.16	0.44	0.09	0.657	0.14	0.375	0.23	0.268
	Synovitis	0.11	0.612	-0.04	0.866	0.16	0.463	0.23	0.284	0.3	0.159
	DAS28	0.24	0.459	-0.03	0.939	0.22	0.5	0.28	0.385	0.22	0.489
PIP	JSW	0.07	0.73	-0.03	0.88	0.11	0.59	0.17	0.41	0.17	0.41
	TCT	0.12	0.55	-0.06	0.77	0.15	0.43	0.22	0.27	0.22	0.27
	dGEMRIC	-0.43	0.03	0.07	0.7	-0.39	0.055	-0.51	0.015	-0.51	0.015
	PsAMRIS	0.34	0.089	0.02	0.920	0.34	0.089	0.26	0.205	0.44	0.032
	Synovitis	0.39	0.053	0.14	0.476	0.41	0.042	0.31	0.142	0.45	0.032
	DAS28	0.18	0.568	0.05	0.886	0.2	0.536	0.12	0.708	0.22	0.489
DIP	JSW	-0.1	0.62	-0.1	0.62	-0.03	0.87	-0.01	0.96	-0.25	0.21
	TC	-0.05	0.78	-0.1	0.62	0.01	0.96	0.03	0.87	-0.17	0.41
	dGEMRIC	-0.26	0.22	0.1	0.63	-0.18	0.39	-0.15	0.46	-0.08	0.71
	PsAMRIS	0.54	0.007	0.10	0.621	0.48	0.018	0.46	0.024	0.43	0.032
	Synovitis	0.22	0.294	-0.01	0.956	0.17	0.407	0.15	0.473	0.21	0.294
	DAS28	-0.06	0.848	0.01	0.901	-0.04	0.901	-0.12	0.722	0.07	0.829

Disease Activity Score 28 (DAS 28), JSW and TCT of finger 2–5 at the MCP, PIP, and DIP joint level and overall. p -values < 0.05 were considered significant and are written in bold type.



Also, the synovial involvement of PsA histologically differs from RA regarding the extent of inflammation, synovial thickness, and blood supply (31–33). These differences of synovial changes are potentially due to the different pathogenesis of both entities, with RA being primarily a synovial and PsA being an enthesal-driven disease (34, 35). Therefore, the visual degree of synovitis using PsAMRIS could be over- or underrepresenting synovitis measured by DCE MRI, possibly due to a disease-specific type of synovial involvement. Further, for PsAMRIS scoring, we used coronal and transversal planes, wherein for DCE MRI, we only considered radial and ulnar ROI in coronal slices, which could also contribute to heterogeneous correlations of perfusion parameters and synovitis sub-scores. Additionally, the heterogeneity between MCP, PIP, and DIP joints could be explained by the known circumstances that the state of diffusion equilibrium is reached faster in smaller compared to larger joints (36).

Further, no significant correlations were found between perfusion parameters and clinical disease activity as measured by DAS 28. Previous studies have shown that MRI is more sensitive than clinical scores at the detection of joint inflammation (37, 38). Some studies even demonstrated a radiological progression despite clinical remission and postulated a “silent progression” (39–41). That is why, the lacking correlation of imaging features and clinical data could be due to the superior sensitivity of MRI, especially since a high-field MRI scanner and a dedicated hand-coil have been used resulting in high-resolution imaging.

Our Study Has Limitations

Firstly, our study population of PsA patients had a small sample size. That is why our results should only be considered exploratory and need confirmation by further research with larger populations.

Secondly, we did not use a synovial and cartilage biopsy as a means of validation regarding the extent of synovitis and the cartilage composition. However, previous studies have already histologically validated both DCE MRI and dGEMRIC data (13, 42).

In conclusion, there is a potential association between early cartilage loss and acute synovial inflammation in small finger joints of PsA patients.

REFERENCES

- Sewerin P, Brinks R, Schneider M, Haase I, Vordenbäumen S. Prevalence and incidence of psoriasis and psoriatic arthritis. *Ann Rheum Dis.* (2019) 78:286–7. doi: 10.1136/annrheumdis-2018-214065
- Coates LC, Navarro-Coy N, Brown SR, Brown S, McParland L, Collier H, et al. The TICOPA protocol (Tight COntrol of Psoriatic Arthritis): a randomised controlled trial to compare intensive management versus standard care in early psoriatic arthritis. *BMC Musculoskelet Disord.* (2013) 14:101. doi: 10.1186/1471-2474-14-101
- Singh JA, Guyatt G, Ogdie A, Gladman DD, Deal C, Deodhar A, et al. Special article: 2018 American College of Rheumatology/National psoriasis foundation guideline for the treatment of psoriatic arthritis. *Arthritis Care Res.* (2019) 71:2–29. doi: 10.1002/art.40726
- Coates LC. Treating to target in psoriatic arthritis. *Curr Opin Rheumatol.* (2015) 27:107. doi: 10.1097/BOR.0000000000000140
- Coates LC, Lubrano E, Perrotta FM, Emery P, Conaghan PG, Helliwell PS. What should be the primary target of “treat to target” in psoriatic arthritis? *J Rheumatol.* (2019) 46:38–42. doi: 10.3899/jrheum.180267
- Tillett W, Costa L, Jadon D, Wallis D, Cavill C, McHugh J, et al. The CLASSification for Psoriatic ARthritis (CASPAR) criteria—a retrospective feasibility, sensitivity, and specificity study. *J Rheumatol.* (2012) 39:154–6. doi: 10.3899/jrheum.110845
- Coates LC, Conaghan PG, D’Agostino MA, Wit M de, FitzGerald O, Kvien TK, et al. Remission in psoriatic arthritis—where are we now? *Rheumatology.* (2018) 57:1321–31. doi: 10.1093/rheumatology/kex344
- Yue J, Wu D, Tam L-S. The role of imaging in early diagnosis and prevention of joint damage in inflammatory arthritis. *Expert Rev Clin Immunol.* (2018) 14:499–511. doi: 10.1080/1744666X.2018.1476849

DATA AVAILABILITY STATEMENT

The datasets generated for this study are available on request to the corresponding author.

ETHICS STATEMENT

The studies involving human participants were reviewed and approved by Ethics committee of the Heinrich-Heine University. The patients/participants provided their written informed consent to participate in this study.

AUTHOR CONTRIBUTIONS

DA: acquisition and analysis and interpretation of data. Draft and design of the work. PS: design and conception of the study. Analysis and interpretation of data. Draft and design of the work. Revision of the work. BO, MS, SV, and KR: analysis and interpretation of data. Draft and design of the work. Revision of the work. MF and AM-L: interpretation and analysis of data. Draft and design of the work. Revision of the work. CS: conception and design of the study. Interpretation and analysis of data. Draft and design of the work. Revision of the work. All authors read and approved the final manuscript. All authors contributed to the article and approved the submitted version.

FUNDING

DA was supported by the local research committee of the medical faculty. PS and SV received funding from Pfizer Germany with the Pfizer GIP Inflammation Germany Research Initiative 2014. PS and BO received funding from AbbVie Deutschland GmbH & Co. KG for the Delayed Gadolinium-enhanced MR Imaging of Cartilage—A pilot study to measure the effect of Adalimumab plus MTX vs. Placebo plus MTX on cartilage in early RA patients (CAR-ERA) Study. PS received a grant from the German Bundesministerium für Bildung und Forschung (BMBF), ArthroMark (01EC1009).

ACKNOWLEDGMENTS

We thank Mrs. Erika Rädtsch for conducting all MRI studies.

9. Ostergaard M, McQueen F, Wiell C, Bird P, Boyesen P, Ejlberg B, et al. The OMERACT psoriatic arthritis magnetic resonance imaging scoring system (PsAMRIS): definitions of key pathologies, suggested MRI sequences, and preliminary scoring system for PsA Hands. *J Rheumatol.* (2009) 36:1816–24. doi: 10.3899/jrheum.090352
10. Müller-Lutz A, Schleich C, Sewerin P, Gross J, Pentang G, Wittsack H-J, et al. Comparison of quantitative and semiquantitative dynamic contrast-enhanced MRI with respect to their correlation to delayed gadolinium-enhanced MRI of the cartilage in patients with early rheumatoid arthritis. *J Comput Assist Tomogr.* (2015) 39:64–9. doi: 10.1097/RCT.0000000000000164
11. Schwenzer NF, Kötter I, Henes JC, Schraml C, Fritz J, Claussen CD, et al. The role of dynamic contrast-enhanced MRI in the differential diagnosis of psoriatic and rheumatoid arthritis. *AJR Am J Roentgenol.* (2010) 194:715–20. doi: 10.2214/AJR.09.2671
12. Cimmino MA, Barbieri F, Boesen M, Paparo F, Parodi M, Kubassova O, et al. Dynamic contrast-enhanced magnetic resonance imaging of articular and extraarticular synovial structures of the hands in patients with psoriatic arthritis. *J Rheumatol Suppl.* (2012) 89:44–8. doi: 10.3899/jrheum.120242
13. Vordenbäumen S, Schleich C, Lögters T, Sewerin P, Bleck E, Pauly T, et al. Dynamic contrast-enhanced magnetic resonance imaging of metacarpophalangeal joints reflects histological signs of synovitis in rheumatoid arthritis. *Arthritis Res Ther.* (2014) 16:452. doi: 10.1186/s13075-014-0452-x
14. Bhattaram P, Chandrasekharan U. The joint synovium: A critical determinant of articular cartilage fate in inflammatory joint diseases. *Semin Cell Dev Biol.* (2017) 62:86–93. doi: 10.1016/j.semcdb.2016.05.009
15. Ostergaard M, Peterfy CG, Bird P, Gandjbakhch F, Glinatsi D, Eshed I, et al. The OMERACT rheumatoid arthritis magnetic resonance imaging (MRI) scoring system: updated recommendations by the OMERACT MRI in arthritis working group. *J Rheumatol.* (2017) 44:1706–12. doi: 10.3899/jrheum.161433
16. Herz B, Albrecht A, Englbrecht M, Welsch GH, Uder M, Renner N, et al. Osteitis and synovitis, but not bone erosion, is associated with proteoglycan loss and microstructure damage in the cartilage of patients with rheumatoid arthritis. *Ann Rheum Dis.* (2014) 73:1101–6. doi: 10.1136/annrheumdis-2012-202850
17. Miese F, Buchbender C, Scherer A, Wittsack H-J, Specker C, Schneider M, et al. Molecular imaging of cartilage damage of finger joints in early rheumatoid arthritis with delayed gadolinium-enhanced magnetic resonance imaging. *Arthritis Rheum.* (2012) 64:394–9. doi: 10.1002/art.33352
18. van Tiel J, Kotek G, Reijman M, Bos PK, Bron EE, Klein S, et al. Is T1 ρ mapping an alternative to delayed gadolinium-enhanced MR imaging of cartilage in the assessment of sulphated glycosaminoglycan content in human osteoarthritic knees? An *in vivo* validation study. *Radiology.* (2016) 279:523–31. doi: 10.1148/radiol.2015150693
19. Abrar DB, Schleich C, Brinks R, Vordenbäumen S, Frenken M, Goertz C, et al. Is a simplified version of PsAMRIS (sPsAMRIS) a potential tool for therapy monitoring in established psoriatic arthritis? *Res Square [Preprint]*. (2019). doi: 10.21203/rs.2.14892/v1
20. Sewerin P, Schleich C, Brinks R, Müller-Lutz A, Fichter F, Eichner M, et al. Assessing associations of synovial perfusion, cartilage quality, and outcome in rheumatoid arthritis using dynamic contrast-enhanced magnetic resonance imaging. *J Rheumatol.* (2020) 47:15–9. doi: 10.3899/jrheum.180832
21. Sewerin P, Schleich C, Brinks R, Müller-Lutz A, Fichter F, Eichner M, et al. Synovial perfusion assessed by dynamic contrast-enhanced MRI is associated to treatment response, remission, and cartilage quality in rheumatoid arthritis. *J Rheumatol.* (2019). doi: 10.3899/jrheum.180832. [Epub ahead of print].
22. Tofts PS. T1-weighted DCE imaging concepts: modelling, acquisition and analysis. *MAGNETOM Flash.* (2010) 2010:30–9.
23. Miese F, Kröpil P, Ostendorf B, Scherer A, Buchbender C, Quentin M, et al. Motion correction improves image quality of dGEMRIC in finger joints. *Eur J Radiol.* (2011) 80:e427–31. doi: 10.1016/j.ejrad.2011.01.006
24. Miese FR, Ostendorf B, Wittsack H-J, Reichelt DC, Mamisch TC, Zilkens C, et al. Metacarpophalangeal joints in rheumatoid arthritis: delayed gadolinium-enhanced MR imaging of cartilage—a feasibility study. *Radiology.* (2010) 257:441–7. doi: 10.1148/radiol.10100459
25. Sewerin P, Müller-Lutz A, Abrar DB, Odendahl S, Eichner M, Schneider M, et al. Prevention of the progressive biochemical cartilage destruction under methotrexate therapy in early rheumatoid arthritis. *Clin Exp Rheumatol.* (2019) 37:179–85.
26. Sewerin P, Schleich C, Vordenbäumen S, Ostendorf B. Update on imaging in rheumatic diseases: cartilage. *Clin Exp Rheumatol.* (2018) 36 Suppl 114:139–44.
27. Hodgson R, Grainger A, O'Connor P, Barnes T, Connolly S, Moots R. Dynamic contrast enhanced MRI of bone marrow oedema in rheumatoid arthritis. *Ann Rheum Dis.* (2008) 67:270–2. doi: 10.1136/ard.2007.077271
28. Boesen M, Kubassova O, Bouert R, Axelsen MB, Ostergaard M, Cimmino MA, et al. Correlation between computer-aided dynamic gadolinium-enhanced MRI assessment of inflammation and semi-quantitative synovitis and bone marrow oedema scores of the wrist in patients with rheumatoid arthritis—a cohort study. *Rheumatology.* (2012) 51:134–43. doi: 10.1093/rheumatology/ker220
29. Wojciechowski W, Tabor Z, Urbanik A. Assessing synovitis based on dynamic gadolinium-enhanced MRI and EULAR-OMERACT scores of the wrist in patients with rheumatoid arthritis. *Clin Exp Rheumatol.* (2013) 31:850–6.
30. Sudoł-Szopińska I, Pracoń G. Diagnostic imaging of psoriatic arthritis. Part II: magnetic resonance imaging and ultrasonography. *J Ultrason.* (2016) 16:163–74. doi: 10.15557/JoU.2016.0018
31. Narváez J, Narváez JA, Albert M de, Gómez-Vaquero C, Nolla JM. Can magnetic resonance imaging of the hand and wrist differentiate between rheumatoid arthritis and psoriatic arthritis in the early stages of the disease? *Semin Arthritis Rheum.* (2012) 42:234–45. doi: 10.1016/j.semarthrit.2012.03.016
32. Sankowski AJ, Lebkowska UM, Cwikła J, Walecka I, Walecki J. Psoriatic arthritis. *Pol J Radiol.* (2013) 78:7–17. doi: 10.12659/PJR.883763
33. Sudoł-Szopińska I, Plaza M, Pracoń G. Selected issues in diagnostic imaging of spondyloarthritides: psoriatic arthritis and juvenile spondyloarthritis. *Reumatologia.* (2016) 54:310–7. doi: 10.5114/reum.2016.64908
34. McGonagle D, Hermann K-GA, Tan AL. Differentiation between osteoarthritis and psoriatic arthritis: implications for pathogenesis and treatment in the biologic therapy era. *Rheumatology.* (2015) 54:29–38. doi: 10.1093/rheumatology/keu328
35. Schett G, Coates LC, Ash ZR, Finzel S, Conaghan PG. Structural damage in rheumatoid arthritis, psoriatic arthritis, and ankylosing spondylitis: traditional views, novel insights gained from TNF blockade, and concepts for the future. *Arthritis Res Ther.* (2011) 2011:S4. doi: 10.1186/1478-6354-13-S1-S4
36. Peterfy CG. MR imaging. *Baillieres Clin Rheumatol.* (1996) 10:635–78. doi: 10.1016/S0950-3579(96)80055-0
37. Ostergaard M, Hansen M, Stoltenberg M, Jensen KE, Szkudlarek M, Pedersen-Zbinden B, et al. New radiographic bone erosions in the wrists of patients with rheumatoid arthritis are detectable with magnetic resonance imaging a median of two years earlier. *Arthritis Rheum.* (2003) 48:2128–31. doi: 10.1002/art.11076
38. Ejlberg BJ, Vestergaard A, Jacobsen S, Thomsen HS, Østergaard M. The smallest detectable difference and sensitivity to change of magnetic resonance imaging and radiographic scoring of structural joint damage in rheumatoid arthritis finger, wrist, and toe joints: a comparison of the OMERACT rheumatoid arthritis magnetic resonance imaging score applied to different joint combinations and the Sharp/van der Heijde radiographic score. *Arthritis Rheum.* (2005) 52:2300–6. doi: 10.1002/art.21207
39. Moller-Bisgaard S, Hørslev-Petersen K, Ejlberg BJ, Boesen M, Hetland ML, Christensen R, et al. Impact of a magnetic resonance imaging-guided treat-to-target strategy on disease activity and progression in patients with rheumatoid arthritis (the IMAGINE-RA trial): study protocol for a randomized controlled trial. *Trials.* (2015) 16:178. doi: 10.1186/s13063-015-0693-2
40. Sewerin P, Vordenbaeumen S, Hoyer A, Brinks R, Buchbender C, Miese F, et al. Silent progression in patients with rheumatoid arthritis: is DAS28 remission an insufficient goal in RA? Results from the German Remission-plus cohort. *BMC Musculoskelet Disord.* (2017) 18:163. doi: 10.1186/s12891-017-1528-y

41. Hetland ML, Stengaard-Pedersen K, Junker P, Østergaard M, Ejbjerg BJ, Jacobsen S, et al. Radiographic progression and remission rates in early rheumatoid arthritis - MRI bone oedema and anti-CCP predicted radiographic progression in the 5-year extension of the double-blind randomised CIMESTR trial. *Ann Rheum Dis.* (2010) 69:1789–95. doi: 10.1136/ard.2009.125534
42. Schmaranzer F, Arendt L, Liechti EF, Nuss K, Rechenberg B von, Kircher PR, et al. Do dGEMRIC and T2 imaging correlate with histologic cartilage degeneration in an experimental ovine FAI model? *Clin Orthop Relat Res.* (2019) 477:990–1003. doi: 10.1097/CORR.0000000000000593

Conflict of Interest: The authors declare that the research was conducted in the absence of any commercial or financial relationships that could be construed as a potential conflict of interest.

Copyright © 2020 Abrar, Schleich, Müller-Lutz, Frenken, Radke, Vordenbäumen, Schneider, Ostendorf and Sewerin. This is an open-access article distributed under the terms of the Creative Commons Attribution License (CC BY). The use, distribution or reproduction in other forums is permitted, provided the original author(s) and the copyright owner(s) are credited and that the original publication in this journal is cited, in accordance with accepted academic practice. No use, distribution or reproduction is permitted which does not comply with these terms.

Article

Introduction of a Simplified Psoriatic Arthritis Magnetic Resonance Imaging Score (sPsAMRIS): A Potential Tool for Treatment Monitoring in Peripheral Psoriatic Arthritis

Daniel B. Abrar ^{1,*}, Christoph Schleich ¹, Ralph Brinks ², Christine Goertz ², Miriam Frenken ¹, Matthias Schneider ², Sven Nebelung ^{1,†} and Philipp Sewerin ^{2,†}

¹ Department of Diagnostic and Interventional Radiology, Medical Faculty, University Dusseldorf, D-40225 Dusseldorf, Germany; Christoph.Schleich@med.uni-duesseldorf.de (C.S.); Miriam.Frenken@med.uni-duesseldorf.de (M.F.); Sven.Nebelung@med.uni-duesseldorf.de (S.N.)

² Department and Hiller-Research-Unit for Rheumatology, UKD, Heinrich-Heine University Dusseldorf, D-40225 Dusseldorf, Germany; Ralph.Brinks@med.uni-duesseldorf.de (R.B.); christine.goertz@med.uni-duesseldorf.de (C.G.); matthias.schneider@med.uni-duesseldorf.de (M.S.); philipp.sewerin@med.uni-duesseldorf.de (P.S.)

* Correspondence: danielbenjamin.abrar@med.uni-duesseldorf.de; Tel.: +49-211-81-08505

† These authors contributed equally to this work.

Received: 17 November 2020; Accepted: 14 December 2020; Published: 15 December 2020



Abstract: Background: To evaluate whether a simplified (s) version of the psoriatic arthritis magnetic resonance imaging score (PsAMRIS), sPsAMRIS, is a potential tool for therapy monitoring in psoriatic arthritis (PsA). Methods: Seventeen patients with active psoriatic arthritis (PsA) underwent magnetic resonance imaging (MRI) at 3 T of the clinically dominant hand at baseline and after 6 months. Scoring was performed by two musculoskeletal radiologists in terms of the PsAMRIS and sPsAMRIS, which is a simplified version with reduced item numbers based on prior evaluation of responsiveness to change by standardized response means (SRMs). Both scores were compared by calculation of overall and each sub-score's SRMs and relative efficacy (RE) after bootstrapping. Results: PsAMRIS sub-scores of MCP joints 3 and 4, and proximal interphalangeal (PIP) joint 4 had the highest SRM (−0.07 each), indicating highest responsiveness to change, and were, therefore, included in sPsAMRIS. Compared to PsAMRIS, sPsAMRIS was characterized by higher SRMs (sPsAMRIS: −0.13 vs. PsAMRIS: −0.02) and higher RE (29.46). sPsAMRIS and PsAMRIS were highly correlated at baseline ($r = 0.75$, $p < 0.01$ (Pearson's correlation)) and at 6-month follow-up ($r = 0.64$, $p = 0.01$). Mean time burden for completion of scoring per MRI study was significantly reduced when using PsAMRIS (469 ± 87.03 s) as compared to sPsAMRIS (140.1 ± 21.25 s) ($p < 0.001$). Conclusion: Due to its similar responsiveness to change compared to standard PsAMRIS, and time efficiency, sPsAMRIS might be a potential diagnostic tool to quantitatively assess and monitor therapy in PsA.

Keywords: psoriatic arthritis; PsAMRIS; magnetic resonance imaging; OMERACT

1. Introduction

Psoriatic arthritis (PsA) is a chronic inflammatory disorder that results in progressive joint destruction if left untreated [1,2]. With a global prevalence of 0.05–0.25%, PsA constitutes one of the most common inflammatory joint diseases alongside rheumatoid arthritis (RA) and gout [3]. PsA may manifest in a variety of manifestations such as dactylitis, enthesitis, synovitis, or bone erosions [4]. Similar to RA, early diagnosis and targeted treatment of PsA are crucial for improved clinical outcomes,

i.e., clinical remission or low disease activity [5]. Current treatment strategies suggest escalation of therapy in patients that do not demonstrate sufficient treatment response [6]; hence, early detection of treatment failure is of paramount importance. Consequently, there is a true clinical need for reliable tools for therapy monitoring in PsA.

Even though it is not part of the Classification Criteria for Psoriatic Arthritis (CASPAR) [7], magnetic resonance imaging (MRI) becomes increasingly important as a tool for early detection and monitoring of PsA-related joint involvement [5,8]. MRI is a reliable tool for detecting early PsA-related pathologies such as soft tissue swelling, enthesitis, bone marrow edema, and bone erosion [9,10]. In 2003, the Outcome Measures in Rheumatology Clinical Trials (OMERACT) working group presented a diagnostic scoring tool, the RA MRI Score (RAMRIS), for evaluation of changes related to RA, which has been validated used for outcome measurement ever since [11]. Subsequently, in 2007 the OMERACT Psoriatic Arthritis Magnetic Resonance Imaging Scoring System (PsAMRIS) was introduced [12]. PsAMRIS is a semi-quantitative scoring system that includes typical changes of peripheral PsA such as enthesitis, synovitis, tenosynovitis, periarticular inflammation, bone edema, bone erosion, and bone proliferation in 24 joints, resulting in a sum score [13]. PsAMRIS is an increasingly accepted diagnostic scoring tool for reliable and objective outcome measurements in controlled clinical trials investigating PsA [14]. A major drawback of PsAMRIS is the considerable time needed for scoring that may have prevented its more widespread implementation in clinical practice.

The aim of this study was to systematically evaluate in a clinical cohort of PsA which components of PsAMRIS are of superordinate diagnostic relevance to be included in its simplified version, termed sPsAMRIS. Hence, our hypothesis was that sPsAMRIS is as diagnostically reliable as PsAMRIS, while reducing the time burden and complexity associated with standard scoring procedures of PsAMRIS.

2. Materials and Methods

2.1. Patients

Seventeen patients with PsA (mean age, 53.7 ± 11.6 years; range, 26–72 years; male/female, 9/8), fulfilling the CASPAR criteria [15] with a mean disease duration 4.0 ± 3.6 years and peripheral joint involvement of at least two metacarpophalangeal (MCP) joints and dactylitis of at least one finger were prospectively recruited for the “Analysis of the DActylic Melange” (ADAM) research initiative [16]. At baseline, all patients received methotrexate (MTX) monotherapy. After a baseline MRI scan, they were escalated to Etanercept (Enbrel® 50 mg s.c.) fortnightly and thereafter received a combination therapy of MTX and Etanercept. Follow-up data, including the follow-up MRI scan and clinical and laboratory tests, were available in 13 patients (mean age, 57.0 ± 9.0 years; range, 42–73 years; male/female, 7/6) at 6.2 ± 0.9 months (range 5–8 months) after escalation of treatment. Four of the initial 17 patients had to be excluded from the study prior to the follow-up MRI scan, because they had moved away. In the entire cohort, the Disease Activity Score 28 (DAS 28) [17] was 2.42 ± 0.72 (range, 1.8–4.3; median, 2.2) at baseline and 2.06 ± 0.27 (range, 1.6–2.5; median, 2.1). C-reactive protein (CRP) levels were 0.87 ± 1.35 mg/dL (range, 0.1–5.8 mg/dL; median, 0.3 mg/dL) at baseline and 0.43 ± 0.27 mg/dL (range, 0.1–1.1 mg/dL; median, 0.4 mg/dL) at follow-up. Patient recruitment took place at the Department of Rheumatology from June 2015 until January 2017. The study was approved by the local ethics committee (Medical Faculty, University Dusseldorf, 4962R, date of approval: 1 April 2015). Written and oral informed consent was obtained from all patients before the initiation of the study.

2.2. MRI

Baseline (T0) and follow-up (T1) MR imaging of the clinically dominant hand was performed using a 3T MRI scanner (Magnetom Skyra, Siemens Healthineers, Erlangen, Germany) and a dedicated 16-channel receive-only hand coil (3T Tim Coil, Siemens Healthineers) as previously published by our

department [16]. Patients were imaged in the prone position with their arms extended overhead and palms facing down (“superman” position).

The imaging protocol was implemented in accordance with the recommendations of the OMERACT working group and included pre- and post-contrast (0.4 mL/kg body weight gadoteric acid [Gd-DOTA], Dotarem, Guerbet Villepinte, France) T1-weighted and non-contrast fat-saturated T2-weighted or short tau inversion recovery (STIR) sequences in two different orthogonal planes.

Detailed sequence parameters are given in Table 1.

Table 1. Detailed Magnetic Resonance Imaging (MRI) Sequence Parameters.

Sequence	Orientation	TR/TE (ms)	Flip Angle (°)	Slice Thickness (mm)	FoV (mm × mm)	Acquisition Matrix (pixels)	Pixel Size (mm/pixel)
T1w TSE	Coronal	862/27	150	2.5	140 × 140	512 × 512	0.27 × 0.27
T1w TSE + contrast	Coronal	862/27	150	2.5	140 × 140	512 × 512	0.27 × 0.27
STIR	Coronal	5560/31	120	2.5	140 × 140	448 × 314	0.31 × 0.41
T2w TSE fs	Transversal	5694	89	3.0	160 × 160	512 × 358	0.31 × 0.45
PD TSE fs	Sagittal	3150/47	150	2.5	150 × 150	448 × 182	0.33 × 0.82
T1 TSE fs + contrast	Transversal	807/16	90	2.5	130 × 130	384 × 288	0.31 × 0.42

Imaging plane, echo and repetition time (TE/TR), flip angle, slice thickness, field of view (FoV), pixel size, and number of slices are given for all sequences (Short Tau Inversion Recovery, T2-weighted fat-saturated turbo spin echo (T2w TSE fs), T1w TSE, Proton Density TSE fs (PD)).

2.3. Image Analysis

MR images were independently read and analyzed by two musculoskeletal radiologists (DBA and CS with 3 and 8 years of experience) according to the OMERACT PsAMRIS guidelines [13, 14]. The readers were blinded to patients’ and treatment data. Baseline and follow-up scans were independently evaluated in random order. In the case of different scores, cases were discussed by both readers with the assisting opinion of a third reader (PS, trained in musculoskeletal imaging with 8 years of experience) until consensus was reached. Images were scored according to the OMERACT PsAMRIS guidelines [13]. They were evaluated for synovitis (score, 0–3), flexor tenosynovitis (score, 0–3), periarticular inflammation (score, 0 or 1), bone edema (score, 0–3), bone erosion (score, 0–10), and bone proliferation (score, 0 or 1) for the metacarpophalangeal (MCP), proximal and distal interphalangeal (PIP and DIP) joints of digits 2–5. In all joints, the proximal and distal or the dorsal and palmar aspects of the joint were analyzed separately for the presence of bone edema, bone erosions and periarticular inflammation. Scoring was repeated applying a simplified version of PsAMRIS (sPsAMRIS) by the same raters. The time needed to complete the scoring of PsAMRIS and sPsAMRIS per MRI study was recorded throughout the study and comparatively evaluated using Student’s *t*-test.

2.4. Development of a Simplified Psoriatic Arthritis MRI Score (sPsAMRIS) and Statistical Analysis

For the development of a simplified scoring system, sPsAMRIS, we applied a single-site weighted summation approach. Priority was assigned to the joints with the highest standardized response mean (SRM) for the change of overall PsAMRIS at baseline (t0) versus follow up (t1). The SRM is an effect size index commonly used to assess a score’s responsiveness to change.

All statistical analyses were performed using The R Project for Statistical Computing, a dedicated software environment for this purpose (version 3.5.1 “feather spray”, the R foundation, <https://www.R-project.org>).

For descriptive analysis, means, standard deviations, minima, and maxima were determined. The sensitivity for change and their responsiveness was calculated by division of the mean score change by the standard deviation of the change [18]. For PsAMRIS and sPsAMRIS as well as each sub-score, SRM was calculated based on the following Equation (1):

$$\text{SRM} = (\text{mean score } t_0 - \text{mean score } t_1) / (\text{SD mean score } t_0 - \text{mean score } t_1). \quad (1)$$

SRMs were defined according to Middel and van Sonderen [19] as large, moderate, small, and trivial responsiveness to therapy based on SRM values of $SRM \geq 0.8$, $0.8 > SRM \geq 0.5$, $0.5 > SRM \geq 0.2$, and $SRM < 0.2$.

Relative efficacy (RE) was calculated for sPsAMRIS compared to PsAMRIS as reference using the following Equation (2):

$$RE = ((sPsAMRIS\ SRM)/(PsAMRIS\ SRM))^2 \quad (2)$$

Confidence bounds for RE were estimated by the bootstrap method (based on $B = 5000$ bootstraps with replacement) and application of the percentile method [20]. RE values > 1 indicate that sPsAMRIS is more efficient than PsAMRIS in detecting change, while RE values < 1 indicate the opposite. For correlation analyses, Pearson's product-moment correlation with Pearson's correlation coefficient, r , was determined. Correlation strength was stratified as small ($0.1 \leq r < 0.3$), medium ($0.3 \leq r < 0.5$), and large ($0.5 \leq r < 1$) according to Cohen [21].

p -values of $p < 0.05$ were considered significant. Inter- and intra-rater reliability was calculated by two-way mixed intraclass correlation coefficients, i.e., single-measure ICC (sICC) for intra-rater and average-measure ICC (aICC) for inter-rater reliability based on the initial findings of the two readers before consensus was reached.

3. Results

3.1. Simplified Score: sPsAMRIS

Changes of overall PsAMRIS and each PsAMRIS sub-score between baseline and follow-up in terms of SRM are summarized in Table 2. For overall PsAMRIS, the MCP joints of digits 3 and 4 and the PIP joint of digit 4 showed the highest SRM values of 0.07, -0.07 , and -0.07 , respectively, and were hence combined to give the new simplified score sPsAMRIS. The topographical distribution of the regions and subregions to be included in sPsAMRIS as compared to PsAMRIS is detailed in Figure 1.

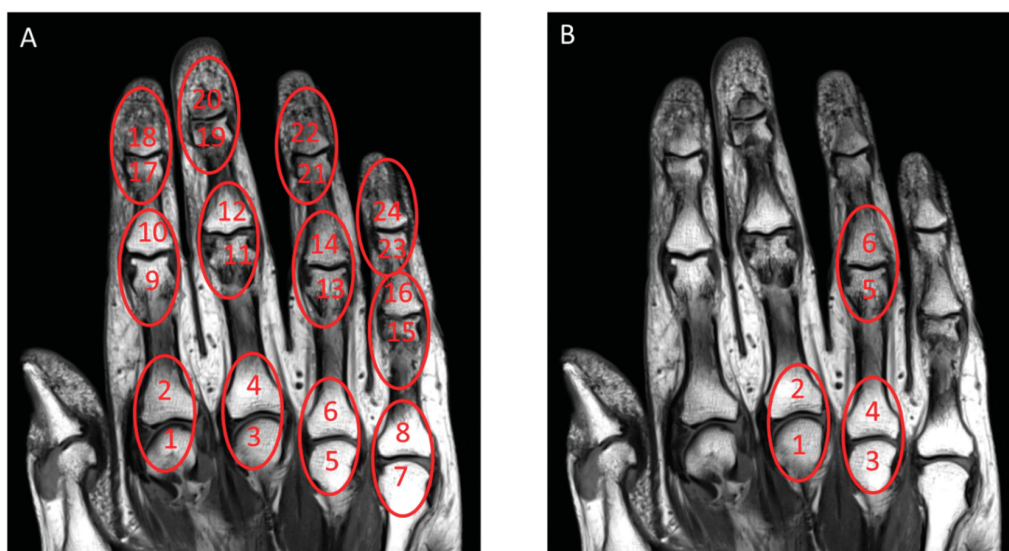


Figure 1. Joint regions and sub-regions in Psoriatic Arthritis Magnetic Resonance Imaging Score (PsAMRIS) versus simplified (s) PsAMRIS. Coronal T1-weighted MR image of a representative patient suffering from psoriatic arthritis (PsA). (A) In the full PsAMRIS, inflammatory and destructive changes associated with PsA are assessed in distinct regions and subregions of the hand. Circles indicate scored joints (i.e., regions), while numbers indicate joint sites (i.e., subregions). (B) Simplified (s) PsAMRIS. In A, 24 joint sites and/or 12 joints were evaluated, while in B, this number is reduced to 3 joints and/or 6 joint sites that were determined to be most responsive to clinical change.

Table 2. Changes between T0 and T1 for the overall psoriatic arthritis resonance imaging score (PsAMRIS) and its sub-scores assessed by standardized response means (SRM) ($SRM = \frac{\text{mean score T0} - \text{mean score T1}}{SD \text{ mean score T0} - \text{mean score T1}}$) at the metacarpophalangeal (MCP), proximal interphalangeal (PIP) and distal interphalangeal (DIP) joints of digits 2–5 in a clinical cohort of PsA patients. NaN—not available due to absence of the feature in the study population.

PsAMRIS Sub-Score	MCP				PIP				DIP			
	2	3	4	5	2	3	4	5	2	3	4	5
Overall	−0.01	0.07	−0.07	−0.03	−0.01	0	−0.07	0.00	0	−0.01	0	−0.03
Synovitis	−0.02	0.05	−0.07	−0.04	0.02	−0.03	−0.11	−0.03	−0.05	−0.05	−0.04	−0.04
Flexor tenosynovitis	0.05	0.09	0	0.01	0.01	0.04	−0.05	−0.08	0.04	0.1	0.04	−0.02
Bone Proliferation	−0.01	NaN	−0.01	NaN	−0.01	−0.01	−0.01	−0.01	−0.01	−0.01	0.03	NaN
Periarticular inflammation	−0.03	0.01	−0.01	0	−0.06	−0.05	−0.13	0.00	−0.03	0.01	−0.01	−0.06
Bone edema	−0.02	0.05	−0.07	−0.04	0.02	−0.03	−0.11	−0.03	−0.05	−0.05	−0.04	−0.04
Bone erosion	−0.04	0	−0.04	−0.05	−0.02	−0.01	0.03	0.03	0	−0.04	0.01	0

3.2. PsAMRIS and sPsAMRIS during Therapy

The PsAMRIS and sPsAMRIS scores and sub-scores at baseline (i.e., under MTX therapy) and at follow-up (i.e., after escalation to etanercept), are summarized in Table 3. Synovitis, flexor tenosynovitis, and periarticular inflammation were frequently observed in our patient cohort, which is thus reflected in both PsAMRIS and sPsAMRIS (Figure 2). Bone edema and bone erosions, on the other hand were less frequently seen, whereas bone proliferations were rarely detected.

Table 3. Descriptive analysis of PsAMRIS and short (s) PsAMRIS at baseline and at follow-up regarding the overall scores and each sub-score. For each values the mean ± standard deviation (SD), the median and range are presented.

PsAMRIS Sub-Score	Baseline PsAMRIS/sPsAMRIS				Follow-Up PsAMRIS/sPsAMRIS				p-Value
	Mean	SD	Range	Median	Mean	SD	Range	Median	
Overall	65.4 /16.3	±17.4 /±4.4	37–93 /9–25	64.0 /15.0	67.5/ 17.2	±14.4 /±3.1	49–98 /14–25	68.0 /16.5	0.958 /0.436
Synovitis	22.1 /6.4	±5.7 /±1.5	13–33 /5–9	22.0 /6.0	24.0 /6.9	±4.7 /±1.3	17–32 /5–9	23.5 /7.0	0.689 /0.149
Flexor tenosynovitis	10.5 /2.9	±5 /±1	3–22 /2–5	10.0 /3.0	9.6 /2.8	±3.1 /±0.7	5–16 /2–4	10.0 /3.0	0.592 /0.602
Bone Proliferation	1.1 /0.2	±1.4 /±0.5	0–4 /0–2	1.0 /0.0	1.1 /0.2	±1.4 /±0.6	0–4 /0–2	1.0 /0.0	1 /0.956
Periarticular inflammation	17.7 /4.5	±3.1 /±1.4	10–22 /1–6	18.0 /5.0	18.9 /4.9	±3.7 /±0.8	9–23 /4–6	19.5 /5.0	0.299 /0.055
Bone edema	6.6 /0.5	±5.5 /±1.2	1–20 /0–4	5.0 /0.0	5.6 /0.4	±6 /±0.9	0–23 /0–3	4.0 /0.0	0.449 /0.336
Bone erosion	7.5 /1.8	±5.5 /±1.6	1–20 /0–5	6.0 /1.0	8.2 /1.9	±5.6 /±1.3	1–19 /0–5	7.0 /1.5	0.316 /0.637

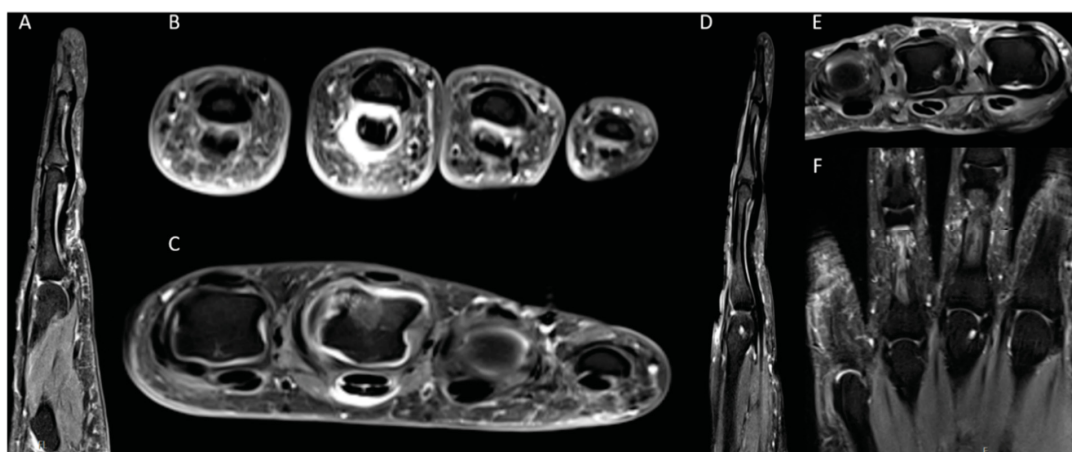


Figure 2. Representative MRI findings in a 57-year-old (A–C) and a 43-year-old (D–F) patient suffering from peripheral PsA. (A) and (D) Sagittal proton density-weighted (PD) fat-saturated (fs) image of the fourth (A) and third (D) digit (B,C,E) Transversal T1-weighted (T1w) fs image after contrast agent application through the level of proximal interphalangeal (PIP) joints of digits 2–5 (B), metacarpophalangeal (MCP) joints of digits 2–5 (D) and digits 2–4 (E). (F) Coronal short tau inversion recovery (STIR) sequence of the MCP joints of the digits 2–5 and the PIP joints of the digits 3 and 4. (A,B) show distinct periarticular inflammation and flexor tenosynovitis at the PIP joints of digits 3 and 4 and less distinct of the second digit. (C) illustrates synovitis, flexor tenosynovitis, bone marrow edema and a subtle erosion of the MCP joint of the third digit and moderate periarticular inflammation at the dorsal portion of the MCP joint of the fourth and at the palmar portion of the fifth digit. D–F depict a distinct bone erosion at the MCP joint of the third digit and periarticular inflammation at the MCP joints of the digits 2–4.

At follow-up, overall PsAMRIS and sPsAMRIS values alongside the sub-scores for synovitis, periarticular inflammation, and bone erosions, were increased as compared to baseline, however, non-significantly. The sub-scores for flexor tenosynovitis and bone edema, on the other hand, were slightly decreased, again non-significantly, at follow-up.

3.3. PsAMRIS and sPsAMRIS Sensitivity to Change (Responsiveness) in Terms of Standardized Response Means (SRMs)

The sensitivity to change of PsAMRIS and sPsAMRIS as assessed by the SRMs [22] is summarized in Table 4. Overall, there is mostly trivial sensitivity to change for both PsAMRIS and sPsAMRIS, whereas for the latter, we determined slightly higher absolute SRMs indicating higher sensitivity to change. Only for the sub-scores periarticular inflammation and bone erosion (PsAMRIS) as well as synovitis (sPsAMRIS) did we find slightly higher, yet still low, sensitivity to change (Table 4).

Table 4. Standardized Response Means of PsAMRIS and sPsAMRIS and Their Sub-Scores. Sensitivity to change, i.e., responsiveness, of PsAMRIS, sPsAMRIS, and their sub-scores between baseline and follow-up as assessed by SRMs. NaN—not available due to absence of the feature in the study population.

PsAMRIS Sub-Score	PsAMRIS	sPsAMRIS
Overall	−0.02	−0.13
Synovitis	−0.11	−0.21
Flexor tenosynovitis	0.15	0.08
Bone Proliferation	NaN	NaN
Periarticular inflammation	−0.31	−0.16
Bone edema	0.2	−0.13
Bone erosion	−0.29	0.12

3.4. RE and Degrees of Agreement

RE for sPsAMRIS as compared to PsAMRIS was calculated as 29.46 (confidence bounds 2.5/97.5%: 0.00/59.88). Intra- and inter-rater reliability for both scoring systems was high (aICC = 0.95, sICC = 0.92).

3.5. Correlation of PsAMRIS and sPsAMRIS

Details of the correlations of PsAMRIS with sPsAMRIS are shown in Table 5. Strong significant correlations between both scores were found for the overall values at baseline and follow-up (baseline, $r = 0.75$, $p < 0.01$; follow-up, 0.64 , $p < 0.05$) as well as for the majority of sub-scores.

Table 5. Pearson's correlation coefficients r of PsAMRIS and sPsAMRIS for the overall score as well as each sub-score at baseline and follow-up. p -values of $p < 0.05$ were considered significant and are given in **bold** type.

PsAMRIS Sub-Score	Baseline			Follow-Up		
	Correlation Coefficient r	95% Confidence Interval	p -Value	Correlation Coefficient r	95% Confidence Interval	p -Value
Overall	0.75	0.42; 0.90	<0.001	0.64	0.17; 0.87	0.013
Synovitis	0.84	0.61; 0.94	<0.001	0.74	0.34; 0.91	0.002
Flexor tenosynovitis	0.72	0.36; 0.89	0.001	0.59	0.09; 0.85	0.025
Bone proliferation	0.66	0.27; 0.87	0.004	0.66	0.23; 0.88	0.007
Periarticular inflammation	0.79	0.50; 0.92	<0.001	0.35	−0.22; 0.74	0.223
Bone edema	0.31	−0.2; 0.69	0.221	0.85	0.58; 0.95	<0.001
Bone erosion	0.8	0.51; 0.92	<0.001	0.74	0.35; 0.91	0.002

3.6. Comparative Analysis of Time Burden

Overall, the time needed for scoring was variable as a function of the number of lesions detected. Per MRI study, significantly higher time burden was recorded for PsAMRIS (mean \pm standard deviation, 469 ± 87.03 s; median, 428 s; range, 300–607 s) than for sPsAMRIS (140.1 ± 21.25 s; median, 141 s; 95–174 s) ($p < 0.001$) (Figure 3).

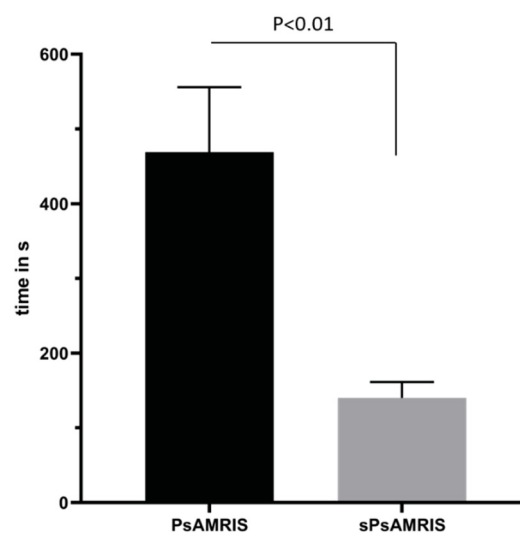


Figure 3. Mean time burden for completion of scoring based on PsAMRIS and sPsAMRIS per MRI study. Scoring on the basis of sPsAMRIS was completed in significantly less time than scoring on the basis of PsAMRIS ($p < 0.01$).

4. Discussion

The most important finding of the present study is that sPsAMRIS is a potent diagnostic tool to quantitatively assess and monitor therapy in PsA because of its excellent reliability, higher responsiveness to change, and time efficiency as compared to PsAMRIS.

In 2009, the OMERACT working group established the PsAMRIS [13] for detecting and grading PsA-related findings. The PsAMRIS is increasingly used for structured semi-quantitative evaluation of peripheral joint changes related to PsA [22–24]. Even though PsAMRIS is a sensitive and validated tool for detecting early PsA-related changes [14,25,26], it is of limited use in clinical practice and, hence, primarily used in research, not least because of the substantial time burden. Up to now, however, there has been no alternative to the OMERACT PsAMRIS for semi-quantitative evaluation of joint changes. Therefore, some authors have developed and applied abbreviated versions of PsAMRIS in the context of their research. Feletar et al. scored osteitis, tenosynovitis, and synovitis, without demonstrating correlation with regular PsAMRIS [27]. Our group previously demonstrated that an abbreviated version of the OMERACT Rheumatoid Arthritis Magnetic Resonance Imaging Score (RAMRIS), RAMRIS-5, is a time- and resource-saving alternative to the original version [28]. Similar to our approach for the RAMRIS-5, we reduced the current PsAMRIS to a simplified and abbreviated version that scores 36 instead of 144 items in 3 instead of 12 joints. We found a strong correlation between sPsAMRIS and PsAMRIS at baseline and follow-up after six months of etanercept therapy. Further, sPsAMRIS indicated a very high RE compared to PsAMRIS, which is well in line with other studies [29] and, thus, can be considered to be sufficiently sensitive to change. Additionally, sPsAMRIS significantly decreased the time burden associated with scoring as compared to the regular PsAMRIS. Hence, sPsAMRIS may be a time- and resource-saving alternative for semi-quantitative scoring of PsA-related joint changes of the hand, in particular when screening of large numbers of MRI studies is performed. As PsAMRIS is of limited clinical use due to its time burden, sPsAMRIS is better applicable in clinical and distinct research settings, for example when screening and stratifying potentially eligible patients in disease modifying drug trials. For this purpose, excellent reliability, similar responsiveness to change compared to standard PsAMRIS, and time efficiency have been demonstrated for sPsAMRIS, rendering this scoring system a potential tool in clinical research and clinical work.

Nonetheless, we do not intend to fully replace PsAMRIS by sPsAMRIS because its wide-spread application in clinical research.

Following Ostergaard et al. and Glinatsi et al., who stated potential difficulties in scoring especially DIP and, to a lesser extent, PIP joints, due to a lack of spatial resolution, there are additional arguments for an abbreviation with focus on the MCP joint regions [13,14]. Using a clinical MRI scanner with high field strength of 3 T and a dedicated 16-channel hand coil, we managed to improve spatial resolution considerably, making analysis of the PIP region more accurate. Yet, accurate assessment of the sub-millimeter thin cartilage layers of the PIP and DIP joints remains challenging because of inherent limitations in terms of spatial resolution, signal-to-noise ratio, and partial volume effects [30]. With dedicated wrist coils, let alone specialized high-resolution coils for finger joints, not widely available in radiology departments and clinical scanning of hands oftentimes performed on 1.5 T MRI scanners, the focus on the evaluation of the MCP and PIP joints (as in sPsAMRIS) may strengthen the score's clinical applicability, validity, and reliability.

Our study has limitations. Since PsA is a disease with several clinical and radiological manifestations, this study focused more on a well-defined and homogeneous patient collective. However, due to our small patient collective included in this exploratory study, our results must be considered preliminary. Further investigations using larger and more varied patient cohorts are required to corroborate our findings and the applicability of sPsAMRIS. Additionally, sPsAMRIS is a data-driven and weighted approach that is derived from this well-defined patient collective, which limits general transferability to other PsA collectives. Since PsA is a very heterogeneous and complex disease, a “one-fits-all” scoring system that is both sensitive and time saving may be even more difficult to establish compared to RA, which tends to be a more homogeneous disease entity.

5. Conclusions

The simplified MRI scoring system for PsA-related changes in hands, sPsAMRIS, is a reliable and time-efficient diagnostic scoring tool that is strongly correlated with standard PsAMRIS. Due to its similar responsiveness to change compared to regular PsAMRIS, sPsAMRIS may potentially be used for quantitative assessment and therapy monitoring in PsA. Its clinical applicability beyond our patient collective needs to be demonstrated in larger future study populations.

Author Contributions: D.B.A.: acquisition, analysis and interpretation of data; drafting the article; final approval of the version to be published; agree to be accountable for all aspects of the work. C.S.: conception and design of the study, analysis of data; revising the article critically for important intellectual content; final approval of the version to be published; agree to be accountable for all aspects of the work. R.B.: analysis and interpretation of data; revising the article critically for important intellectual content; final approval of the version to be published; agree to be accountable for all aspects of the work. C.G.: acquisition and analysis of data; revising the article critically for important intellectual content; final approval of the version to be published; agree to be accountable for all aspects of the work. M.F.: acquisition and analysis of data; revising the article critically for important intellectual content; final approval of the version to be published; agree to be accountable for all aspects of the work. M.S.: conception and design of the study; revising the article critically for important intellectual content; final approval of the version to be published; agree to be accountable for all aspects of the work. S.N.: analysis and interpretation of data; revising the article critically for important intellectual content; final approval of the version to be published; agree to be accountable for all aspects of the work. P.S.: conception and design of the study, analysis and interpretation of data; revising the article critically for important intellectual content; final approval of the version to be published; agree to be accountable for all aspects of the work. All authors have read and agreed to the published version of the manuscript.

Funding: The project was funded by the “Pfizer GIP Inflammation Germany Research Initiative 2014” to P.S. and by a grant from the German “Bundesministerium für Bildung und Forschung”(BMBF), ArthroMark (01EC1009). D.B.A. was supported by an internal research grant of the local research committee of the medical faculty. German “Bundesministerium für Bildung und Forschung” (BMBF), ArthroMark (01EC1009). S.N. has been supported by grants from the “Deutsche Forschungsgemeinschaft” (DFG) (NE 2136/3-1).

Acknowledgments: We thank Erika Rädisch for the technical acquisition of all images.

Conflicts of Interest: The authors declare no conflict of interest.

References

1. Castaneda, S.; Gonzalez-Juanatey, C.; Gonzalez-Gay, M.A. Inflammatory Arthritis and Heart Disease. *Curr. Pharm. Des.* **2018**, *24*, 262–280. [[CrossRef](#)]
2. Koo, J.; Marangell, L.B.; Nakamura, M.; Armstrong, A.; Jeon, C.; Bhutani, T.; Wu, J.J. Depression and suicidality in psoriasis: Review of the literature including the cytokine theory of depression. *J. Eur. Acad. Dermatol. Venereol. JEADV* **2017**, *31*, 1999–2009. [[CrossRef](#)] [[PubMed](#)]
3. Sewerin, P.; Brinks, R.; Schneider, M.; Haase, I.; Vordenbäumen, S. Prevalence and incidence of psoriasis and psoriatic arthritis. *Ann. Rheum. Dis.* **2019**, *78*, 286–287. [[CrossRef](#)] [[PubMed](#)]
4. Kim, Y.; Oh, H.C.; Park, J.W.; Kim, I.S.; Kim, J.Y.; Kim, K.C.; Chae, D.S.; Jo, W.L.; Song, J.H. Diagnosis and Treatment of Inflammatory Joint Disease. *Hip Pelvis* **2017**, *29*, 211–222. [[CrossRef](#)]
5. McQueen, F.; Lassere, M.; Østergaard, M. Magnetic resonance imaging in psoriatic arthritis: A review of the literature. *Arthritis Res. Ther.* **2006**, *8*, 207. [[CrossRef](#)] [[PubMed](#)]
6. Mc Ardle, A.; Flatley, B.; Pennington, S.R.; Fitzgerald, O. Early biomarkers of joint damage in rheumatoid and psoriatic arthritis. *Arthritis Res. Ther.* **2015**, *17*, 1–12. [[CrossRef](#)]
7. Hermann, K.G.A.; Ohrndorf, S.; Werner, S.G.; Finzel, S.; Backhaus, M. Bildgebende Verfahren bei Psoriasisarthritis. *Z. Rheumatol.* **2013**, *72*, 771–778. [[CrossRef](#)]
8. Gossec, L.; Coates, L.C.; De Wit, M.; Kavanaugh, A.; Ramiro, S.; Mease, P.J.; Ritchlin, C.T.; Van Der Heijde, D.; Smolen, J.S. Management of psoriatic arthritis in 2016: A comparison of EULAR and GRAPPA recommendations. *Nat. Rev. Rheumatol.* **2016**, *12*, 743–750. [[CrossRef](#)]
9. Taylor, W.; Gladman, D.; Helliwell, P.; Marchesoni, A.; Mease, P.; Mielants, H. Classification criteria for psoriatic arthritis: Development of new criteria from a large international study. *Arthritis Rheum.* **2006**, *54*, 2665–2673. [[CrossRef](#)] [[PubMed](#)]

10. Poggenborg, R.P.; Sørensen, I.J.; Pedersen, S.J.; Østergaard, M. Magnetic resonance imaging for diagnosing, monitoring and prognostication in psoriatic arthritis. *Clin. Exp. Rheumatol.* **2015**, *33*, 66–69.
11. Agten, C.A.; Rosskopf, A.B.; Jonczy, M.; Brunner, F.; Pfirrmann, C.W.A.; Buck, F.M. Frequency of inflammatory-like MR imaging findings in asymptomatic fingers of healthy volunteers. *Skelet. Radiol.* **2018**, *47*, 279–287. [[CrossRef](#)] [[PubMed](#)]
12. Sudol-Szopińska, I.; Pracoń, G. Diagnostic imaging of psoriatic arthritis. Part II: Magnetic resonance imaging and ultrasonography. *J. Ultrason.* **2016**, *16*, 163–174. [[CrossRef](#)]
13. Østergaard, M.; Peterfy, C.; Conaghan, P.; OMERACT Rheumatoid Arthritis Magnetic Resonance Imaging Studies. Core set of MRI acquisitions, joint pathology definitions, and the OMERACT RA-MRI scoring system. *J. Rheumatol.* **2003**, *30*, 1385–1386.
14. Østergaard, M.; McQueen, F.; Bird, P.; Peterfy, C.; Haavardsholm, E.; Ejbjerg, B.; Lassere, M.; O'Connor, P.; Emery, P.; Edmonds, J.; et al. The OMERACT Magnetic Resonance Imaging Inflammatory Arthritis Group—Advances and priorities. *J. Rheumatol.* **2007**, *34*, 852–853. [[PubMed](#)]
15. Østergaard, M.; McQUEEN, F.I.; Wiell, C.; Bird, P.; Bøyesen, P.; Ejbjerg, B.; Peterfy, C.; Gandjbakhch, F.; Duer-Jensen, A.; Coates, L.; et al. The OMERACT psoriatic arthritis magnetic resonance imaging scoring system (PsAMRIS): Definitions of key pathologies, suggested MRI sequences, and preliminary scoring system for PsA Hands. *J. Rheumatol.* **2009**, *36*, 1816–1824. [[CrossRef](#)] [[PubMed](#)]
16. Glinatsi, D.; Bird, P.; Gandjbakhch, F.; Mease, P.J.; Bøyesen, P.; Peterfy, C.G.; Conaghan, P.G.; Østergaard, M. Validation of the OMERACT Psoriatic Arthritis Magnetic Resonance Imaging Score (PsAMRIS) for the Hand and Foot in a Randomized Placebo-controlled Trial. *J. Rheumatol.* **2015**, *42*, 2473–2479. [[CrossRef](#)]
17. Schleich, C.; Buchbender, C.; Sewerin, P.; Miese, F.; Aissa, J.; Brinks, R.; Schneider, M.; Antoch, G.; Ostendorf, B. Evaluation of a simplified version of the Rheumatoid Arthritis Magnetic Resonance Imaging Score (RAMRIS) comprising 5 joints (RAMRIS5). *Clin. Exp. Rheumatol.* **2015**, *33*, 209–215.
18. Bøyesen, P.; McQueen, F.M.; Gandjbakhch, F.; Lillegraven, S.; Coates, L.; Wiell, C.; Haavardsholm, E.A.; Conaghan, P.G.; Peterfy, C.G.; Bird, P.; et al. The OMERACT Psoriatic Arthritis Magnetic Resonance Imaging Score (PsAMRIS) is reliable and sensitive to change: Results from an OMERACT workshop. *J. Rheumatol.* **2011**, *38*, 2034–2038. [[CrossRef](#)]
19. Michelsen, B.; Fiane, R.; Diamantopoulos, A.P.; Soldal, D.M.; Hansen, I.J.; Sokka, T.; Kavanaugh, A.; Haugeberg, G. A comparison of disease burden in rheumatoid arthritis, psoriatic arthritis and axial spondyloarthritis. *PLoS ONE* **2015**, *10*, e0123582. [[CrossRef](#)]
20. de Socio, A.; Perrotta, F.M.; Grasso, G.M.; Lubrano, E. Incidence of rheumatoid arthritis, psoriatic arthritis and polymyalgia rheumatica in an inland area of central Italy: Results of the CAMPO-RHE study. *Postgrad. Med.* **2018**, *130*, 137–141. [[CrossRef](#)]
21. Michelsen, B.; Uhlig, T.; Sexton, J.; van der Heijde, D.; Hammer, H.B.; Kristianslund, E.K.; Wierød, A.; Bakland, G.; Rødevand, E.; Krøll, F.; et al. Health-related quality of life in patients with psoriatic and rheumatoid arthritis: Data from the prospective multicentre NOR-DMARD study compared with Norwegian general population controls. *Ann. Rheum. Dis.* **2018**. [[CrossRef](#)] [[PubMed](#)]
22. Coates, L.C.; Hodgson, R.; Conaghan, P.G.; Freeston, J.E. MRI and ultrasonography for diagnosis and monitoring of psoriatic arthritis. *Best pract. Res. Clin. Rheumatol.* **2012**, *26*, 805–822. [[CrossRef](#)] [[PubMed](#)]
23. Watad, A.; Eshed, I.; McGonagle, D. Lessons learned from Imaging on Enthesitis in PsoA. *Isr. Med. Assoc. J. IMAJ* **2017**, *19*, 708–711. [[PubMed](#)]
24. Coates, L.C.; Helliwell, P.S. Treat to target in psoriatic arthritis-evidence, target, research agenda. *Curr. Rheumatol. Rep.* **2015**, *17*, 517. [[CrossRef](#)]
25. Tan, A.L.; Fukuba, E.; Halliday, N.A.; Tanner, S.F.; Emery, P.; McGonagle, D. High-resolution MRI assessment of dactylitis in psoriatic arthritis shows flexor tendon pulley and sheath-related enthesitis. *Ann. Rheum. Dis.* **2015**, *74*, 185–189. [[CrossRef](#)]
26. Zubler, V.; Agten, C.A.; Pfirrmann, C.W.A.; Weiss, B.G.; Dietrich, T.J. Frequency of Arthritis-Like MRI Findings in the Forefeet of Healthy Volunteers Versus Patients With Symptomatic Rheumatoid Arthritis or Psoriatic Arthritis. *AJR Am. J. Roentgenol.* **2017**, *208*, W45–W53. [[CrossRef](#)]
27. Mcqueen, F.I.; Lassere, M.; Duer-Jensen, A.; Wiell, C.; Conaghan, P.G.; Gandjbakhch, F.; Hermann, K.G.; Bird, P.; Bøyesen, P.; Peterfy, C.; et al. Testing an OMERACT MRI scoring system for peripheral psoriatic arthritis in cross-sectional and longitudinal settings. *J. Rheumatol.* **2009**, *36*, 1811–1815. [[CrossRef](#)]

28. Yanaba, K.; Sadaoka, A.; Yonenaga, T.; Saeki, H.; Umezawa, Y.; Tojo, S.; Ito, T.; Kikuchi, S.; Fukuda, K.; Nakagawa, H. Adalimumab markedly improves enthesitis in patients with psoriatic arthritis: Evaluation with a magnetic resonance imaging scoring system. *J. Dermatol.* **2015**, *42*, 1153–1159. [[CrossRef](#)]
29. Mease, P.; Genovese, M.C.; Gladstein, G.; Kivitz, A.J.; Ritchlin, C.; Tak, P.P.; Wollenhaupt, J.; Bahary, O.; Becker, J.C.; Kelly, S.; et al. Abatacept in the treatment of patients with psoriatic arthritis: Results of a six-month, multicenter, randomized, double-blind, placebo-controlled, phase II trial. *Arthritis Rheum.* **2011**, *63*, 939–948. [[CrossRef](#)]
30. Coates, L.C.; Conaghan, P.G.; D’Agostino, M.A.; De Wit, M.; FitzGerald, O.; Kvien, T.K.; Lories, R.; Mease, P.; Nash, P.; Schett, G.; et al. Remission in psoriatic arthritis—Where are we now? *Rheumatology* **2018**. [[CrossRef](#)]

Publisher’s Note: MDPI stays neutral with regard to jurisdictional claims in published maps and institutional affiliations.



© 2020 by the authors. Licensee MDPI, Basel, Switzerland. This article is an open access article distributed under the terms and conditions of the Creative Commons Attribution (CC BY) license (<http://creativecommons.org/licenses/by/4.0/>).

Article

DGEMRIC in the Assessment of Pre-Morphological Cartilage Degeneration in Rheumatic Disease: Rheumatoid Arthritis vs. Psoriatic Arthritis

Daniel B. Abrar ^{1,*} , Christoph Schleich ¹, Miriam Frenken ¹, Stefan Vordenbäumen ², Jutta Richter ², Matthias Schneider ², Benedikt Ostendorf ², Sven Nebelung ^{1,†}  and Philipp Sewerin ^{2,†} 

¹ Medical Faculty, Department of Diagnostic and Interventional Radiology, University Dusseldorf, 40225 Düsseldorf, Germany; Christoph.Schleich@med.uni-duesseldorf.de (C.S.); Miriam.Frenken@med.uni-duesseldorf.de (M.F.); sven.nebelung@med.uni-duesseldorf.de (S.N.)

² Department and Hiller Research Unit for Rheumatology, Heinrich Heine University Düsseldorf, Moorenstrasse 5, 40225 Düsseldorf, Germany; Stefan.Vordenbaeumen@med.uni-duesseldorf.de (S.V.); jutta.richter@med.uni-duesseldorf.de (J.R.); matthias.schneider@med.uni-duesseldorf.de (M.S.); ostendorf@rheumatologie-am-hofgarten.de (B.O.); philipp.sewerin@med.uni-duesseldorf.de (P.S.)

* Correspondence: DanielBenjamin.Abrar@med.uni-duesseldorf.de

† Authors contributed equally.

Abstract: Background: Even though cartilage loss is a known feature of psoriatic (PsA) and rheumatoid arthritis (RA), research is sparse on its role in the pathogenesis of PsA, its potential use for disease monitoring and for differentiation from RA. We therefore assessed the use of delayed gadolinium-enhanced magnetic resonance imaging of cartilage (dGEMRIC) to evaluate biochemical cartilage changes in metacarpophalangeal (MCP) and proximal interphalangeal (PIP) joints in PsA patients and compared these to RA patients. Materials and Methods: A total of 17 patients with active PsA and 20 patients with active RA were evaluated by high-resolution 3 Tesla dGEMRIC using a dedicated 16-channel hand coil. Images were analyzed by two independent raters for dGEMRIC indices and joint space width (JSW) at MCP and PIP joint levels. Results: No significant differences of dGEMRIC values could be found between both study populations (PsA 472.25 ms, RA 461.11 ms; $p = 0.763$). In all RA and most PsA patients, PIP joints showed significantly lower dGEMRIC indices than MCP joints (RA: D2: $p = 0.009$, D3: $p = 0.008$, D4: $p = 0.002$, D5: $p = 0.002$; PsA: D3: $p = 0.001$, D4: $p = 0.004$). Most joint spaces had similar widths in both disease entities and no significant differences were found. Conclusions: As evaluated by dGEMRIC, the molecular composition of the MCP and PIP joint cartilage of PsA patients is similar to that of RA patients, demonstrating the scientific and clinical feasibility of compositional magnetic resonance (MR) imaging in these disease entities. Patterns and severity of compositional cartilage degradation of the finger joints may therefore be assessed beyond mere morphology in PsA and RA patients.

Keywords: psoriatic arthritis; rheumatoid arthritis; cartilage; magnetic resonance imaging; dGEMRIC; compositional imaging



Citation: Abrar, D.B.; Schleich, C.; Frenken, M.; Vordenbäumen, S.; Richter, J.; Schneider, M.; Ostendorf, B.; Nebelung, S.; Sewerin, P. DGEMRIC in the Assessment of Pre-Morphological Cartilage Degeneration in Rheumatic Disease: Rheumatoid Arthritis vs. Psoriatic Arthritis. *Diagnostics* **2021**, *11*, 147. <https://doi.org/10.3390/diagnostics11020147>

Received: 9 December 2020

Accepted: 18 January 2021

Published: 20 January 2021

Publisher's Note: MDPI stays neutral with regard to jurisdictional claims in published maps and institutional affiliations.



Copyright: © 2021 by the authors. Licensee MDPI, Basel, Switzerland. This article is an open access article distributed under the terms and conditions of the Creative Commons Attribution (CC BY) license (<https://creativecommons.org/licenses/by/4.0/>).

1. Introduction

Cartilage damage and bone destruction are the main features of progressive rheumatoid arthritis (RA) [1,2]. Even though the exact pathogenesis of rheumatoid arthritis (RA) is subject to ongoing research, three main patho-mechanisms are considered to eventually lead to cartilage destruction: a. synovial inflammation leading to secondary infiltration and destruction of bone and cartilage (outside-in-model) [3]; b. primary inflammation of subchondral bone marrow that secondarily involves cortical bone and cartilage [3–5]; c. primary affection of joint cartilage by deposition of immune complexes [6]. Eventually, all mechanisms lead to functional disability of joints, wherein cartilage damage is considered to be pivotal [7,8]. Unlike RA, the research on cartilage damage in psoriatic arthritis (PsA) is

sparse, even though it is a known feature of the disease [9]. In particular, studies evaluating biomarkers such as cartilage oligo-matrix protein (COMP) and osteo-protegerin (OPG) could demonstrate an involvement of cartilage in PsA that was not limited to late stages of the disease [10–13]. Research has also shown that bone and cartilage damage in RA is frequently associated with enthesal insertion sites due to mechanical stress and spreading inflammation [14]. Considering that PsA is an enthesal disease, driven by inflammation of the so-called synovio–enthesal complex, an enthesal-driven involvement of bone and cartilage seems evident [15,16].

Early diagnosis and treatment are pivotal for a favorable clinical outcome in both entities, RA and PsA. Hence, treat-to-target strategies have emerged over the past decade [17–19]. However, the role of magnetic resonance imaging (MRI) in clinical strategies is less clear. On the one hand, in RA, bone marrow edema and MRI erosions are highly predictive of future erosions, even though there is only little evidence for this in PsA; on the other hand, a recent trial failed to demonstrate any benefit from an MRI-remission strategy [20]. Thus, more research is clearly needed. Morphological MR imaging is commonly used in clinical contexts and beyond, for example, by the Outcome Measures in RA Clinical Trials (OMERACT) working group for the quantitative assessment of RA and PsA in research studies. Additionally, there are several compositional MRI techniques available that allow the detection of cartilage changes on a molecular level preceding morphological damage [21]. Delayed gadolinium-enhanced MRI of cartilage (dGEMRIC) is the gold-standard technique for compositional cartilage imaging that allows the visualization of proteoglycan depletion in cartilage by analysis of the fixed-charge density [22]. The negatively charged side chains of proteoglycans bring about charge repulsion of equally negatively charged gadolinium molecules after intravenous administration and diffusion into cartilage tissue. Consequently, the concentration of proteoglycans is inversely proportional to the concentration of gadolinium; dGEMRIC is considered the best validated and most robust technique for quantifying proteoglycan content in vivo and in clinical trials [23].

Using dGEMRIC, several studies have shown a strong correlation of local joint inflammation and early cartilage alterations in RA [24,25]. However, to the best of our knowledge, no such data exists for PsA patients. Accordingly, the aim of our study was to assess articular cartilage composition by dGEMRIC across a cohort of PsA patients as compared to RA patients and to evaluate both patterns and severity of compositional (i.e., pre-morphological) cartilage degradation in both disease entities. Our study's hypotheses were a) patterns and severity of compositional cartilage degradation of the finger joints could be assessed by dGEMRIC in PsA patients; and b) these were significantly different in PsA patients as compared to RA patients.

2. Materials and Methods

2.1. Study Population

21 patients with PsA (mean age 47 ± 6 , range 26–72 years, male/female 11/10) fulfilling the classification criteria for psoriatic arthritis (CASPAR), mean disease duration 4 ± 3.6 years and suffering from peripheral joint involvement and dactylitis were prospectively recruited for the “Analysis of the DActylic Melange” (ADAM) research initiative [26]. All patients had failed methotrexate (MTX) monotherapy and were escalated to Etanercept (Enbrel® 50 mg s.c. fortnightly, Pfizer). 17 patients (mean age 53.7 ± 11.6 ; minimum/maximum 26/72 years, male/female 9/8) were included, and four patients did not want to participate in the study.

20 patients (mean age 46 ± 15.7 , range 19–67 years, male/female 9/11) fulfilling the American College of Rheumatology (ACR)/European League Against Rheumatism (EULAR) 2010 criteria for RA with a mean disease duration <6 months (mean duration 8 weeks, range 2–22 weeks) from the ‘Cartilage in early RA’ (CAR-ERA) study were similarly included. Patients maintained either MTX monotherapy or received a combination of MTX and adalimumab. Patients were blinded for their therapy regime.

The study was approved by the local ethics committee (Ethics committee of the medical faculty of the Heinrich-Heine-University Dusseldorf, 4962R, MO-LKP-719, approved on 01 April 2015 and 17 September 2015). Written and informed consent was obtained from all patients before initiation of the study. Patient recruitment and consecutive MRI measurements were performed between 01/2015 and 12/2017.

2.2. MR Imaging

For all patients, we used a clinical 3T MRI scanner (Magentom Skyra, Siemens Healthineers, Erlangen, Germany) and a receive-only 16-channel hand coil (3T Tim Coil, Siemens).

All patients were scanned in the prone position with the clinically dominant hand extended overhead, palm facing down ('superman position').

The morphologic MRI protocols were designed according to the recommendations of the OMERACT working group for PsA and RA [27,28].

In practical terms, the imaging protocol included pre- and post-contrast coronal T1-weighted turbo spin echo (TSE) sequences before and after intravenous administration of a gadolinium-based contrast agent (Gd-DOTA-], Dotarem, Guerbet Villepinte, France) in a double dose, i.e., 0.4 mmol/kg bodyweight). Additionally, post-contrast fat-saturated T1-weighted sequences in at least two different orthogonal planes and non-contrast enhanced, fat-saturated T2-weighted/short tau inversion recovery (STIR) sequences were acquired. Further, two 3D fast low angle shot (3D-FLASH) sequences using two different excitation flip angles (5° and 26°) were obtained for T1 mapping.

For the entire study population, compositional MRI using the dGEMRIC technique of the MCP and PIP joints of fingers 2–5 was conducted 40 min after intravenous injection of Gd-DOTA-. We used a flip-angle three-dimensional gradient-echo imaging (FLASH) sequence with two excitation flip angles (5° and 26°). 40 sagittal slices were obtained perpendicular to each joint's surface. The total acquisition time was approximately 2 min 25 sec. The detailed sequence parameters were as follows: coronal T1 TSE (TR/TE in ms, PsA: 862/27, RA: 25/860; flip angle in °, PsA: 150, RA: 150; slice thickness in mm, PsA: 2.5, RA: 2.5; field of view in mm, PsA: 140, RA: 120), coronal STIR (TR/TE in ms, PsA: 5560/31, RA: 31/5560; flip angle in °, PsA: 120, RA: 120; slice thickness in mm, PsA: 2.5, RA: 2.5; field of view in mm, PsA: 140, RA: 120), transversal T1 SE fat-saturated after iv contrast (TR/TE in ms, PsA: 807/16, RA: 807/16; flip angle in °, PsA: 90, RA: 90; slice thickness in mm, PsA: 3.0, RA: 3.0; field of view in mm, PsA: 130, RA: 130), coronal T1 TSE after iv contrast (TR/TE in ms, PsA: 862/27, RA: 25/120; flip angle in °, PsA: 150, RA: 150; slice thickness in mm, PsA: 2.5, RA: 2.5; field of view in mm, PsA: 140, RA: 120), flip-angle three-dimensional gradient-echo imaging (FLASH, TR/TE in ms, PsA: 5.8/1.9, RA: 5.8/1.9; flip angle in °, PsA: 8/26, RA: 8/26; slice thickness in mm, PsA: 3.0, RA: 3.0; field of view in mm, PsA: 140, RA: 140, imaging matrix in PsA and RA 312 × 384).

2.3. Image Analysis

For the quantitative analysis of joint space widths (JSW), T1-weighted images obtained perpendicularly to the joint surfaces were used. Following the approach of Herz et al. [29] and using the caliper tool of the in-house picture archiving and communication system (PACS, IDS 7, Sectra AB, Linköping, Sweden), JSW was measured in mm at each radial, ulnar and central aspect of the joint as the distance between the proximal and distal cortical bone. For compositional analyses of cartilage quality with dGEMRIC, motion correction was performed using STROKETOOL (Digital Image Solutions, Frechen, Germany) for all images to reduce movement artifacts. This tool has been validated for dGEMRIC analyses of the finger joints and corrects for patient motion between the measurements using a dedicated image registration method [30].

T1 maps were analyzed using region of interest (ROI) measurements to evaluate biochemical cartilage quality. T1 values were calculated per pixel. Gradient-echo (GE) images with a flip angle of 5° were applied for anatomical identification of articular cartilage. ROI were drawn into the proximal and distal portion of the articular cartilage

of MPC and PIP joints 2–5 on a single sagittal slice. Readers were allowed to adjust the window settings as required to guarantee optimal visualization of ROI. After ROI placement a second reader confirmed the optimal placement before the ROI were transferred to a simultaneously registered T1 map. DGEMRIC indices were recorded in ms. All images were analyzed by two readers (DBA and CS, radiologists trained in musculoskeletal imaging with three and eight years of experience) who were blinded for patients' data; in case of different findings, the analysts decided by common agreement. For JSW and dGEMRIC measurements, mean values were calculated.

2.4. Statistical Analysis

All statistical analyses were performed using SPSS software (IBM, version 22, Armonk, NY, USA) by DBA. For descriptive analysis, mean, standard deviation, minimum and maximum values were calculated. Datasets were tested for normality by Kolmogorov-Smirnov test with Lilliefors significance correction. Means were compared by student's t-test. *p*-values < 0.05 were considered to be significant.

3. Results

The descriptive analysis (mean, standard deviation and range) of dGEMRIC values at MCP and PIP joints in both study populations is displayed in Table 1. Mean dGEMRIC indices at the MCP joint level D2-5 ranged from 516.2 to 552.1 ms in PsA patients and from 519.3 to 575.8 ms in RA patients. At the PIP joint level D2-5 mean dGEMRIC indices ranged from 338.6 to 450.0 ms in PsA patients and from 399.5 to 439.4 ms in RA patients, respectively. By trend, dGEMRIC indices tended to be higher in PsA patients than in RA patients, yet these differences were not significant (Table 1).

Table 1. Descriptive analysis (mean values, standard deviations (SD) and range (minimum/maximum)) of delayed gadolinium-enhanced magnetic resonance imaging of cartilage (dGEMRIC) indices [ms] of metacarpophalangeal (MCP) and proximal interphalangeal (PIP) joints D2-5 in psoriatic arthritis (PsA) and rheumatoid arthritis (RA) patients.

dGEMRIC [ms]	D2		D3		D4		D5	
	MCP	PIP	MCP	PIP	MCP	PIP	MCP	PIP
PsA								
Mean	523.68	420.81	516.2	338.62	552.07	407.88	537.35	450.01
SD	180.69	113.73	147.05	98.52	123.11	125.44	143.22	118.0
Minimum	272.0	202.9	259.3	190.6	348.3	235.5	327.3	277.2
Maximum	951.4	639.6	717.0	49.4	806.4	678.7	861.9	674.3
RA								
Mean	519.27	399.53	545.12	415.59	576.81	439.39	537.52	435.97
SD	106.11	146.95	117.0	139.65	126.65	106.33	99.82	85.97
Minimum	349.1	225.6	335.5	249.2	298.7	312.6	366.3	307.8
Maximum	679.6	777.9	764.9	671.2	834.1	644.3	739.3	607.8

JSW of MCP and PIP joints of both study populations are presented in Table 2. Only PIP joints 2 and 3 showed significantly wider joint spaces in PsA than in RA patients ($p = 0.005$). All other joints displayed no significant disease-related differences in JSW.

The comparative analysis of dGEMRIC indices of PsA and RA patients is illustrated in Table 3. There was no significant difference between the mean dGEMRIC indices of PsA and RA patients, neither at the MCP nor at the PIP joint level.

Table 2. Descriptive and comparative analysis of joint space width (JSW) (mm) of MCP and PIP 2–5 in RA and PsA patients. *p*-values < 0.05 are considered significant and are given in bold type.

JSW [mm]	D2		D3		D4		D5	
	PsA	RA	PsA	RA	PsA	RA	PsA	RA
MCP								
Mean	1.59	1.65	1.57	1.44	1.34	1.31	1.44	1.35
SD	0.19	0.33	0.26	0.22	0.24	0.24	0.23	0.26
Minimum	1.30	1.13	1.15	1.13	0.92	1.02	1.08	0.98
Maximum	1.96	2.55	2.03	1.86	1.80	1.90	1.80	1.88
<i>p</i> -value	0.536		0.109		0.640		0.271	
PIP								
Mean	1.09	0.88	1.14	0.88	0.95	0.85	0.90	0.82
SD	0.33	0.14	0.30	0.17	0.35	0.16	0.30	0.24
Minimum	0.68	0.56	0.66	0.65	0.54	0.59	0.49	0.54
Maximum	1.72	1.12	1.62	1.19	1.75	1.17	1.59	1.59
<i>p</i> -value	0.005		0.005		0.272		0.364	

Table 3. Mean differences in dGEMRIC indices [ms] at MCP and PIP joints D2–5 comparing PsA and RA patients. Positive differences indicate higher dGEMRIC values in PsA than RA patients for the specific finger joint, and vice versa. CI: confidence interval.

dGEMRIC [ms] PsA vs. RA	D2		D3		D4		D5	
	MCP	PIP	MCP	PIP	MCP	PIP	MCP	PIP
Mean difference	4.41	21.28	−28.92	−76.97	−24.74	−31.51	−0.17	14.03
95% CI lower limit	−98.71	−74.57	−124.16	−168.54	−113.91	−116.74	−86.7	−165.89
95% CI upper limit	107.54	117.14	66.33	14.6	64.43	53.72	86.36	129.04
<i>p</i> -value	0.931	0.653	0.540	0.096	0.576	0.456	0.997	0.798

The comparative analysis of dGEMRIC indices of MCP and PIP joints within each study population is shown in Table 4. In RA patients we found significantly lower dGEMRIC indices at PIP than at MCP joints (D2: $p = 0.009$; D3: $p = 0.008$; D4: $p = 0.002$; D5: $p = 0.002$). This finding was partly reflected in PsA patients, as their PIP joints 3 and 4 showed significantly lower dGEMRIC indices than the corresponding MCP joints (D3: $p = 0.001$; D4: $p = 0.004$). Representative dGEMRIC maps are visualized in Figure 1.

Table 4. dGEMRIC values of PsA and RA patients comparing MCP and PIP joints D2–5. CI: confidence interval. *p*-values < 0.05 were considered to be significant and are given in bold type.

dGEMRIC. MCP vs. PIP	D2		D3		D4		D5	
	PsA	RA	PsA	RA	PsA	RA	PsA	RA
Mean difference	102.87	119.74	177.58	129.53	144.19	137.41	87.34	101.54
95% CI lower limit	−10.05	31.97	82.82	36.88	51.23	55.13	−13.06	38.44
95% CI upper limit	215.79	207.51	272.34	222.18	237.15	219.69	187.74	164.65
<i>p</i> -value	0.073	0.009	0.001	0.008	0.004	0.002	0.086	0.002

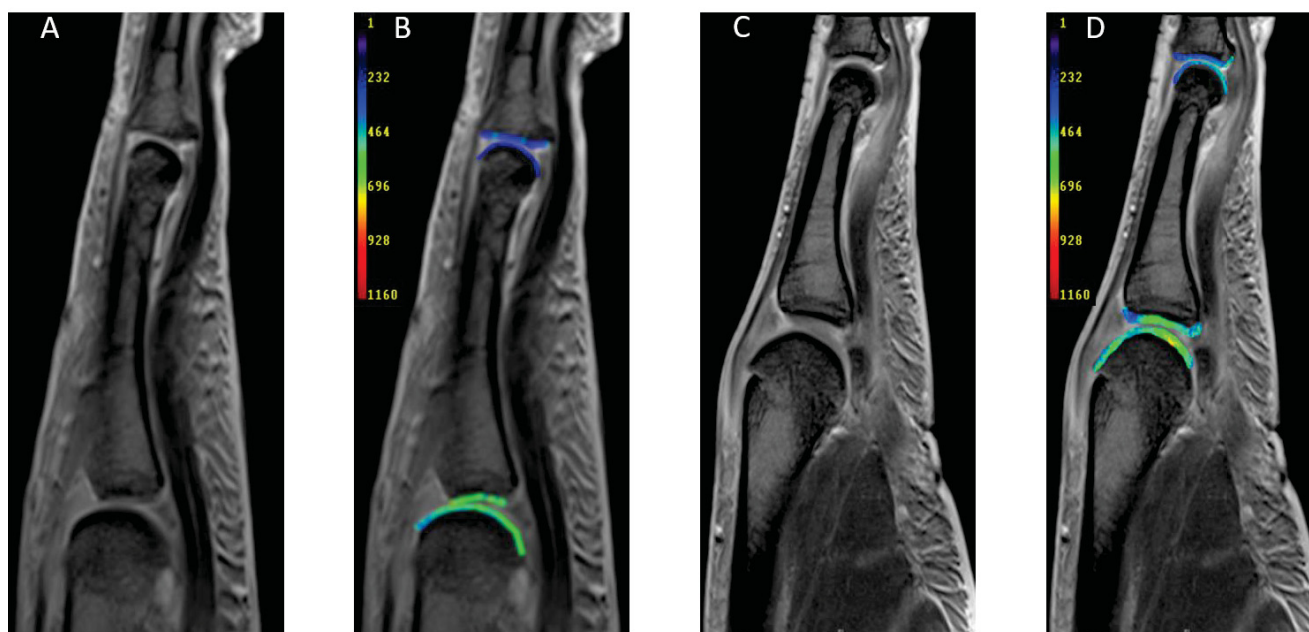


Figure 1. Representative sagittal magnetic resonance (MR) images of MCP and PIP joints of the 2nd digit of patients suffering from PsA (A,B) and RA (C,D). (A,C) give the morphological T1 maps, while (B,D) give the corresponding dGEMRIC maps of the same patients. 62-year-old male with PsA (A,B) and 57-year-old female with RA (C,D).

4. Discussion

The most important finding of this study is that the degree of proteoglycan loss at the MCP and PIP joints (as assessed by dGEMRIC) is not significantly different between PsA and RA patients.

RA and PsA are chronic inflammatory disorders that cause bone and cartilage destruction and eventually lead to joint mutilation and functional disability. Albeit cartilage damage has been investigated both in terms of morphology and composition for RA, it has not yet been the focus of research in PsA. As imaging biomarkers that allow a more clear-cut differentiation of RA, PsA and other inflammatory and non-inflammatory joint diseases such as osteoarthritis are still lacking, we set out to introduce dGEMRIC for the evaluation of proteoglycan loss in PsA patients and to compare the degree of early cartilage loss to RA patients [31,32].

According to our findings the degree of proteoglycan loss at MCP and PIP joints is equally distributed in both, PsA and RA patients. Even though cartilage damage is a known feature in PsA, research is sparse on its role in pathogenesis and it is widely considered a late feature of the disease, especially as compared to RA [33–35]. Cartilage loss in RA, on the other hand, has been the focus of intense research over the last decades and has helped to further delineate the association between cartilage damage and joint inflammation [6]. Even though the question of whether cartilage damage is the reason for, or result of, inflammation remains open, unequivocal evidence suggests that disease activity is closely related to cartilage damage [6]. In the context of our study, a higher degree of early cartilage degradation could have been assumed in RA patients. Similarly, early cartilage loss in PsA could be of significance to the pathogenesis of the disease and provide a potential diagnostic tool beyond the initial diagnosis, i.e., also for disease monitoring, as it is in RA [27]. Therefore, future studies should investigate the association of early cartilage changes detected by MRI and clinical inflammation as well as serum biomarkers in patients with PsA.

Despite roughly similar dGEMRIC indices in RA and PsA patients, we found significantly lower dGEMRIC values, indicating a higher degree of proteoglycan loss in PIP than in MCP joints in both entities. Even though not included in the OMERACT RA MRI

score (RAMRIS), it is long known that RA commonly and severely affects PIP next to MCP and wrist joints [27,36]. PsA, on the other hand, is a more heterogeneous disease that is traditionally divided into five subtypes and can affect various joints, one of them commonly being the PIP joint. This explains why PIP joints are included in the OMCERACT PsAMRIS [28]. It is known that RA and PsA share pathophysiological features and that a distinction between the two can be difficult, especially in cases of symmetrical joint involvement [31]. Our findings of equal dGEMRIC values in both entities with a predominant proteoglycan loss of the PIP joint cartilage confirm the known dilemma of the potentially difficult differentiation between the two disease entities.

Generalizability of the study is hampered by a few limitations. Firstly, we used a small study population. Therefore, further research with a larger sample size is needed. Nonetheless, comparative evaluation was rendered feasible by the application of consistent imaging protocols and strict inclusion criteria for both disease entities. Second, some patients of our study population were older than 60 years of age. Therefore, coexisting osteoarthritis might have been a confounding factor. Third, the mean disease duration of the PsA and RA study population differed by approximately 192 weeks (RA 8, PsA 200 weeks). Applying current definitions, we hence compared “non-early” PsA to “early” RA populations (“early” RA: disease duration <12 months; “early” PsA: disease duration <24 months) [37,38]. Thus, the comparability of both populations is potentially limited in this respect. That is why, future studies using more strictly defined study cohorts (e.g., “early” RA versus “early” PsA) in the assessment of compositional MRI techniques need to corroborate our findings, especially if a distinction between both entities was the aim. In addition, as absolute dGEMRIC indices vary among different studies and protocols, inter-study comparability is limited, and absolute values cannot be readily translated. Fourth, we used Magnevist for our dGEMRIC technique in RA patients since it is the best validated technique for assessment of proteoglycans [39]. However, the European Medical Association (EMA) banned Magnevist due to its potential complications, e.g., cerebral and cerebellar gadolinium depositions [40]. That is why we applied a different, non-linear contrast agent (Dotarem) for the PsA study group, which has been used in prior studies for dGEMRIC [41]. Due to the ban on linear gadolinium-based contrast agents, future studies need to be based on gadolinium-based contrast agents that are potentially less harmful.

5. Conclusions

In conclusion, the molecular cartilage composition at MCP and PIP joints of “non-early” PsA patients is similar to that of a control group of “early” RA patients. Hence, biochemical compositional imaging on the basis of dGEMRIC could be of value for disease monitoring in PsA patients, as it is in RA. This study demonstrates scientific and clinical feasibility of compositional MR imaging in PsA and RA patients, thereby providing a potential framework for more elaborate assessment of patterns and severity of compositional cartilage degradation of the finger joints beyond mere morphology. Prospectively, compositional MR imaging may be applied in the context of diagnostic differentiation and assessment of both disease entities and other inflammatory and non-inflammatory joint disorders, as well as in the monitoring of disease activity under treatment.

Author Contributions: D.B.A.: acquisition, analysis and interpretation of data; drafting the article; final approval of the version to be published; agree to be accountable for all aspects of the work. C.S.: conception and design of the study, analysis of data; revising the article critically for important intellectual content; final approval of the version to be published; agree to be accountable for all aspects of the work. S.V.: analysis and interpretation of data; revising the article critically for important intellectual content; final approval of the version to be published; agree to be accountable for all aspects of the work. J.R.: acquisition and analysis of data; revising the article critically for important intellectual content; final approval of the version to be published; agree to be accountable for all aspects of the work. M.F.: acquisition and analysis of data; revising the article critically for important intellectual content; final approval of the version to be published; agree to be accountable for all aspects of the work. M.S.: conception and design of the study; revising the article critically for

important intellectual content; final approval of the version to be published; agree to be accountable for all aspects of the work. B.O.: conception and design of the study; revising the article critically for important intellectual content; final approval of the version to be published; agree to be accountable for all aspects of the work. S.N.: analysis and interpretation of data; revising the article critically for important intellectual content; final approval of the version to be published; agree to be accountable for all aspects of the work. P.S.: conception and design of the study, analysis and interpretation of data; revising the article critically for important intellectual content; final approval of the version to be published; agree to be accountable for all aspects of the work. All authors have read and agreed to the published version of the manuscript.

Funding: D.B.A. was supported by the local research committee of the medical faculty. P.S. and S.V. received funding from Pfizer Germany with the “Pfizer GIP Inflammation Germany Research Initiative 2014”. P.S. and B.O. received funding from AbbVie Deutschland GmbH & Co. KG for the “Delayed Gadolinium-enhanced MR Imaging of Cartilage—A pilot study to measure the effect of Adalimumab plus MTX versus Placebo plus MTX on cartilage in early RA patients (CAR-ERA) Study”. P.S. received a grant from the German “Bundesministerium für Bildung und Forschung” (BMBF), ArthroMark (01EC1009). S.N. was supported by a grant from the Deutsche Forschungsgemeinschaft (DFG, NE 2136/3-1). Funding institutions had no influence on the design of the study and collection, analysis, and interpretation of data.

Institutional Review Board Statement: Ethics committee of the medical faculty of the Heinrich-Heine-University Dusseldorf, 4962R, MO-LKP-719, approved on 01 April 2015 and 17 September 2015.

Informed Consent Statement: Informed consent was obtained from all subjects involved in the study.

Data Availability Statement: Data can be obtained from the authors upon reasonable request.

Acknowledgments: Erika Rädisch technically performed all MRI scans.

Conflicts of Interest: The authors declare no conflict of interest.

References

- Schett, G.; Coates, L.C.; Ash, Z.R.; Finzel, S.; Conaghan, P.G. Structural damage in rheumatoid arthritis, psoriatic arthritis, and ankylosing spondylitis: Traditional views, novel insights gained from TNF blockade, and concepts for the future. *Arthritis Res. Ther.* **2011**, *13*, S4. [[CrossRef](#)] [[PubMed](#)]
- Ostrowska, M.; Maśliński, W.; Prochorec-Sobieszek, M.; Nieciecki, M.; Sudół-Szopińska, I. Cartilage and bone damage in rheumatoid arthritis. *Reumatologia* **2018**, *56*, 111–120. [[CrossRef](#)] [[PubMed](#)]
- Buchbender, C.; Ostendorf, B.; Mattes-György, K.; Wittsack, H.J.; Quentin, M.; Specker, C.; Schneider, M.; Antoch, G.; Müller, H.W.; Scherer, A. Synovitis and bone inflammation in early rheumatoid arthritis: High-resolution multi-pinhole SPECT versus MRI. *Diagn. Interv. Radiol.* **2013**, *19*, 20–24. [[PubMed](#)]
- Bugatti, S.; Caporali, R.; Manzo, A.; Vitolo, B.; Pitzalis, C.; Montecucco, C. Involvement of subchondral bone marrow in rheumatoid arthritis: Lymphoid neogenesis and in situ relationship to subchondral bone marrow osteoclast recruitment. *Arthritis Rheum.* **2005**, *52*, 3448–3459. [[CrossRef](#)] [[PubMed](#)]
- Jimenez-Boj, E.; Redlich, K.; Türk, B.; Hanslik-Schnabel, B.; Wanivenhaus, A.; Chott, A.; Smolen, J.S.; Schett, G. Interaction between Synovial Inflammatory Tissue and Bone Marrow in Rheumatoid Arthritis. *J. Immunol.* **2005**, *175*, 2579–2588. [[CrossRef](#)]
- Smolen, J.S.; Aletaha, D.; Steiner, G. Does damage cause inflammation? Revisiting the link between joint damage and inflammation. *Ann. Rheum. Dis.* **2009**, *68*, 159–162. [[CrossRef](#)]
- Aletaha, D.; Funovits, J.; Smolen, J.S. Physical disability in rheumatoid arthritis is associated with cartilage damage rather than bone destruction. *Ann. Rheum. Dis.* **2011**, *70*, 733–739. [[CrossRef](#)]
- Hayer, S.; Bauer, G.; Willburger, M.; Sinn, K.; Alasti, F.; Plasenzotti, R.; Shvets, T.; Niederreiter, B.; Aschauer, C.; Steiner, G.; et al. Cartilage damage and bone erosion are more prominent determinants of functional impairment in longstanding experimental arthritis than synovial inflammation. *Dis. Model. Mech.* **2016**, *9*, 1329–1338. [[CrossRef](#)]
- Bhattaram, P.; Chandrasekharan, U.M. The joint synovium: A critical determinant of articular cartilage fate in inflammatory joint diseases. *Semin. Cell Dev. Biol.* **2017**, *62*, 86–93. [[CrossRef](#)]
- Bartosinska, J.; Michalak-Stoma, A.; Juszkiewicz-Borowiec, M.; Kowal, M.; Chodorowska, G. The Assessment of Selected Bone and Cartilage Biomarkers in Psoriatic Patients from Poland. *Mediat. Inflamm.* **2015**, *2015*, 1–8. [[CrossRef](#)]
- Chandran, V.; Abji, F.; Perruccio, A.V.; Gandhi, R.; Li, S.; Cook, R.J.; Gladman, D.D. Serum-based soluble markers differentiate psoriatic arthritis from osteoarthritis. *Ann. Rheum. Dis.* **2019**, *78*, 796–801. [[CrossRef](#)] [[PubMed](#)]

12. Farouk, H.M.; Mostafa, A.A.A.; Youssef, S.S.; Elbeblawy, M.M.S.; Assaf, N.Y.; Elokda, E.S.E. Value of Enthesal Ultrasonography and Serum Cartilage Oligomeric Matrix Protein in the Preclinical Diagnosis of Psoriatic Arthritis. *Clin. Med. Insights: Arthritis Musculoskelet. Disord.* **2010**, *3*, 7–14. [[CrossRef](#)] [[PubMed](#)]
13. Mortezaei, M.; Thiele, R.; Ritchlin, C. The joint in psoriatic arthritis. *Clin. Exp. Rheumatol.* **2015**, *2015*, 20–25.
14. McGonagle, D.; Tan, A.L.; Møller Døhn, U.; Ostergaard, M.; Benjamin, M. Microanatomic studies to define predictive factors for the topography of peri-articular erosion formation in inflammatory arthritis. *Arthritis Rheum.* **2009**, *60*, 1042–1051. [[CrossRef](#)] [[PubMed](#)]
15. McGonagle, D.; Tan, A. The enthesis in psoriatic arthritis. *Clin. Exp. Rheumatol.* **2015**, *33*, 36–39.
16. McGonagle, D.; Lories, R.J.U.; Tan, A.L.; Benjamin, M. The concept of a “synovio-entheseal complex” and its implications for understanding joint inflammation and damage in psoriatic arthritis and beyond. *Arthritis Rheum.* **2007**, *56*, 2482–2491. [[CrossRef](#)]
17. Coates, L.C. Treating to target in psoriatic arthritis. *Curr. Opin. Rheumatol.* **2015**, *27*, 107–110. [[CrossRef](#)]
18. Van Vollenhoven, R. Treat-to-target in rheumatoid arthritis—are we there yet? *Nat. Rev. Rheumatol.* **2019**, *15*, 180–186. [[CrossRef](#)]
19. Van den Bosch, F.; Coates, L. Clinical management of psoriatic arthritis. *Lancet* **2018**, *391*, 2285–2294. [[CrossRef](#)]
20. Møller-Bisgaard, S.; Hørslev-Petersen, K.; Ejbjerg, B.; Hetland, M.L.; Ørnberg, L.M.; Glinatsi, D.; Møller, J.; Boesen, M.; Christensen, R.; Stengaard-Pedersen, K. Effect of Magnetic Resonance Imaging vs Conventional Treat-to-Target Strategies on Disease Activity Remission and Radiographic Progression in Rheumatoid Arthritis: The IMAGINE-RA Randomized Clinical Trial. *JAMA* **2019**, *321*, 461–472. [[CrossRef](#)]
21. Miese, F.R.; Ostendorf, B.; Wittsack, H.-J.; Reichelt, D.C.; Mamisch, T.C.; Zilkens, C.; Lanzman, R.S.; Schneider, M.; Scherer, A. Metacarpophalangeal Joints in Rheumatoid Arthritis: Delayed Gadolinium-enhanced MR Imaging of Cartilage—A Feasibility Study. *Radiology* **2010**, *257*, 441–447. [[CrossRef](#)] [[PubMed](#)]
22. Miese, F.; Buchbender, C.; Scherer, A.; Wittsack, H.-J.; Specker, C.; Schneider, M.; Antoch, G.; Ostendorf, B. Molecular imaging of cartilage damage of finger joints in early rheumatoid arthritis with delayed gadolinium-enhanced magnetic resonance imaging. *Arthritis Rheum.* **2012**, *64*, 394–399. [[CrossRef](#)] [[PubMed](#)]
23. Van Tiel, J.; Kotek, G.; Reijman, M.; Bos, P.K.; Bron, E.E.; Klein, S.; Nasserinejad, K.; van Osch, G.J.; Verhaar, J.A.; Krestin, G.P.; et al. Is T1ρ Mapping an Alternative to Delayed Gadolinium-enhanced MR Imaging of Cartilage in the Assessment of Sulphated Glycosaminoglycan Content in Human Osteoarthritic Knees? An in Vivo Validation Study. *Radiology* **2016**, *279*, 523–531. [[CrossRef](#)] [[PubMed](#)]
24. Schleich, C.; Schleich, C.; Sewerin, P.; Ostendorf, B.; Buchbender, C.; Schneider, M.; Antoch, G.; Miese, F. Intra-individual assessment of inflammatory severity and cartilage composition of finger joints in rheumatoid arthritis. *Skelet. Radiol.* **2014**, *44*, 513–518. [[CrossRef](#)] [[PubMed](#)]
25. Sewerin, P.; Müller-Lutz, A.; Abrar, D.B.; Odendahl, S.; Eichner, M.; Schneider, M.; Ostendorf, B.; Schleich, C. Prevention of the progressive biochemical cartilage destruction under methotrexate therapy in early rheumatoid arthritis. *Clin. Exp. Rheumatol.* **2018**, *37*, 179–185.
26. Abrar, D.B.; Schleich, C.; Nebelung, S.; Frenken, M.; Radke, K.L.; Vordenbäumen, S.; Brinks, R.; Schneider, M.; Ostendorf, B.; McGonagle, D.; et al. High-resolution MRI of flexor tendon pulleys using a 16-channel hand coil: Disease detection and differentiation of psoriatic and rheumatoid arthritis. *Arthritis Res.* **2020**, *22*, 1–10. [[CrossRef](#)] [[PubMed](#)]
27. Østergaard, M.; Peterfy, C.G.; Bird, P.; Gandjbakhch, F.; Glinatsi, D.; Eshed, I.; Haavardsholm, E.A.; Lillegraven, S.; Bøyesen, P.; Ejbjerg, B.; et al. The OMERACT Rheumatoid Arthritis Magnetic Resonance Imaging (MRI) Scoring System: Updated Recommendations by the OMERACT MRI in Arthritis Working Group. *J. Rheumatol.* **2017**, *44*, 1706–1712. [[CrossRef](#)]
28. Østergaard, M.; McQueen, F.; Wiell, C.; Bird, P.; Bøyesen, P.; Ejbjerg, B.; Peterfy, C.; Gandjbakhch, F.; Duer-Jensen, A.; Coates, L.; et al. The OMERACT Psoriatic Arthritis Magnetic Resonance Imaging Scoring System (PsAMRIS): Definitions of Key Pathologies, Suggested MRI Sequences, and Preliminary Scoring System for PsA Hands. *J. Rheumatol.* **2009**, *36*, 1816–1824. [[CrossRef](#)]
29. Herz, B.; Albrecht, A.; Englbrecht, M.; Welsch, G.H.; Uder, M.; Renner, N.; Schlechtweg, P.M.; Paul, D.; Lauer, L.; Engelke, K.; et al. Osteitis and synovitis, but not bone erosion, is associated with proteoglycan loss and microstructure damage in the cartilage of patients with rheumatoid arthritis. *Ann. Rheum. Dis.* **2013**, *73*, 1101–1106. [[CrossRef](#)]
30. Miese, F.; Kröpil, P.; Ostendorf, B.; Scherer, A.; Buchbender, C.; Quentin, M.; Lanzman, R.S.; Blondin, D.; Schneider, M.; Bittersohl, B.; et al. Motion correction improves image quality of dGEMRIC in finger joints. *Eur. J. Radiol.* **2011**, *80*, e427–e431. [[CrossRef](#)]
31. Merola, J.; Espinoza, L.R.; Fleischmann, R. Distinguishing rheumatoid arthritis from psoriatic arthritis. *RMD Open* **2018**, *4*, e000656. [[CrossRef](#)] [[PubMed](#)]
32. Braum, L.S.; McGonagle, D.; Bruns, A.; Philipp, S.; Hermann, S.; Aupperle, K.; Tan, A.L.; Diekhoff, T.; Hamm, B.; Hermann, K.-G. Characterisation of hand small joints arthropathy using high-resolution MRI—Limited discrimination between osteoarthritis and psoriatic arthritis. *Eur. Radiol.* **2013**, *23*, 1686–1693. [[CrossRef](#)] [[PubMed](#)]
33. Yue, J.; Wu, D.; Tam, L.-S. The role of imaging in early diagnosis and prevention of joint damage in inflammatory arthritis. *Expert Rev. Clin. Immunol.* **2018**, *14*, 499–511. [[CrossRef](#)] [[PubMed](#)]
34. McGonagle, D.; Hermann, K.-G.A.; Tan, A.L. Differentiation between osteoarthritis and psoriatic arthritis: Implications for pathogenesis and treatment in the biologic therapy era. *Rheumatology* **2015**, *54*, 29–38. [[CrossRef](#)] [[PubMed](#)]
35. Sankowski, A.J.; Lebkowska, U.M.; Cwikła, J.; Walecka, I.; Walecki, J. Psoriatic arthritis. *Pol. J. Radiol.* **2013**, *78*, 7–17.
36. Harrison, S.H. The proximal interphalangeal joint in rheumatoid arthritis. *Hand* **1971**, *3*, 125–130. [[CrossRef](#)]
37. Heidari, B. Rheumatoid Arthritis: Early diagnosis and treatment outcomes. *Casp. J. Intern. Med.* **2011**, *2*, 161–170.

38. Gladman, D.D. Early Psoriatic Arthritis. *Rheum. Dis. Clin. North. Am.* **2012**, *38*, 373–386. [[CrossRef](#)]
39. Sewerin, P.; Ostendorf, B.; Schleich, C. MRT-Diagnostik bei entzündlichen Gelenk- und Wirbelsäulenerkrankungen: Protokolle und Spezialsequenzen: Wann und wozu? *Z. Rheumatol.* **2018**, *77*, 538–548. [[CrossRef](#)]
40. Kanda, T.; Nakai, Y.; Hagiwara, A.; Oba, H.; Toyoda, K.; Furui, S. Distribution and chemical forms of gadolinium in the brain: A review. *Br. J. Radiol.* **2017**, *90*. [[CrossRef](#)]
41. Zilkens, C.; Miese, F.; Kim, Y.-J.; Jäger, M.; Mamisch, T.C.; Hosalkar, H.; Antoch, G.; Krauspe, R.; Bittersohl, B. Direct comparison of intra-articular versus intravenous delayed gadolinium-enhanced MRI of hip joint cartilage. *J. Magn. Reson. Imaging* **2014**, *39*, 94–102. [[CrossRef](#)] [[PubMed](#)]

Article

Non-Specific Low Back Pain and Lumbar Radiculopathy: Comparison of Morphologic and Compositional MRI as Assessed by gagCEST Imaging at 3T

Miriam Frenken ^{1,†}, Sven Nebelung ^{1,†}, Christoph Schleich ¹, Anja Müller-Lutz ¹, Karl Ludger Radke ¹, Benedikt Kamp ¹, Matthias Boschheidgen ¹, Lena Wollschläger ², Bernd Bittersohl ², Gerald Antoch ¹, Markus R. Konieczny ² and Daniel B. Abrar ^{1,*}

¹ Department of Diagnostic and Interventional Radiology, Medical Faculty, University Dusseldorf, D-40225 Dusseldorf, Germany; Miriam.Frenken@med.uni-duesseldorf.de (M.F.); sven.nebelung@med.uni-duesseldorf.de (S.N.); Christoph.Schleich@med.uni-duesseldorf.de (C.S.); Anja.Lutz@med.uni-duesseldorf.de (A.M.-L.); Ludger.Radke@med.uni-duesseldorf.de (K.L.R.); Benedikt.Kamp@med.uni-duesseldorf.de (B.K.); Matthias.Boschheidgen@med.uni-duesseldorf.de (M.B.); Antoch@med.uni-duesseldorf.de (G.A.)

² Department of Orthopedic and Trauma Surgery, University Hospital of Duesseldorf, D-40225 Dusseldorf, Germany; Lena.wollschlaeger@med.uni-duesseldorf.de (L.W.); Bernd.Bittersohl@med.uni-duesseldorf.de (B.B.); Markus.Konieczny@med.uni-duesseldorf.de (M.R.K.)

* Correspondence: danielbenjamin.abrar@med.uni-duesseldorf.de

† Authors contributed equally.

Citation: Frenken, M.; Nebelung, S.; Schleich, C.; Müller-Lutz, A.; Radke, K.L.; Kamp, B.; Boschheidgen, M.; Wollschl, L.; Bittersohl, B.; Antoch, G.; et al. Non-specific Low Back Pain and Lumbar Radiculopathy: Comparison of Morphologic and Compositional MRI as Assessed by gagCEST Imaging at 3T. *Diagnostics* **2021**, *11*, 402. <https://doi.org/10.3390/diagnostics11030402>

Academic Editor: Rute Santos

Received: 8 January 2021

Accepted: 23 February 2021

Published: 26 February 2021

Publisher's Note: MDPI stays neutral with regard to jurisdictional claims in published maps and institutional affiliations.



Copyright: © 2021 by the authors. Licensee MDPI, Basel, Switzerland. This article is an open access article distributed under the terms and conditions of the Creative Commons Attribution (CC BY) license (<http://creativecommons.org/licenses/by/4.0/>).

Abstract: Using glycosaminoglycan Chemical Exchange Saturation Transfer (gagCEST) magnetic resonance imaging (MRI), this study comparatively evaluated the GAG contents of lumbar intervertebral disks (IVDs) of patients with non-specific low back pain (nsLBP), radiculopathy, and asymptomatic volunteers to elucidate the association of clinical manifestation and compositional correlate. A total of 18 patients (mean age 57.5 ± 22.5 years) with radiculopathy, 16 age-matched patients with chronic nsLBP and 20 age-matched volunteers underwent standard morphologic and compositional gagCEST MRI on a 3T scanner. In all cohorts, GAG contents of lumbar IVDs were determined using gagCEST MRI. An assessment of morphologic IVD degeneration based on the Pfirrmann classification and T2-weighted sequences served as a reference. A linear mixed model adjusted for multiple confounders was used for statistical evaluation. IVDs of patients with nsLBP showed lower gagCEST values than those of volunteers (nsLBP: 1.3% [99% confidence intervals (CI): 1.0; 1.6] vs. volunteers: 1.9% [99% CI: 1.6; 2.2]). Yet, IVDs of patients with radiculopathy (1.8% [99% CI: 1.4; 2.1]) were not different from patients with nsLBP or volunteers. In patients with radiculopathy, IVDs directly adjacent to IVD extrusions demonstrated lower gagCEST values than distant IVDs (adjacent: 0.9% [99% CI: 0.3; 1.5], distant: 2.1% [99% CI: 1.7; 2.5]). Advanced GAG depletion in nsLBP and directly adjacent to IVD extrusions in radiculopathy indicates close interrelatedness of clinical pathology and compositional degeneration.

Keywords: gagCEST; spine; compositional MRI; disk degeneration; low back pain; radiculopathy; disk extrusion; IVD

1. Introduction

Low back pain (LBP) is a major global health burden that is associated with limited physical activity, increased disability, and absence from work [1]. Therefore, LBP is characterized by an enormous individual and socioeconomic disease burden. The majority of LBP is non-specific (nsLBP), i.e., without an unequivocal structural cause such as vertebral fractures [2,3]. One potential contributor to nsLBP is lumbar degenerative disk disease (LDDD), which is an accelerated type of age-related intervertebral disk (IVD)

degeneration [4,5]. A very common structural disorder leading to LBP is lumbar IVD extrusion with radiculopathy [6–8]. To this date, the importance of magnetic resonance imaging (MRI) at LBP is still controversial, especially in the acute and subacute setting, and therefore, it is not recommended for primary diagnostics by current guidelines [9,10]. However, it is the most widely used imaging technique for the direct assessment of the characteristic morphologic changes in LDDD [11,12], such as IVD dehydration and loss of IVD height. In the clinical routine, these changes are commonly visualized by T2-weighted (T2w) images and allow for the differentiation of degenerated and non-degenerated IVDs according to validated grading systems such as the Pfirrmann classification [13,14]. However, these standard clinical MRI techniques allow assessment of mere morphology and cannot depict early, potentially reversible changes of IVD composition such as glycosaminoglycan (GAG) depletion that precede structural changes. Consequently, compositional MRI techniques such as GAG Chemical Exchange Saturation Transfer (gagCEST) imaging that evaluate tissue properties beyond morphology are of ever-increasing clinical and scientific interest [15–19]. As a non-invasive imaging technique, gagCEST measures the chemical exchange of hydroxy protons between GAG and bulk water molecules [20–22]. To induce the CEST effect in the tissue, a frequency-specific radiofrequency (RF) pulse is used to saturate a pool of solute protons at different frequency offsets around the water resonance. These saturated protons are subsequently transferred to the bulk water pool by chemical exchange, consequently reducing its signal. The signal decrease is then used to assess the CEST effect at a GAG-specific frequency range of 0.9–1.9 ppm [22,23]. The resulting magnetization transfer ratio asymmetry (MTR_{asym}), i.e., the gagCEST effect size, correlates with the underlying GAG concentration of the given IVD [23,24]. In previous studies, our group has provided preliminary evidence that gagCEST imaging of the lumbar spine may help to differentiate degenerative and non-degenerative IVDs based on their respective GAG contents [24–26]. Yet, the association of compositional changes, i.e., GAG depletion, and common clinical manifestations of disorders of the lumbar spine remains to be elucidated.

Against this background, the aim of this study was to systematically assess the GAG contents of lumbar IVDs in common disorders of the lumbar spine, i.e., nsLBP and radiculopathy, and to compare them to asymptomatic volunteers, both overall and on a segmental level and to elucidate a potential influence of IVD extrusions on the GAG contents of adjacent IVDs. We hypothesized that (a) the GAG contents in patients with nsLBP and radiculopathy are significantly lower than in asymptomatic volunteers and that (b) the GAG contents of lumbar IVDs adjacent to extruded IVDs is significantly lower than of non-adjacent IVDs.

2. Materials and Methods

2.1. Study Population

A total of 18 patients (mean age: 57.5 ± 22.5 years, range: 14–96 years; 10 female, 8 male) with subacute (4–12 weeks duration) [25] radiculopathy and IVD extrusion and 16 age-matched patients with chronic nsLBP (mean age: 59.0 ± 17.5 years, range: 22.5–83.5 years; 10 female, 6 male) were prospectively recruited at the outpatient clinic of the Department of Orthopedic and Trauma Surgery of the University Hospital Duesseldorf. In patients with radiculopathy, IVD extrusion had been diagnosed earlier during previous MRI scanning sessions and was based on the recommendations of the combined task forces of the North American Spine Society, American Society of Spine Radiology, and American Society of Neuroradiology [26]. Accordingly, extrusion was defined as being present when any distance between the edges of the disc material beyond the disc space was greater than the distance between the edges of the base. Additionally, 20 age-matched asymptomatic volunteers (mean age: 54.5 ± 11.5 years, range: 39.5–76.5 years; 11 female, 9 male) were included as a control group. Chronic LBP was defined as persistent LBP symptoms beyond three months [27]. Exclusion criteria for all participants were prior

spine surgery, chronic inflammatory diseases affecting the musculoskeletal system, congenital spine deformities, and a body mass index <18.5 or >30 kg/m². For the control group, the exclusion criteria were expanded to acquired spinal deformities, radiculopathy, and chronic LBP. For the LBP group, the exclusion criteria were expanded to presence of radiculopathy. All patients were treated conservatively. Written and informed consent was obtained from all participants or their legal guardians prior to the initiation of the study. The study was approved by the local ethical committee (Ethical Committee, Medical Faculty, University of Düsseldorf, Germany, study number 5087R, 29 June 2015). Demographic and clinical characteristics of the study population and the three study cohorts are presented in Table 1.

Table 1. Demographic and clinical information of the study population.

	Patients with Non-Specific Low Back Pain	Patients with Radiculopathy	Volunteers
Cohort size (<i>n</i>)	16	18	20
Age (years)	59 ± 17.5	57.5 ± 22.5	54.5 ± 11.5
Gender female/male	10/6	10/8	11/9
IVD extrusion (*)	0	18 (one in each patient)	0
IVD protrusion	19	9	8
LBP (<i>n</i>)	16	18	0
Radicular pain (<i>n</i>)	0	18	0
Sensory deficit (<i>n</i>)	0	14	0
Muscle weakness (<i>n</i>)	0	0	0

Age data are presented as means ± standard deviations. For each study cohort, age, sex, the presence and distribution of IVD extrusions as well as the clinical presentation are given. Abbreviations: IVD – intervertebral disc. Detailed distribution of IVD extrusions: L1/2 (*n* = 0), L2/3 (*n* = 0), L3/4 (*n* = 0), L4/5 (*n* = 9), L5/S1 (*n* = 9). (*) IVD extrusion was defined as present when the base of the protruded disk material was narrower than its dome. IVD protrusion was defined as present when the base of the protruded disk was broader than its dome. LBP: low back pain.

2.2. Clinical Assessment

Patients were clinically assessed at the outpatient clinic of the Department of Orthopedic and Trauma Surgery by a board-certified orthopedic surgeon (MRK, 10 years of experience as a spine surgeon). Patients and volunteers underwent a focused neurologic exam of the motor and sensory systems as well as the reflex status. More specifically, back and leg pain with a particular focus on radicular pain, distal sensation and muscle strength were evaluated. Wherever radicular pain, i.e., pain in a nerve-root distribution, sensory loss or muscle weakness were present, the level of nerve affection was clinically localized using the corresponding dermatoma or myotoma.

2.3. Imaging

MRI studies of the lumbar spines of all participants were performed on a clinical 3 Tesla (T) MRI scanner (Magnetom Prisma, Siemens Healthineers, Erlangen, Germany) with a 32-channel body and a 24-channel spine matrix coil (Siemens Healthineers, Erlangen, Germany) in the supine position.

In line with earlier studies, the MRI exams comprised both morphologic and compositional sequences. The morphologic sequences included T1-weighted (T1w), T2-weighted (T2w), and short-tau-inversion-recovery (STIR) sequences in the sagittal orientation and a T2w sequence in the transversal orientation. Compositional imaging included CEST and Water Saturation Shift Referencing (WASSR) sequences to

compensate for magnetic field inhomogeneities in the sagittal orientation. Detailed sequence parameters are presented in Table 2.

Table 2. Detailed Magnetic Resonance Imaging (MRI) Sequence Parameters.

	Sequence					
	STIR	T2w TSE	T1w TSE	T2w TSE	CEST	WASSR
Imaging Plane	Sagittal	Sagittal	Sagittal	Transversal	Midsagittal	Midsagittal
TE (ms)	57	95	9.5	106	5.1	5.1
TR (ms)	3800	3500	650	5200	10	10
Flip Angle (°)	150	160	150	160	10	10
Slice Thickness (mm)	4	4	4	4	5	5
FoV (mm × mm)	300 × 300	300 × 300	300 × 300	190 × 190	300 × 300	300 × 300
Pixel Size (mm × mm)	0.8 × 0.8	0.7 × 0.7	0.7 × 0.7	0.6 × 0.6	1.6 × 1.6	1.6 × 1.6
Number of Slices	15	15	15	38	1	1

Imaging plane, echo time (TE), repetition time (TR), flip angle, slice thickness, field of view (FoV), pixel size, and number of slices are given for all sequences (Short Tau Inversion Recovery (STIR), T2-weighted turbo spin echo (T2w TSE), T1w TSE, chemical exchange saturation transfer (CEST) and water saturation shift referencing (WASSR) sequences).

2.4. Image Analysis

The raters were blinded to the participants' diagnoses and demographics. The lumbar IVDs (segments L1/L2–L5/S1) of all participants were graded individually and independently on sagittal T2w images according to the Pfirrmann classification by two radiologists with long-standing experience in musculoskeletal imaging (DBA and CS with four and ten years of experience in musculoskeletal imaging) [11]. In case of diverging findings, consensus was reached with assistance of a third clinical radiologist (SN, eight years of experience in musculoskeletal imaging). The Pfirrmann classification allows distinction of non-degenerative (grades 1 and 2) and degenerative IVDs (grades 3–5) on the basis of signal intensity, structure, and height as well as the distinction of the nucleus pulposus (NP) and annulus fibrosus (AF).

In addition, all images and all lumbar segments were analyzed by the same raters for the presence of IVD extrusions according to the recommendations of the Combined Task Forces of the North American Spine Society, American Society of Spine Radiology, and American Society of Neuroradiology [26]. Consequently, extrusion was defined as being present when any distance between the edges of the disc material beyond the disc space was greater than the distance between the edges of the base. As published in previous studies [16,28], we first used WASSR images to correct B_0 field inhomogeneities by the maximum-symmetry algorithm with calculation of a pixel-wise frequency offset curve. Second, the corrected CEST curves divided by the signal without pre-saturation (S_0) were defined as the so-called z-spectra ($Z(\omega)$). The maximum frequency offset of each z-spectrum was $\Delta\omega = 3$ ppm. MTR_{asym} (defined as $MTR_{\text{asym}}(\Delta\omega) = Z(-\Delta\omega) - Z(\Delta\omega)$) was used for the assessment of the gagCEST effect [16]. We calculated MTR_{asym} maps by using the average value of MTR_{asym} in the GAG-specific frequency range of $\Delta\omega = 0.9$ – 1.9 ppm. MTR_{asym} values, i.e., the gagCEST effect sizes, are given in [%] [29]. As previously published by our group, regions of interest (ROIs) were defined in the midsagittal plane by a customized in-house script implemented in Matlab (MATLAB, R2018a, The MathWorks, Inc., MA, USA) that automatically identifies lumbar segments and analyzes the gagCEST effect [30].

The disk segmentation approach was based on Bayes classification to divide bone and ligaments from disk cartilage [31]. All ROIs were visually confirmed for correct positioning by a board-certified radiologist (CS). No ROIs had to be manually corrected. In the following, MTR_{asym} values are referred to as gagCEST values for better readability. As shown in previous studies, gagCEST values correlate with the IVD's GAG content [16,28]. Therefore, lower gagCEST values reflect lower GAG contents.

2.5. Statistical Analysis

SPSS software (v27, SPSS Inc., Chicago, IL, USA) was used for all statistical analyses performed by KLR and DBA. Descriptive statistics of gagCEST values were calculated for volunteers and patients. Based on a linear mixed model (LMM), the three study cohorts, i.e., asymptomatic volunteers, patients with nsLBP and patients with radiculopathy, IVD regions, i.e., NP and AF, and IVD segments, i.e., L1/2 to L5/S1 were comparatively evaluated as multivariable statistics. The model included a subject-specific random intercept, the factors healthy volunteer/patient, age, gender, Pfirrmann grading, and the interaction of these factors and was fitted using a restricted maximum likelihood approach [32]. Based on another LMM, IVDs adjacent to IVD extrusions, i.e., directly above or below, and non-adjacent IVDs were comparatively evaluated. The model included the factors adjacent/non-adjacent IVD, age, gender, Pfirrmann grading and the interaction of these factors. Based on these final models, the mean differences of gagCEST values were calculated. Not assuming normal distributions, mean Pfirrmann grades were compared between the three study cohorts using the Kruskal–Wallis test followed by Dunn’s post-hoc test wherever appropriate. The presentation of *p*-values for the illustration of statistical significance was deliberately avoided [33].

3. Results

3.1. Morphologic Analysis

Detailed findings of IVD extrusion and IVD degradation are given in Tables 1 and 3, respectively. Only patients with radiculopathy were found to demonstrate IVD extrusions at the IVD segments L4/5 and L5/S1, while patients with nsLBP or asymptomatic volunteers showed none (Table 1).

The grading of IVDs according to the Pfirrmann classification was as follows: entire study population: grade 1: (*n* = 0), grade 2: (*n* = 192), grade 3: (*n* = 79), grade 4: (*n* = 29), and grade 5: (*n* = 2); patients with radiculopathy: grade 1: (*n* = 0), grade 2: (*n* = 48), grade 3: (*n* = 31), grade 4: (*n* = 11), and grade 5: (*n* = 0); patients with nsLBP: grade 1: (*n* = 0), grade 2: (*n* = 37), grade 3: (*n* = 30), grade 4: (*n* = 11), and grade 5: (*n* = 2); asymptomatic volunteers: grade 1: (*n* = 0), grade 2: (*n* = 70), grade 3: (*n* = 19), grade 4: (*n* = 7), and grade 5: (*n* = 0). At each individual lumbar segment, we did not find distinct differences for the Pfirrmann grades between the three study cohorts. However, when considering all lumbar segments, patients with nsLBP had lower overall Pfirrmann grades than asymptomatic volunteers (nsLBP: 2.7 [99% CI: 2.6; 2.9] vs. volunteers: 2.4 [99% CI: 2.2; 2.5]). No distinct differences in Pfirrmann grades were found between patients with nsLBP and patients with radiculopathy and between patients with radiculopathy and asymptomatic volunteers (Table 3).

Table 3. Mean imaging measures as a function of the study cohort, i.e., patients with radiculopathy, non-specific low back pain (nsLBP) and asymptomatic volunteers, and intervertebral disc (IVD) segment level, i.e., L1/2–L5/S1. Data are given as means [99% confidence intervals]. Glycosaminoglycan chemical exchange saturation transfer (gagCEST) values were compared using a linear mixed model comprising a subject-specific random intercept, while the Pfirrmann grades were compared using the Kruskal–Wallis test followed by Dunn’s post-hoc test wherever appropriate.

		Segment					Overall
		L1/2	L2/3	L3/4	L4/5	L5/S1	
gagCEST values (%)	Radiculopathy	2.5 [1.4; 3.5]	2.1 [1.3; 2.8]	1.7 [1.0; 2.3]	1.2 [0.6; 1.9]	1.5 [0.5; 2.6]	1.8 [1.4; 2.1]
	nsLBP	1.3 [0.5; 2.1]	1.1 [0.5; 1.7]	1.2 [0.6; 1.8]	1.1 [0.5; 1.7]	2.3 [1.3; 3.3]	1.3 [1.0; 1.6]
	Volunteers	2.5 [1.7; 3.2]	2.0 [1.3; 2.5]	1.5 [1.0; 2.0]	1.7 [1.2; 2.2]	2.1 [1.2; 3.0]	1.9 [1.6; 2.2]
Pfirrmann grade (1–5)	Radiculopathy	2.3 [2.0; 2.7]	2.4 [2.0; 2.6]	2.6 [2.2; 2.9]	2.8 [2.5; 3.1]	2.9 [2.6; 3.2]	2.6 [2.4; 2.7]
	nsLBP	2.5 [2.1; 2.9]	2.7 [2.0; 2.7]	2.6 [2.2; 3.0]	2.8 [2.3; 3.2]	3.1 [2.6; 3.6]	2.7 [2.6; 2.9]
	Volunteers	2.2 [1.9; 2.5]	2.3 [2.0; 2.6]	2.4 [2.0; 2.7]	2.4 [2.2; 2.6]	2.5 [2.2; 2.8]	2.4 [2.2; 2.5]

3.2. Multivariable Comparative Analyses of gagCEST Values

In all IVDs, irrespective of the study cohort, the NPs showed higher gagCEST values than the AFs (AF: 1.2% [99% CI: 1.0; 1.4] vs. NP: 2.1% [99% CI 1.8; 2.4], $p < 0.001$). GagCEST values were affected by morphologic IVD degeneration as assessed by the Pfirrmann grade. Overall, IVDs with Pfirrmann grades ≤ 2 , i.e., non-degenerated IVDs, had higher gagCEST values (2.0% [99% CI: 1.7; 2.2]) than IVDs with Pfirrmann grades ≥ 3 , i.e., degenerated IVDs (1.3% [99% CI: 1.0; 1.6]) ($p < 0.001$). No distinct differences were found between gagCEST values of all IVDs of the different lumbar segments: L1/2: 1.9% [99% CI: 1.5; 2.3]; L2/3: 1.6% [99% CI: 1.2; 1.9]; L3/4: 1.5% [99% CI: 1.1; 1.8], L4/5: 1.4% [99% CI: 1.1; 1.7], L5/S1: 1.9% [99% CI: 1.4; 2.5].

Comparative analyses of gagCEST values of lumbar IVDs in the three study cohorts are presented in Table 3 and Figure 1.

Overall, the lumbar IVDs of patients with nsLBP showed lower gagCEST values (1.3% [99% CI: 1.0; 1.6]) than those of asymptomatic volunteers (1.9% [99% CI: 1.6; 2.2]) and lower values than those of patients with radiculopathy (1.8% [99% CI: 1.4; 2.1]). No distinct differences in gagCEST values were found between patients with radiculopathy and asymptomatic volunteers or between female (1.7% [99% CI: 1.5; 2.0]) and male individuals (1.6% [99% CI: 1.3; 1.8]) in the entire study population.

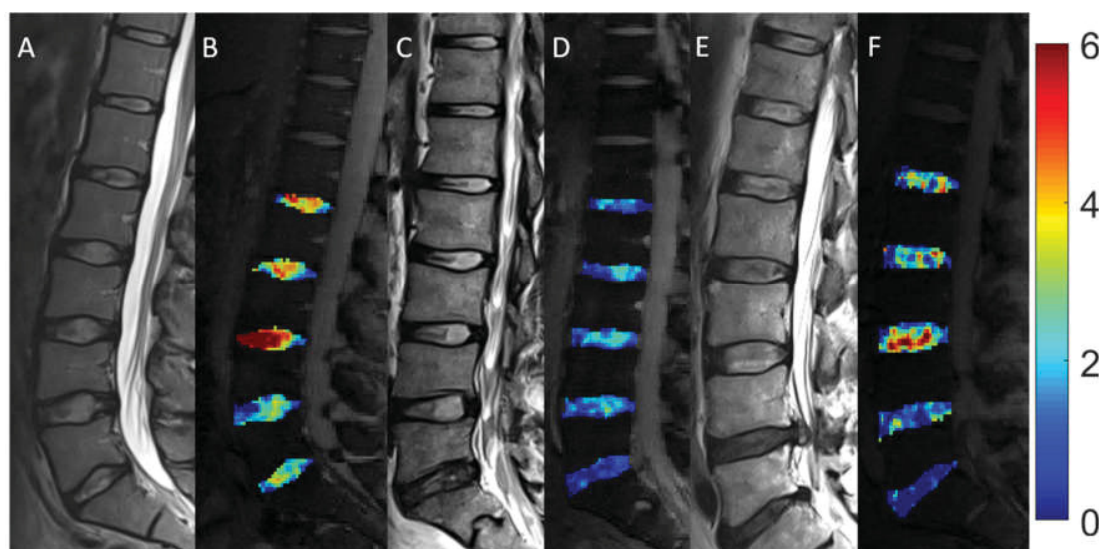


Figure 1. Morphologic and compositional imaging findings of lumbar intervertebral discs of an asymptomatic volunteer (A,B), a patient with nonspecific low back pain (C,D), and a patient with radiculopathy (E,F). A, C and E: Sagittal T2-weighted (T2w) images show the absence of morphologic signs of relevant IVD degeneration (A), substantial dehydration at the L4/L5 segment (C) and the L5/S1 segment (C,E) accompanied by extrusion at the L4/L5 segment (E). B, D and F: Sagittal glycosaminoglycan Chemical Exchange Saturation Transfer (gagCEST) images with overlaid color-coded maps to visualize the GAG contents of the IVD segments. Low GAG content is depicted in blue, and high GAG content is depicted in red. The unit of scale on the right is gagCEST effect in %. The lowest values are found in the patient with nsLBP, while the highest values are seen in the asymptomatic volunteer.

Comparative analyses of gagCEST values of IVDs adjacent and non-adjacent to IVD extrusions in patients with radiculopathy are displayed in Table 4.

IVDs adjacent to an IVD extrusion, i.e., directly above and/or below, demonstrated lower gagCEST values (0.9% [99% CI: 0.3; 1.5]) than IVDs that were non-adjacent, i.e., distant, to an extruded IVD (1.9% [99% CI: 1.7; 2.5]). No distinct differences, however, were found compared to extruded IVDs.

Table 4. Comparative analysis of glycosaminoglycan chemical exchange saturation transfer (gagCEST) values of intervertebral discs (IVDs) adjacent to IVD extrusions and IVDs non-adjacent to IVD extrusions of patients with radiculopathy. Data are means [99% confidence intervals]. The mean gagCEST values were compared with a linear mixed model comprising a subject-specific random intercept.

gagCEST values (%)	Cohort	Mean [99% CI]
	Patients with radiculopathy	
	IVDs adjacent to IVD extrusions	0.9% [0.3; 1.5]
	IVDs non-adjacent to IVD extrusions	2.1% [1.7; 2.5]
	Extruded IVDs	1.0% [0.2; 1.8]

4. Discussion

In this study, we found that lumbar IVDs directly adjacent to IVD extrusions showed lower gagCEST values than IVDs non-adjacent to extrusions. Furthermore, lumbar IVDs of patients with nsLBP exhibited the lowest overall gagCEST values, lower than the controls and slightly lower than patients with radiculopathy.

Lumbar IVD extrusions are a known and common cause of LBP that not only lead to local pain, but frequently are accompanied by radicular pain, sensory deficits and/or muscle weakness due to the affection of nerve roots [34,35]. Pathophysiologically, proteoglycan depletion of IVDs results in tissue dehydration (of both AF and NP) that brings about decreases in IVD height. These changes are characteristic of LDDD and subsequently increases each IVD's susceptibility to mechanical stress that predisposes to tears and fissures of the AF, and eventually results in IVD extrusions [36]. In the present study, patients who suffered from radiculopathy demonstrated IVD extrusions in their MRI scans. The extruded IVDs showed substantially lower gagCEST values than those of asymptomatic volunteers, which is not surprising since proteoglycan depletion corresponds well with the pathophysiologic concept of IVD degeneration preceding extrusion [37]. Interestingly, IVDs adjacent to the extruded IVD, i.e., directly above and/or below, also demonstrated lower gagCEST values than IVDs that were non-adjacent to the extruded IVD. It remains speculative whether the distinct proteoglycan depletion of the adjacent IVDs was caused by the extrusion and the subsequently altered biomechanics or whether it was simply altered due to exposure to the same mechanical stress that eventually led to IVD extrusion. In favor of the former, overall gagCEST values of patients with radiculopathy were similar to those of asymptomatic volunteers and did not demonstrate signs of advanced degeneration. Thus, one could argue that IVD extrusions affect the biomechanical integrity of the surrounding spine leading to advanced segmental degeneration that originates at the adjacent segments. In favor of this hypothesis, Masui et al. designed a longitudinal study and followed 21 patients over seven years. They found that progressive IVD degeneration regularly occurred after conservative treatment of symptomatic IVD extrusions [38]. Most of their patients showed no signs of morphologic IVD degeneration at baseline (morphologic MRI). Notably, compositional MRI techniques that may allow for the detection of premorphologic IVD changes were not performed in their study. Concurring findings were presented in a systematic review by Schroeder et al. [39], who also concluded that such changes were likely physiological. Keeping these preliminary findings in mind, it would be of interest to prospectively investigate the development of the progressive degeneration of adjacent segments following IVD extrusion in a longitudinal manner. This might contribute to a better understanding of the relationship between IVD extrusion, LBP, and LDDD. Eventually, this might facilitate the identification of "IVDs at risk" that in the future, if disease-modifying treatment is available by then, may influence patient care [40–42].

LDDD not only adds to the development of IVD extrusion, but by itself is considered a potential cause and contributor to chronic LBP [43–46], even though it might also occur in asymptomatic individuals [47]. Several studies underlined the high prevalence of degenerative spinal changes in the asymptomatic population [48,49]. Therefore, MR imaging

should be avoided in the setting of acute and subacute LBP [50]. Our results show that patients with nsLBP had significantly lower gagCEST values than asymptomatic volunteers and somewhat lower values than patients with radiculopathy. These findings are well aligned with one of our previous studies that demonstrated patients with non-radicular LBP to show more severe signs of early IVD degeneration than asymptomatic references [19]. Therefore, the results of this study emphasize the potential association of LBP and LDDD [37], even in cases of premorphological degenerative changes of IVDs, as also suggested by previous studies [51,52]. Thus, compositional MRI could potentially be used in the primary diagnostic work-up of patients with LBP and in follow-up measurements after therapeutic intervention to evaluate treatment success. However, the limited correlation between morphologic changes and clinical outcome as shown in previous studies should be considered in this respect [53].

When interpreting our results, some limitations have to be considered.

First, despite including a sizable study population, each study cohort was relatively small. Therefore, our results have to be considered as preliminary and future studies are required to confirm our findings in larger clinical populations. Second, gagCEST imaging still requires histological validation in human subjects. However, for obvious ethical circumstances, our gagCEST data were not histologically correlated. Such validation remains to be performed directly, in human cadaveric studies, or indirectly, via IVD biopsy during surgery. Third, patients with nsLBP suffered from more severe GAG depletion and higher morphologic IVD degeneration (quantified by Pfirrmann grades ≥ 3) than asymptomatic volunteers. However, to mitigate this limitation, we statistically corrected for differences in Pfirrmann grading in the LMM. Fourth, we only performed one single compositional MRI technique, i.e., gagCEST, while other promising methods for the detection of premorphologic degenerative changes of IVDs, such as T2* mapping [54], were not assessed and remain to be studied. Fifth, the study population was rather heterogeneous, e.g., with a wide age range, which was partially mitigated by matching across the three cohorts. Sixth, gagCEST imaging is ideally performed at 7 T, and there is ongoing discussion as to whether it is feasible at 3 T MRI systems. In addition, it is worth noting that, to this day, gagCEST imaging lacks a standardized protocol as well as normative values and is highly dependent on the individual scanning system, overall hampering the comparability between different sites. To expand gagCEST imaging beyond feasibility studies, expert imaging recommendations as for other imaging biomarkers seem most valuable [55].

5. Conclusions

In conclusion, more advanced GAG depletion in nsLBP and in IVDs adjacent to IVD extrusions in radiculopathy indicates close interrelatedness of clinical pathology and compositional and structural IVD changes in lumbar spine degeneration. These findings underline the potential diagnostic value of non-invasive gagCEST imaging in (a) quantifying tissue composition and detecting premorphological IVD degeneration; (b) in differentiating patterns of IVD degeneration in common clinical disorders of the lumbar spine, and (c) in identifying “IVDs at risk”.

Author Contributions: Conceptualization, M.F., C.S., A.M.-L., B.B., G.A., M.R.K. and D.B.A.; data curation, S.N., L.W. and D.B.A.; formal analysis, K.L.R., B.K., M.B. and L.W.; funding acquisition, G.A.; investigation, M.F., S.N., K.L.R., B.K., M.B. and L.W.; methodology, A.M.-L., K.L.R., B.K. and M.R.K.; project administration, C.S. and B.B.; software, A.M.-L.; supervision, G.A. and M.R.K.; writing—original draft, M.F.; writing—review and editing, S.N., C.S., M.B., L.W., B.B., M.R.K. and D.B.A. All authors have read and agreed to the published version of the manuscript.

Funding: This research was funded by a grant of the Medical Faculty of the Heinrich Heine University Dusseldorf and a grant of the Deutsche Forschungsgemeinschaft (DFG) (NE 2136/3-1).

Institutional Review Board Statement: The study was conducted according to the guidelines of the Declaration of Helsinki, and approved by the Institutional Review Board (or Ethics Committee) of the Medical Faculty, University of Dusseldorf, Germany (protocol code 5078R and date of approval: 29 June 2015).

Informed Consent Statement: Informed consent was obtained from all subjects involved in the study.

Data Availability Statement: Data can be provided by the authors upon reasonable request.

Acknowledgments: We thank Erika Rädisch for the technical acquisition of all images.

Conflicts of Interest: The authors declare no conflict of interest.

References

1. Wu, A.; March, L.; Zheng, X.; Huang, J.; Wang, X.; Zhao, J.; Blyth, F.M.; Smith, E.; Buchbinder, R.; Hoy, D. Global low back pain prevalence and years lived with disability from 1990 to 2017: Estimates from the Global Burden of Disease Study 2017. *Ann. Transl. Med.* **2020**, *8*, 299.
2. Billis, E.V.; McCarthy, C.J.; Oldham, J.A. Subclassification of low back pain: A cross-country comparison. *Eur. Spine J.* **2007**, *16*, 865–879.
3. Dewitte, V.; de Pauw, R.; de Meulemeester, K.; Peersman, W.; Danneels, L.; Bouche, K.; Roets, A.; Cagnie, B. Clinical classification criteria for nonspecific low back pain: A Delphi-survey of clinical experts. *Musculoskelet. Sci. Pract.* **2018**, *34*, 66–76.
4. Deane, J.A.; McGregor, A.H. Current and future perspectives on lumbar degenerative disc disease: A UK survey exploring specialist multidisciplinary clinical opinion. *BMJ Open* **2016**, *6*, e011075.
5. Taher, F.; Essig, D.; Lebl, D.R.; Hughes, A.P.; Sama, A.A.; Cammisa, F.P.; Girardi, F.P. Lumbar Degenerative Disc Disease: Current and Future Concepts of Diagnosis and Management. *Adv. Orthop.* **2012**, *2012*, doi:10.1155/2012/970752.
6. Chou, R.; Qaseem, A.; Snow, V.; Casey, D.; Cross, J.T.; Shekelle, P.; Owens, D.K. Diagnosis and treatment of low back pain: A joint clinical practice guideline from the American College of Physicians and the American Pain Society. *Ann. Intern. Med.* **2007**, *147*, 478–491.
7. Yang, H.; Liu, H.; Li, Z.; Zhang, K.; Wang, J.; Wang, H.; Zhen, Z. Low back pain associated with lumbar disc herniation: Role of moderately degenerative disc and annulus fibrous tears. *Int. J. Clin. Exp. Med.* **2015**, *8*, 1634–1644.
8. McCall, I.W. Lumbar herniated disks. *Radiol. Clin. N. Am.* **2000**, *38*, 1293–1309.
9. Chou, R.; Qaseem, A.; Owens, D.K.; Shekelle, P. Diagnostic imaging for low back pain: Advice for high-value health care from the American College of Physicians. *Ann. Intern. Med.* **2011**, *154*, 181–189.
10. Carragee, E.; Alamin, T.; Cheng, I.; Franklin, T.; van den Haak, E.; Hurwitz, E. Are first-time episodes of serious LBP associated with new MRI findings? *Spine J.* **2006**, *6*, 624–635.
11. Ogon, I.; Takebayashi, T.; Takashima, H.; Morita, T.; Terashima, Y.; Yoshimoto, M.; Yamashita, T. Imaging diagnosis for intervertebral disc. *JOR Spine* **2019**, *3*, e1066.
12. Brinjikji, W.; Diehn, F.E.; Jarvik, J.G.; Carr, C.M.; Kallmes, D.F.; Murad, M.H.; Luetmer, P.H. MRI Findings of Disc Degeneration are More Prevalent in Adults with Low Back Pain than in Asymptomatic Controls: A Systematic Review and Meta-Analysis. *AJNR Am. J. Neuroradiol.* **2015**, *36*, 2394–2399.
13. Pfirrmann, C.W.; Metzendorf, A.; Zanetti, M.; Hodler, J.; Boos, N. Magnetic resonance classification of lumbar intervertebral disc degeneration. *Spine* **2001**, *26*, 1873–1878.
14. Urrutia, J.; Besa, P.; Campos, M.; Cikutovic, P.; Cabezon, M.; Molina, M.; Cruz, J.P. The Pfirrmann classification of lumbar intervertebral disc degeneration: An independent inter- and intra-observer agreement assessment. *Eur. Spine J.* **2016**, *25*, 2728–1733.
15. Melkus, G.; Grabau, M.; Karampinos DC.; Majumdar, S. Ex vivo Porcine Model to Measure pH Dependence of gagCEST in the Inter-Vertebral Disc. *Magn. Reson. Med.* **2013**, *71*, 1743–1749.
16. Müller-Lutz, A.; Schleich, C.; Pentang, G.; Schmitt, B.; Lanzman RS.; Matuschke, F.; Wittsack HJ.; Miese, F. Age-dependency of glycosaminoglycan content in lumbar discs: A 3t gagCEST study. *J. Magn. Reson. Imaging* **2015**, *42*, 1517–1523.
17. Müller-Lutz, A.; Schleich, C.; Schmitt, B.; Topgöz, M.; Pentang, G.; Antoch, G.; Wittsack, H.J.; Miese, F. Improvement of gagCEST imaging in the human lumbar intervertebral disc by motion correction. *Skeletal Radiol.* **2015**, *44*, 505–511.
18. Haneder, S.; Apprigh SR.; Schmitt, B.; Michaely HJ.; Schoenberg SO.; Friedrich KM.; Trattnig, S. Assessment of glycosaminoglycan content in intervertebral discs using chemical exchange saturation transfer at 3.0 Tesla: Preliminary results in patients with low-back pain. *Eur. Radiol.* **2013**, *23*, 861–868.
19. Pulickal, T.; Boos, J.; Konieczny, M.; Sawicki, L.M.; Müller-Lutz, A.; Bittersohl, B.; Gerß, J.; Eichner, M.; Wittsack, H.J.; Antoch, G.; Schleich, C. MRI identifies biochemical alterations of intervertebral discs in patients with low back pain and radiculopathy. *Eur. Radiol.* **2019**, *29*, 6443–6446.
20. Kogan, F.; Hargreaves, B.A.; Gold, G.E. Volumetric multislice gagCEST imaging of articular cartilage: Optimization and comparison with T1rho. *Magn. Reson. Med.* **2017**, *77*, 1134–1141.

21. Wei, W.; Jia, G.; Flanigan, D.; Zhou, J.; Knopp, M.V. Chemical exchange saturation transfer MR imaging of articular cartilage glycosaminoglycans at 3 T: Accuracy of B0 Field Inhomogeneity corrections with gradient echo method. *Magn. Reson. Imaging* **2014**, *32*, 41–47.
22. Saar, G.; Zhang, B.; Ling, W.; Regatte, R.R.; Navon, G.; Jerschow, A. Assessment of glycosaminoglycan concentration changes in the intervertebral disc via chemical exchange saturation transfer. *NMR Biomed.* **2012**, *25*, 255–261.
23. Ling, W.; Regatte, R.R.; Navon, G.; Jerschow, A. Assessment of glycosaminoglycan concentration in vivo by chemical exchange-dependent saturation transfer (gagCEST). *Proc. Natl. Acad. Sci. USA* **2008**, *105*, 2266–2270.
24. Brinkhof, S.; Nizak, R.; Sim, S.; Khlebnikov, V.; Quenneville, E.; Garon, M.; Clomp, D.; Saris, D. In vivo biochemical assessment of cartilage with gagCEST MRI: Correlation with cartilage properties. *NMR Biomed.* **2021**, *34*, e4463.
25. Casser, H.-R.; Seddigh, S.; Rauschmann, M. Acute Lumbar Back Pain. *Dtsch. Arztebl. Int.* **2016**, *113*, 223–234.
26. Fardon, D.F.; Milette, P.C. Nomenclature and classification of lumbar disc pathology. Recommendations of the Combined task Forces of the North American Spine Society.; American Society of Spine Radiology.; and American Society of Neuroradiology. *Spine* **2001**, *26*, E93–E113.
27. Rozenberg, S. Lomبالغie Chronique, Définition Et Prise En Charge. *La Revue du Praticien* **2008**, *58*, 265–272.
28. Müller-Lutz, A.; Schleich, C.; Schmitt, B.; Antoch, G.; Matuschke, F.; Quentin, M.; Wittsack, H.J.; Miese, F.; Gender, B. BMI and T2 dependencies of glycosaminoglycan chemical exchange saturation transfer in intervertebral discs. *Magn. Reson. Imaging* **2016**, *34*, 271–275.
29. Schleich, C.; Müller-Lutz, A.; Blum, K.; Boos, J.; Bittersohl, B.; Schmitt, B.; Gerß, J.; Matuschke, F.; Wittsack, H.J.; Antoch, G.; Miese, F. Facet tropism and facet joint orientation: Risk factors for the development of early biochemical alterations of lumbar intervertebral discs. *Osteoarthr. Cartil.* **2016**, *24*, 1761–1768.
30. Schleich, C.; Müller-Lutz, A.; Matuschke, F.; Sewerin, P.; Sengewein, R.; Schmitt, B.; Ostendorf, B.; Wittsack, H.J.; Stanke, K.; Antoch, G.; Miese, F. Glycosaminoglycan chemical exchange saturation transfer of lumbar intervertebral discs in patients with spondyloarthritis. *J. Magn. Reson. Imaging* **2015**, *42*, 1057–1063.
31. Zhang, S.; Keupp, J.; Wang, X.; Dimitrov, I.; Madhuranthakam, A.J.; Lenkinski, R.E.; Vinogradov, E. Z-spectrum appearance and interpretation in the presence of fat: Influence of acquisition parameters. *Magn. Reson. Med.* **2017**, *79*, 2731–2737.
32. Beaumont, C. Comparison of Henderson’s Method I and restricted maximum likelihood estimation of genetic parameters of reproductive traits. *Poult. Sci.* **1991**, *70*, 1462–1468.
33. Turkiewicz, A.; Luta, G.; Hughes, H.V.; Ranstam, J. Statistical mistakes and how to avoid them - lessons learned from the reproducibility crisis. *Osteoarthr. Cartil.* **2018**, *26*, 1409–1411.
34. Amin, R.M.; Andrade, N.S.; Neuman, B.J. Lumbar Disc Herniation. *Curr. Rev. Musculoskelet. Med.* **2017**, *10*, 507–516.
35. Vialle, L.R.; Vialle, E.N.; Suárez Henao, J.E.; Giraldo, G. Lumbar disc herniation. *Rev. Bras. Ortop.* **2010**, *45*, 17–22.
36. Oichi, T.; Taniguchi, Y.; Oshima, Y.; Tanaka, S.; Saito, T. Pathomechanism of intervertebral disc degeneration. *JOR Spine* **2020**, *3*, e1076.
37. Donnally, C.J., III.; Hanna, A.; Varacallo, M. *Statpearls: Lumbar Degenerative Disk Disease*; StatPearls Publishing: Treasure Island, FL, USA, 2020.
38. Masui, T.; Yukawa, Y.; Nakamura, S.; Kajino, G.; Matsubara, Y.; Kato, F.; Ishiguri, N. Natural history of patients with lumbar disc herniation observed by magnetic resonance imaging for minimum 7 years. *J. Spinal Disord. Tech.* **2005**, *18*, 121–126.
39. Schroeder, J.E.; Dettori, J.R.; Brodt, E.D.; Kaplan, L. Disc degeneration after disc herniation: Are we accelerating the process? *Evid. Based Spine. Care J.* **2012**, *3*, 33–40.
40. Lurie, J.D.; Tosteson, T.D.; Tosteson, A.N.A.; Zhao, W.; Morgan, T.S.; Abdu, W.A.; William, A.; Herkowitz, H.; Weinstein, J. Surgical versus nonoperative treatment for lumbar disc herniation: Eight-year results for the spine patient outcomes research trial. *Spine* **2014**, *39*, 3–16.
41. Rotherl, R.D.; Woertgen, C.; Brawanski, A. When should conservative treatment for lumbar disc herniation be ceased and surgery considered? *Neurosurg. Rev.* **2002**, *25*, 162–165.
42. Weinstein, J.N.; Tosteson, T.D.; Lurie, J.D.; Tosteson, A.N.A.; Hanscom, B.; Skinner, J.S.; Abdu, W.; Hilibrand, A.; Boden, S.; Deyo, R. Surgical vs nonoperative treatment for lumbar disc herniation: The Spine Patient Outcomes Research Trial (SPORT): A randomized trial. *JAMA* **2006**, *296*, 2441–2450.
43. Zheng, C.-J.; Chen, J. Disc degeneration implies low back pain. *Theor. Biol. Med. Model.* **2015**, *12*, 24.
44. Khan, A.N.; Jacobsen, H.E.; Khan, J.; Filippi, C.G.; Levine, M.; Lehman, R.A.; Riew, D.; Lenke, L.; Chahine, N. Inflammatory biomarkers of low back pain and disc degeneration: A review. *Ann. N. Y. Acad. Sci.* **2017**, *1410*, 68–84.
45. Kos, N.; Gradisnik, L.; Velnar, T. A Brief Review of the Degenerative Intervertebral Disc Disease. *Med. Arch.* **2019**, *73*, 421–424.
46. Ito, K.; Creemers, L. Mechanisms of intervertebral disk degeneration/injury and pain: A review. *Global Spine J.* **2013**, *3*, 145–152.
47. Jensen, M.C.; Brant-Zawadzki, M.N.; Obuchowski, N.; Modic, M.T.; Malkasian, D.; Ross, J.S. Magnetic resonance imaging of the lumbar spine in people without back pain. *N. Engl. J. Med.* **1994**, *331*, 69–73.
48. Jarvik, J.G.; Meier, E.N.; James, K.T.; Gold, L.S.; Tan, K.W.; Kessler, L.G.; Suri, P.; Kallmes, D.; Cherkin, D.; Deyo, R. The Effect of Including Benchmark Prevalence Data of Common Imaging Findings in Spine Image Reports on Health Care Utilization Among Adults Undergoing Spine Imaging: A Stepped-Wedge Randomized Clinical Trial. *JAMA Netw. Open* **2020**, *3*, e2015713.
49. Brinjikji, W.; Luetmer, P.H.; Comstock, B.; Bresnahan, B.W.; Chen, L.E.; Deyo, R.A.; Halabi, S.; Turner, J.; Avins, A.; James, K. Systematic literature review of imaging features of spinal degeneration in asymptomatic populations. *AJNR Am. J. Neuroradiol.* **2015**, *36*, 811–816.

50. Darlow, B.; Forster BB.; O'Sullivan, K.; O'Sullivan, P. It is time to stop causing harm with inappropriate imaging for low back pain. *Br. J. Sports. Med.* **2017**, *51*, 414–415.
51. Togao, O.; Hiwatashi, A.; Wada, T.; Yamashita, K.; Kikuchi, K.; Tokunaga, C.; Keupp, J.; Yoneyama, M.; Honda, H. A Qualitative and Quantitative Correlation Study of Lumbar Intervertebral Disc Degeneration Using Glycosaminoglycan Chemical Exchange Saturation Transfer.; Pfirrmann Grade.; and T1-ρ. *AJNR Am. J. Neuroradiol.* **2018**, *39*, 1369–1375.
52. Xiong, X.; Zhou, Z.; Figini, M.; Shangguan, J.; Zhang, Z.; Chen, W. Multi-parameter evaluation of lumbar intervertebral disc degeneration using quantitative magnetic resonance imaging techniques. *Am. J. Transl. Res.* **2018**, *10*, 444–454.
53. el Barzouhi, A.; Vleggeert-Lankamp, C.L.A.M.; Lycklama à Nijeholt, G.J.; van der Kallen, B.F.; van den Hout, W.B.; Jacobs, W.C.H.; Koes, B.; Peul, W. Magnetic resonance imaging in follow-up assessment of sciatica. *N. Engl. J. Med.* **2013**, *368*, 999–1007.
54. Guermazi, A.; Alizai, H.; Crema, M.D.; Trattng, S.; Regatte, R.R.; Roemer, F.W. Compositional MRI techniques for evaluation of cartilage degeneration in osteoarthritis. *Osteoarthr. Cartil.* **2015**, *23*, 1639–1653.
55. Qiba Biomarker Committee. (Ed.) Qiba Profile:Mr-Based Cartilage Compositional Biomarkers (T1ρ, T2) for Risk Prediction, Early Diagnosis and Monitoring of Treatment of Degenerative Joint Disease. 2020. Available online: https://qibawiki.rsna.org/images/2/20/QIBA_Profile_MSK-Cartilage-Stage1_Profile.pdf. (accessed on 29 October 2020).

Article

Evaluating Lumbar Intervertebral Disc Degeneration on a Compositional Level Using Chemical Exchange Saturation Transfer: Preliminary Results in Patients with Adolescent Idiopathic Scoliosis

Lena M. Wollschläger ^{1,2,*}, Sven Nebelung ¹, Christoph Schleich ¹, Anja Müller-Lutz ¹, Karl L. Radke ¹, Miriam Frenken ¹, Matthias Boschheidgen ¹, Max Prost ², Gerald Antoch ¹, Markus R. Konieczny ² and Daniel B. Abrar ¹

¹ Department of Diagnostic and Interventional Radiology, Medical Faculty, University Dusseldorf, D-40225 Dusseldorf, Germany; sven.nebelung@med.uni-duesseldorf.de (S.N.); schleich@radiologie-duesseldorf-mitte.de (C.S.); anja.lutz@med.uni-duesseldorf.de (A.M.-L.); ludger.radke@med.uni-duesseldorf.de (K.L.R.); miriam.frenken@med.uni-duesseldorf.de (M.F.); matthias.boschheidgen@med.uni-duesseldorf.de (M.B.); antoch@med.uni-duesseldorf.de (G.A.); danielbenjamin.abrar@med.uni-duesseldorf.de (D.B.A.)

² Department of Orthopedics and Trauma Surgery, Medical Faculty, University Dusseldorf, D-40225 Dusseldorf, Germany; max.prost@med.uni-duesseldorf.de (M.P.); markus.konieczny@med.uni-duesseldorf.de (M.R.K.)

* Correspondence: lena.wollschlaeger@med.uni-duesseldorf.de



Citation: Wollschläger, L.M.; Nebelung, S.; Schleich, C.; Müller-Lutz, A.; Radke, K.L.; Frenken, M.; Boschheidgen, M.; Prost, M.; Antoch, G.; Konieczny, M.R.; et al. Evaluating Lumbar Intervertebral Disc Degeneration on a Compositional Level Using Chemical Exchange Saturation Transfer: Preliminary Results in Patients with Adolescent Idiopathic Scoliosis. *Diagnostics* **2021**, *11*, 934. <https://doi.org/10.3390/diagnostics11060934>

Academic Editor: Rute Santos

Received: 28 April 2021

Accepted: 21 May 2021

Published: 22 May 2021

Publisher's Note: MDPI stays neutral with regard to jurisdictional claims in published maps and institutional affiliations.



Copyright: © 2021 by the authors. Licensee MDPI, Basel, Switzerland. This article is an open access article distributed under the terms and conditions of the Creative Commons Attribution (CC BY) license (<https://creativecommons.org/licenses/by/4.0/>).

Abstract: Lumbar intervertebral disc (IVD) degeneration is characterized by structural and compositional changes. This study aimed to assess the glycosaminoglycan (GAG) content of IVDs of patients with adolescent idiopathic scoliosis (AIS) and healthy controls using GAG chemical exchange saturation transfer (gagCEST) imaging. Ten AIS patients (mean age 18.3 ± 8.2 years) and 16 healthy controls (mean age 25.5 ± 1.7 years) were included. Clinical standard morphologic MR images (T1w-, T2w-, and STIR-sequences), to rule out further spinal disorders and assess IVD degeneration using the Pfirrmann score, and compositional gagCEST sequences were acquired on a 3T MRI. In AIS patients, the most distal scoliotic curve was determined on whole-spine conventional radiographs and morphological MRI and IVDs were divided as to whether they were affected by scoliotic deformity, i.e., proximal (affected, aIVDs) or distal (unaffected, uaIVDs) to the stable vertebra of the most distal scoliotic curve. Linear mixed models were used to compare mean gagCEST-values. Over all segments, AIS-patients' IVDs exhibited significantly lower gagCEST-values than the controls: 2.76 [2.32, 3.20]% (AIS), 3.51 [3.16, 3.86]% (Control); $p = 0.005$. Meanwhile, no significant differences were found for gagCEST values comparing aIVDs with uaIVDs. In conclusion, as a powerful diagnostic adjunct, gagCEST imaging may be prospectively applied to detect early compositional degenerative changes in patients suffering from AIS.

Keywords: advanced MRI techniques; Idiopathic scoliosis; gagCEST; compositional magnetic resonance imaging of cartilage; disc degeneration

1. Introduction

Adolescent idiopathic scoliosis (AIS) is the most common subtype of all idiopathic scolioses with an overall prevalence of 0.5–5.2% and a female predominance [1]. With the disease progressing continuously during the growth of patients, AIS can cause significant back pain, restricted mobility, severe rib deformity, and, ultimately, thoracic insufficiency in advanced stages [2,3]. Scoliotic deformity in AIS leads to remodeling of the intervertebral discs (IVDs) with consecutive morphologic IVD degeneration, frequently associated with lower back pain [4–6]. In severe AIS, the treatment of choice is spinal 3-dimensional

deformity correction and fusion after skeletal maturity. Over the years, surgical concepts have evolved. Presently, selective fusion [7] is performed by sparing fusion of minor curves, i.e., less affected spinal segments. Short segment fusion leads to less frequent IVD degeneration and pain [8,9]. However, only little is known about preoperative IVD degeneration in patients with AIS [10].

As of today, magnetic resonance tomography (MRI) is the most sensitive imaging technique for the evaluation of degenerative alterations in IVDs [4,11]. While non-degenerative, morphologically unremarkable IVDs exhibit a high signal in T2-weighted (T2-w) sequences due to their high intra-tissue water content [6,12,13], degenerative IVDs have a lower signal due to their decreased water content [4,6]. These signal changes of IVDs are used for the well-known Pfirrmann classification, a validated grading system for the differentiation of non-degenerative and degenerative IVDs based on imaging criteria [12]. However, standard clinical morphologic MRI techniques cannot detect early changes in the nucleus pulposus, i.e., glycosaminoglycan (GAG) depletion, as an early and potentially reversible change indicative of IVD degeneration [14]. GAGs are negatively charged linear polysaccharides that attract water and, alongside the central core protein, make up the proteoglycan (PGs) and tissue solid extracellular matrix components. Primarily in the nucleus pulposus (NP), PGs play a vital role for IVD hydration, thus providing resistance to mechanical stress through high osmotic pressure [4]. Consequently, the PG content of the IVDs provides a quantitative indicator of the structure's composition and configuration in health and disease, and a potent diagnostic target. In the context of AIS, quantitative evaluation of the PG content may therefore open up diagnostic opportunities in detecting early degeneration and monitoring treatment efficacy beyond mere morphologic evaluation.

The gold standard of compositional cartilage imaging using biochemically sensitive MRI sequences is delayed gadolinium-enhanced MRI of cartilage (dGEMRIC). However, due to recent restrictions on gadolinium-based contrast agents (GBCA) [15], alternative compositional imaging techniques have come into focus that do not rely on GBCA. GAG chemical exchange saturation transfer (gagCEST) imaging is a technique that measures the chemical exchange of hydroxyl (-OH)-protons between GAG and bulk water. To induce the CEST effect, a frequency-specific radiofrequency (RF) pulse is applied to first saturate the solute-bound proton pool at different offset frequencies and then transfer these protons to the bulk water pool through chemical exchange, subsequently reducing its signal. The resultant signal decrease is then used to quantitatively assess the CEST effect at the specific frequency range of GAG, i.e., at 0.9–1.9 ppm [16–18]. Previous pioneering studies have demonstrated the close association of CEST effect and GAG content that may be used to quantify IVD GAG content [17–19]. Consequently, a solid body of evidence indicates that degenerative and non-degenerative IVDs can be distinguished through quantification of GAG content using gagCEST imaging [19–21].

As of today, gagCEST imaging has not yet been used for the evaluation of proteoglycan depletion as one of the earliest degenerative changes in lumbar IVDs of patients with AIS. The aim of our study was to compare the GAG contents of (a) lumbar IVDs in AIS patients with healthy controls and (b) of those IVDs in AIS patients that were part of the scoliotic curve and those that were not. We hypothesized that gagCEST values of (a) lumbar IVDs of patients with AIS are significantly lower than corresponding IVDs of the control group and (b) that in AIS patients the same is true for IVDs of the scoliotic curve as compared to those that are not part of the scoliotic curve.

2. Materials and Methods

2.1. Study Design and Population

This study was designed as a prospective comparative clinical imaging study assessing the proteoglycan content of lumbar IVDs in patients with AIS as compared to healthy controls. Prior to study initiation, approval by the local Ethical Committee (Medical Faculty, University of Düsseldorf, Germany, study number 2019-551) and written informed

consent were attained from all participants included, or, in underaged patients, from their legal guardians.

A total of 11 patients with AIS (mean age 18.3 ± 8.2 years; 7 females, 4 males, disease duration 59.2 ± 102.0 months) and 16 healthy controls (mean age 25.5 ± 1.7 years; 8 females, 8 males) without any previous history of spine disease were prospectively recruited during consultation hours at the Department of Orthopedic and Trauma Surgery (University Hospital Düsseldorf) and among the hospital staff, and were included in this study. Of the 11 AIS patients, 4 were treated with physical therapy only, 5 received bracing therapy, and 2 patients received bracing therapy with subsequent surgery. None of the patients had received surgery prior to study initiation. Table 1 gives details on both study populations.

Table 1. Demographic, clinical, and therapeutic information of the study population.

	AIS Patients	Controls
Age [years]	18.3 ± 8.2	25.5 ± 1.7
Gender [female/male]	7/4	8/8
Number of involved vertebrae [n]		
• Major curve	7.5 ± 3.2 (4–15)	n/a
• Minor curve	6 ± 0.5 (5–6)	n/a
Orientation of major curve [dextro-, levoscoliosis]	Dextroscoliosis $n = 6$ Levoscoliosis $n = 5$	n/a
Cobb angle [°] major curve	34.8 ± 21.5 (15–73)	n/a
Cobb angle [°] minor curve	21.8 ± 10.2 (11–37)	n/a
Disease duration [months]	59.2 ± 102.0	n/a
Type of treatment		n/a
• Physical therapy	4	n/a
• Bracing (conservative)	5	n/a
• Bracing (+subsequent surgery)	2	n/a

Data for the radiographic analysis (Cobb angle of the major and minor curve, the number of involved vertebrae, the orientation of the major curve, and the disease duration) and type of treatment are given for AIS patients. Means \pm standard deviations and the range are presented. Abbreviations: AIS—adolescent idiopathic scoliosis; n/a—not applicable.

For all participants, predefined exclusion criteria were a history of spine surgery, musculoskeletal chronic inflammatory diseases, congenital spine conditions including non-idiopathic scoliosis, previous spinal trauma, known IVD extrusion as detected by a potential previous MRI scan or pathological body mass index ranges <18.5 or >30 kg/m². However, due to excessive motion artifacts, one female AIS patient had to be excluded from the gagCEST analysis. Acquired spinal deformities and chronic lower back pain were defined as additional exclusion criteria for the control group. Clinically indicated and independent of this study, all included patients had received standard conventional radiographs (CR) of the whole spine in anteroposterior and lateral projections prior to initiation of the study.

2.2. MR Imaging

All participants underwent MR imaging of their lumbar spine on a whole-body clinical 3.0T MRI system (Magnetom Prisma, Siemens Healthineers, Erlangen, Germany). Patients were examined in the supine position and imaged with a 32-channel body and a 24-channel spine matrix coil (both Siemens Healthineers). The imaging protocol consisted of a clinical routine protocol, i.e., T1- (T1w) and T2-weighted (T2w) sequences and a short tau inversion recovery (STIR) sequence, and compositional sequences using gagCEST and water saturation shift referencing (WASSR) imaging. All sequences were acquired in the sagittal orientation. Detailed sequence parameters are given in Table 2.

Table 2. Morphological and compositional magnetic resonance imaging (MRI) sequence parameters.

	Sequence				
	STIR	T2w TSE	T1w TSE	gagCEST	WASSR
Orientation	Sagittal	Sagittal	Sagittal	Sagittal	Sagittal
TE/TR [ms]	57/3800	95/3500	9.5/650	5.1/10	5.1/10
Flip Angle [°]	150	160	150	10	10
Slice Thickness [mm]	4	4	4	5	5
FoV [mm × mm]	300 × 300	300 × 300	300 × 300	300 × 300	300 × 300
Pixel Size [mm × mm]	0.8 × 0.8	0.7 × 0.7	0.7 × 0.7	1.6 × 1.6	1.6 × 1.6

Orientation, echo and repetition time, flip angle, slice thickness, field of view, pixel size, and number of slices are given for all sequences. Abbreviations: TE—echo time; TR—repetition time; FOV—field of view; STIR—short tau inversions recovery; T2w—T2-weighted; T1w T2-weighted; TSE—turbo spin-echo; gagCEST—glycosaminoglycan chemical exchange saturation transfer; WASSR—water saturation shift referencing.

2.3. MR Image Analysis

For image analysis, two clinical radiologists (DBA and CS with 5 and 8 years of experience in musculoskeletal imaging, respectively), blinded to patient data, independently read the MR images. In case of divergent findings, consensus was arbitrated with the assistance of a third clinical radiologist (SN, 8 years of experience in musculoskeletal imaging).

All participants' lumbar IVDs (segments L1/L2–L5/S1) were individually graded on sagittal T2w images according to the Pfirrmann classification, an MRI-based five-step grading system for lumbar disc degeneration that enables distinction of degenerated (grade ≥ 3) and non-degenerated (grade ≤ 2) IVDs based on signal intensity and structure of the NP, disc height and the NPs distinction from the annulus fibrosus (AF) [12].

On anteroposterior CR of AIS, the Cobb angle and the apical, end, and stable vertebrae were determined using Cobb's method [22]. By convention, the apical vertebra is the vertebra with the farthest deviation from the center of the vertebral column, while the end vertebrae are those vertebrae that are most tilted towards the apex of the curve. The latter ones are used to measure the Cobb angle by determining the intersection of a tangent drawn along the superior endplate of the superior end vertebra and of a tangent drawn along the inferior endplate of the inferior end vertebra. The stable vertebra is defined as the first vertebra below the lowest curve which is bisected by the central sacral vertical line [23].

In all AIS patients, the stable vertebra was situated in the lumbar spine. To further evaluate the influence of scoliotic deformity on GAG content in IVDs in AIS patients, all IVDs proximal to the stable vertebra were compared to those IVDs distal to the stable vertebra and thus not part of the scoliotic curve. To this end, all IVDs of AIS patients, i.e., L1/L2–L5/S1, were divided into two groups depending on whether they were situated proximal or distal to the stable vertebra of the most distal scoliotic curve. For the sake of readability, IVDs situated proximal or distal to the stable vertebra of the most distal scoliotic curve are referred to as "affected" IVDs (aIVDs) or "non affected" IVDs (uaIVDs). For both groups, gagCEST values were determined and statistically analyzed.

For our study, all gagCEST analyses were performed as before [20,24]. Briefly, gagCEST values were derived using a customized in-house script implemented in Matlab (R2018a, The MathWorks Inc., Natick, MA, USA). By means of a diffeomorphic image registration technique integrated into the fMRLung software (Siemens Healthcare), motion correction was conducted for both WASSR (water saturation shift referencing) and CEST images [18]. Using the WASSR maximum-symmetry algorithm to determine a pixel-wise frequency offset curve, B0-field inhomogeneities were corrected as previously published [21,25]. To this end, pixel-wise frequency offset-corrected CEST-curves were determined and divided by the signal without presaturation (S_0) to establish the z-spectrum ($Z(\omega)$), with a maximum frequency offset of $\Delta\omega = 3$ ppm for each z-spectrum. With $\Delta\omega$ defined as the specified frequency shift difference, the gagCEST effect was further evaluated using the maximum magnetization transfer asymmetry (MTR_{Asym}): $MTR_{Asym}(\Delta\omega) = Z(-\Delta\omega) - Z(\Delta\omega)$ [21]. More specifically, using the average value of MTR_{Asym} in the GAG-specific

frequency range ($\Delta\omega = 0.9\text{--}1.9$ ppm) in which hydroxyl protons of GAG can function as CEST agents [16], MTRasym maps were calculated with MTRasym values provided in %.

To determine the CEST effect, disc segmentation was performed according to the Naïve Bayes classification for image segmentation, which differentiates disc tissue from osseous and ligamentous structures of the lumbar spine [26]. To this end, region-of-interest (ROI) definition was automatically conducted by computed segmentation of lumbar IVDs using a customized in-house script implemented in Matlab with the ROIs subsequently positioned in the lumbar IVDs. A radiologist (CS) visually verified the correct ROI position for every IVD. If necessary, mispositioned ROIs were repositioned, yet no ROI size had to be modified manually. Hereafter, MTRasym values are referred to as gagCEST values for easier readability.

2.4. Statistical Analysis

Statistical analyses were performed by KLR and LMW using SPSS (v27, SPSS Inc., Chicago, IL, USA). Summary statistics of gagCEST values were determined for healthy controls and AIS patients. Based on a linear mixed model (LMM), both cohorts (i.e., healthy controls and AIS patients), regions (i.e., NP and AF), and IVD group (i.e., uaIVDs and aIVDs) were comparatively evaluated as multivariable statistics. The LMMs included a subject-specific random intercept, independent variables (i.e., gender, age, cohort, Pfirrmann score, IVD segment level, scoliotic affection), and their interactions. Employing a restricted maximum likelihood approach, the LMMs were fitted [27]. Mean differences of gagCEST values were determined based on the established LMMs and analyzed for significance. Due to this study's exploratory character, p -values ≤ 0.05 indicated statistical significance.

3. Results

3.1. Study Population

The characteristics of the study population are displayed in Table 1. A total of 80 lumbar IVDs of 16 healthy controls and 50 lumbar IVDs of 10 AIS patients (both L1/L2–L5/S1) were analyzed. For both groups, significant differences in age distribution were found with AIS patients being significantly younger than healthy controls ($p < 0.001$). The covariates were corrected for an age of 23.1 years.

3.2. Morphologic Grading of IVD Degeneration

Based on the Pfirrmann classification, degeneration in IVDs was quantified as follows: total study population: grade 2: ($n = 127$), grade 3: ($n = 3$); healthy controls: grade 2: ($n = 79$), grade 3: ($n = 1$); AIS patients: grade 2: ($n = 48$), grade 3: ($n = 2$). No IVD grades 1, 4, or 5 were present.

3.3. GagCEST Values: Healthy Controls vs. AIS Patients

In all lumbar IVDs of both groups, significantly higher gagCEST values were observed in the NP than the AF (NP: 3.90 [confidence interval (CI) 3.49, 4.31]%, AF: 2.37 [CI 2.03, 2.70]%; $p = 0.001$).

Over all segments, IVDs in AIS patients exhibited significantly lower mean gagCEST values compared to those of healthy controls (AIS: 2.76 [CI 2.32, 3.20]%, C: 3.51 [CI: 3.16, 3.86]%; $p = 0.005$). Considering each lumbar segment by itself, gagCEST values only significantly differed at segment L5/S1 (AIS 1.38 [0.66, 2.1]%, C: 3.39 [2.87, 3.90]%; $p < 0.001$).

Mean gagCEST values in healthy controls and AIS patients as well as the corresponding comparative analysis are further outlined in Table 3. GagCEST maps of both study groups illustrate these findings (Figure 1).

Table 3. Analysis of compositional imaging features of lumbar intervertebral discs (IVDs).

Score	L1/2	L2/3	L3/4	L4/5	L5/S1	All Segments	
gagCEST values [%]	Controls	3.340 [2.721, 3.959]	3.466 [2.844, 4.089]	3.218 [2.586, 3.850]	3.679 [2.082, 5.276]	3.389 [2.877, 3.902]	3.510 [3.159, 3.861]
	AIS	2.867 [2.005, 3.729]	2.646 [1.831, 3.461]	3.908 [3.079, 4.736]	3.700 [1.581, 5.818]	1.381 [0.661, 2.102]	2.759 [2.320, 3.199]
	<i>p</i>-values	0.399	0.139	0.220	0.988	<0.001	0.005

Mean glycosaminoglycan chemical exchange saturation transfer (gagCEST) values of the two study cohorts (i.e., 16 healthy controls and 10 AIS patients) in all patients as a function of segment levels. Using linear mixed models including a subject-specific intercept, mean gagCEST values were compared. Data are corrected mean + 95% confidence interval [square brackets] (%) of gagCEST values of the nucleus pulposus (NP). The covariates were corrected for an age of 23.1 years. *p*-values < 0.05 are given in bold type. Abbreviations: L—lumbar; n/a—not applicable.

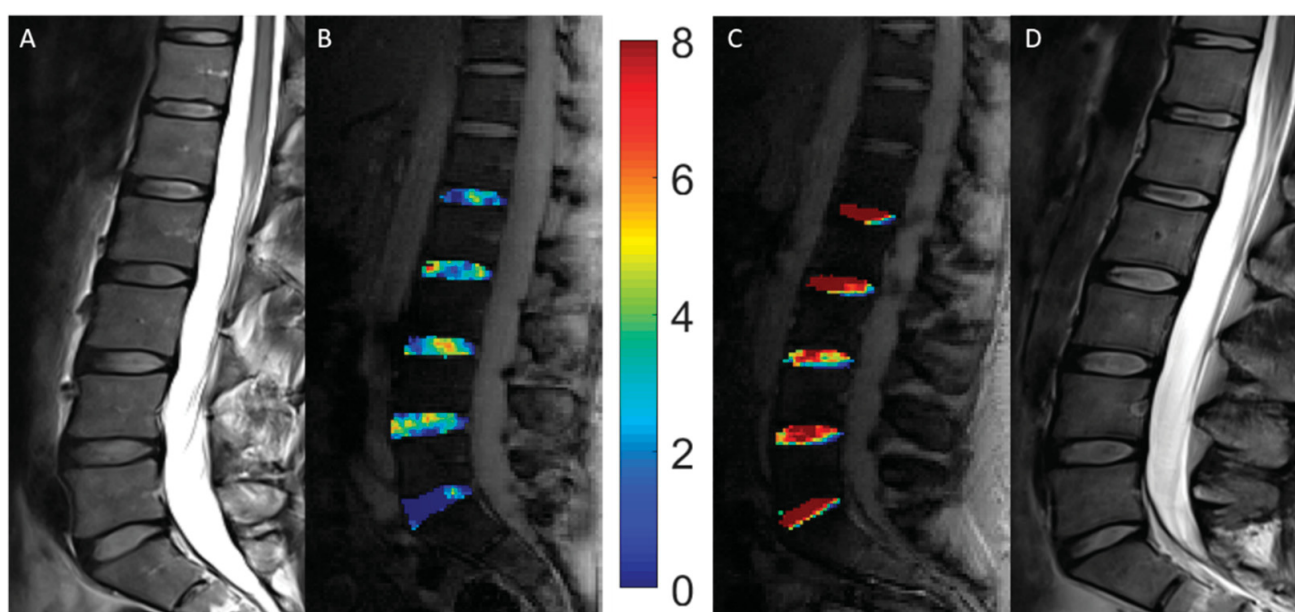


Figure 1. Representative morphologic and compositional imaging findings of the lumbar intervertebral discs (IVDs) of a patient with adolescent idiopathic scoliosis (AIS, **A,B**) and a healthy control (**C,D**). (**A,D**): Sagittal T2-weighted images show the absence of morphologic signs of relevant intervertebral disc degeneration. (**B,C**): Sagittal gagCEST images with overlaid color-coded gagCEST maps to indicate the GAG content reveal distinct differences in GAG contents. Lower GAG content is indicated in blue, while high GAG content is illustrated in red. This patient with AIS demonstrated a lower GAG content than this healthy control despite non-degenerated IVDs in both individuals.

3.4. GagCEST Values: Affected vs. Unaffected IVDs

In AIS patients, 44% of IVDs (22/50) were found to be affected by scoliotic deformity (aIVDs). Correspondingly, 56% of IVDs (28/50) were identified as unaffected (uaIVDs). The 22 aIVDs in the AIS patients were distributed across the different segment levels as follows: 9 aIVDs were located in segment L1/2, 6 aIVDs in segment L2/3, 4 aIVDs in segment L3/4 and 3 aIVDs in segment L4/5. In segment L5/S1 no IVD was affected by scoliotic deformity. Over all segments, no significant differences were found for mean gagCEST values between uaIVDs and aIVDs (uaIVDs: 2.32 [CI 0.93, 3.70]%, aIVD: 2.93 [CI 1.48, 4.38]%; $p = 0.258$) as detailed in Table 4. Representative morphological and compositional imaging findings are shown in Figure 2.

Table 4. Analysis of scoliotic affection on compositional imaging features of lumbar intervertebral discs (IVDs) in AIS patients. Mean glycosaminoglycan chemical exchange saturation transfer (gagCEST) values as a function of scoliotic affection (affected and unaffected IVDs of AIS patients) and IVD segment levels. Using a linear mixed model including a subject-specific intercept, mean values of gagCEST were compared. Data are corrected mean + 95% confidence interval [square brackets] (%) of gagCEST values of the nucleus pulposus (NP). The covariates were corrected for an age of 23.1 years. *p*-values < 0.05 were considered significant. Abbreviations: L—lumbar; n/a—not applicable.

Score	Segment						<i>p</i> -Value	
	L1/2	L2/3	L3/4	L4/5	L5/S1	All Segments		
IVDs affected by scoliosis	Yes	3.171 [0.129, 4.213]	2.886 [2.155, 3.616]	5.103 [2.686, 7.520]	1.520 [0.377, 2.663]	n/a	2.929 [1.479, 4.379]	0.258
	No	−0.004 [−3.666, 3.659]	2.666 [1.179, 4.153]	3.100 [2.093, 4.107]	5.762 [1.116, 10.408]	2.186 [0.942, 3.429]	2.316 [0.936, 3.697]	

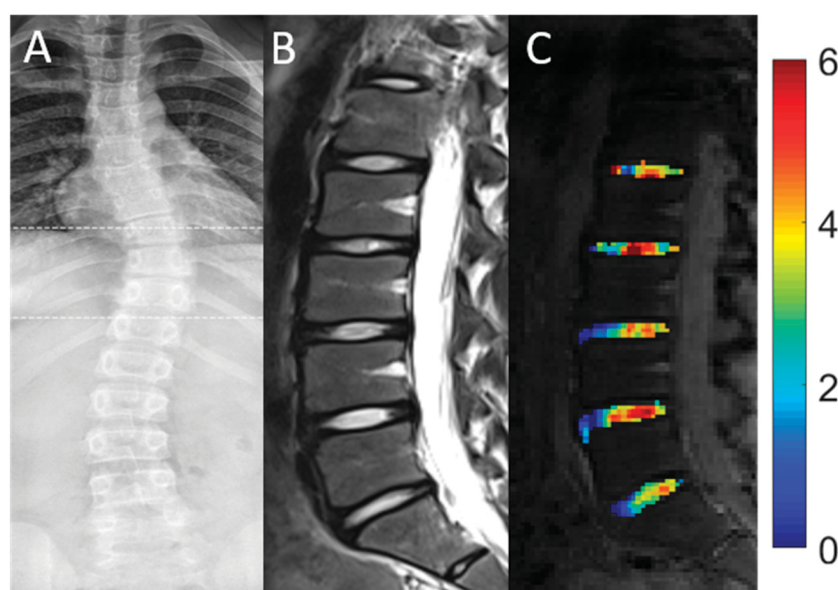


Figure 2. Representative conventional radiograph (A) and morphologic (B) and compositional (C) imaging findings of the spine of a 15-year-old female patient. (A): Conventional whole-spine radiograph in coronal orientation reveals the extent of the scoliotic curve. (B): Sagittal T2-weighted image indicates the absence of significant degenerative changes of the lumbar IVDs. (C): Sagittal gagCEST images with overlaid color-coded gagCEST maps to illustrate the GAG content indicates that no significant differences of the GAG content are seen in scoliotic compared to non-scoliotic IVDs.

4. Discussion

The most important finding of this study was that gagCEST values in lumbar IVDs of AIS patients were significantly lower than those of healthy controls, thereby indicating premorphologic IVD degeneration secondary to the specific biomechanics associated with scoliotic curvatures.

GAG depletion is considered the initial, yet reversible, step in cartilage degeneration, e.g., in degenerative disc disease of the lumbar spine [4,17]. GagCEST is a novel imaging technique that enables the quantification of GAG content in IVDs without the application of GBCA, thus rendering feasible the evaluation of early cartilage changes at the premorphologic level [20]. Decreasing gagCEST values are associated with increasing IVD degeneration, as classified using Pfirrmann grading [19,20].

In line with the results of previous studies [4,17,19,20,22], we found that gagCEST values of the NPs in all lumbar IVDs were significantly higher than those of the AF. In healthy IVDs, GAG content is physiologically highest in the NP and lowest in the AF [4,19,20]. Our group previously demonstrated significantly lower gagCEST values in

the AF than the NP in a healthy cohort [20]. In a histological study, Urban et al. examined disc composition in patients with neuromuscular scoliosis and found the GAG and water content to be highest in the disc center with a steady decrease towards the periphery, i.e., the NP–AF transition [28]. Accordingly, our study revealed the same basic IVD structure, i.e., an expected GAG gradient from central (NP) to distal (AF), in both healthy controls and AIS patients.

Overall, gagCEST values in lumbar IVDs of AIS patients were significantly lower as compared to those of healthy controls. Lower GAG concentrations bring about a loss in hydration, thus reducing biomechanical resistance [13,24,29]. Previous studies have indicated that such compositional changes in lumbar IVDs occur before morphologic degeneration [14], thereby underscoring the diagnostic potential of gagCEST imaging in the detection of early, premorphologic degeneration. Accordingly, our results suggest that IVDs of AIS patients already suffer from more severe GAG depletion and hence early degenerative changes at a significantly younger age. Once these patients have attained skeletal maturity, their lumbar spines are characterized by ongoing compositional disintegration secondary to their aberrant biomechanics. As these changes may progress further with increasing age [21], thereby underscoring the clinical need to diagnose early degeneration, timely diagnosis is a prerequisite for timely treatment. In severe cases of scoliotic deformity, with a Cobb angle of over 50°, spinal fusion surgery remains the treatment of choice in AIS patients [8,9] after skeletal maturity. As of today, it is still controversially discussed whether spinal fusion in the lower lumbar segments leads to the development of premature disc degeneration and subsequent back pain in AIS patients by reducing the number of mobile segments or if the disease itself might be the cause due to mechanical stress of the spinal curvature [30,31]. However, progression of IVD degeneration has not yet been correlated to Cobb angle. Nonetheless, reducing the number of fixed segments influences the development of disc degeneration and may lead to less lumbar back pain [32]. So far, only a few studies have evaluated the rates of preoperative disc degeneration in the lumbar spines of AIS patients [10]. In a retrospective study, Jones et al. found that only 3.9% of AIS patients undergoing surgical interventions exhibited degenerative disc changes preoperatively, which is comparable to the general pediatric population [10]. With most of the preoperative morphologic MRI scans appearing normal in AIS patients, they concluded that surgical interventions should be aimed at preserving motion in the lumbar spine segments [10]. However, in our study, lower gagCEST values in conservatively treated AIS patients indicate early compositional changes of the IVDs, suggesting that early degenerative disc changes might already be prevalent preoperatively even if not yet visible morphologically. Even though it remains speculative whether the established diagnosis of premorphologic IVD degeneration is truly reversible or alters treatment type and course, the fact that IVD composition may be assessed non-invasively extends and refines the treating physician's diagnostic armamentarium. Nonetheless, further clinical research is necessary to demonstrate the clinical value of diagnosing early compositional IVD changes by means of gagCEST imaging, for example in the preoperative work-up of AIS patients.

Another important finding of our study was that gagCEST values were not significantly different in those IVDs that were a part of the major scoliotic curve as compared to those that were not. In neuromuscular scoliosis, histologic evaluation revealed the highest GAG contents at the apical IVD, i.e., at the apex of the scoliotic curve, compared to adjacent discs one or two levels below, suggesting increased mechanical load in the convex region of the curve [28]. Increasing mechanical stress applied to the disc induces a decrease in disc hydration, thereby increasing relative GAG content (as a percentage of wet weight) [28]. Regardless of the exact relationship of solid and fluid IVD components, histologic data suggest that decreases or depletion of GAGs are not present in severely scoliotic segments. These results also indicate that aberrant loading, as it occurs in patients with neuromuscular scoliosis, does not directly affect GAG content [28], which is in accordance with our study. Although the exact reason for the preserved GAG contents in lumbar

IVDs remains speculative, the AIS patients' ages need to be considered. At a mean age of 18.3 ± 8.2 years, the AIS patients may be too young to manifest such compositional changes that are commonly considered the result of long-standing biomechanical aberration. However, due to differences in the rate of curve progression, severity of final curvature, and rigidity of the scoliotic deformity [33–35], patients with AIS and neuromuscular scoliosis may not be directly compared. Yet, due to the small number of patients with AIS enrolled in our study, our data might only be considered preliminary and should thus be validated in a larger and more homogenous patient cohort.

Our study has limitations. First, the small patient numbers are the main limitation of our study. Even though the analysis included 130 separate IVDs, these were necessarily interrelated. Consequently, with $n = 10$ AIS patients included, our results can only be considered preliminary. However, this is the first study using gagCEST imaging for the compositional evaluation of lumbar IVDs in patients with AIS that could be a starting point for future larger studies. Second, our study population was not age matched. The significantly lower mean age in AIS patients may potentially have affected our results since GAG content is known to decrease with increasing age [21]. Yet, in favor of our central hypothesis, we still found significantly lower gagCEST values in AIS patients, who, because of their younger age, ought to have higher GAG values than in healthy controls. Since the onset of AIS most commonly manifests in early puberty, a very young patient cohort was expected [1,2]. Due to ethical reasons, however, MRI exams of minors as healthy age-matched controls could not be performed. However, the significant difference in age distribution of both cohorts may be considered of minor relevance since (i) the factor "age" was accounted for in the LMM and (ii) age itself is a risk factor for GAG depletion. Third, the imaging data could not be validated through reference analyses, e.g., by histology, for ethical reasons. Fourth, evaluation of GAG content was only performed in lumbar IVDs. Though thoracic IVDs are often more severely affected by scoliotic deformity and thoracic scoliotic deformities tend to progress more rapidly [36], we only evaluated GAG content in lumbar IVDs, as thoracic IVDs are prone to considerable motion artifacts caused by respiratory motion. Fifth, the severity of scoliotic deformity, as indicated by the Cobb angle, was quite heterogeneous among our AIS patients, ranging from 11° to 73° , which may explain increased statistical variability, yet only demonstrates clinical reality. Still, future studies should include a larger study population that accounts for the various clinical and diagnostic factors such as disease duration, degree of curve deformity, and shape and degree of the Cobb angle by large enough patient numbers and sufficient statistical power.

5. Conclusions

In conclusion, the lumbar IVDs of adolescent and adult AIS patients revealed significantly lower gagCEST values indicative of compositional proteoglycan depletion that precedes structural changes and were not (yet) visible morphologically. Thus, as a powerful non-invasive and contrast-agent-free diagnostic adjunct, gagCEST imaging may be prospectively applied to quantify IVD composition and to detect early compositional changes of the degenerative cascade in patients affected by AIS.

Author Contributions: Conceptualization, L.M.W., S.N., G.A., M.R.K., and D.B.A.; Methodology, L.M.W., S.N., M.R.K., and D.B.A.; Software, L.M.W., S.N., K.L.R., A.M.-L., and D.B.A.; Validation, L.M.W., S.N., M.R.K., and D.B.A.; Formal Analysis, L.M.W., S.N., K.L.R., M.F., M.B., M.P., and D.B.A.; Investigation, L.M.W., S.N., C.S., K.L.R., M.R.K., and D.B.A.; Resources, L.M.W., S.N., K.L.R., A.M.-L., M.R.K., and D.B.A.; Data Curation, L.M.W., S.N., C.S., K.L.R., and D.B.A.; Writing—Original Draft Preparation, L.M.W., S.N., and D.B.A.; Writing—Review and Editing, L.M.W., S.N., C.S., A.M.-L., K.L.R., M.F., M.B., M.P., G.A., M.R.K., and D.B.A.; Visualization, L.M.W., S.N., C.S., A.M.-L., K.L.R., M.F., M.B., M.P., G.A., M.R.K., and D.B.A.; Supervision, L.M.W., S.N., G.A., M.R.K., and D.B.A.; Project Administration, L.M.W., S.N., M.R.K. and D.B.A.; Funding Acquisition, L.M.W., S.N., M.F., and D.B.A. All authors have read and agreed to the published version of the manuscript.

Funding: L.M.W., M.F., S.N. and D.B.A. were supported by the local Research Committee of the Medical Faculty of Heinrich-Heine-University Düsseldorf. SN was additionally supported by grants from the “Deutsche Forschungsgemeinschaft” (DFG) (NE 2136/3-1).

Institutional Review Board Statement: The study was conducted according to the guidelines of the Declaration of Helsinki and approved by the Institutional Ethics Committee of the Heinrich-Heine-University Düsseldorf (2019-551, 26 April 2021).

Informed Consent Statement: Informed consent was obtained from all subjects or, if applicable, from the legal guardians involved in the study. Written informed consent has been obtained from the patients and healthy volunteers to publish this paper.

Data Availability Statement: The data presented and/or analyzed in this study are available on reasonable request from the corresponding author. The data are not publicly available due to ethical reasons.

Acknowledgments: We thank Erika Rädisch for the technical acquisition of all MRI studies.

Conflicts of Interest: The authors declare no conflict of interest.

References

1. Konieczny, M.R.; Senyurt, H.; Krauspe, R. Epidemiology of adolescent idiopathic scoliosis. *J. Child. Orthop.* **2013**, *7*, 3–9. [[CrossRef](#)]
2. Cheng, J.C.; Castelein, R.M.; Chu, W.C.; Danielsson, A.J.; Dobbs, M.B.; Grivas, T.B.; Gurnett, C.A.; Luk, K.D.; Moreau, A.; Newton, P.O.; et al. Adolescent idiopathic scoliosis. *Nat. Rev. Dis. Primer* **2015**, *1*, 15030. [[CrossRef](#)]
3. Horne, J.P.; Flannery, R.; Usman, S. Adolescent Idiopathic Scoliosis: Diagnosis and Management. *Am. Fam. Physician* **2014**, *89*, 6.
4. Urban, J.P.G.; Winlove, C.P. Pathophysiology of the intervertebral disc and the challenges for MRI. *J. Magn. Reson. Imaging* **2007**, *25*, 419–432. [[CrossRef](#)]
5. Bertram, H.; Steck, E.; Zimmermann, G.; Chen, B.; Carstens, C.; Nerlich, A.; Richter, W. Accelerated intervertebral disc degeneration in scoliosis versus physiological ageing develops against a background of enhanced anabolic gene expression. *Biochem. Biophys. Res. Commun.* **2006**, *342*, 963–972. [[CrossRef](#)]
6. Griffith, J.F.; Wang, Y.-X.J.; Antonio, G.E.; Choi, K.C.; Yu, A.; Ahuja, A.T.; Leung, P.C. Modified Pfirrmann Grading System for Lumbar Intervertebral Disc Degeneration. *Spine* **2007**, *32*, E708. [[CrossRef](#)] [[PubMed](#)]
7. Lenke, L.G.; Betz, R.R.; Harms, J.; Bridwell, K.H.; Clements, D.H.; Lowe, T.G.; Blanke, K. Adolescent idiopathic scoliosis: A new classification to determine extent of spinal arthrodesis. *J. Bone Jt. Surg. Am.* **2001**, *83*, 1169–1181. [[CrossRef](#)]
8. Daher, M.T.; Melo, N.C.; Nascimento, V.N.; Felisbino, P., Jr.; Araújo, B.C.R.; Daher, S.; Rabahi, M.F. What Is the Best Distal Level of Arthrodesis in Lumbar Fusion in Patients with Adolescent Idiopathic Scoliosis: L3 or L4? *Coluna/Columna* **2019**, *18*, 200–204. [[CrossRef](#)]
9. Akazawa, T.; Kotani, T.; Sakuma, T.; Minami, S.; Orita, S.; Fujimoto, K.; Shiga, Y.; Takaso, M.; Inoue, G.; Miyagi, M.; et al. Spinal fusion on adolescent idiopathic scoliosis patients with the level of L4 or lower can increase lumbar disc degeneration with sagittal imbalance 35 years after surgery. *Spine Surg. Relat. Res.* **2017**, *1*, 72–77. [[CrossRef](#)]
10. Jones, M.; Badreddine, I.; Mehta, J.; Ede, M.N.; Gardner, A.; Spilsbury, J.; Marks, D. The Rate of Disc Degeneration on MRI in Preoperative Adolescent Idiopathic Scoliosis. *Spine J.* **2017**, *17*, S332. [[CrossRef](#)]
11. An, H.S.; Anderson, P.A.; Haughton, V.M.; Iatridis, J.C.; Kang, J.D.; Lotz, J.C.; Natarajan, R.N.; Oegema, T.R.J.; Roughley, P.; Setton, L.A.; et al. Introduction: Disc Degeneration: Summary. *Spine* **2004**, *29*, 2677–2678. [[CrossRef](#)]
12. Pfirrmann, C.W.; Metzendorf, A.; Zanetti, M.; Hodler, J.; Boos, N. Magnetic resonance classification of lumbar intervertebral disc degeneration. *Spine* **2001**, *26*, 1873–1878. [[CrossRef](#)] [[PubMed](#)]
13. Urban, J.P.G.; McMullin, J.F. Swelling pressure of the intervertebral disc: Influence of proteoglycan and collagen contents. *Biorheology* **1985**, *22*, 145–157. [[CrossRef](#)]
14. Chen, C.; Huang, M.; Han, Z.; Shao, L.; Xie, Y.; Wu, J.; Zhang, Y.; Xin, H.; Ren, A.; Guo, Y.; et al. Quantitative T2 Magnetic Resonance Imaging Compared to Morphological Grading of the Early Cervical Intervertebral Disc Degeneration: An Evaluation Approach in Asymptomatic Young Adults. *PLoS ONE* **2014**, *9*. [[CrossRef](#)]
15. Gulani, V.; Calamante, F.; Shellock, F.G.; Kanal, E.; Reeder, S.B. International Society for Magnetic Resonance in Medicine Gadolinium deposition in the brain: Summary of evidence and recommendations. *Lancet Neurol.* **2017**, *16*, 564–570. [[CrossRef](#)]
16. Ling, W.; Regatte, R.R.; Navon, G.; Jerschow, A. Assessment of glycosaminoglycan concentration in vivo by chemical exchange-dependent saturation transfer (gagCEST). *Proc. Natl. Acad. Sci. USA* **2008**, *105*, 2266–2270. [[CrossRef](#)] [[PubMed](#)]
17. Saar, G.; Zhang, B.; Ling, W.; Regatte, R.R.; Navon, G.; Jerschow, A. Assessment of GAG Concentration Changes in the Intervertebral Disc via CEST. *Nmr Biomed.* **2012**, *25*, 255–261. [[CrossRef](#)]
18. Müller-Lutz, A.; Schleich, C.; Schmitt, B.; Topgöz, M.; Pentang, G.; Antoch, G.; Wittsack, H.-J.; Miese, F. Improvement of gagCEST imaging in the human lumbar intervertebral disc by motion correction. *Skelet. Radiol.* **2015**, *44*, 505–511. [[CrossRef](#)] [[PubMed](#)]
19. Haneder, S.; Apprigh, S.R.; Schmitt, B.; Michaely, H.J.; Schoenberg, S.O.; Friedrich, K.M.; Trattng, S. Assessment of glycosaminoglycan content in intervertebral discs using chemical exchange saturation transfer at 3.0 Tesla: Preliminary results in patients with low-back pain. *Eur. Radiol.* **2013**, *23*, 861–868. [[CrossRef](#)]

20. Schleich, C.; Müller-Lutz, A.; Eichner, M.; Schmitt, B.; Matuschke, F.; Bittersohl, B.; Zilkens, C.; Wittsack, H.-J.; Antoch, G.; Miese, F. Glycosaminoglycan Chemical Exchange Saturation Transfer of Lumbar Intervertebral Discs in Healthy Volunteers. *Spine* **2016**, *41*, 146–152. [[CrossRef](#)]
21. Müller-Lutz, A.; Schleich, C.; Pentang, G.; Schmitt, B.; Lanzman, R.S.; Matuschke, F.; Wittsack, H.-J.; Miese, F. Age-dependency of glycosaminoglycan content in lumbar discs: A 3t gageEST study. *J. Magn. Reson. Imaging JMRI* **2015**, *42*, 1517–1523. [[CrossRef](#)] [[PubMed](#)]
22. Kim, M.; Chan, Q.; Anthony, M.-P.; Cheung, K.M.C.; Samartzis, D.; Khong, P.-L. Assessment of glycosaminoglycan distribution in human lumbar intervertebral discs using chemical exchange saturation transfer at 3 T: Feasibility and initial experience. *NMR Biomed.* **2011**, *24*, 1137–1144. [[CrossRef](#)] [[PubMed](#)]
23. Kim, H.; Kim, H.S.; Moon, E.S.; Yoon, C.-S.; Chung, T.-S.; Song, H.-T.; Suh, J.-S.; Lee, Y.H.; Kim, S. Scoliosis Imaging: What Radiologists Should Know. *RadioGraphics* **2010**, *30*, 1823–1842. [[CrossRef](#)]
24. Schleich, C.; Müller-Lutz, A.; Blum, K.; Boos, J.; Bittersohl, B.; Schmitt, B.; Gerß, J.; Matuschke, F.; Wittsack, H.-J.; Antoch, G.; et al. Facet tropism and facet joint orientation: Risk factors for the development of early biochemical alterations of lumbar intervertebral discs. *Osteoarthr. Cartil.* **2016**, *24*, 1761–1768. [[CrossRef](#)] [[PubMed](#)]
25. Müller-Lutz, A.; Schleich, C.; Schmitt, B.; Antoch, G.; Matuschke, F.; Quentin, M.; Wittsack, H.-J.; Miese, F. Gender, BMI and T2 dependencies of glycosaminoglycan chemical exchange saturation transfer in intervertebral discs. *Magn. Reson. Imaging* **2016**, *34*, 271–275. [[CrossRef](#)]
26. Zhang, Z. Naïve Bayes classification in R. *Ann. Transl. Med.* **2016**, *4*, 241. [[CrossRef](#)]
27. Beaumont, C. Comparison of Henderson’s Method I and restricted maximum likelihood estimation of genetic parameters of reproductive traits. *Poult. Sci.* **1991**, *70*, 1462–1468. [[CrossRef](#)]
28. Urban, M.R.; Fairbank, J.C.T.; Bibby, S.R.S.; Urban, J.P.G. Intervertebral Disc Composition in Neuromuscular Scoliosis: Changes in Cell Density and Glycosaminoglycan Concentration at the Curve Apex. *Spine* **2001**, *26*, 610–617. [[CrossRef](#)]
29. Lyons, G.; Eisenstein, S.M.; Sweet, M.B.E. Biochemical changes in intervertebral disc degeneration. *Biochim. Biophys. Acta BBA Gen. Subj.* **1981**, *673*, 443–453. [[CrossRef](#)]
30. Danielsson, A.J.; Cederlund, C.G.; Ekholm, S.; Nachemson, A.L. The prevalence of disc aging and back pain after fusion extending into the lower lumbar spine: A matched MR study twenty-five years after surgery for adolescent idiopathic scoliosis. *Acta Radiol.* **2001**, *42*, 187–197. [[CrossRef](#)]
31. Nohara, A.; Kawakami, N.; Tsuji, T.; Ohara, T.; Saito, T.; Kawakami, K. Intervertebral Disc Degeneration During Postoperative Follow-up More Than 10 Years After Corrective Surgery in Idiopathic Scoliosis: Comparison Between Patients With and Without Surgery. *Spine* **2018**, *43*, 255–261. [[CrossRef](#)]
32. Connolly, P.J.; Von Schroeder, H.P.; Johnson, G.E.; Kostuik, J.P. Adolescent idiopathic scoliosis. Long-term effect of instrumentation extending to the lumbar spine. *JBJS* **1995**, *77*, 1210–1216. [[CrossRef](#)] [[PubMed](#)]
33. Müller, E.B.; Nordwall, A.; Odén, A. Progression of Scoliosis in Children with Myelomeningocele. *Spine* **1994**, *19*, 147–150. [[CrossRef](#)] [[PubMed](#)]
34. Lonstein, J.E.; Carlson, J.M. The prediction of curve progression in untreated idiopathic scoliosis during growth. *J. Bone Jt. Surg. Am.* **1984**, *66*, 1061–1071. [[CrossRef](#)]
35. Saito, N.; Ebara, S.; Ohotsuka, K.; Kumeta, H.; Takaoka, K. Natural history of scoliosis in spastic cerebral palsy. *Lancet Lond. Engl.* **1998**, *351*, 1687–1692. [[CrossRef](#)]
36. Weinstein, S.L.; Dolan, L.A.; Cheng, J.C.; Danielsson, A.; Morcuende, J.A. Adolescent idiopathic scoliosis. *Lancet* **2008**, *371*, 1527–1537. [[CrossRef](#)]



Contents lists available at ScienceDirect

Journal of Science and Medicine in Sport

journal homepage: www.elsevier.com/locate/jsams

Original research

Imaging of exercise-induced spinal remodeling in elite rowers

M. Frenken^{a,*}, C. Schleich^a, K.L. Radke^a, A. Müller-Lutz^a, C. Benedikter^b, A. Franz^b, G. Antoch^a, B. Bittersohl^b, D.B. Abrar^{a,1}, S. Nebelung^{a,1}^a Department of Diagnostic and Interventional Radiology, Medical Faculty, University Dusseldorf, Germany^b Department of Orthopedics and Trauma Surgery, University of Düsseldorf, Medical Faculty, Germany

ARTICLE INFO

Article history:

Received 6 May 2021

Received in revised form 29 July 2021

Accepted 31 July 2021

Available online xxxx

Keywords:

Water sports

Spine

Intervertebral disc

Cartilage remodeling

gagCEST

Magnetic resonance imaging

ABSTRACT

Objectives: As in-vivo knowledge of training-induced remodeling of intervertebral discs (IVD) is scarce, this study assessed how lumbar IVDs change as a function of long-term training in elite athletes and age-matched controls using compositional Magnetic Resonance Imaging (MRI).

Design: Prospective case-control study.

Methods: Prospectively, lumbar spines of 17 elite rowers (ERs) of the German national rowing team (mean age: 23.9 ± 3.3 years) were imaged on a clinical 3.0 T MRI scanner. ERs were imaged twice during the annual training cycle, i.e., at training intensive pre-season preparations (t_0) and 6 months later during post-competition recovery (t_1). Controls ($n = 22$, mean age: 26.3 ± 1.9 years) were imaged once at corresponding time points (t_0 : $n = 11$; t_1 : $n = 11$). Segment-wise, the glycosaminoglycan (GAG) content of lumbar IVDs ($n = 195$) was determined using glycosaminoglycan chemical exchange saturation transfer (gagCEST). Linear mixed models were set up to assess the influence of cohort and other variables on GAG content.

Results: During pre-season, IVD GAG values of ERs were significantly higher than those of controls (ERs(t_0): $2.58 \pm 0.27\%$ (mean \pm standard deviations); controls(t_0): $1.43 \pm 0.36\%$; $p \leq 0.001$), while during post-competition recovery, such differences were not present anymore (ERs(t_1): $2.11 \pm 0.18\%$; controls(t_1): $1.89 \pm 0.24\%$; $p = 0.362$).

Conclusions: Professional elite-level rowing is transiently associated with significantly higher gagCEST values, which indicate increased lumbar IVD-GAG content and strong remodeling effects in response to training. Beyond professional rowing, core-strengthening full-body exercise may help to enhance the resilience of the lumbar spine as a potential therapeutic target in treating back pain.

© 2021 Sports Medicine Australia. Published by Elsevier Ltd. All rights reserved.

Practical implications

- Lumbar IVDs of elite rowers during pre-season preparation had significantly higher GAG values than IVDs of controls, indicating a training-induced healthier disc structure.
- During post-competition recovery, GAG values were not significantly different anymore, indicating a transient effect of training on cartilage with broader therapeutic implications for back-strengthening exercise and resilience.
- Beyond simple anatomical imaging, gagCEST is a modern non-invasive contrast agent-free imaging technique to study lumbar IVD composition and to monitor the effects of interventions such as training.

1. Introduction

Rowing is one of the traditional Olympic sports and highly competitive. Consequently, athletes are constantly pushing their limits. The lower back acts as a lever with each stroke and is the most important connection in the transmission of power from the legs to the rudder.¹ Therefore, the lumbar intervertebral discs (IVDs) are exposed to repetitive cyclic compression under high axial loads.¹ The rowing stroke may be divided into two phases, the drive and the recovery. In the drive phase, the rudder enters the water and the rower transmits the power impulse. At the end of this phase the rudder is lifted out of the water. In between, the rower moves from a fully flexed position of the lumbar spine to a relatively extended position.^{2,3} During this process, the lumbar intervertebral discs (IVDs) are exposed to repetitive cyclic motion under high axial loads.¹

Exercise in general has many positive effects on the human body, especially on the musculoskeletal and cardiovascular systems.⁴ Yet, focusing on the IVD, intensive athletic exercise at professional level is associated with early degenerative changes, including disc herniation.^{5,6} Premature IVD degeneration has been observed after frequent torsional

* Corresponding author.

E-mail address: Miriam.frenken@med.uni-duesseldorf.de (M. Frenken).¹ These authors have contributed equally to this work.

motion or recurrent spinal trauma.^{7,8} Despite these clinical observations, there is little data on how the IVD is affected by physical stress. In rats, dynamic loading positively and reversibly stimulated glycosaminoglycan (GAG) production.⁹ GAGs are components of the IVD cartilage matrix that influence its biomechanical properties. Whereas healthy IVDs have a high GAG content, IVD degeneration results in the depletion of GAGs, which may result in structural damage and mechanical loss of IVD function,¹⁰ such as a decrease in cartilage elasticity.¹¹ While dynamic compression of the IVD largely stimulated the production of the extracellular matrix constituents, particularly proteoglycans, static compression had opposite effects.¹² In humans, dynamic loading of IVDs during walking and running led to altered IVD composition in terms of increased water and proteoglycan contents, even with strenuous cumulative activity such as >50 km of weekly running.¹³

These findings support the theory that mechanical stimuli regulate the intricate cellular and metabolic processes within the IVD and that the effects of static and dynamic loading of the spine are distinctly different.¹⁴ Yet, the mechanisms by which articular cartilage responds to exercise in form of mechanical stimuli are difficult to study in vivo. Consequently, advanced imaging techniques sensitive to tissue composition have become increasingly important and are commonly referred to as *compositional MRI techniques*. Of these, GAG Chemical Exchange Saturation Transfer (gagCEST) can be applied to determine the gagCEST effect, which is a surrogate parameter for the tissue's GAG content. GagCEST is particularly promising because of its potential to assess early IVD degeneration.¹⁵ GagCEST is based on the principle that bound hydroxyl protons resonate with other frequencies than bulk water protons and can be selectively saturated. The resultant saturation transfer may be used for GAG quantification.¹⁶ Accordingly, the IVD GAG contents may thus be determined in vivo.¹⁵ Decreased IVD GAG content has been associated with increasing age,¹⁷ progressive spinal degeneration, low back pain,^{18,19} and spondyloarthritis.²⁰

Despite the substantial clinical evidence linking GAG values with age- and pathology-associated changes, the role of gagCEST in providing quantitative imaging markers of IVD composition remains to be defined. In particular, the effects of therapeutic interventions, e.g. intense physical exercise, on the IVD composition is unclear and warrants further research. Rowing lends itself to such an interventional study as the seated position in the boat and the fixed sculls and rowing oars determine dynamic sequences of movements that are synchronized to perfection by professional athletes. Unexpected sudden high loads or shearing movements are effectively prevented throughout the movements sequence, unlike impact or ball sports, because of the restricted corridor of movement. Consequently, rowers are particularly well suited to investigate the effects of dynamic full-body physical exercise and consecutive loading on the lumbar spine.

This study aimed to longitudinally determine IVD GAG contents of the lumbar spines in elite rowers of the German national team at two different stages in their annual training cycle in the pre-Olympic year 2019, to compare these changes to age-matched controls, and to relate GAG contents to morphologic imaging features. We hypothesized that intense core-strengthening full-body training would induce adaptive remodeling processes in elite rowers in terms of increased IVD-GAG content during peak training and normalized IVD-GAG content during post-competition recovery.

2. Methods

For this study, 20 elite rowers (ERs) (mean age 23.9 ± 3.0 years; 9 females, 11 males) and 22 age-matched controls not engaged in competitive sports (mean age 26.3 ± 1.9 years; 12 females, 10 males) were recruited. ERs were recruited at one of the central German federal rowing bases. With the agreement of the national coaches and team physicians, the athletes of the under-23 and senior German National Rowing Team ($n = 32$ athletes altogether) were offered to participate. Of these, 20 athletes were willing to participate and were included in

this study. One ER exhibited excessive motion artifacts during both MRI studies, thereby obviating reliable quantification, and two ERs were lost to follow-up and excluded. MRI studies were acquired during the peak of the preseason preparations (t_0), when ERs completed a maximum of rowing-specific on-water training sessions, and during post-competition recovery, i.e., approximately 6 months later (t_1).

As levels of physical activity in non-competitive athletes vary with seasonality, particular weather, and may unduly influence GAG contents,²¹ controls were not followed longitudinally but allocated to two groups based on the date of their MRI study. Matching the annual training cycle of ERs, controls were thus assigned to two equal age- and sex-matched groups, i.e., the t_0 group ($n = 11$, mean age 26.1 ± 1.6 years; 6 females, 5 males) and the t_1 group ($n = 11$, mean age 26.4 ± 2.1 years; 6 females, 5 males). Present or past recurrent symptoms of low back pain, surgery to the spine, and minor age were defined as exclusion criteria. Consequently, the total study population of 39 individuals consisted of 17 ERs (mean age 23.9 ± 3.3 years; 8 females, 9 males) and 22 controls (as described above) that underwent serial MRI studies at t_0 and t_1 .

Lumbar spines were imaged in the supine position on a clinical whole-body 3.0 T MRI scanner (MAGNETOM Prisma, Siemens Healthineers, Erlangen, Germany) and a dedicated 32-channel spine coil (Siemens Healthineers). The imaging protocol included morphologic and compositional sequences as indicated in Table 1 and -intentionally- no contrast-enhanced sequences. Sagittal and transverse T2-weighted (T2-w), sagittal short tau inversion recovery (STIR), and sagittal T1-weighted (T1-w) sequences were acquired as morphologic sequences. For compositional assessment of IVDs, a previously validated gagCEST sequence was acquired, supplemented by a water saturation shift referencing (WASSR) sequence to correct B_0 -field inhomogeneity.²² Asymmetric spin-lock ratio (SLRasym) maps were calculated as in previous studies.¹⁷ They serve as surrogate parameters for the GAG content in lumbar IVDs and are given in [%].²³

To determine the gagCEST effect in terms of SLRasym, the lumbar IVD segments L1/L2–L5/S1 were defined as regions-of-interest (ROIs) and automatically selected by a customized image processing algorithm implemented in MATLAB software (R2018a, The Mathworks, Inc., Natick, MA, USA).²⁴ Bayes classification was used to separate bone and ligaments from the disc tissue. Once the entire IVD was segmented based on the different tissue signal intensities of non-saturated and saturated images, the segmentation outlines were divided into nucleus pulposus (NP) (central 60%) and annulus fibrosus (AF) (bilaterally adjacent tissue regions, 40%). Both subregions contributed to the IVD GAG content in the subsequent evaluation and underwent statistical analysis as outlined below. Blinded to group allocation and other clinical details, DBA (resident radiologist with 5 years of musculoskeletal imaging experience) semi-quantitatively assessed the IVDs on sagittal T2-w images according to the Pfirrmann classification of disc degeneration.²⁵ Briefly, the Pfirrmann classification is a five-step system that grades discs as non-degenerative (grades 1 and 2) or degenerative (grades 3–5) based on the intensity and structure of the NP, its distinction from the AF, and disc height. All automatically positioned ROIs were visually verified by CS (senior consultant radiologist with 10 years of musculoskeletal imaging experience). No segmentation outlines or subdivisions had to be repositioned. In total, 195 IVDs were thus analyzed in this study.

Statistical analysis was performed using MATLAB and SPSS software (IBM, version 25, Armonk, NY, USA) by KLR and MF. To investigate mean differences in GAG contents between ERs and controls, multivariate statistical analyses were performed based on linear mixed models (LMMs). The LMMs included the variables (i) group allocation, i.e., ER vs. control, (ii) IVD subregion, i.e., NP vs. AF, (iii) gender, i.e., male vs. female, (iv) disc height, (v) age, and (vi) morphologic Pfirrmann score, and was fit using a restricted maximum likelihood approach.²⁶ Starting with a full model that included all variables, stepwise variable selection was applied to attain a reduced model. Based on the final model, mean differences of GAG contents were calculated and assessed for statistical

Table 1
Acquisition parameters of morphologic and compositional MRI sequences.

	T2	T2	STIR	T1	CEST	WASSR
Orientation	sag	ax	sag	sag	sag	sag
TE [ms]	95	106	57	9.5	5.1	5.1
TR [ms]	3500	5200	3800	650	10	10
Flip angle [°]	160	160	150	150	10	10
Slice thickness [mm]	4	4	4	4	5	5
FoV [mm ²]	260 × 260	190 × 190	300 × 300	300 × 300	300 × 300	300 × 300
Basic resolution [pixels ²]	384 × 288	320 × 272	384 × 269	448 × 314	192 × 192	192 × 192
Slice number [n]	15	22/16	15	15	1	1
Max. frequency offset [ppm]	n/a	n/a	n/a	n/a	4	1
Number of dynamic scans [n]					32	22
Frequency range [ppm]					-4 to 4	-1 to 1
Number of pulses [n]					6	1
Pulse duration [ms]					100	100
Interpulse duration [ms]					100	100
B1 amplitude [µT]					1.2	0.1
Duty cycle					0,5	0,5

n/a - not applicable, sag - sagittal, ax - axial.

STIR - short tau inversion recovery.

CEST - chemical exchange saturation transfer.

WASSR - water saturation shift referencing.

ppm - parts per million.

significance. More specifically, separate LMMs were set up to determine group differences at t_0 and t_1 . GagCEST values as surrogates of GAG contents of lumbar IVDs were assumed to be normally distributed. For ERs, longitudinal intra-individual comparisons between t_0 and t_1 were made using paired Student's *t*-test. For controls, inter-individual comparisons between t_0 and t_1 were based on another separate LMM that took the variables (ii) to (vi) (see above) into account to assess GAG values serially. Unless specified otherwise, data are given as means ± standard deviations (95% confidence intervals [CI]). *P*-values ≤ 0.05 were considered statistically significant.

3. Results

A total of 195 lumbar IVDs of 17 ERs ($n = 85$ IVDs) and 22 controls ($n = 110$ IVDs) were analyzed. Lumbar IVDs of ERs were scored as grades I ($n = 1/85 = 1.2\%$), II ($n = 70/85 = 82.4\%$) and III ($n = 14/85 = 16.5\%$). Similarly, lumbar IVDs of controls were assigned grades II ($n = 106/110 = 96.4\%$) and III ($n = 4/110 = 3.6\%$) (Table 2). No grades IV or V were assigned. Based on a threshold of grade ≤ II for non-degenerative IVDs (and, correspondingly, grades ≥ III for degenerative IVDs),²⁴ the vast majority of IVDs in both cohorts were not degenerated at the time of study.

GagCEST values as surrogates of GAG contents of lumbar IVDs of ERs were significantly higher than those of age-matched controls at the peak of pre-season preparations (t_0 : ERs: $2.58 \pm 0.27\%$ [CI: 2.04–3.11]; controls: $1.43 \pm 0.36\%$ [CI: 0.72–2.14]; $p \leq 0.001$), while at post-competition recovery, the GAG values of ERs were decreased and demonstrated no significant inter-group differences anymore (t_1 : ERs: $2.11 \pm 0.18\%$ [CI: 1.76–2.45]; controls: $1.89 \pm 0.24\%$ [CI: 1.43–2.35]; $p = 0.362$) (Fig. 1). Intra-individual longitudinal assessment between t_0 and t_1 revealed these differences in GAG values to be significant in ERs ($p = 0.035$). An elite rower's representative gagCEST images indicate that these decreases

Table 2

Segment-wise percentages of non-degenerated intervertebral discs, defined as Pfirrmann grades ≤ 2 [%], in elite rowers and controls.

Pfirrmann grade ≤ 2		L1/L2	L2/L3	L3/L4	L4/L5	L5/S1
Elite Rowers	t_0	100.0	88.2	76.5	82.4	70.6
	t_1	100.0	88.2	75.0	76.5	70.6
Controls nr.1	t_0	100.0	100.0	100.0	100.0	100.0
	t_1	100.0	100.0	100.0	90.9	72.7

were observed in all lumbar segments, yet to variable degrees, and were not identifiable on morphologic images (Fig. 2). In contrast, time-wise differences in GAG values were not significant in controls ($p = 0.884$).

At t_0 and t_1 , mean IVD GAG values were significantly higher in the NP than the AF, both in ERs and controls (t_0 [all]: NP: $2.74 \pm 0.32\%$ [CI: 2.11–3.38]; AF: $1.26 \pm 0.30\%$ [CI: 0.68–1.85]; $p \leq 0.001$; t_1 [all]: NP: $2.71 \pm 0.22\%$ [CI: 2.28–3.14]; AF: $1.29 \pm 0.19\%$ [CI: 0.93–1.66]; $p \leq 0.001$). Moreover, mean IVD GAG values were also significantly higher in Pfirrmann scores ≤ 2 than scores > 2, both at t_0 ([all]: Pfirrmann scores ≤ 2: $3.18 \pm 0.15\%$ [CI: 2.89–3.47]; Pfirrmann scores > 2: $0.83 \pm 0.54\%$ [CI: -0.23 – 1.88]; $p \leq 0.001$) and at t_1 ([all]: Pfirrmann scores ≤ 2: $2.88 \pm 0.13\%$ [CI: 2.63–3.13], Pfirrmann scores > 2: $1.12 \pm 0.30\%$ [CI: 0.53–1.71]; $p \leq 0.001$). Men tended to have higher GAG values than women, although this difference was not significant (t_0 [all]: males: $2.17 \pm 0.31\%$ [CI: 1.56–2.78]; females: $1.84 \pm 0.31\%$ [CI: 1.23–2.44]; $p = 0.199$; t_1 [all]: males: $2.04 \pm 0.20\%$ [CI: 1.65–2.43]; females: $1.96 \pm 0.20\%$ [CI: 1.56–2.36]; $p = 0.698$).

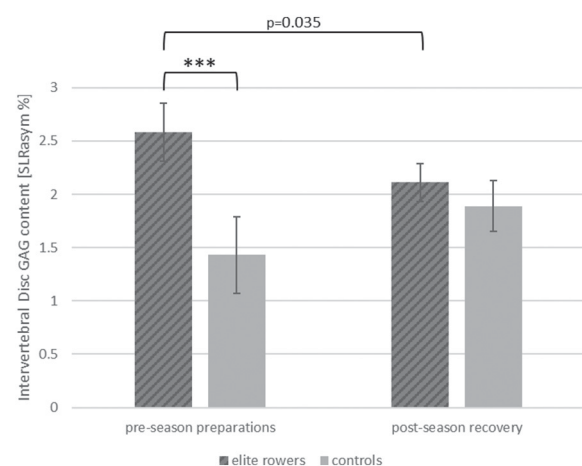


Fig. 1. Lumbar intervertebral disc GAG contents of elite rowers (hatched dark grey) and age-matched controls (plain light grey) during the pre-season preparations and the post-season recovery. GAG contents were determined using gagCEST imaging and are presented as asymmetric spin-lock ratios (SLRasym [%]). Triple asterisks denote highly significant differences [$p \leq 0.001$]. Bars and whiskers indicate means and standard deviations. Note that elite rowers [$n = 17$] were imaged serially, thereby allowing longitudinal and intra-individual assessment, while controls were imaged once at each time point [$n = 11$ each], thereby allowing cross-sectional and inter-individual comparative evaluation.

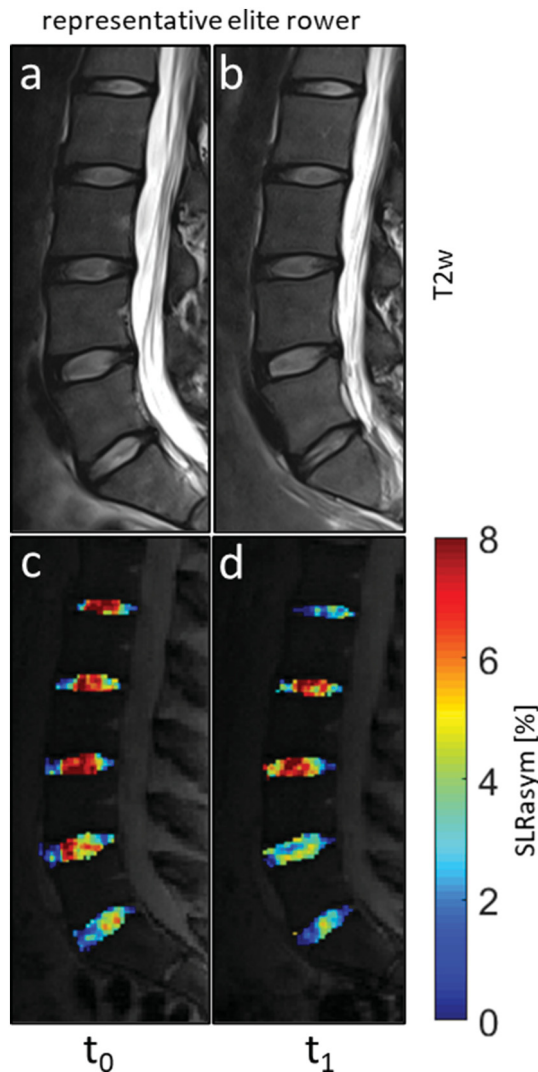


Fig. 2. Mid-sagittal T2-weighted (T2w) morphologic (a, b) and corresponding gagCEST images (c, d) of a representative elite rower. Elite rowers were imaged at the peak of the pre-season preparations (t_0) and during post-season recovery (t_1). While morphologic features of the lumbar intervertebral discs remained constant, decreases in GAG contents were found throughout the entire lumbar spine at t_1 as compared to t_0 . Color-coded display of GAG contents of intervertebral discs in lumbar segments L1/2–L5/S1. GAG contents are indicated as SLRasym [%] and are overlaid onto the corresponding WASSR mid-sagittal sequences (c, d).

Level of disc segment was not of significant relevance to IVD GAG values (t_0 [all]: $p = 0.064$, t_1 [all]: $p = 0.617$), whereas age was of significant relevance, yet only at t_1 and not at t_0 (t_0 [all]: $p = 0.800$; t_1 [all]: $p = 0.022$).

4. Discussion

This study's most important finding is that professional elite-level is transiently associated with significantly higher gagCEST values, which indicate increased lumbar IVD-GAG content and strong training-induced adaptive remodeling effects of spinal composition with potentially wide-ranging diagnostic and therapeutic implications beyond the world of professional athleticism.

Rowing belongs to the traditional Olympic sports and is performed by many young athletes.^{1,27}

The biomechanics of rowing are complex, and the spine is one of the important force transmission elements in this cyclic movement. In the drive phase of the boat, it is initially fully flexed and then transitions to a relative extended position.^{28,29} Up to now, the effects of rowing

on the lumbar IVDs remain to be elucidated to protect young athletes from possible damage and provide scientifically sound guidance on whether rowing can be considered protective for the lumbar spine.

Our main finding is that the IVD GAG values as surrogate for GAG contents in young ERs were higher under intense training than in age-matched controls and decreased during post-season recovery. Since GAGs are components of the cartilage extracellular matrix and important for the structure and functionality of intervertebral discs, especially their elasticity, our results suggest an improvement of IVD quality during exercise. This is consistent with earlier in-vivo data of improved IVD hydration and GAG contents in physically active humans¹³ and the response to mechanical stimulation of rat IVDs when dynamically loaded.⁹ In the present study, ERs showed higher GAG values under exercise, which dropped considerably to age-normalized levels during recovery. Denoch While decreases in GAG content are considered an early sign of IVD degeneration,¹⁹ corresponding increases have been demonstrated for runners.¹³ Building on this body of scientific evidence, our study suggests that substantial anabolic adaptive processes in the IVD result from core-strengthening full-body physical exercise such as rowing.

Nevertheless, it is still unclear how these beneficial training-induced remodeling processes in the IVD can be reconciled with increased disc herniations and premature degenerative changes of the spine in active athletes - as previously reported in the literature and also observed -by trend- in this study.^{5,6} Possible explanations involve the theory of a "likely anabolic loading window"^{13,30} that suggests that loading within a specific range allows for optimal adaptation of the IVD. If, however, pressures on the discs are lower or higher than this range, adaptive processes are reduced. The observation of high-impact loading causing damage to the IVD and the vertebral endplates³¹ supports this theory. Even though rowing may be more protective for the lumbar spine than high-impact sports, our data also indicate that the high-power transmission of forces via the lumbar spine at elite-level intensities may predispose the lumbar spine to premature degeneration. Whether or not lower loading intensities at the recreational level have the same effect on the lumbar spine remains speculative. Similarly, the effects of other sports activities such as running on IVD GAG values are unclear, too, and require systematic longitudinal comparisons between the different types of sports with standardization of the activity level, if possible.

Focusing on factors influencing IVD GAG content, age and gender need to be considered, too.^{17,32} At t_1 , we noticed significant decreases in the GAG contents of ERs that were more pronounced with increasing age. This finding is in line with earlier results that indicated age-dependent reductions in IVD GAG contents¹⁷ and may be associated with altered metabolic capacity. By deliberately including young athletes in their twenties, we aimed to limit the effects of age-related pre-morphologic degenerative changes and to control the effects of such confounders. At t_0 , however, age did not significantly affect IVD GAG values, which may be due to the overpowering training effects induced by elite-level rowing. Gender was not significantly associated with IVD GAG contents, even though men tended to have higher GAG values than women. Given the small overall sample size, these relations need to be further elucidated in future studies.

Morphologic assessment of IVDs as based on the Pfirrmann score indicated that most IVDs were not degenerated. Despite the low morphologic variation, a strong inverse correlation between the IVDs' molecular composition, i.e., GAG values, and morphologic degeneration, i.e., Pfirrmann scores, was found. Such associations have been reported before¹⁵ and indicate that gagCEST imaging provides a specific and valid imaging marker of pre-morphologic IVD changes.

Biomechanical data indicate that during loading, the lumbar spine is heterogeneously and non-linearly stressed.³³ Hence, it is surprising that we did not find any significant segment-wise differences in GAG values between L1/L2–L5/S1. Possibly due to the levering mechanisms that transfer loads en bloc to the lumbar spine, competitive rowing seems

to bring about homogeneously altered disc pressures and increased GAG synthesis. An earlier study on 12 volunteers, whose activity level was not further specified, found lower GAG contents at lower IVD levels.³⁴ Yet, the considerably older cohort in that study with a mean age of 30 years (range: 25–53 years) must be considered, as this relationship may be confounded by increasing degeneration as a function of age.

There are limitations. First, both cohorts were not exactly matched in terms of age with slightly younger ERs than controls. Even though the mean difference was just two years, previous studies have indicated the dominant effects of age on GAG quantity. 10-year differences were associated with considerable decreases in GAG values.¹⁷ Second, sample size was limited. Yet, given the fact that the elite squad of the German Rowing Federation consists of 32 athletes altogether, we consider our efforts to put together this consistent study cohort of elite athletes quite successful. Third, we did not evaluate intra- and inter-observer reliability because the primary parameter of interest, i.e., SLRasym value, was determined using an automatic segmentation algorithm, thereby obviating the need for intra- and inter-observer analysis. Fourth, among the many advanced MRI techniques available, we only performed gagCEST imaging. Alternative functional techniques such as T2 or T1 ρ mapping may offer additional insights into the adaptive compositional changes of the lumbar spine in response to training. Fifth, while ERs were imaged twice (at t_0 and t_1) during their annual training cycle and thus could be assessed longitudinally and intra-individually, controls were only imaged once, at either t_0 or t_1 , which only allows inter-individual comparisons. This limitation in study design is partially offset because controls were not followed up longitudinally and thus not enticed to engage in physical activities beyond non-competitive recreational sports. Yet, the limited group sizes accounted for substantial inter-individual variability between the control cohorts at t_0 and t_1 . Future studies should thus address this methodological limitation by including longitudinal follow-up of controls, too. Lastly, it should be noted that correlations between the gagCEST effect, i.e. SLRasym and the GAG content have been demonstrated using gagCEST, allowing GAG monitoring in IVDs in vivo.³⁵ However, a histological validation of the method and also the clarification to what extent T2 relaxation times represent a possible bias on the gagCEST effect³⁶ is still pending and should be addressed in further studies.

5. Conclusion

In conclusion, professional elite-level rowing is transiently associated with significantly higher gagCEST values, which indicate increased lumbar IVD-GAG content and strong training-induced GAG remodeling effects and adaptations of the lumbar spine at the pre-morphological level. Beyond the world of elite rowing, physical core-strengthening full-body exercise seems to be therapeutically beneficial in strengthening the lumbar spine's resilience. In efforts to prevent premature lumbar degeneration, this study indicates that exercise within an anabolic window may be beneficial for the spine and used to guide preventive and/or therapeutic measures.

Funding information

M. Frenken, D.B. Abrar and S. Nebelung have been supported by research grants of the Medical Faculty of Heinrich-Heine-University Düsseldorf (Research Commission of the Medical Faculty). This project was also funded by the Deutsche Forschungsgemeinschaft (grant number: NE 2136/3-1).

Declaration of interest statement

None declared.

Confirmation of ethical compliance

This prospective study was approved by the local ethical committee (Ethical Committee, Medical Faculty, University of Düsseldorf, Germany, study number 5087R). Written informed consent was obtained from all participants prior to the study.

Acknowledgements

CS, MF, BB, CB, AF, GA, DBA and SN conceptualized the study. The study was performed by DBA, MF, CB, CS, AF, SN with AM-L and KLR completing the image acquisition. MF drafted the manuscript. KLR, conducted the data analysis. MF, AM-L, DAB and SN interpreted data and contributed to the manuscript draft. The authors would like to thank Erika Rädisch for the assistance in performing the MRI studies.

References

- Hosea TM, Hannafin JA. Rowing injuries. *Sports Health* 2012;4(3):236-245. doi:10.1177/1941738112442484.
- Wilson F, Gissane C, Gormley J et al. Sagittal plane motion of the lumbar spine during ergometer and single scull rowing. *Sports Biomech* 2013;12(2):132-142. doi:10.1080/14763141.2012.726640.
- Pollock CL, Jenkyn TR, Jones IC et al. Electromyography and kinematics of the trunk during rowing in elite female rowers. *Med Sci Sports Exerc* 2009;41(3):628-636. doi:10.1249/MSS.0b013e31818c1300.
- Huonker M, Halle M, Keul J. Structural and functional adaptations of the cardiovascular system by training. *Int J Sports Med* 1996;17(Suppl 3):S164-S172. doi:10.1055/s-2007-972919.
- Witwit WA, Kovac P, Sward A et al. Disc degeneration on MRI is more prevalent in young elite skiers compared to controls. *Knee Surg Sports Traumatol Arthrosc* 2018;26(1):325-332. doi:10.1007/s00167-017-4545-3.
- Abdalkader M, Guermazi A, Engebretsen L et al. MRI-detected spinal disc degenerative changes in athletes participating in the Rio de Janeiro 2016 summer Olympics games. *BMC Musculoskelet Disord* 2020;21(1):45. doi:10.1186/s12891-020-3057-3.
- Schmidt H, Heuer F, Wilke HJ. Dependency of disc degeneration on shear and tensile strains between annular fiber layers for complex loads. *Med Eng Phys* 2009;31(6):642-649. doi:10.1016/j.medengphy.2008.12.004.
- Kartal A, Yildiran I, Senkoylu A et al. Soccer causes degenerative changes in the cervical spine. *Eur Spine J* 2004;13(1):76-82. doi:10.1007/s00586-003-0623-y.
- Ueta RHS, Tarini VAF, Franciozi CES et al. Effects of training and overtraining on intervertebral disc proteoglycans. *Spine (Phila Pa 1976)* 2018;43(1):E1-E6. doi:10.1097/BRS.0000000000002368.
- Liu X, Krishnamoorthy D, Lin L et al. A method for characterising human intervertebral disc glycosaminoglycan disaccharides using liquid chromatography-mass spectrometry with multiple reaction monitoring. *Eur Cell Mater* 2018;35:117-131. doi:10.22203/eCM.v035a09.
- Zwierzchowski TJ, Janus J, Konecki W et al. The quantitative evaluation of the impact of viable medial meniscus graft type on the biochemical and biomechanical properties of the rabbit tibial cartilage. *J Orthop Surg Res* 2015;10:170. doi:10.1186/s13018-015-0311-8.
- Grodzinsky AJ, Levenston ME, Jin M et al. Cartilage tissue remodeling in response to mechanical forces. *Annu Rev Biomed Eng* 2000;2:691-713. doi:10.1146/annurev.bioeng.2.1.691.
- Belavy DL, Quittner MJ, Ridgers N et al. Running exercise strengthens the intervertebral disc. *Sci Rep* 2017;7:45975. doi:10.1038/srep45975.
- Brisby H, Wei AQ, Molloy T et al. The effect of running exercise on intervertebral disc extracellular matrix production in a rat model. *Spine (Phila Pa 1976)* 2010;35(15):1429-1436. doi:10.1097/BRS.0b013e3181e0f5bc.
- Togao O, Hiwatashi A, Wada T et al. A qualitative and quantitative correlation study of lumbar intervertebral disc degeneration using glycosaminoglycan chemical exchange saturation transfer, Pfirrmann grade, and T1-rho. *AJNR Am J Neuroradiol* 2018;39(7):1369-1375. doi:10.3174/ajnr.A5657.
- Vinogradov E, Sherry AD, Lenkinski RE. CEST: from basic principles to applications, challenges and opportunities. *J Magn Reson* 2013;229:155-172. doi:10.1016/j.jmr.2012.11.024.
- Muller-Lutz A, Schleich C, Pentang G et al. Age-dependency of glycosaminoglycan content in lumbar discs: a 3t gagCEST study. *J Magn Reson Imaging* 2015;42(6):1517-1523. doi:10.1002/jmri.24945.
- Haneder S, Apprich SR, Schmitt B et al. Assessment of glycosaminoglycan content in intervertebral discs using chemical exchange saturation transfer at 3.0 Tesla: preliminary results in patients with low-back pain. *Eur Radiol* 2013;23(3):861-868. doi:10.1007/s00330-012-2660-6.
- Pulickal T, Boos J, Konieczny M et al. MRI identifies biochemical alterations of intervertebral discs in patients with low back pain and radiculopathy. *Eur Radiol* 2019;29(12):6443-6446. doi:10.1007/s00330-019-06305-6.
- Schleich C, Muller-Lutz A, Matuschke F et al. Glycosaminoglycan chemical exchange saturation transfer of lumbar intervertebral discs in patients with spondyloarthritis. *J Magn Reson Imaging* 2015;42(4):1057-1063. doi:10.1002/jmri.24877.
- Tucker P, Gilliland J. The effect of season and weather on physical activity: a systematic review. *Public Health* 2007;121(12):909-922. doi:10.1016/j.puhe.2007.04.009.

22. Muller-Lutz A, Matuschke F, Schleich C et al. Improvement of water saturation shift referencing by sequence and analysis optimization to enhance chemical exchange saturation transfer imaging. *Magn Reson Imaging* 2016;34(6):771-778. doi:10.1016/j.mri.2016.03.013.
23. Muller-Lutz A, Ljimini A, Stabinska J et al. Comparison of B0 versus B0 and B1 field inhomogeneity correction for glycosaminoglycan chemical exchange saturation transfer imaging. *MAGMA* 2018. doi:10.1007/s10334-018-0689-5.
24. Schleich C, Muller-Lutz A, Eichner M et al. Glycosaminoglycan chemical exchange saturation transfer of lumbar intervertebral discs in healthy volunteers. *Spine (Phila Pa 1976)* 2016;41(2):146-152. doi:10.1097/BRS.0000000000001144.
25. Pfirrmann CW, Metzendorf A, Zanetti M et al. Magnetic resonance classification of lumbar intervertebral disc degeneration. *Spine (Phila Pa 1976)* 2001;26(17):1873-1878.
26. Beaumont C. Comparison of Henderson's method I and restricted maximum likelihood estimation of genetic parameters of reproductive traits. *Poult Sci* 1991;70(7):1462-1468. doi:10.3382/ps.0701462.
27. Smoljanovic T, Bojanic I, Hannafin JA et al. Traumatic and overuse injuries among international elite junior rowers. *Am J Sports Med* 2009;37(6):1193-1199. doi:10.1177/0363546508331205.
28. Wilson F, Gissane C, McGregor A. Ergometer training volume and previous injury predict back pain in rowing; strategies for injury prevention and rehabilitation. *Br J Sports Med* 2014;48(21):1534-1537. doi:10.1136/bjsports-2014-093968.
29. Wilson F, Thornton JS, Wilkie K et al. 2021 consensus statement for preventing and managing low back pain in elite and subelite adult rowers. *Br J Sports Med* 2021. doi:10.1136/bjsports-2020-103385.
30. Wilke HJ, Neef P, Cimi M et al. New in vivo measurements of pressures in the intervertebral disc in daily life. *Spine (Phila Pa 1976)* 1999;24(8):755-762. doi:10.1097/00007632-199904150-00005.
31. Schmidt H, Kettler A, Heuer F et al. Intradiscal pressure, shear strain, and fiber strain in the intervertebral disc under combined loading. *Spine (Phila Pa 1976)* 2007;32(7):748-755. doi:10.1097/01.brs.0000259059.90430.c2.
32. Muller-Lutz A, Schleich C, Schmitt B et al. Gender, BMI and T2 dependencies of glycosaminoglycan chemical exchange saturation transfer in intervertebral discs. *Magn Reson Imaging* 2016;34(3):271-275. doi:10.1016/j.mri.2015.10.024.
33. Shirazi-Adl A. Biomechanics of the lumbar spine in sagittal/lateral moments. *Spine (Phila Pa 1976)* 1994;19(21):2407-2414. doi:10.1097/00007632-199411000-00007.
34. Kim M, Chan Q, Anthony MP et al. Assessment of glycosaminoglycan distribution in human lumbar intervertebral discs using chemical exchange saturation transfer at 3 T: feasibility and initial experience. *NMR Biomed* 2011;24(9):1137-1144. doi:10.1002/nbm.1671.
35. Ling W, Regatte RR, Navon G et al. Assessment of glycosaminoglycan concentration in vivo by chemical exchange-dependent saturation transfer (gagCEST). *Proc Natl Acad Sci U S A* 2008;105(7):2266-2270. doi:10.1073/pnas.0707666105.
36. Peterson P, Olsson E, Svensson J. T2 relaxation time bias in gagCEST at 3T and 7T: comparison of saturation schemes. *Magn Reson Med* 2019;81(2):1044-1051. doi:10.1002/mrm.27465.